DEVELOPMENT AND ASSESSMENT OF GASTRIC-RETENTIVE SUSTAINED RELEASE METRONIDAZOLE MICROCAPSULES

by

Anjana Makan

A Thesis Submitted to Rhodes University in

Fulfilment of the Requirements for the Degree of

MASTER OF SCIENCE (PHARMACY)

in

PHARMACEUTICS

February 2017

Faculty of Pharmacy

RHODES UNIVERSITY

Grahamstown

South Africa

ABSTRACT

Helicobacter pylori is one of the most common pathogenic bacterial infections and is the leading cause of gastritis, gastroduodenal ulcer disease and gastric cancers. Studies have revealed the prevalence of *Helicobacter pylori* is high in many countries around the globe. Although *Helicobacter pylori* is highly sensitive to antimicrobial agents *in vitro* the clinical eradication rate of the disease is still low. The instability of API at gastric pH, low concentration of API in the gastric mucosa and short gastric residence times are the main reasons for poor eradication rates. The high prevalence rate of this disease necessitates the design and development of gastric-retentive site specific oral dosage forms for the optimized delivery of existing therapeutic molecules and may be an approach to improving the eradication rate of *Helicobacter pylori.* Metronidazole (MTZ) is a 5-nitroimidazole derivative that exhibits antibiotic and antiprotozoal activity. MTZ is used in combination with other compounds for the treatment of *Helicobacter pylori* in peptic ulcer disease. MTZ is a potential candidate for inclusion in a sustained release gastric-retentive delivery system that acts in the stomach and since it is unstable in the intestinal/colonic environment enhancing gastric residence time would be a therapeutic advantage. MTZ is a cost-effective therapy that exhibits good anti-microbial activity and has a favourable pharmacokinetic profile. A sustained release gastric-retentive formulation is therefore proposed as an approach to enhance the local delivery of MTZ and improve treatment outcomes for patients infected with *Helicobacter pylori*.

A stability indicating Reversed-Phase High Performance Liquid Chromatography (RP-HPLC) method for the quantitation of MTZ in pharmaceutical dosage forms was developed and optimised using a Central Composite Design (CCD) approach. The RP-HPLC method was found to be linear, accurate, precise, sensitive, selective, and was applied to the analysis of MTZ in commercially available medicines.

Preformulation studies were conducted as preparative work prior to manufacture gastric-retentive sustained release MTZ microcapsules. The experiments conducted were tailored for the development of sustained release MTZ microcapsules using a solvent evaporation method. The particle size and shape of the microcapsules was investigated using Scanning Electron Microscopy (SEM). MTZ- excipient compatibility studies were performed using Fourier Transform Infra-red Spectroscopy (FTIR), Differential Scanning Calorimetry (DSC)

and X-Ray Diffraction (XRD). The results revealed that no definite interaction between MTZ and intended excipients to be used for manufacture of MTZ formulations occurred.

A solvent evaporation procedure was used for the manufacture of MTZ microcapsules. Preliminary formulations were manufactured using two different grades of Methocel® at various levels. In addition the impact of processing parameters on performance was also investigated. The formulations were assessed in terms of *in vitro* release, buoyancy, yield, encapsulation efficiency and microcapsule size. Formulation optimisation was undertaken using a CCD approach and numerical optimisation was used to predict an optimised formulation composition that would produce minimal initial MTZ release, maximum MTZ release at 12 hours and maximum buoyancy, encapsulation efficiency and yield.

The kinetics of MTZ release from microcapsules was established by fitting *in vitro* release data to different mathematical models. Higuchi model and first-order model appeared to best fit the data as majority of the formulation batches had highest R^2 values for these models. Short-term stability assessment of the optimised formulation was established by undertaking stability studies at 25°C/60% RH and 40°C/75%RH. No significant changes in any of the CQA were observed over 30 days of stability testing.

A gas chromatographic (GC) method was developed and validated for the quantitation of residual acetone and n-hexane. The optimised formulation contained 213.60 ppm/g acetone and 25.23 ppm/g n-hexane which are well below the limits set for residual solvents.

In conclusion, gastric-retentive sustained release MTZ microcapsules with potential for further development and optimisation have been successfully developed and assessed in these studies.

This thesis is dedicated to the following:

To my parents Mr Baloo Makan and Mrs Usha Makan and my sister Priya

ACKNOWLEDGEMENTS

I would like to express my sincere gratitude to the following people:

My supervisor, Professor R.B. Walker for giving me the opportunity to be part of his research group. I thank him for his support, guidance, assistance, understanding and patience during the research and writing of this thesis

Dr S. M. M. Khamanga for his constant academic support and positive encouragement during the difficult times of this research

Dr R. Tandlich for the opportunity to utilize the Gas Chromatography equipment, his dedication, assistance and supervision is appreciated.

The Henderson Scholarship for funding and giving me the opportunity to complete my post-graduate studies.

Mr L. Purdon, Mr C. Nontyi, Ms L. Emslie, Mrs T. Kent and Mr T. Fleck for their technical assistance during my studies.

Professor Watkins, for allowing me to use the DSC and FTIR in the Chemistry Department. Ms S. Pinchuck and Mr M. Randall for their technical assistance at the Electron Microscopy Unit.

My colleagues and friends in the Biopharmaceutics Research Laboratory, Biopharmaceutics Research Institute, Pharmaceutical Chemistry Department and Mr P. Ngoepe from the Chemistry Faculty.

My parents, Mr B. Makan and Mrs U. Makan for their love, motivation, prayers and support. Without them, nothing would have been possible. I am forever thankful and indebted to my parents for the sacrifices they made to support my education .

My sister, Ms P Makan-Machhi and my brother in-law, Mr D. Machhi for all their love, encouragement and support.

Nitesh for his support, care, sacrifices and patience during the trials and tribulations of this research.

The Almighty for giving me the strength and protection to succeed throughout my life.

STUDY OBJECTIVES

Helicobacter pylori infection affects approximately 50% to 75% of the global population [1,2]. *Helicobacter pylori* is a major cause of peptic ulcer disease and gastric malignancies such as mucosa associated lymphoid tissue lymphoma and gastric adenocarcinoma [1]. Treatment remains a challenge, since many determinants for successful therapy including antibiotic resistance, mucosal drug concentration, short gastric residence time of drugs, side-effect profile and cost reduce success [2,3]. Metronidazole is one of the agents used for the treatment of *Helicobacter pylori* infection and is a suitable candidate for inclusion in gastric-retentive delivery systems, since it acts in the stomach and is unstable in the intestinal/colonic environment [4–7]. MTZ is almost completely absorbed following oral administration and exhibits a bioavailability of > 90% [8,9]. MTZ is widely distributed in the biological system and has an apparent volume of distribution of 0.6 - 0.9 l/kg [10]. The high rate of prevalence of this disease and need for the manufacture of gastric-retentive site specific oral dosage forms for the optimum delivery of existing drug molecules may be an approach to improving eradication of *Helicobacter pylori*.

The objectives of this study were:

i. To collect, analyse and interpret information relating to the physicochemical, pharmacological and clinical properties of MTZ.
ii. To develop and validate a RP-HPLC method with the necessary selectivity and sensitivity to quantitate MTZ in dosage forms with the necessary accuracy and precision for quality control purposes.
iii. To conduct preformulation studies to determine the compatibility of MTZ with intended excipients.
iv. To develop and manufacture sustained release gastric-retentive MTZ microcapsules using solvent evaporation manufacture.
v. To investigate the effect of formulation and manufacturing variables on encapsulation efficiency, yield, buoyancy and MTZ release.
vi. To use Response Surface Methodology (RSM) to optimise the formulation.
vii. To use model-dependent approaches to establish the kinetics of MTZ.
viii. To undertake short term stability studies on the optimised formulation.
ix. To develop and validate a GC method for residual acetone and n-hexane determination in the optimised formulation.

TABLE OF CONTENTS

LIST OF TABLES

LIST OF FIGURES

LIST OF ACRONYMS

ACN	Acetonitrile
ANOVA	Analysis of Variance
API	Active Pharmaceutical Ingredient
BBD	Box Behnken Design
CCD	Central Composite Design
CQA	Critical Quality Attributes
DoE	Design of Experiments
DSC	Differential Scanning Calorimetry
EE	Encapsulation Efficiency
FID	Flame Ionisation Detector
FDA	Food and Drug Administration
FTIR	Fourier Transform Infrared Spectroscopy
GC	Gas Chromatography
HPLC	High Performance Liquid Chromatography
HPMC	Hydroxypropyl Methylcellulose
ICH	International Conference on Harmonisation
LOD	Limit of Detection
LOQ	Limit of Quantitation
MeOH	Methanol
MTZ	Metronidazole
MCC	Microcrystalline cellulose
ODZ	Ornidazole
PTF	Peak Tailing Factor
RSD	Relative Standard Deviation
RSM	Response Surface Methodology

RT	Retention Time
SD	Standard Deviation
SEM	Scanning Electron Microscopy
USP	United States Pharmacopiea
UV	Ultraviolet
XRD	X-ray Diffraction

CHAPTER ONE
METRONIDAZOLE

1.1 INTRODUCTION

Metronidazole (MTZ) is a 5-nitroimidazole derivative developed following the discovery of azomycin [11,12]. Azomycin exhibited antibacterial and trichomonacidal activity however, it was found to be toxic when used clinically. Consequently through the synthesis of a series of analogs the development of MTZ was accomplished [11,12]. MTZ was initially thought to be effective against protozoal organisms but was later found to exhibit activity against anaerobic bacteria [11,13]. The 5-nitroimidazole series of compounds exhibits anti-protozoal and antibiotic properties and examples of this group of compounds include tinidazole, ornidazole, secnidazole and ternidazole [14].

MTZ is used for the treatment of protozoal infections including trichomoniasis, giardiasis and amoebiasis [15]. MTZ is active against anaerobic bacteria such as *Bacteroides* and *Clostridium* species and can be used to treat specific bacterial infections such as acute necrotizing ulcerative gingivitis, periodontitis, bacterial vaginosis and pelvic inflammatory disease [16–18]. MTZ has been used for the treatment of bacterial vaginosis since 1980 and is used in combination with other molecules such as omeprazole and amoxicillin or clarithromycin to treat *Helicobacter pylori* (*H. Pylori)* infections in peptic ulcer disease [16,19,20].

MTZ is administered orally in the form of immediate release tablets, capsules or extended release tablets and is administered as the benzoate salt in suspensions [16]. It is also available as a cream or gel for topical or vaginal use [17]. MTZ has been incorporated into suppository formulations and intravenous dosage forms of MTZ or the hydrochloride salt are also available [16]. Commercially available MTZ products in South Africa include Flagyl®, Metrazole®, Metrogel lV®, Trichazole® and Rozex® [16,17].

1.2 PHYSICO-CHEMICAL PROPERTIES

1.2.1 Description

MTZ is a white to pale yellow crystalline powder that is odourless and bitter to taste [16,21]. MTZ has the chemical name 1-(2-hydroxyethyl)-2-methyl-5-nitroimidazole and is a low molecular weight compound with a molecular weight of 171.16 and a molecular formula of $C_6H_9N_3O_3$ [21,22]. The chemical structure of MTZ is depicted in Figure 1.1.

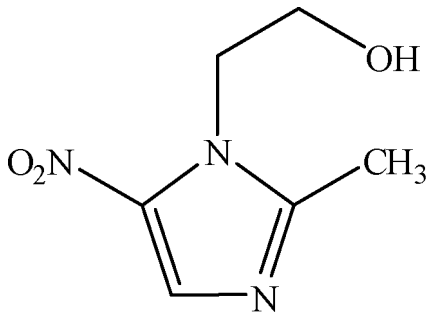

Figure 1.1 Chemical structure of MTZ

1.2.2 Solubility

The solubility of MTZ in different solvents at 25°C is summarised in Table 1.1.

Table 1.1 Solubility of MTZ in different solvents [21].

Solvent	Solubility mg/ml
Water	10.5
Methanol	32.5
Ethanol	15.4
Chloroform	3.8
Heptane	<0.01

1.2.3 Dissociation constant (pKa)

MTZ is a weakly basic compound with a pKa of 2.62 [23–25].

1.2.4 Partition coefficient

Knowledge of the oil/water partition coefficient of a compound is crucial for drug and product design as in order for effective absorption, distribution and metabolism to occur the compound must cross the phospholipid membranes of cells and tissues [24,26]. In order to establish the partition coefficient of a molecule octanol is used as it represents the oleaginous phase that corresponds to the lipid components of a membrane [27].

The logarithm of the octanol-water partition ratio (logP) is a measure of the lipophilicity or hydrophobicity of a substance and the most common approach to the measurement of logP is to establish the extent of partitioning of a compound between octanol and water [27,28]. The hydrophobic nature of a drug is an important parameter as it facilities an understanding of enzyme-ligand interactions, drug receptor interactions and transport of a molecule to active sites *in vivo* [28–30]. The log P of MTZ at 25°C in n-octanol and in a n-octanol/0.1M sodium diphosphate buffer of pH 7.4 is 0.75 and -0.02, respectively [31,32].

1.2.5 Infrared absorption spectrum

The vibrational spectrum of a molecule is a unique physical property of that molecule and is used to identify the compound and infrared spectroscopy is used to identify functional groups that make up a molecule [33,34]. The structural features of a molecule produce characteristic and consistent absorption bands in the electromagnetic spectrum from which the structural characteristics of a molecule can be elucidated [33,35].

The presence of linear or branched chains, unsaturated bonds and/or aromatic rings can be identified as can the orientation and location of functional groups within the structure [33].The infrared spectrum of MTZ was determined using a Spectrum 100 FT-IR spectrophotometer (Perkin-Elmer®, Beaconsfield, England). The spectrum was generated over the range 4000-650 cm^{-1} using 4 scans at a resolution of 4 cm^{-1}. The infrared absorption spectrum of MTZ is depicted in Figure 1.2 and the band assignments for the spectrum are summarised in Table 1.2. The principle peaks observed in the spectrum are similar to previously reported data [21,33,36].

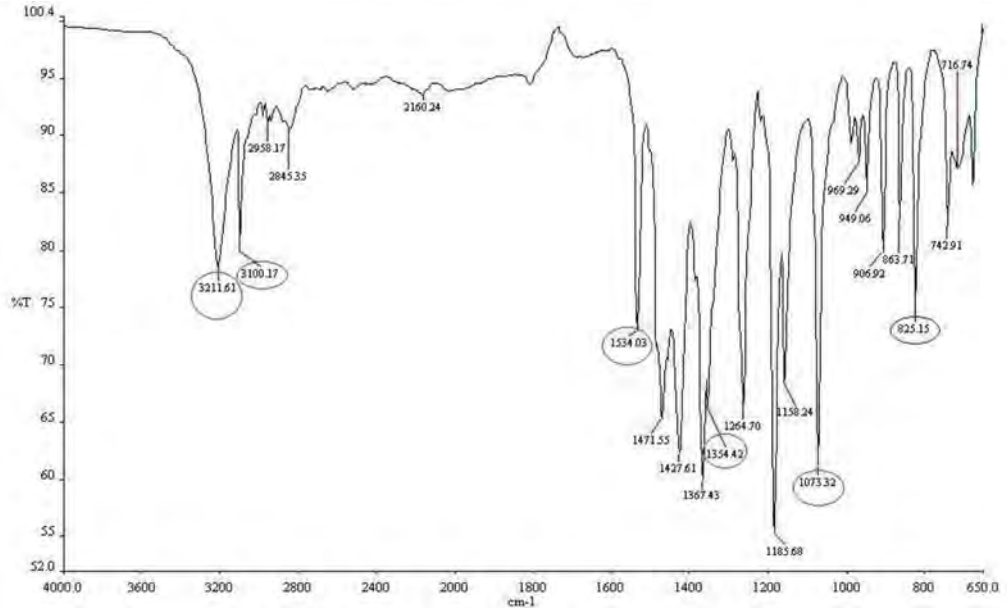

Figure 1.2 Infrared absorption spectrum of MTZ.

Table 1.2 Absorption bands assignments for MTZ

Assignment	Band cm^{-1}
OH stretch	3200-3570
C=CH, C-H stretch	3100-3070
NO2; NO stretch	1320-1355;1540-1560
C-OH, C-O stretch	1050-1085
C-NO2; C-N stretch	920-830

The FT-IR spectrum of MTZ reveals the presence of characteristic bands at frequencies of 3211.61cm^{-1}due to an O-H stretch and at 3100.17 cm^{-1} due to C=CH and C-H stretching. The peaks at 1354.42 cm^{-1} and 1534.03 cm^{-1} correspond to a nitro group vibration [21,37]. Further peaks at 1073.32 cm^{-1} and 825.15 cm^{-1} are due to C-O and C-N stretching, respectively [21,36,38].

1.2.6 Ultraviolet (UV) absorption spectrum

UV absorption spectroscopy is used extensively for pharmaceutical analysis including chromatographic separations and characterisation of the kinetics of reactions, amongst others. The UV absorption spectrum originates from the excitation of electrons and is dependent on the nature of the chemical bonds in a molecule [39,40].

The UV absorption spectrum of MTZ in methanol acidified with 0.1N sulphuric acid revealed a wavelength of maximum absorption (λ_{max}) of 276 nm (Figure 1.3) which is similar to a λ_{max} of 274 nm reported in literature. The literature value may be different due to the type of solvent used [21]. The UV absorption spectrum of MTZ generated using a Lambda 25 UV/VIS Spectrometer (Perkin Elmer®, Beaconsfield, England) at a scan speed of 480 nm

min^{-1} over the wavelength range of 200-700 nm in a solution of 0.04M potassium dihydrogen orthophosphate (KH_2PO_4) buffer of pH 4 and acetonitrile in a ratio of 81:19 v/v revealed a λ_{max} of 319 nm (Figure 1.4) for MTZ.

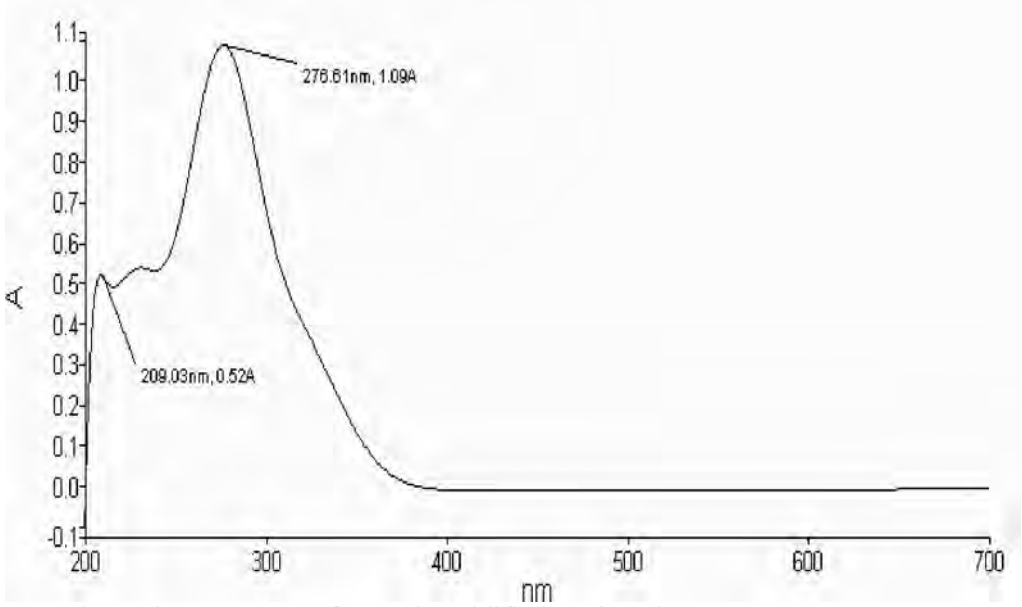

Figure 1.3 UV absorption spectrum of MTZ in acidified methanol

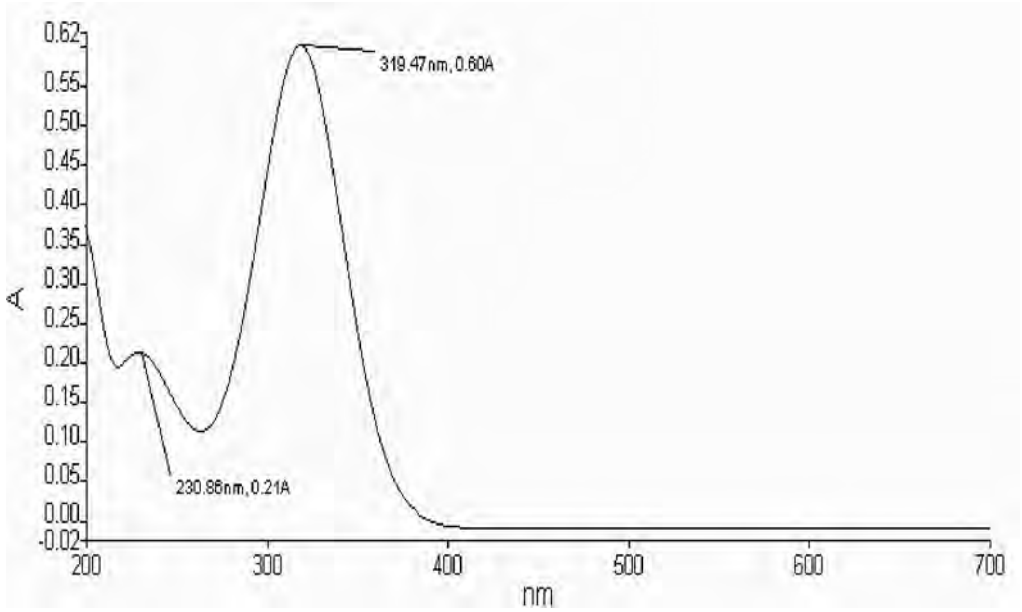

Figure 1.4 UV spectrum of MTZ in 0.04M KH_2PO_4 buffer (pH =4) and acetonitrile in a ratio of 81:19 v/v

1.2.7 Melting Range

The melting range of MTZ is 159°C-163°C [21,41,42]. Differential Scanning Calorimetry (DSC) was used to determine the melting point of MTZ. DSC scanning was performed using

a Model DSC 6 (Perkin Elmer®, Norwalk, USA).The DSC scans were generated between 30-445°C at a heating rate of 10°C/min and a nitrogen flow rate of 20 ml/min using a sealed aluminium pan as a reference. The DSC thermogram depicted in Figure 1.5 reveals a melting endotherm at 163.37°C and a broad endotherm at 252.91°C.

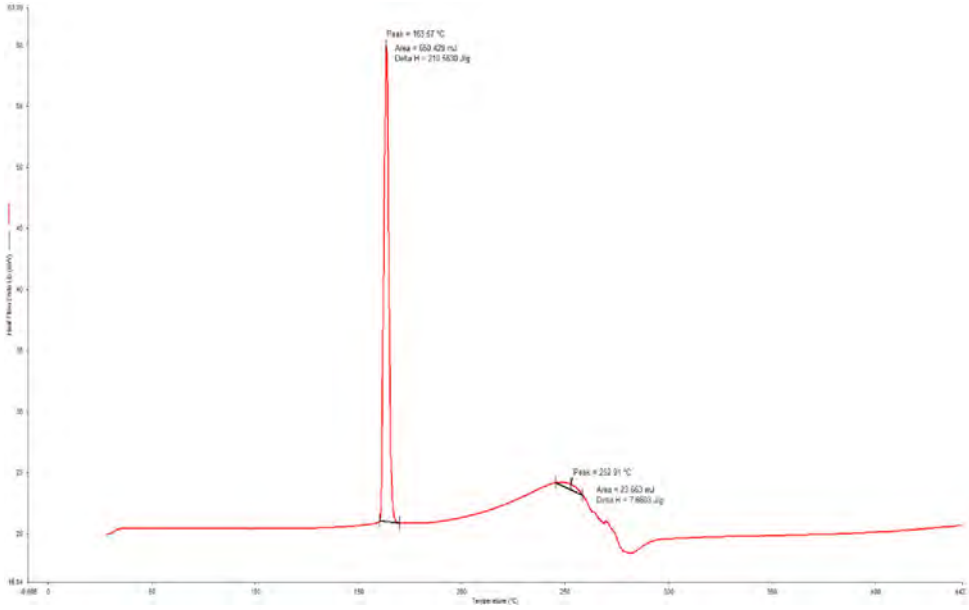

Figure 1.5 DSC thermogram of MTZ

1.3 SYNTHESIS OF MTZ

MTZ has been synthesised from tartaric acid and o-phenylene diamine with the formation of a crucial intermediate, 2-methyl-imidazole [43]. The simplest single stage method of manufacturing this intermediate is to synthesise the compound from glyoxal, aldehyde and ammonia. However due to the scarcity and high cost of glyoxal this approach is not useful for large-scale synthesis of MTZ and ethylenediamine is preferred as a starting material, since it is relatively cheap and readily available [43].The synthesis of MTZ from ethylenediamine starting material is depicted in Figure 1.6.

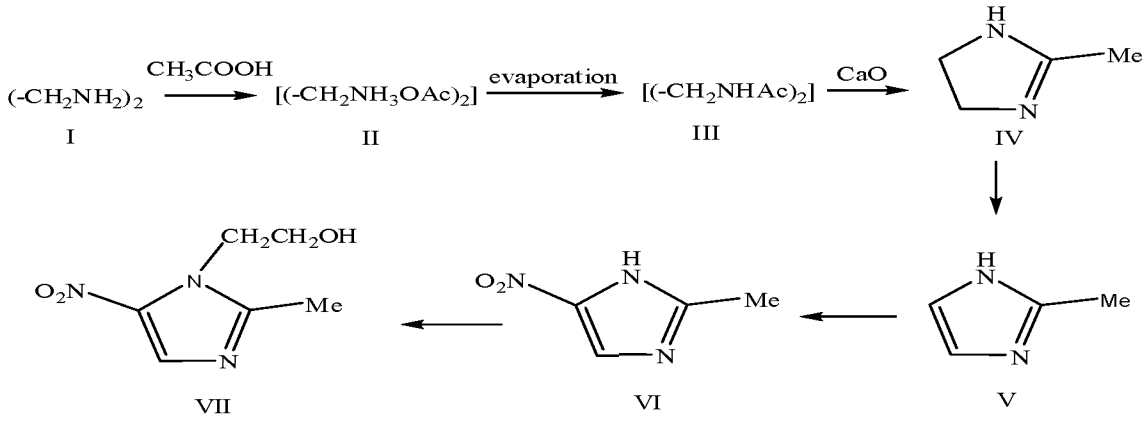

Figure 1.6 Synthesis of MTZ from ethylenediamine, adapted from [43]

An aqueous solution of ethylenediamine (I) and acetic acid (CH_3COOH) is mixed in 1:2 mole ratio at high (70-79%) and low (10-40%) concentration to produce the diacetic salt of ethylenediamine (II). This is converted to N,N'-diacetylethylenediamine (III) following evaporation of water and without isolation and further purification the N,N'-diacetylethylenediamine is treated with quick lime (CaO) to produce compound IV. Compound IV is dehydrogenated rapidly in the presence of raney nickel or non-pyrophoric nickel to form compound V. The nitration of compound V is completed using a mixture of nitric (HNO_3) and sulphuric (H_2SO_4) acid in the presence of sodium sulphate (Na_2SO_4) and sodium hydrogen sulphate ($NaHSO_4$) to produce compound VI. The yield of compound VI is approximately 63-66% and is greater than the yield of 48-52% reported when nitration of compound V is achieved using inorganic nitrate compounds. Hydroxy ethylation of compound VI with ethylene oxide is achieved in a homogenous medium of phosphoric and acetic acid to produce MTZ (VII) [43].

1.4 STABILITY OF MTZ

MTZ is photolabile, therefore adequate protection from light is required during storage and handling of the drug and dosage forms [44,45]. The photochemical decomposition of MTZ progresses according to a first order kinetic process and the reactivity of nitroimidazoles is based on the electrophilic properties of substituents on position N_1 and C_5 of the nitroimidazole ring [46]. MTZ undergoes a typical nitro group photoreaction as depicted in Figure 1.7 [47].

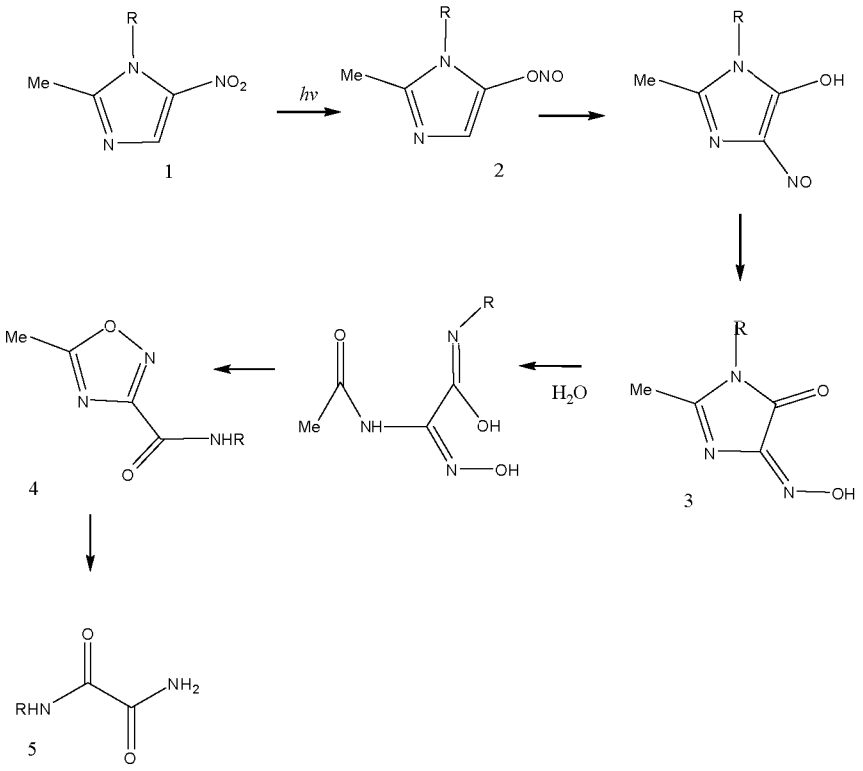

Figure 1.7 Schematic representation of the photodegradation of MTZ [43]

Photodegradation of MTZ commences with a nitro-nitrite rearrangement (1) to produce compound 2 followed by a shift of the NO group to the vicinal position [47]. Hydrolytic ring-opening – closure from the oxime (3) produces 1,2,4-oxadiazol-3-carboxamide (4) that under undergoes photo-accelerated hydrolysis to form an oxaldiamide (5) [47].

The photodecomposition of MTZ is dependent on factors such as solvent type, pH, temperature and the light source [48]. The rate of decomposition in water, methanol, isopropanol and chloroform was 0.21, 0.32, 1.02 and 1.6h^{-1} respectively, which indicates that the rate of decomposition increases with decreasing solvent polarity and that the rate of decomposition increases when using solvents that readily form reactive species. This suggests that radical formation by the solvent is implicated in decomposition reactions [48]. The rate of decomposition of MTZ increased with increasing temperature, pH and intensity of radiation and the presence or absence of oxygen has a limited effect on the rate of photodecomposition of the compound, which suggests that oxidation and/or reduction may not be a consequence of decomposition of MTZ [48]. Negligible degradation of MTZ occurred when MTZ was exposed to 3% v/v H_2O_2 for 6 hours and 30% degrades when exposed to 30% v/v H_2O_2 for 48 hours [49]. The degradation of MTZ in acidic and alkaline

media follows a first order reaction process. Maximum stability is observed at a pH between 4 and 6 [50]. In another study MTZ degraded by approximately 20% when heated to 80°C in 0.1M HCL for 12 hours and formed low molecular weight compounds in the presence of acid [49]. Under alkaline conditions MTZ decomposes to form ammonia and acetic acid and an unknown compound that is pink to violet in colour when mixed with ninhydrin reagent [49,51]. Heating of MTZ at 80°C in 0.1 NaOH for 2 hours resulted in approximately 95% degradation [49].

1.5 CLINICAL PHARMACOLOGY

1.5.1 Mode of action

MTZ is a prodrug that is activated once the compound enters the cell of an organism [52]. The drug enters the cell via passive diffusion and is activated when an electron is transferred to the nitro functional group. This results in the formation of a nitroso free radical [52,53]. The resultant reduction product has cytotoxic effects as it binds covalently to and damages deoxyribose nucleic acid (DNA) [52,54]. The resultant damage to DNA is a consequence of oxidation resulting in breakage of single-and double strands of DNA, loss of the helical structure and impaired template function. This ultimately leads to apoptosis [52,54]. The activation process results in a concentration gradient that facilitates an increase in the uptake of the MTZ by the target organism [52]. In susceptible anaerobic bacteria the redox potential of components of the electron transport chain is sufficiently negative to reduce the nitro group, which results in electron donation from ferredoxin or flavodoxin, dependent on the type of organism [52].

1.5.2 Indications

MTZ is used for the treatment and prophylaxis of anaerobic bacterial infections [16,55]. Bacterial infections treated with MTZ include acute necrotising ulcerative gingivitis, pelvic inflammatory disease and urethritis [16,17,56]. MTZ can also be used to treat infections such as amoebiasis, balantidiasis, giardiasis and trichomoniasis [57].

MTZ is used in combination with other compounds for the treatment of *Helicobacter pylori* in peptic ulcer disease [16,17]. It can be administered topically to treat rosacea and has been used to treat bacterial vaginosis including vaginosis due to *Gardnerella vaginalis*, *Bacteroides* species and *Mycoplasma hominis* [17,58]. MTZ has been used to treat guineaworm (dracunculosis) where it exhibits anti-inflammatory activity and facilitates removal of parasites from infected tissues. MTZ exhibits radio-sensitising effects and has

been used for the treatment of malignant neoplasma and is also indicated for the treatment of Crohn's disease, meningitis and brain abscess [16,17,58].

1.5.3 Antimicrobial action

MTZ is active against anaerobic bacteria including Gram negative anaerobes such as *Bacteroides fragilis*, *Prevotella* species and *Fusobacterium* species [9,16]. Gram positive anaerobes susceptible to MTZ include *Peptococcus niger*, *Peptostreptococcus*, *Clostridium* species and strains of *Eubacterium* [16,59]. MTZ is active against most anaerobic protozoa including *Balantidium coli, Blastocystis hominis, Entamoeba histolytica, Giardia intestinalis* and *Trichomonas vaginalis* [7,16]. MTZ is bactericidal and has variable activity against facultative anaerobes such as *Gardnerella vaginalis* and *Helicobacter pylori* [7].

1.5.4 Resistance

The mechanisms of resistance to MTZ in anaerobic bacteria that have been identified vary depending on the type and species of organism [7]. Resistance takes the form of a decreased uptake of MTZ or through modified efficiency of a reduction reaction in the organism [7,54]. The two mechanisms of resistance may act in combination as is the case when reduced activity of the nitro-reductase enzymes lead to a decreased uptake of MTZ [7]. Distinct resistance conferring genes impart resistance for nitroimidazole compounds have been isolated in different genera of Gram positive and negative anaerobic bacteria including those of the *Bacteroides* species [7]. This type of gene encodes for a modified reductase enzyme that converts nitroimidazole to a non- toxic form [7]. Other mechanisms of resistance in *Bacteroides* species include up-regulation of efflux pumps [54,60]. Furthermore, the modification of DNA repair systems also plays an important role in resistance to MTZ in *Helicobacter pylori*. MTZ resistant strains of *Helicobacter pylori* have been isolated however the use of combination therapy including MTZ is still indicated for treatment of such infections [7,61].

1.5.5 Dosage

To successfully treat rosacea a thin film of a 0.75% w/w MTZ gel is applied to the affected area(s) twice daily [17,52]. A 200 mg oral dose taken three times daily for three days is used for the treatment of necrotizing ulcerative gingivitis in adults whereas 200 mg dosed orally three times daily for two weeks is used to treat periodontitis [17,62,63]. The adult dose for the treatment of guineaworm is 250 mg dosed three times daily for ten days [64]. MTZ is used in combination with a proton pump inhibitor and either clarithromycin or amoxicillin for

the treatment of *Helicobacter pylori* infection and is dosed at 400mg twice daily for seven days [65].

Bacterial vaginosis is treated using a vaginal gel (0.75% w/w) inserted intra-vaginally at bedtime for five days [17,66]. Alternatively MTZ delivered orally can also be administered as a single 2 g dose or as a 5-7 day course of 400 or 500 mg administered twice daily [67]. The adult and paediatric dosage for the treatment of anaerobic infections amoebiasis, giardiasis and urogenital trichomoniasis are summarised in Table 1.3 [16,17]

Table 1.3 Adult and paediatric doses for treatment of anaerobic infection, amoebiasis and giardiasis [16,17]

Type of infection	Adult	Paediatric
Anaerobic infection	Oral:800 mg initially, then 400 mg 8 hourly for 7 days	Oral:7.5 mg/kg 8 hourly
	Rectal:1 g 8 hourly for 3 days, then 1 g 12 hourly	Rectal:5-12 years approximately half the adult rectal dose
	IV:500 mg 8 hourly	IV:7.5 mg/kg 8 hourly
Amoebiasis	Oral:400-800 mg 8 hourly for 5-10 days	Oral:1-3 years, 100-200 mg 3 times daily, for 5-10 days 3-7 years, 100-200 mg 4 times daily, for 5-10 days 7-10 years, 200-400 mg 3 times daily, for 5-10 days Alternatively,35-50 mg/kg/day in divided doses for 5-10 days
Giardiasis	Oral:2 g daily for 3 days or 400 mg 8 hourly for 5 days	Oral:1-3 years, 500 mg/day, for 3 days 3-7 years, 600-800 mg/day, for 3 days 7-10 years, 1 g/day, for 3 days Alternatively,15 mg/kg/day in divided doses
Urogenital trichomoniasis	Oral:2 g as a single dose	Oral: 1-3 years,50 mg 3 times daily, for 7 days
	Alternatively, 200 mg 3 times daily for 7 days, or 400 mg twice daily for 7 days	3-7 years,100-200 mg 4 times daily, for 7 days 7-10 years,100 mg 3 times daily, for 7 days Alternatively, 15 mg/kg/day in divided doses.

1.5.6 Drug Interactions

Concurrent use of MTZ with alcohol results in a disulfiram-like reaction as MTZ inhibits the aldehyde dehydrogenase enzyme resulting in accumulation of acetaldehyde in the body

[32,68,69]. Symptoms of accumulation include sweating, abdominal cramps, nausea and vomiting [17]. MTZ also interacts with disulfiram resulting in confusion and psychotic episodes [17,70]. MTZ interacts with cimetidine and metabolism is reduced and the half-life of MTZ is prolonged [52,71]. Concomitant use of MTZ and lithium results in a rise in lithium concentrations and phenobarbital increases the metabolism of MTZ thereby reducing the half- life due to the induction of enzyme systems [70,72]. MTZ results in an increase in the plasma levels of phenytoin and increases the anticoagulant effects of warfarin necessitating prothrombin time monitoring [52,73,74].

1.5.7 Adverse effects

Common side effects of MTZ include nausea, anorexia, headache and a metallic taste in the mouth [16,75]. Abdominal pain, vomiting and diarrhoea may also occur and symptoms that have been reported include weakness, ataxia, headache, drowsiness, insomnia, hallucinations and changes in mood such as depression or confusion [76,77]. Peripheral neuropathy and epileptiform seizures are associated with high doses and prolonged treatment with MTZ and adverse effects of MTZ are usually dose related [16,70]. Rash, urticaria, pruritus, raised liver enzyme levels, cholestatic hepatitis, jaundice and pancreatitis may occur occasionally [17,78]. Rare side effects include agranulocytosis, leucopenia, pancytopenia, and thrombocytopenia [79]. Thrombophlebitis may occur following intravenous use of MTZ. Vaginal administration of MTZ may result in adverse effects such as vaginal candidiasis, vulvovaginal itching, burning or swelling, increased pelvic pressure, and abnormal vaginal discharge [17,66,80].

1.5.8 Guidelines for use

Blood count monitoring should be undertaken if MTZ is used chronically, in older patients and if the patient has a history of a blood dyscrasia [81]. Alcohol should not be used during therapy and for 48 hours following discontinuation of therapy [17,82]. MTZ tablets should be taken with half a glass of water with or after meals and patients should be advised of the possibility of dark colouration of urine [57,83]. MTZ is suitable for treating both intestinal and extra-intestinal amoebiasis, however higher doses are required to treat invasive amoebiasis [17].

1.5.9 Precautions

MTZ should be used with caution in patients suffering from epilepsy or other CNS disease such as aseptic meningitis or encephalopathy, impaired hepatic function and porphyria

[16,52]. Neurotoxic symptoms such as peripheral neuropathy and transient epileptic type seizures have been associated with long term or intense treatment with MTZ [17,84]. Special precautions should be taken when MTZ is used during pregnancy, lactation and in geriatric patients and the use of MTZ in these patients groups is described in Sections 1.5.9.1-1.5.9.3.

1.5.9.1 Geriatric patients

There is an increased risk of blood dyscrasia when high doses or treatment periods extend for longer than a week [16,17,52]. Dose adjustment may be required due to decreased hepatic function in this group of patients [85].

1.5.9.2 Pregnancy

The use of MTZ during the first trimester of pregnancy should preferably be avoided [86,87]. MTZ readily crosses the placenta however the risk of teratogenicity is low and it is classified as a pregnancy Category B drug [16,88,89]. The risk benefit should be carefully considered when using MTZ during pregnancy [17,64]. Studies have shown that there is no association between treatment with MTZ use during the first or later trimesters of pregnancy and preterm birth, low birth weight or the incidence of congenital anomalies [90,91]. However there have been reports of an association between vaginal treatment during the first and second months of gestation and congenital hydrocephalus hence, MTZ should be used with caution during pregnancy [92].

1.5.9.3 Lactation

MTZ is excreted in breast milk and should only be used during lactation if no other treatment is suitable [70,74,93]. Breast-feeding should be withheld for 24 hours following a single dose of MTZ [16,17,94].

1.6 CLINICAL PHARMACOKINETICS OF MTZ

1.6.1 Absorption

MTZ is almost completely absorbed following oral administration and exhibits good bioavailability of > 90% [8,9]. Following a single dose of 250 mg or 500 mg the peak plasma concentration was approximately 6 µg/ml and 12 µg/ml observed within 1-2 hours of dosing [16]. Accumulation of the drug may occur and as a result concentrations are higher when multiple doses are administered. Absorption may be delayed but not reduced in the presence of food [95,96]. The use of MTZ benzoate suspension administered orally results in hydrolysis of the ester in the gastrointestinal tract to release MTZ, which is then absorbed

[16,97]. Rectal absorption of MTZ is slower and bioavailability of MTZ following rectal administration is between 60 to 80% with peak plasma concentrations approximately half those observed following oral administration of equivalent doses [16,17,98]. Absorption following vaginal administration using pessaries is poor with a resultant bioavailability of between 20 and 25% and a C_{max} of 2 µg/ml following a 500 mg dose [16,99].

1.6.2 Distribution

The apparent volume of distribution of MTZ is 0.6-0.9 l/kg [10]. MTZ is widely distributed in the biological system and has been isolated in tissues and fluid including bile, bone, breast milk, cerebral abscesses, CSF, liver and liver abscesses, saliva, seminal fluid, and vaginal secretions [100,101]. It reaches concentrations in these locations similar to those observed in plasma. MTZ crosses the placenta and enters foetal circulation [86,102]. Approximately < 20% MTZ is bound to plasma proteins following administration [85,103].

1.6.3 Metabolism

Approximately 90% of MTZ is metabolised in the liver to oxidative products, the metabolism of MTZ occurs in the liver due to side-chain oxidation and glucuronide formation [24,64,104,105]. The main metabolites formed include 1-(2-hydroxyethyl)-2-hydroxymethyl-5-nitroimidazole and 2-methyl-5-nitroimidazole-1-acetic acid [16,24,79]. The hydroxy metabolite exhibits antibacterial activity 30-65% that of MTZ, and has been isolated in plasma and urine [9,104]. The acid metabolite has only 5% antibacterial activity and is not detectable in plasma but is excreted in the urine [16,52,105]. A small amount of reduction metabolites, acetamide and *N*-(2-hydroxyethyl) oxamic acid (HOA) has been detected in the urine [16,24].

1.6.4 Elimination

The elimination half-life of MTZ is approximately 8 hours [16,52,106]. It has been reported that the elimination half-life is inversely related to gestational age [105–107]. The elimination half-life for a 28 week gestation infant and 30 weeks gestation infant was found to be 109 and 60 hours, respectively [106]. In renally impaired patients the elimination half-life of MTZ is approximately 10 hours [103]. The metabolites and 10-20% unchanged drug is excreted in the urine [17,96].

1.7 CONCLUSIONS

Helicobacter pylori is a Gram negative urease-producing bacterium that is common in humans [2]. The organism resides in the gastric antrum and metaplasia in the duodenum. It is the primary causative agent in the development of chronic gastritis, gastric and duodenal ulceration, gastric B-cell lymphoma and distal gastric cancer [2].

Gastro-duodenal disease is common in Africa, with a high prevalence in Sub-Saharan Africa, Congo and the coastal regions of West Africa [108]. It is estimated that *Helicobacter pylori* affects up to 50% of the global population [2]. Infection is more frequent and acquired at an early age in developing countries, when compared to European populations [2]. The prevalence rate of infection is approximately 80-95% in developing countries. It is now clear that there is a high incidence of gastro-duodenal ulcers in Africa including, regions that historically exhibited a low prevalence of the disease [2,108].

Helicobacter pylori infects one third of northern European and American adults, whereas Eastern European, South American and Asian populations have been associated with > 50% prevalence of the disease [109]. Consequently the treatment of *Helicobacter pylori* is critical for the rapid resolution of peptic ulcers. Such treatment limits the recurrence of peptic ulcer disease and associated complications such as dyspepsia and gastric cancer [110,111].

Major obstructions to the eradication of *Helicobacter pylori* include antibiotic-resistant bacteria, adverse reactions and poor patient adherence [3]. *Helicobacter pylori* is relatively sensitive to single antimicrobial agent therapy, however clinical eradication is poor as many antibiotics are unstable at gastric pH also, only low concentrations of drug in deep gastric mucosa where the bacterium resides are achieved. The process is further complicated by the short residence time of the antibiotic in the stomach [3]. Therefore prolonging the gastric residence time of drugs is one approach to overcome these challenges [3,5]. Oral site-specific drug delivery systems that increase the durability of therapy at the target site may be more effective for such infections [6].

Gastric-retentive dosage forms are an example of oral site-specific drug delivery systems that may prolong gastric retention time in addition to sustained release of a drug over an extended period [5,6]. This approach may result in an increase in the concentration of MTZ at the target site, reduce the dosing frequency and therefore improved patient adherence. While no new drugs have been developed to treat *Helicobacter pylori,* infections, current therapeutic

approaches include the use of a combination of antibiotics and anti-secretory agents [1]. The standard first line combination therapy consists of a proton pump inhibitor and two antibiotics such as metronidazole and amoxicillin or clarithromycin [1,112].

MTZ is a cost-effective drug due to low cost, has good antimicrobial activity, favourable pharmacokinetic properties and minimal side effect profile [7]. MTZ is the drug of choice for the treatment of *Helicobacter pylori* infection and is a suitable candidate for inclusion in gastric-retentive delivery systems, since it acts in the stomach and is unstable in the intestinal/colonic environment [4–6,23]. The objective of this research was to design a floating gastric-retentive drug delivery system for metronidazole with the intention of producing a drug delivery system that prolongs the gastric residence time of MTZ and ensures sustained release of the compound at the target site. This approach would enhance the local delivery of MTZ, improve treatment outcomes and ultimately patient adherence.

CHAPTER TWO
DEVELOPMENT AND VALIDATION OF A RP-HPLC METHOD FOR THE ANALYSIS OF METRONIDAZOLE

2.1 INTRODUCTION

2.1.1 Overview

Chromatography is a technique used to separate components of a mixture due to the difference in the time taken by each component to move across a stationary phase when carried by a mobile phase [113,114]. The stationary phase may be a solid or a liquid supported on a solid backbone and the mobile phase may be a liquid or gas. The separation is a result of distinct interactions between compounds in the sample and the stationary and mobile phases [79,115]. Chromatography was first used by Tswett in 1903. He was able to separate plant pigments using chalk ($CaCO_3$) packed in glass columns [113,116]. Tswett described the effect of different materials and particle size on the separation [117]. The importance of his work was not realised until the 1930s when Lederer and others described their work on the separation of plant pigments such as carotenoids and xanthophylls [117,118]. This led to the emergence of various chromatographic techniques including paper, thin layer, ion exchange partition, gas-liquid and liquid-liquid chromatography [117,119].

Several analytical techniques have been reported for the analysis of metronidazole alone or in combination with other drugs in a variety of matrices [51]. These techniques include spectrophotometry, thin layer chromatography, supercritical fluid chromatography, electrochemistry, gas chromatography and high-performance liquid chromatography (HPLC) [49,51,120]. Compendial methods for bulk drug analysis include non-aqueous titration, UV spectrophotometry and HPLC for the quantitation of metronidazole in dosage forms [41,49,121]. The objective of this study was to develop, optimise and validate a simple, sensitive, stability-indicating RP-HPLC method for the analysis and quantitation of metronidazole in pharmaceutical dosage forms.

2.1.2 Principles of HPLC

Liquid chromatography separates molecules in a sample with a liquid mobile phase and a solid stationary phase and can be used for analytical or preparative applications [122]. Generally, column chromatography viz., adsorption, partition or ion exchange, thin layer

chromatography and modern liquid chromatography are examples of liquid chromatography [115,123]. Modern liquid chromatographic techniques include High Pressure or High Performance Liquid Chromatography and Ultra-Performance Liquid Chromatography (UPLC) [115].

Modern liquid chromatography has many advantages in terms of accuracy, convenience and speed when compared to traditional liquid chromatography [115]. Modern HPLC instruments separate mixtures using a column, the majority of which are stainless steel tubes packed with small particles of 1-5 μm in diameter that are rigid porous materials [116,124]. The packing material is retained inside the column while the mobile phase is pumped through the column [116]. The column is the part of the instrumentation in which separation occurs [116,125]. The principle of liquid chromatography has remained the same since first described, however, improvements such as the use of automated sample injection, continuous solvent pumping and reusable columns have improved the technique [116]. The detector is a key component of an HPLC system as a means of identifying the components of a mixture [126]. Common detectors used in HPLC include ultraviolet (UV) absorbance, refractive index, fluorescence, conductivity, photodiode array and mass spectrometery detectors [127,128]. HPLC is used for qualitative and quantitative analysis in the pharmaceutical industry. HPLC use in the pharmaceutical industry is governed by guidelines developed by the U.S. Food and Drug Administration (FDA) and other regulatory authorities [127]. HPLC is also used in the food industry, forensics biochemical and phytochemical research [116,129,130].

The main components of a basic HPLC system are depicted in Figure 2.1. A reservoir containing mobile phase is connected to a high pressure pump that forces the mobile phase at a specific flow rate via an injector that introduces the sample into the continuously flowing mobile phase that carries the sample through the stationary phase [113,126,131,132]. The column is the site at which separation occurs due to interactions between packing materials and the physico-chemical properties of the components [116,133]. The detector is used to monitor the effluent as the components of the mixture elute from the column [122,126].

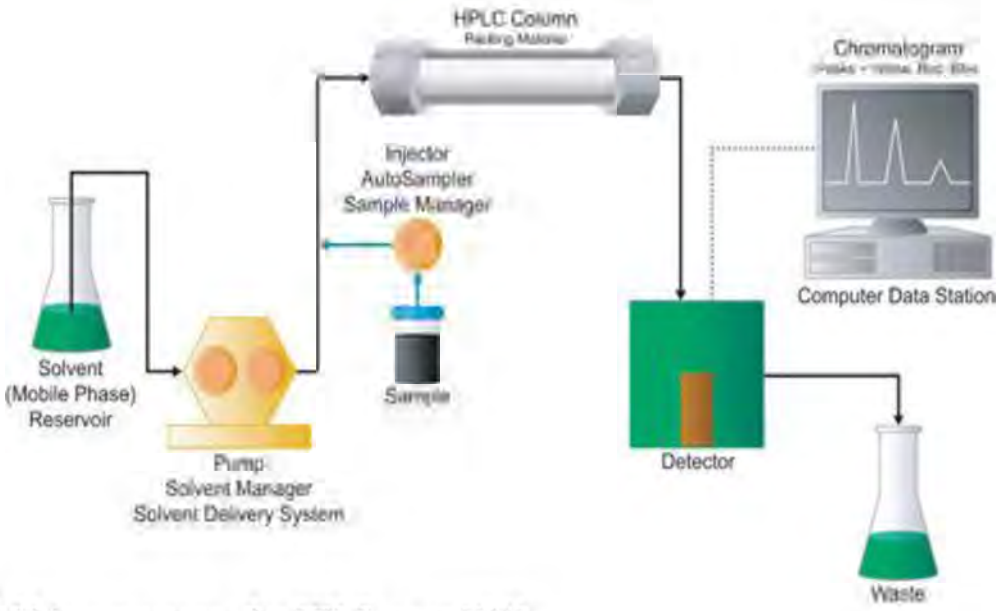

Figure 2.1 Main components of an HPLC system[134]

HPLC techniques can be classified into four types viz., normal phase, reversed-phase, ion-exchange and size exclusion chromatography [135,136]. Each technique is defined by the dominant type of molecular interactions that effect a separation [135].

2.2 CLASSIFICATION OF HPLC

2.2.1 Normal Phase HPLC

Normal phase (NP) HPLC is also known as liquid-solid or adsorption chromatography and is a traditional separation technique that is based on the adsorption of an analyte onto a polar stationary phase [116,137]. The backbone of the stationary phase is usually porous silica or aluminium oxide with hydroxyl groups that are densely packed on the surface making the material polar [138]. This technique uses differences in the strength of the polar interactions of analytes with the stationary phase to separate the components [138]. The stronger the interaction between an analyte and stationary phase the longer that analyte will be retained [130]. Analyte molecules continuously compete with molecules of the mobile phase for adsorption sites on the surface of the stationary phase [138,139].

In NP HPLC the mobile phase is comprised of non-polar solvents such as heptane or hexane with a small addition of polar solvents such as methanol, isopropanol or ethanol [116,140]. Using different concentrations of the polar components ensure control of the retention of an analyte on the column [138]. NP HPLC is primarily used for the analysis of hydrophobic

compounds as the mobile phase uses non polar solvents in which components are likely to be soluble [138,141].

2.2.2 Reversed-phase HPLC (RP-HPLC)

Reversed-phase chromatography is the most commonly used chromatographic technique and approximately 90% of all analysis of low molecular weight compounds is performed using this approach [138]. In RP-HPLC the stationary phase is non-polar and the mobile phase polar [132,142]. This form of chromatography is dependent on dispersive forces and is suitable for the separation of closely related compounds [138]. Commonly used stationary phases are chemically modified porous silica materials of different carbon length chemically bonded to a silica backbone [122,143]. Chemically bonded octadecylsilane and n-alkane with 18 carbon atoms are most often used as a stationary phase. Shorter alkyl chains, cyclohexyl groups and phenyl groups can also be used as stationary phases [143,144]. A mixture of methanol or acetonitrile with water are typical mobile phases and the polarity of the mobile phase may be altered by the addition of different proportions of organic solvent [145–147]. Non-polar compounds are retained longer than polar compounds since the stationary phase is non-polar [146]. Increasing the polarity and strength of the mobile phase in RP-HPLC will result in non-polar compounds retention for prolonged periods [145,148]. It is suggested that the pH of the eluent be maintained in the range 2-8 due to potential hydrolysis or cleavage of the stationary phase that may occur at extreme pH [117].

2.2.3 Ion Exchange HPLC

Ion exchange chromatography is useful for analysis of ionic and biological compounds such as amino acids, proteins and polynucleotides [149]. Separation is achieved when ionic analytes are exchanged with counter-ions attached to the stationary phase [126].

2.2.4 Size exclusion HPLC

Separation in size exclusion chromatography is based on the molecular size of an analyte and large molecules are excluded from pores and move rapidly down the stationary phase, whereas small molecules penetrate into pores and migrate slowly through the system [150,151].

2.3 METHODS FOR THE ANALYSIS OF METRONIDAZOLE

A literature review of HPLC methods for the analyses of MTZ was conducted and a summary of the conditions reported in those methods are listed in Table 2.1.

It is evident that most methods for the analysis of MTZ were used to analyse pharmaceutical dosage forms and plasma [152–157]. A number of methods use RP-HPLC with silica matrix C_8 or C_{18} stationary phases and in some cases a phenyl based column was used. Most methods report a retention time < 10 minutes. The most commonly used organic modifiers were acetonitrile (ACN) and methanol (MeOH) the content of which ranged between 5-25% and 20-50% for ACN and MeOH, respectively [152–156,158–160].

Most methods used a phosphate buffer of pH between 4 and 4.5 in proportions ranging between 20 and 95% v/v. Flow rates of 1 to 1.5 ml/min were used and UV was the preferred method of detection at wavelengths between 254 and 370 nm. The separation of ionic molecules can be accomplished in systems in which the mobile phase is buffered [161]. Since MTZ is a weak base it may be necessary to use buffer systems to achieve an adequate separation, however mobile phases without buffer systems have been used [153,158,161].

Table 2.1 Analytical method for the analysis of MTZ

Sample	Column	Technique	Mobile phase	Flow rate ml/min	λ nm	RT min	Internal standard	Ref.
Raw material	Eurospher®,C_8, 250 mm x4.6 mm,5µm,Knauer®	RP-HPLC	Acetonitrile: water (20:80% v/v)	1.5	318	4.1	-	[162]
Tablets	Octadecyl®,C_8, 250 mm x 4.6 mm, 10µm, Phenomenax®	RP-HPLC	0.05M phosphate buffer (pH=4): methanol: acetonitrile (30:45:25% v/v)	1.0	277	3.28	-	[158]
Tablets and powders	Kromasil®, C_{18}, 250 mm x4.6 mm, 5 µm	RP-HPLC	Methanol:0.1% phosphoric acid (20:80% v/v)	1.0	317	5.04	-	[152]
Tablets	InertsilODS®,C_{18},250 mm x4.6 mm, 5 µm	RP-HPLC	Phosphate buffer(pH=4.5): methanol: acetonitrile (30:50:20% v/v)	1.2	271	2.92	-	[153]
Homogenate of rat stomach	YMC Pack AM12S05 ODS®, 150 mm x 6 mm, 5µm, YMC®	RP-HPLC	Methanol: water: perchloric acid (60%): sodium perchlorate monohydrate (50:950:1:5,v/v/v/w)	1.0	370	9.7	-	[154]
Blood	MOS-Hypersil®,C_8, 100 mm x 4.6 mm, 5µm	RP-HPLC	MeOH:10mM KH_2PO_4 (30:70%v/v)	0.2	318	2.45	-	[159]
Human Plasma	Eclipse XDB-phenyl®, 250 mm x 4.6 mm, 5µm, Agilent®	RP-HPLC	0.05M sodium acetate: acetonitrile: glacial acetic acid (75:25:1% v/v/v), (pH=4)	1.0	320	4.06	Carbamazepine	[163]
Human Plasma	Symmetry shield®, C_{18}, 150 mm x 4.5 mm, 5µm, Waters®	RP-HPLC	0.05M sodium acetate (pH=4): acetonitrile (85:15% v/v)	1.0	320	3.7	Tinidazole	[155]
Human Plasma	µBondapak® phenyl,300 mm × 3.9 mm,10 µm,Waters®	RP-HPLC	0.1M potassium dihydrogen phosphate (pH=4.5): acetonitrile (95:5%v/v)	1.5	324	4.9	Ranitidine	[160]
Human Plasma	Varian® C_{18},150mm x 4.6 mm,5µm, Microssorb®	HPLC/MS/MS	Acetonitrile:10mM ammonium acetate (20:80 %v/v)	1.0	-	3	Zidovudine	[156]
Pessary	µ-Bondapak C_{18},300 mm x 3.9 mm,10 µm, Waters®	RP-HPLC	Methanol: water (40:60% v/v)	1.0	254	5	Sulfamethoxazole	[164]

2.4 EXPERIMENTAL

2.4.1 Chemicals and reagents

MTZ USP reference and ornidazole (ODZ) analytical standards were purchased from Sigma Aldrich (St Louis, Missouri, USA). HPLC grade acetonitrile (ACN) 200 far UV Romil-SpSTM Super Purity Solvent (Romil® Ltd, Waterbeach, Cambridge) was purchased from Microsep (Port Elizabeth, South Africa). Potassium dihydrogen orthophosphate was purchased from Merck Laboratories (Wadeville, South Africa). HPLC grade water was used for all analysis and was purified using a Milli-RO® water purification system (Millipore®, Bedford, MA, USA), consisting of two ion-exchange cartridges, an Organex-Q® and a Super-C carbon cartridge. The water was filtered through a 0.22 µm Millipak® stack filter (Millipore®, Bedford, MA, USA). Flagyl® 200 mg and 400 mg tablets were purchased from a local pharmacy. Sodium hydroxide pellets were purchased from Merck Chemicals Ltd (Modderfontein, Gauteng, South Africa).

2.4.2 Instrumentation

The HPLC system used consisted of a Waters® Alliance Model 2695 separation module equipped with a solvent delivery module, auto sampler, online degasser and a Model 2489 UV/Vis Detector (Milford, MA, USA). Data acquisition, processing and reporting were achieved using Waters® Empower 2 software (Milford, MA, USA). The stationary phase was a Macherey-Nagel Nucleosil® C8 column 250 mm x 4 mm i.d x 10 µm (Separations®, Randburg, South Africa). A Crison GLP21 pH-meter (Crison Instruments, Johannesburg, South Africa) was used to measure pH. A Colora® ultra-thermostat water bath (Colora®, Lorch, Germany) was used to maintain temperature for stress testing studies and an Atlas SUNTEST® CPS+ was used for photolytic degradation studies. HVLP Durapore® membrane filters 0.45µm (Millipore®, Bedford, MA, USA) were used to filter sample solutions. A Branson® B12 sonicator (Branson®, Shelton, USA) was used to sonicate sample solutions.

2.4.3 Preparation of stock solutions

Stock solutions were prepared on a daily basis and were protected from light using aluminium foil. Approximately 20 mg of MTZ was accurately weighed using a Mettler® Model AE 163 analytical balance (Mettler®, Zurich, Switzerland) and was quantitatively transferred to a 100 ml A-grade volumetric flask and made up to volume using a mixture of buffer: ACN in a 81:19 % v/v ratio to produce a stock solution of 200 µg/ml. The stock

solution was sonicated for 15 minutes and then serially diluted in 10 ml A-grade volumetric flasks to produce 0.4, 5, 20, 40, 80, 100, 120 µg/ml MTZ solutions.

A stock solution of the internal standard was prepared by accurately weighing out 60 mg ODZ using a Mettler® Model AE 163 analytical balance (Mettler® Inc., Zurich, Switzerland) and quantitatively transferring to 100 ml A-grade volumetric flask and made up to volume using a mixture of buffer: ACN in a 81:19 % v/v ratio to produce a stock solution of 600 µg/ml. A 1 ml aliquot of the stock solution was transferred to a 10 ml A-grade volumetric flask and made up to volume to produce a solution of 60 µg/ml.

2.4.4 Preparation of mobile phase

The mobile phase was comprised of a 0.04M KH_2PO_4 buffer of pH 4 and ACN in an 81:19 % v/v ratio that was prepared daily. The KH_2PO_4 buffer (0.04M) was prepared by accurately weighing 5.44 g of KH_2PO_4 and quantitatively transferring to a 1000 ml A-grade volumetric flask and making it up to volume with HPLC grade water. The buffer pH was adjusted to 4.0 using a 0.1M sodium hydroxide solution. The KH_2PO_4 buffer was filtered through a 0.45 µm Millipore® membrane HVLP filter (Millipore®, Bedford, MA, USA) and degassed under vacuum using an Eyela® Aspirator A-2S vacuum pump (Rikakikai® Co. Ltd, Tokyo, Japan) prior to use. The KH_2PO_4 buffer was transferred to a 1000 ml Schott® Duran bottle (Schott® Duran GmbH, Wertheim, Germany). A litre (1000 ml) of ACN was measured using a 1000ml A-grade measuring cylinder and transferred in a Schott® Duran bottle. The KH_2PO_4 buffer and the ACN were mixed online in an 81:19 % v/v ratio.

2.5 SYSTEM SUITABILITY TESTING

System suitability testing was used to establish whether an instrument was functioning as required for an application [165]. Prior to developing an HPLC method, performance tests on the column were undertaken to ensure the performance characteristics of that column. The tests that were undertaken included assessing the number of theoretical plates, peak asymmetry factor, resolution factor and capacity factor for the separation [115,144].

2.5.1 Column efficiency

The number of theoretical plates (N) is a quantitative measure of column efficiency and can be calculated using either Equation 2.1 or 2.2 [121,133].

$$N = 16\left(\frac{t_R}{W}\right)^2 \qquad \textit{Equation 2.1}$$

$$N = 5.54\left(\frac{t_R}{W_{h/2}}\right)^2 \qquad \textit{Equation 2.2}$$

Where,

N = Number of theoretical plates in the column (measure of column efficiency)
t_R= Retention time of the analyte
W = Peak width at its base
$W_{h/2}$ = Peak width at half of peak height

The quality of a separation and an increase in resolution result as the value of N increases [144,166]. The value for N is a function of the analyte of interest and is usually constant for a peak developed using a fixed set of conditions [121,166,167]. The value for N is dependent on operating conditions such as flow rate, temperature, quality and uniformity of column packing, internal diameter and column length [121,144]. The value for N can be increased by using densely packed columns, increasing the length of the column, using reduced flow rates and/or low viscosity mobile phases [144,145]. According to FDA Guidelines the theoretical plate number depends on elution time and in general should be > 2000 for a column to be considered suitable for a separation [167].

A column performance test was undertaken by injecting a test solution of phenol, naphthalene and anthracene. The chromatographic conditions were specified in the HPLC column certificate of analysis provided by the supplier. The mobile phase consisted of ACN: water in an 80:20% v/v ratio and the flow rate 1 ml/min while the eluent was monitored at 254 nm. The plate count for this column was calculated using Equation 2.1 and the plate number was approximately 5000 suggesting the column was suitable for use.

2.5.2 Peak Asymmetry Factor

The peak asymmetry factor (A_s), also known as peak tailing factor (PTF) is used to assess band shape and peak symmetry [121,167]. It is important that symmetrical peaks are developed to ensure accurate quantitation of peak area, retention time, peak width and height [168]. The A_s is calculated using 5% peak height using Equation 2.3. An acceptable tailing factor ranges between 0.9 and 1.0 [133]. Peak tailing usually occurs due to adsorption or strong interactions between the analyte and stationary phase [133,166]. Peak fronting may result from column overload, chemical reactions or isomerisation during chromatographic process [133,168]. The A_s for MTZ was 0.92 and was considered appropriate for this separation.

$$A_S = \frac{W_{0.05}}{2f}$$ ***Equation 2.3***

Where,

A_S = Peak asymmetry factor
$W_{0.05}$ = Peak width at 5% height
f = Distance from peak maximum to leading edge of the peak, measured at a point 5% of the peak height from the baseline

2.5.3 Resolution factor

The resolution factor (R_s) is used to assess the degree of separation between components of a mixture and is widely used as a system suitability criterion for chromatographic analysis [121,169]. A resolution factor > 2 is an indication that adequate separation has been achieved between peaks [121,133,167]. Values < 1.5 indicate poor resolution between peaks and the R_s can be calculated using Equation 2.4 [121,170]. The resolution between MTZ and the internal standard ODZ was 8.11 and this was deemed acceptable for this separation.

$$R_S = \frac{t_{R2} - t_{R1}}{0.5(W1+W2)}$$ ***Equation 2.4***

Where,

Rs = Resolution factor
t_{R1} = Retention time of first eluting peak
t_{R2} = Retention time of second eluting peak
W_1 = Width of first eluting peak at base
W_2 = Width of second eluting peak at base

2.5.4 Capacity factor

The capacity factor (k^1) is a measure of the degree of retention of an analyte and is also known as the retention factor and is a measure of the migration rate of an analyte [133,167]. The capacity factor measures the extent of retention of an analyte compared to that of an un-retained compound such as uracil [121]. The capacity factor can be calculated using Equation 2.5 [121].

$$k^1 = \frac{V1 - V0}{V0}$$ ***Equation 2.5***

Where,

k^1 = Capacity factor
V_0 = Void volume
V_1 = Retention volume of the peak of analyte

A value of zero for k^1 indicates that a component is un-retained and will elute with the solvent front whereas a value of one suggests that the component is slightly retained while a value of 20 indicates strong retention and interaction with the stationary phase [133,167]. Capacity factors > 20 are undesirable as run times are long and separations exhibit poor sensitivity and peak broadening [133,166]. The capacity factor for MTZ was 3.1 when compared to uracil and therefore the column was deemed appropriate for use.

2.6 METHOD DEVELOPMENT

2.6.1 Column selection

The stationary phase is located and held in place by frits at each end of the column [139,171]. HPLC columns are made of stainless steel so as to withstand pressures up to 50 MPa [139]. During method development one of the major challenges was to select an appropriate column with desirable selectivity, suitable repeatability and stability for an application [172]. Columns vary in terms of packing material, length, internal diameter and particle size [113,122]. The quality of a separation depends on the physicochemical properties of the analyte and competition between components of a mixture and interaction with the stationary phase [126]. Many particle types used in HPLC columns are fully porous and have a large surface area, allowing for better retention and load capability [172]. Fully porous packing materials are less prone to produce broad peaks with increased injection volumes [172]. The column used in this study was comprised of totally porous spherical silica particles. The pore size should be large enough to allow accessibility of the analytes to the surfaces of the packing material as porosity provides access to surfaces for retention [138,172,173]. Generally a pore size of 10nm (100Å) is suitable for molecules in the molecular weight range 100 to 500 [172]. Since MTZ has a molecular weight of 171.16, a column of 100 Å pore size was used. The length of a column may determine the degree of separation of components in a mixture, however longer run times are inevitable [113]. A suitable column length that results in an adequate separation, does not result in band broadening, long run times and high back pressures, should be selected [113,131,138,171]. The choice of the internal diameter of a column depends on the requirement of analysis. For example, large internal diameters of >10 cm are used for preparative HPLC whereas diameters of 2.1 to 4 mm and normal bore of 4-5 mm are suitable for applications that require quantitation [174,175]. The most common stationary phase used for HPLC is silica based due to inherent mechanical stability that ensures good flow characteristics under high pressure [138,145]. The high strength rigid silica particles exhibit low back pressures and

have long lifetimes. Silica based packing materials are compatible with water and all organic solvents permitting the use of a variety of solvent combinations during gradient elution without changing particle characteristics [166,176]. However silica is soluble at pH 8 precluding the use of mobile phases of extreme pH with silica based columns [166,177]. Following a review of the literature and assessment of the factors affecting column performance, a MachereyNagel Nucleosil®, C8 100Å, 250 mm x 4 mm i.d x 10 µm column was selected for the development of a RP-HPLC method for MTZ.

2.6.2 Choice of internal standard (IS)

The use internal standards improves the accuracy and precision of a separation where sample volume is difficult to control and reduces analytical error [166,177,178]. Examples of error that can be minimised when adding an internal standard include solvent evaporation, injection volume variability, sample loss during preparation, extractions and dilution [178,179]. The IS is added to the sample as a fixed concentration [166]. Peak height and area are used for quantitation and the addition of an internal standard compensates for errors in calculation [180]. The concentration of an analyte is determined by calculating the peak height or area ratio of the analyte of interest to internal standard. The selection of an internal standard is therefore critical for quantitation using these parameters [166,180].

Considerations when selecting an internal standard include structural similarity with the compound of interest, a capacity factor, solubility and detection response that is similar to the compound of interest, complete resolution without interference, absence from the original sample and stability and compatibility with sample components, stationary phase and/or the mobile phase [166,177].

Where a similar compound is not available the selection of internal standard should be made on basis of similar solubility in mobile phase and detector response [166]. Different compounds that could be monitored at a wavelength of 317 nm using a mobile phase comprised of 0.04M KH_2PO_4 buffer (pH=4) and ACN in a 81:19 % v/v ratio at a flow rate of 1ml/min were assessed as potential internal standards and the retention times (RT) are summarised in Table 2.2.

Table 2.2 Evaluation of various internal standards

Internal standard	RT min	Comments
Carbamazepine	5.4	Peaks overlapped retention times too close
Caffeine	2.0	Rapid elution too close to void
Sulfathiazole	2.2	Rapid elution too close to void
Ketoconazole	-	No peak observed after 30 minutes
Propranolol	3.4	Peak elutes too quick, resolution less than 2
Ornidazole	9.1	Retention time, resolution and peak shape were ideal

2.6.3 Mobile phase flow rate selection

The identification of mobile phase composition during method development in order to ensure successful separation is critical and involves evaluation of binary mixtures of organic and aqueous phases [181,182]. The aqueous phase is water or buffer and organic solvents include MeOH, ACN, ethanol, hexane and/or tetrahydrofuran [124,182]. Organic solvents are selected for use based on the type of HPLC separation, properties of the analyte, stationary phase and type of detector [182]. Additives such as salts, acids and bases may be included in the mobile phase at low concentration to produce a specific pH and/or ionic strength [126,182]. Solvents used in RP-HPLC must be of good quality and high purity, free from dissolved gasses, dust particles and other contaminants [183]. Vacuum degassing and filtration of the mobile phase was performed in order to ensure that the mobile phase was free of impurities. The UV cut-off of the organic solvents used in the mobile phase is important as the mobile phase should not absorb UV light at the wavelength used for analysis as this may compromise detection of the analyte/s of interest [184,185]. ACN is commonly used in RP HPLC as it exhibits medium polarity and has a low UV cut-off of 200 nm [182]. Water exhibits a high polarity however the eluting strength of ACN is stronger and therefore an increase in ACN content in the mobile phase reduces the retention time of analytes [182]. The retention time and peak shape of analytes may change with a change in composition of the mobile phase [184]. Acetonitrile was used as it is less viscous than methanol resulting in fewer fluctuations in pressure and a low column back pressure [186]. The pH of the mobile phase is important for analytes that are not neutral and as MTZ is a weak base that exhibits maximum stability at pH between 4 and 6 and therefore pH was considered as a variable during method development [50,184]. Flow rate should be kept constant throughout all experiments to assure precise retention times and good peak shape [166]. Flow rate changes may result in sudden changes in retention times, shift in detector baseline and large variations

in back pressure and occur as a consequence of check valve faults, column blockage and changes of mobile phase viscosity [166].

2.6.4 Method of detection

Detection for RP HPLC methods is primarily based on the physicochemical properties of the analyte of interest [182,187]. The detector transforms a physicochemical property of the analyte to an electrical signal that is represented as a chromatogram [182]. The peaks in a chromatogram are used for the purposes of quantitation and the strength of the signal depends on the concentration of dissolved analyte [182,187]. The majority of HPLC detectors exhibit a linear dependence of peak area or peak height to sample concentration provided the solutions are dilute [166,182]. Non-linear responses may be encountered due to sample overload [166]. A variety of detectors including UV, photodiode array (PDA), fluorescence, refractive index, conductivity and mass spectrometry detectors have been used for HPLC analysis [133]. Approximately 85% of pharmaceutical applications use detectors such as UV or PDA detectors [133]. UV detection is the most common detection approach reported for MTZ. Most manuscripts reported wavelengths between 318 and 370 nm for the detection of MTZ. Prior to method development, a solution of MTZ in 0.04M KH_2PO_4 buffer (pH=4) and ACN in a 81:19 % v/v ratio was scanned over a wavelength range of 200-700nm at a scan speed of 480 nm min^{-1} using a Lambda 25 UV/VIS Spectrometer (Perkin Elmer ® Ltd, Beaconsfield, England). The wavelength of maximum absorption was 317 nm and this wavelength was selected for method development and further studies.

2.7 METHOD OPTIMISATION

2.7.1 Response Surface Methodology (RSM)

The traditional experimental approach of changing one variable at a time involves a large number of experiments to achieve a definite end point, is time consuming, and does not permit evaluation of multiple factors simultaneously [188,189]. The use of an experimental design approach is advantageous as multiple variables that may affect a response can be investigated simultaneously, also permitting evaluation of the degree of effect and possible interactive effects between variables [188,190,191]. When developing a formulation or manufacturing process it is vital to have a full understanding of the effects of modification of multiple factors over the entire experimental domain in order to establish the dependence of a response on input variables in order to predict the response over the entire design space [190,191]. Predication can, if possible, be undertaken if a mathematical model is developed

for each response monitored. The primary aim of Response Surface Methodology (RSM) is to develop such models [190].

RSM is a collection of statistical and mathematical techniques that are suitable for developing, improving and optimising processes [192]. The objective of RSM is to use a sequence of designed experiments to identify an optimal response through use of linear and second-degree polynomial expressions [191,193]. RSM identifies the relationship between a response of interest, say Y and a number of control or input variables denoted X_1, X_2.....X_k and can be approximated, for example, by a low degree polynomial model as denoted by Equation 2.6 [193] .

$$Y = f'(X)\,\beta + \epsilon \qquad \textit{Equation 2.6}$$

Where,

$X = X_1, X_2 \ldots\ldots X_k$,
$f'(X)$ = Vector function of elements that consist of powers and cross-products of powers of X_1, X_2,.....X_k up to adegree denoted by $d \geq 1$
β = a vector of unknown constant coefficients referred to as parameters
ϵ = random experimental error assumed to have a zero mean

The two important models commonly used in RSM are a first degree model (Equation 2.7) and a second degree model (Equation 2.8) [192,193].

First degree model (d=1):

$$Y = \beta_0 + \sum_{i=1}^{k} \beta i\, Xi + \epsilon \qquad \textit{Equation 2.7}$$

Second degree model (d=2):

$$Y = \beta_0 + \sum_{i=1}^{k} \beta i\, Xi + \sum_{i=1}^{k} \sum_{j=i+1}^{k} \beta ij\, Xi\, Xj + \sum_{i=1}^{k} \beta ii\, Xi^2 + \epsilon \qquad \textit{Equation 2.8}$$

Where,

B_0, βi, βii and βij = constant coefficients
Xi and Xj = coded independent factors
ϵ = random experimental error assumed to have a zero mean.

The relationship between Y and X_1, X_2.....X_k can be used to predict response values for a specific set of control or input variables. The significance of a single factor can be determined and the optimum conditions for X_1, X_2.....X_k over a specific region of interest can be identified [192,193]. RSM models and designs are therefore used to identify an optimum response through the use of linear and second degree polynomial models [193,194]. It is

important to select an appropriate design for a response surface model, since the quality of prediction depends on the initial design of the matrix [193,195].

A 2^k factorial design is a commonly used first order design where k represents the number of control variables to be investigated [190,196]. Factorial designs are used for processes in which several input factors or variables are to be investigated [197]. Each of the factors of interest are evaluated at two levels, coded as -1 and +1, corresponding to low and high values. The number of experimental runs, n is equal to 2^k provided that a design point is not replicated [192]. The 2^k design can be used at the beginning of a response surface study where screening experiments are to be performed to identify key process variables [190,192,198].

The Plackett-Burman design is a two-level fractional design that has k = N-1 variables in N runs and can only be used to fit linear models [188]. It requires less experimental runs if the value of k is large. The design can only be used when N, the total number of design points is a multiple of four, thus it can only be used when k is 3, 7, 11,15 etc., [192]. This type of design can only be used to fit linear models making it useful for screening studies where only the main effects are of interest [188,199].

The most common second order design used are 3^k designs and include Central Composite (CCD) and Box-Behnken (BBD) designs [192].The design of 3^k is made up of all combinations of levels and control variables (k) tested at three levels [192,198] coded as -1, 0, +1 for the low, centre and high values [192,198]. If a large number of input variables are investigated there is a corresponding increase in the number of experimental runs required for a 3^k design [192,200].

The CCD design is the most popular design that consists of three sets of experimental runs, the first of which is a complete or fraction of a 2^k factorial design with factor levels coded as -1 and +1 and this is the factorial section [192,201] . The second set include centre points, in which the value for each factor is the median point used for the factorial portion [201,202]. The centre point is replicated in order to improve the precision of the experiment. The third set are the axial points consisting of 2k points for which two points are selected on the axis of each control variable at a distance alpha (α) from the design centre [201]. The first part of the design provides the initial phase to assess the importance of factors for a particular experiment. The additional experiments or the axial and centre point replicates that provide

information may lead to identification of the optimum operating conditions at which the control variables are set [188,190,192].

The BBD evaluates three levels viz., -1, 0 and +1for each variable and is made up of a subset of factorial combinations of the 3^k design [192]. These designs are a class of rotatable or nearly rotatable second order designs. An important characteristic of a BBD is that it is a spherical design and an alternative to the CCD [193]. The number of experiments (N) is defined as N= 2k (k-1), where k is the number of input factors and 2k is the number of centre points [192]. An advantage of the BBD is that it does not contain combinations for which all factors are simultaneously at their highest or lowest levels [190]. Hence these designs are useful when the need to conduct experiments under extreme conditions is unnecessary or for which unsatisfactory results may be generated [188].

RSM is used extensively in industry, particularly in circumstances where several input variables influence performance measures or quality characteristics of a product or process. RSM has been used to develop and optimise a large number of HPLC methods [203–211]. RSM involves performing several experiments in a desired region, fitting the data to a response model and then optimising in order to produce the best conditions to achieve desired responses [212,213].

2.7.2 Experimental design

A Central Composite Design (CCD) approach was selected for the optimisation of process variables for the method developed for the purposes of analysing MTZ. Based on preliminary studies, four independent factors viz., buffer composition, buffer molarity, pH and flow rate were evaluated. The retention times of MTZ and ODZ, resolution and peak tailing of MTZ were the dependent variables or responses monitored. A rotatable design was used as these exhibit reduced prediction error and improved estimation of curvature effects of the models [543]. The independent variables were coded as -1 and +1 where the low and high levels were -1 and +1 respectively. Axial points were located at ($\pm\alpha$, 0, 0), (0, 0, $\pm\alpha$) and (0, $\pm\alpha$, 0) where α is the distance of the axial point from the centre point thereby making the design rotatable. The α value used in this study was 2.0. A rotatable design was used as these designs have reduced prediction error and much improved estimation of curvature effects in the model. The levels of each factor, both coded and actual used in the CCD are listed in Table 2.3 and the experiments performed are listed in Table 2.4. The experiments were performed in a randomised manner and in replicate (n=3) so as to reduce the chance of

uncontrolled factors introducing bias. Design Expert® Version 8.0.2 (Stat-Ease Inc., Minneapolis, USA) statistical software was used for data analysis and to predict values of input variables that would produce the desired responses and produce an adequate separation.

Fisher's statistical test for Analysis of Variance (ANOVA) for the response surface model was used to determine the significance of each factor. The effectiveness of the model was evaluated by computing the F-ratio, Coefficient of Variation (C.V), adequate precision, R squared (R^2), adjusted R^2 and predicted R^2.

Table 2.3 Experimental factors and levels used for the CCD

Factor			**Level**		
Input variable	[-2]	[-1]	[0]	[+1]	[+2]
Buffer composition(%) = X_1	40	50	60	70	80
Buffer molarity (M) = X_2	0.02	0.03	0.04	0.05	0.06
pH = X_3	3	4	5	6	7
Flow rate(ml/min) = X_4	0.7	0.8	0.9	1.0	1.1
Response			**Constraints**		
MTZ retention time (min) = Y_1			$Y_1 = 4.0$		
ODZ retention time (min) = Y_2			$Y_2 = 8.0$		
Resolution factor = Y_3			$Y_3 = 4.0$		
Peak tailing of MTZ= Y_4			Y_4=0.95-1.1		

Table 2.4 CCD experiments with coded and actual values

			Coded values				Actual values			
Experimental run	**Standard run**	**Type**	**pH**	**Buffer Composition %**	**Molarity M**	**Flow rate ml/min**	**pH**	**Buffer Composition %**	**Molarity M**	**Flow rate ml/min**
1	28	Centre	0	0	0	0	5	60	0.04	0.9
2	3	Factorial	-1	1	-1	-1	4	70	0.03	0.8
3	15	Factorial	-1	1	1	1	4	70	0.05	1.0
4	2	Factorial	1	-1	-1	-1	6	50	0.03	0.8
5	8	Factorial	1	1	1	-1	6	70	0.05	0.8
6	23	Axial	0	0	0	-2	5	60	0.04	0.7
7	27	Centre	0	0	0	0	5	60	0.04	0.9
8	25	Centre	0	0	0	0	5	60	0.04	0.9
9	7	Factorial	-1	1	1	-1	4	70	0.05	0.8
10	20	Axial	0	0	0	0	5	80	0.04	0.9
11	22	Axial	0	2	2	0	5	60	0.06	0.9
12	11	Factorial	-1	-1	-1	1	4	70	0.03	1.0
13	18	Axial	2	0	0	0	7	60	0.04	0.9
14	5	Factorial	-1	1	1	-1	4	50	0.05	0.8
15	4	Factorial	1	-1	-1	-1	6	70	0.03	0.8
16	24	Axial	0	0	0	2	5	60	0.04	1.1
17	14	Factorial	1	1	1	1	6	50	0.05	1.0
18	29	Centre	0	0	0	0	5	60	0.04	0.9
19	13	Factorial	-1	-1	1	1	4	50	0.05	1.0
20	30	Centre	0	0	0	0	5	60	0.04	0.9
21	19	Axial	0	-2	0	0	5	40	0.04	0.9
22	16	Factorial	1	1	1	1	6	70	0.05	1.0
23	26	Centre	0	0	0	0	5	60	0.04	0.9
24	6	Factorial	1	-1	1	1	6	50	0.05	0.8
25	1	Factorial	-1	-1	-1	-1	4	50	0.03	0.8
26	21	Axial	0	0	-2	-2	5	60	0.02	0.9
27	9	Factorial	-1	-1	-1	-1	4	50	0.03	1.0
28	17	Axial	-2	0	0	0	3	60	0.04	0.9
29	10	Factorial	1	-1	-1	-1	6	50	0.03	1.0
30	12	Factorial	1	1	-1	-1	6	70	0.03	1.0

2.7.3 Experimental results

Thirty experiments were performed using a CCD approach. A summary of experiments and the responses observed are summarised in Table 2.5. The responses were evaluated using Design Expert® software and the data was fitted to different quadratic models. The capability of each model to describe the relationship between input variables and the response observed was established and ANOVA was used to identify statistically important parameters. The evaluation of model adequacy and ANOVA for the retention time of MTZ, resolution and peak tailing of MTZ only will be discussed in detail vide infra. ANOVA for the retention time of ODZ is not discussed as ODZ was used as an internal standard. The relationships established were used to predict a set of input variables that would yield a desired response for the analytical system to be used.

Table 2.5 CCD experiments and responses observed

Experimental run	Standard run number	pH	Buffer Composition % v/v	Molarity M	Flow rate ml/min	RT of MTZ min	RT of ODZ min	Resolution	Peak tailing of MTZ
1	28	5	60	0.04	0.9	3.42	4.42	2.00	1.04
2	3	4	70	0.03	0.8	3.98	6.39	5.46	1.02
3	15	4	70	0.05	1.0	3.06	5.13	6.04	1.02
4	2	6	50	0.03	0.8	4.16	6.70	4.51	1.71
5	8	6	70	0.05	0.8	6.41	6.91	2.00	1.61
6	23	5	60	0.04	0.7	4.96	5.67	2.01	1.07
7	27	5	60	0.04	0.9	3.70	4.43	2.02	1.04
8	25	5	60	0.04	0.9	3.71	4.40	1.99	1.03
9	7	4	70	0.05	0.8	3.80	6.43	6.19	1.02
10	20	5	80	0.04	0.9	5.71	8.32	4.00	1.10
11	22	5	60	0.06	0.9	3.27	4.39	2.50	1.08
12	11	4	70	0.03	1.0	3.18	5.12	5.42	1.01
13	18	7	60	0.04	0.9	4.33	8.81	4.07	1.95
14	5	4	50	0.05	0.8	3.32	4.18	2.86	1.01
15	4	6	70	0.03	0.8	6.36	7.64	1.90	1.80
16	24	5	60	0.04	1.1	3.11	3.60	1.80	1.07
17	14	6	50	0.05	1.0	3.35	4.48	2.87	1.63
18	29	5	60	0.04	0.9	3.71	4.43	1.99	1.01
19	13	4	50	0.05	1.0	2.66	3.36	2.82	1.03
20	30	5	60	0.04	0.9	3.71	4.43	1.99	1.04
21	19	5	40	0.04	0.9	3.29	3.90	2.02	1.06
22	16	6	70	0.05	1.0	5.15	5.60	1.97	1.65
23	26	5	60	0.04	0.9	3.71	4.43	1.99	1.01
24	6	6	50	0.05	0.8	4.18	5.64	3.03	1.63
25	1	4	50	0.03	0.8	3.68	4.17	1.89	1.00
26	21	5	60	0.02	0.9	4.25	4.80	2.00	1.05
27	9	4	50	0.03	1.0	2.82	3.35	2.29	1.00
28	17	3	60	0.04	0.9	2.96	4.37	5.10	0.90
29	10	6	50	0.03	1.0	3.33	5.38	5.41	1.72
30	12	6	70	0.03	1.0	5.10	6.10	1.89	1.95

2.7.3.1 Evaluation of Model Adequacy for Retention Time of MTZ

The results of model adequacy determination are summarised in Table 2.6. The parameters evaluated to establish model adequacy were the model F-value, coefficient of variation, adequate precision, and R^2 coefficients.

Table 2.6 Summary of model adequacy parameters and values for retention time of MTZ

Parameter	Value	Parameter	Value
Standard deviation	0.27	R^2	0.9597
Mean	3.95	Adjusted R^2	0.9221
% Coefficient of variation	6.92	Predicted R^2	0.7786
F-Value	25.51	Adequate precision	19.449

2.7.3.1.1 Model F-Value

The model F-value is used to test for adequacy and statistical significance of a model and to determine whether data are best fitted to a model [214,215]. The F- value is the ratio of the mean square and the error mean square of a model [216]. A large F-value indicates that variation of the dependent variable is explained by the dependent relationship modelled by the statistical procedure [216]. A large F-value indicates a strong association between the predictors and response and a model F-value of 25.51 implies that the model is significant and there is only 0.01% chance that an F-value this large could occur due to noise [217]. This implies that the model is able to describe the data accurately and there is only 0.01% chance of the model being inaccurate.

2.7.3.1.2 Coefficient of Variation

The coefficient of variation is the ratio of the standard deviation to the mean and a small value for the coefficient variation indicates that the data is uniform or consistent and a value of $< 10\%$ is desirable [218,219]. The CV is a dispersion measurement that compares experimental results involving different variables and measures the reproducibility of a model [219,220]. The value of 6.92 generated was within the limit and implies that the model is able to generate reproducible results.

2.7.3.1.3 Adequate Precision

Adequate precision is a comparison of the range of predicted values at the design points to the average prediction error and a ratio > 4 indicates that there is adequate discrimination in the model [221]. The value of 19.449 for these data is above the limit implying that the model can be used to navigate the design space.

2.7.3.1.4 R^2, Predicted R^2 and Adjusted R^2 Values

The R^2 value is a measure of reduction in variability of dependent variables obtained by using regression variables in the model [192]. The value for R^2 coefficients should fall between 0 and 1 and the closer they are to 1 the better the correlation between observed and predicted responses [222]. Adding a variable to the model will always increase the R^2 value however this is not always the case for the adjusted R^2 value [223]. A difference of < 0.2 between the predicted and adjusted R^2 values indicates the model is suitable [224,225]. The R^2 and adjusted R^2 were >0.9 meaning that there is good correlation between observed and predicted responses. The predicted R^2 of 0.7786 is in reasonable agreement with the adjusted R^2 of 0.9221 and the difference between the two is < 0.2 implying that that the model is suitable.

2.7.3.1.5 Residual analysis for retention time of MTZ

Residual analysis is said to determine model adequacy and is the difference between the observed and predicted responses [226]. Residuals can be examined by use of normal probability plots of residuals and a plot of residuals versus predicted responses [227]. In order for the model to be considered adequate the residuals should be normally distributed around the predicted responses [226,228]. On a normal probability plot of residuals the points should fall on a straight line whereas for the plot of residuals versus predicted responses the points should be scattered or random and not follow a specific pattern [228,229]. The normal plot of residuals and the plot of residuals vs predicted responses are depicted in Figures 2.2 and 2.3 and suggest that this criterion has been met and thus the model is deemed adequate for retention time.

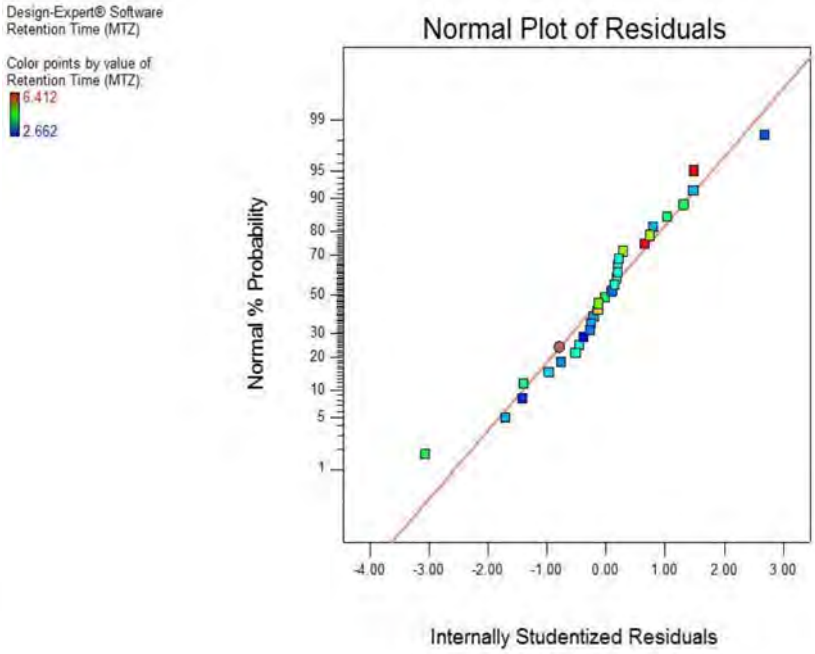

Figure 2.2 Normal probability plot of residuals for retention time of MTZ

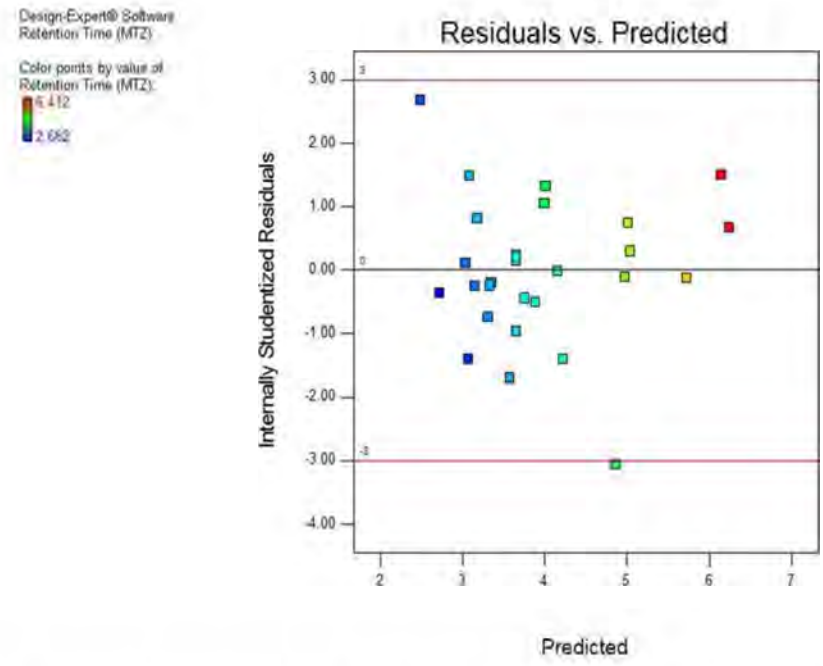

Figure 2.3 Plot of residuals versus predicted responses for retention time of MTZ

2.7.3.1.6 Box-Cox Plot for Power Transformations for the retention time of MTZ

Researchers are constantly faced with data that deviates from normality and as normality is important when parametric tests such as ANOVA and linear models are used, evaluation of

normality is vital [230]. Normality of distribution of data leads to tests that are mathematically traceable and simple to perform [188]. One method of evaluating the normality of data sets is to establish if transformation of data is required and Box-Cox transformation plots is one commonly used in research [231]. Box-Cox plots are used to assess when transformation is required in order to normalise data and improve the applicability of an applied statistical test [230]. In this case, inspection of the Box-Cox plot suggests that transformation of the power λ = -2.27 should be undertaken as depicted in Figure 2.4. However the ratio of maximum to minimum response was 2.40872. A ratio > 10 indicates that transformation is required [232]. Ratios of < 3 indicate power transformations have very little effect on the experimental responses and therefore transformation was not performed for these data [233].

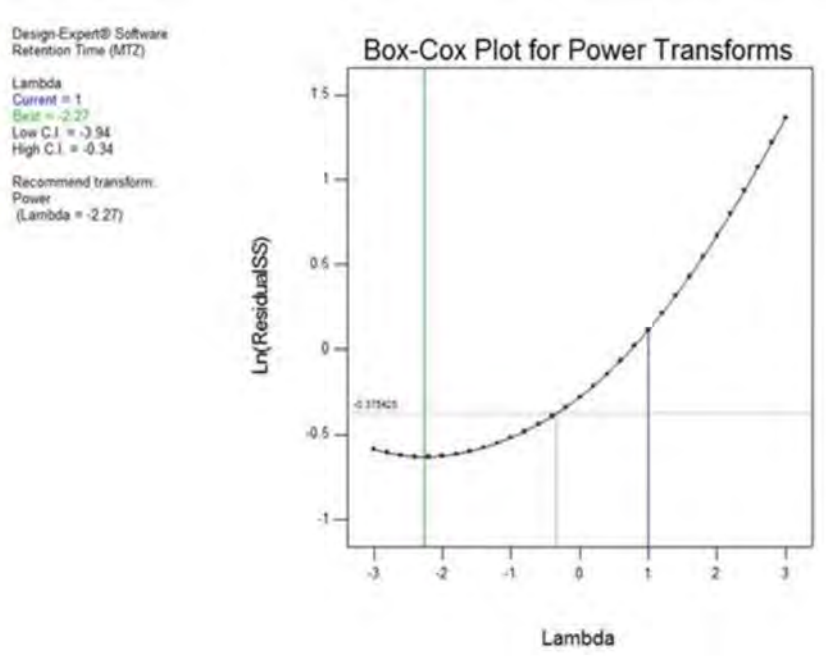

Figure 2.4 Box-Cox plot for power transformation of retention time for MTZ

2.7.3.2 ANOVA for Retention Time of MTZ

2.7.3.2.1 Significant Factors Affecting the Retention Time of MTZ

The results of ANOVA following conduct of the CCD of the significant factors affecting the retention time of MTZ are summarised in Table 2.7. Values of P > F < 0.0500 indicate that the model terms are significant [234].

Table 2.7 ANOVA for response surface quadratic model analysis of variance table (partial sum of squares-type III) for retention time of MTZ

Source	Sum of squares	Df	Mean square	F value	P-value Prob > F
Model	26.66	14	1.90	25.51	< 0.0001
X_1	8.59	1	8.59	115.12	< 0.0001
X_2	0.29	1	0.29	3.88	0.0678
X_3	8.48	1	8.48	113.65	< 0.0001
X_4	5.00	1	5.00	66.92	< 0.0001
X_1X_2	0.246	1	0.246	0.066	0.8006
X_1X_3	2.60	1	2.60	34.89	< 0.0001
X_1X_4	0.049	1	0.049	0.65	0.4327
X_2X_3	0.060	1	0.060	0.81	0.3835
X_2X_4	0.239	1	0.239	0.064	0.8033
X_3X_4	0.083	1	0.083	1.11	0.3097
X_1^2	1.31	1	1.31	17.61	0.0008
X_2^2	0.032	1	0.032	0.43	0.5210
X_3^2	0.121	1	0.121	0.440	0.9263
X_4^2	0.29	1	0.29	3.83	0.0694
Residuals	1.12	15	0.075		
Pure error	0.070	5	0.014		
Cor total	27.78	29			

Values in red indicate significant independent variables

The relationship between independent variables and retention time of MTZ is described mathematically using Equation 2.9.

$$Y_1 = 3.66 + 0.60X_1 - 0.11X_2 + 0.59X_3 - 0.46X_4 + 0.018X_1X_2 + 0.40X_1X_3 - 0.055X_1X_4 + 0.061X_2X_3 + 0.017X_2X_4 - 0.072X_3X_4 + 0.22X_1^2 + 0.034X_2^2 + 0.244X_3^2 + 0.10X_4^2$$

Equation 2.9

The data reveal that the linear contributions of X_1 (buffer composition), X_3 (pH) and X_1X_3 in addition to quadratic interactions of model term X_1^2 had a significant positive effect on retention time for MTZ, as indicated by the positive sign of the model terms in the equation and values of Prob > F < 0.05. The linear contribution of X_4 (flow rate) had a significant antagonistic effect on the retention time of MTZ. Buffer composition and pH had a significant effect on the retention time of MTZ. Increasing the amount of buffer in the mobile phase and pH resulted in a longer retention time for MTZ. An increase in buffer content resulted in an increase in the polarity of the mobile phase and hence MTZ is retained longer on the non-polar stationary phase [145–147]. MTZ is a weak base with a pKa of 2.62, therefore using a mobile phase of pH 2 units higher than the pKa results in less opportunity for protonation of MTZ that remains in the neutral form and is therefore retained on the non-polar stationary phase for longer [138,235]. Decreasing the flow rate results in longer

retention times as indicated by shorter retention times of MTZ when faster mobile phase flow rates were used.

2.7.3.2.2 Response Surface Model Plots for Retention Time of MTZ

The relationship between significant factors and retention time of MTZ can be illustrated using contour plots (Figures 2.5 and 2.6) and 3D response surface plots (Figures 2.7 and 2.8). Increasing mobile phase pH while keeping buffer composition constant resulted in a significant increase in the retention time of MTZ as observed in Figure 2.5 and the retention time of MTZ seems to increase with an increase in buffer content when a mobile phase of constant pH is used.

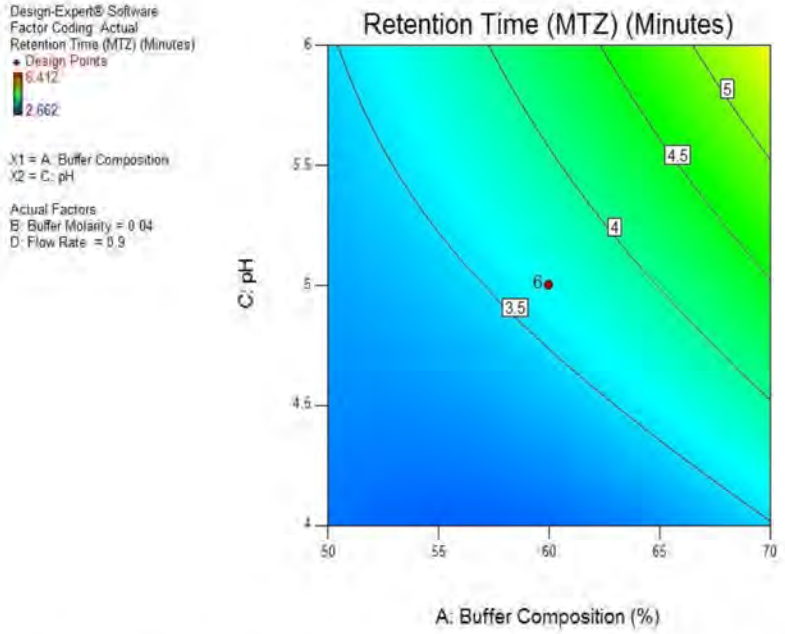

Figure 2.5 Contour plot depicting the impact of changes in pH and buffer content on retention time of MTZ.

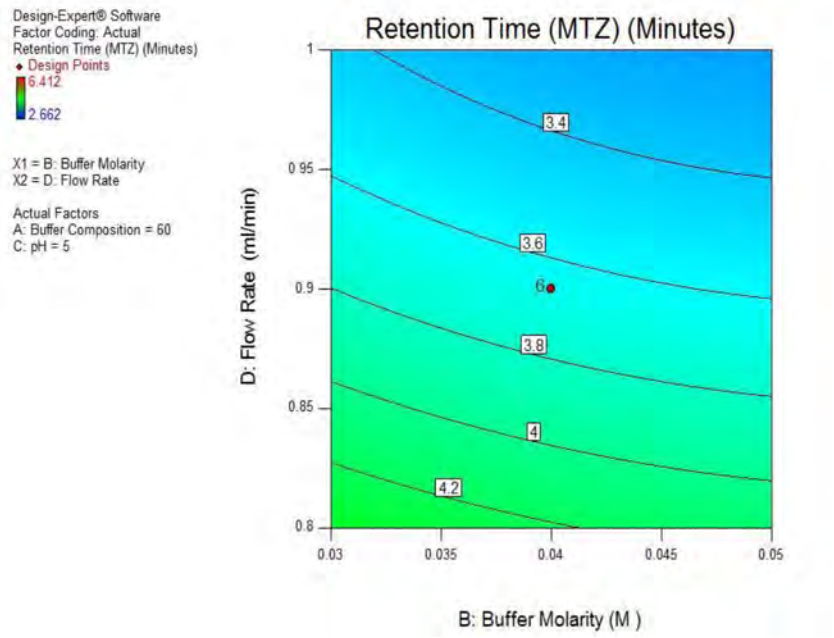

Figure 2.6 Contour plot depicting the impact of flow rate and buffer molarity on retention time of MTZ.

An increase in flow rate with a buffer of constant molarity results in a decrease in the retention time of MTZ whereas an increase in molarity at a constant flow rate has very little or no effect on the retention time of MTZ. This is evident from the almost straight lines observed in the contour plot depicted in Figure 2.6 and value of $P > F > 0.0500$. Figures 2.7 and 2.8 depict 3D response surface plots for retention time of MTZ which illustrate the relationship between retention time and input variable. An increase in pH and a decrease in flow rate results in an increase of retention time of MTZ (Figure 2.7). The 3D plot depicted in Figure 2.8 reveals that an increase in buffer content lengthens the retention time of MTZ however buffer molarity has little or no effect on the retention time of MTZ.

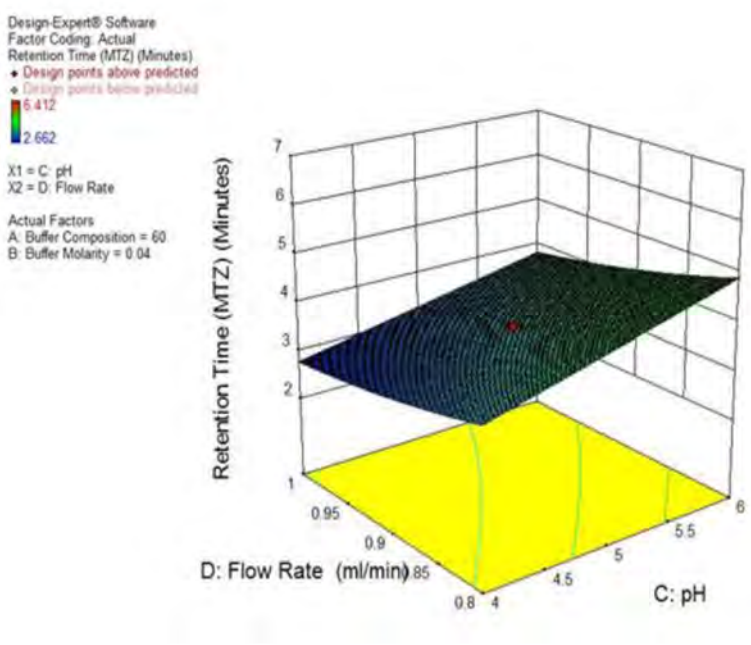

Figure 2.7 3D response surface plot depicting the impact of pH and flow rate on retention time of MTZ

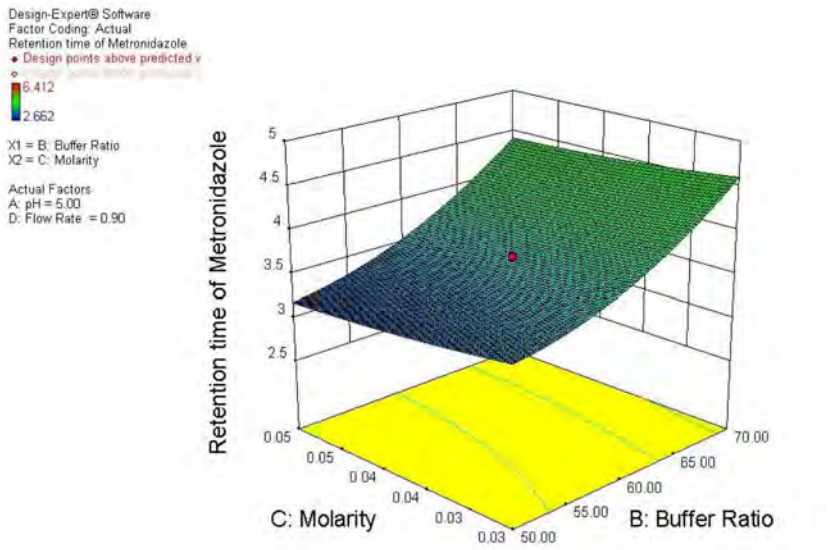

Figure 2.8 3D response surface plot depicting the impact of buffer molarity and composition on retention time of MTZ.

2.7.3.3 Evaluation of Model Adequacy for Resolution

The results of resolution determinations are summarised in Table 2.8. The Model F-value of 14.75 implies the model is significant and that there is only 0.01% chance that an F-value this large could occur due to noise. The predicted R^2 value of 0.6099 is not close to the adjusted R^2 value of 0.8691 and therefore the difference is > 0.2. This may indicate a large block

effect for the prediction of this response when using this model. All other parameters considered for determining the adequacy of the model revealed that the quadratic model that was selected was appropriate to navigate the design space for this separation.

Table 2.8 Summary of model parameters and values used to evaluate adequacy of the model for resolution

Parameter	Value	Parameter	Value
Standard deviation	0.53	R-Squared	0.9323
Mean	3.07	Adjusted R-Squared	0.8691
% Coefficient of variation	7.36	Predicted R-Squared	0.6099
F-Value	14.75	Adequate precision	12.656

2.7.3.3.1 Residual analysis for the resolution

The normal plot of residuals and the plot of residuals vs predicted responses for resolution are depicted in Figures 2.9 and 2.10. The points on the normal plot of residuals follow a straight line, whereas points on the residuals vs predicted responses are scattered. It can thus be concluded that the model is adequate.

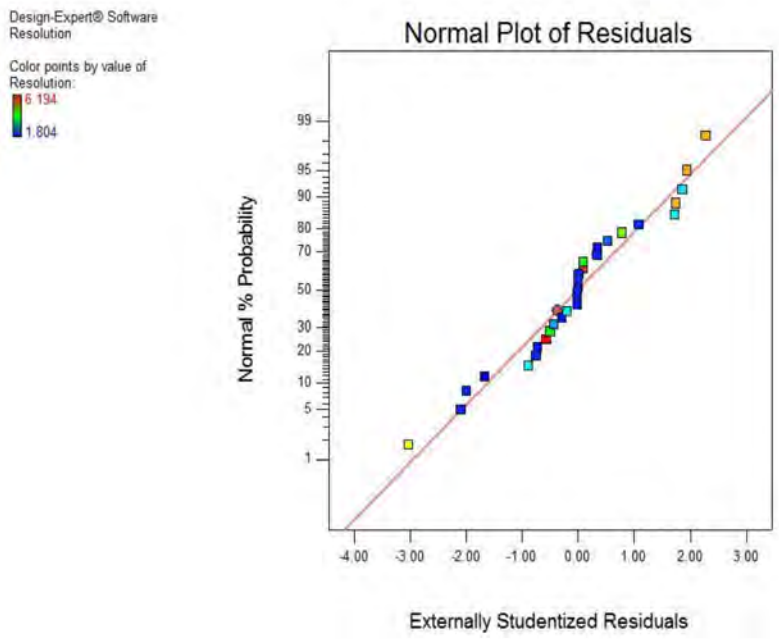

Figure 2.9 Normal plot of residuals for resolution

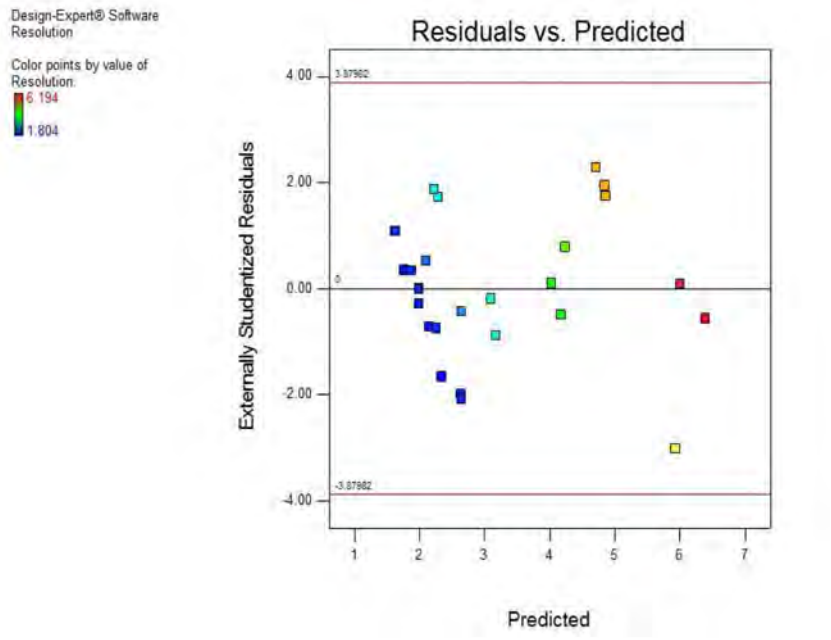

Figure 2.10 Plot of residuals vs predicted responses for resolution

2.7.3.3.2 Box-Cox Plot for Power Transformations for the resolution

The Box-Cox plot for resolution is depicted in Figure 2.11 and evaluation of the plot reveals that there is no need for transformation since $\lambda=1$ and that the data set shows normality.

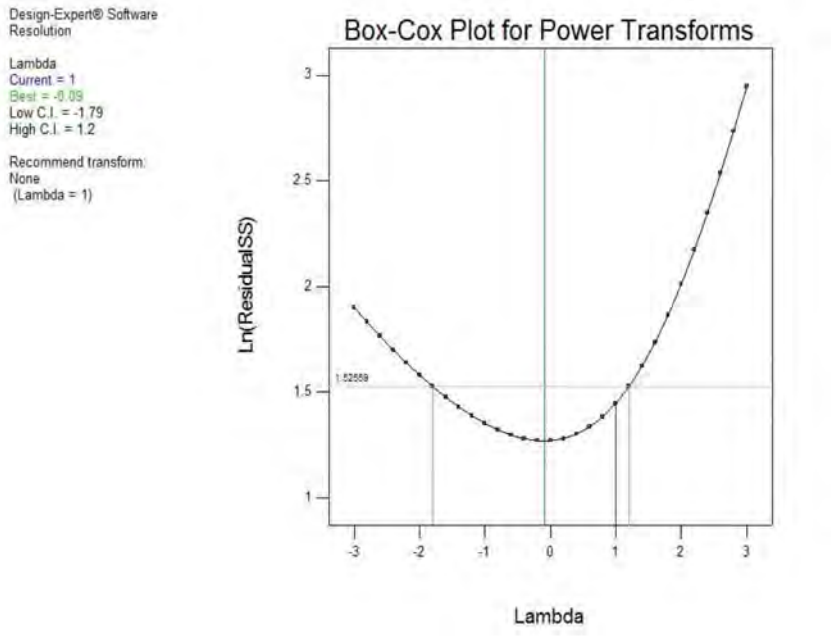

Figure 2.11 Box-Cox plot for the resolution

2.7.3.4 ANOVA for Resolution

2.7.3.4.1 Significant Factors Affecting the Resolution

ANOVA results for establishing factors that significantly affect resolution between MTZ and ODZ are listed in Table 2.9. Model terms with a p-value < 0.05 are considered significant. The relationship between independent variables and resolution is mathematically described by Equation 2.10.

$$Y_3 = 1.99 + 0.38X_1 + 0.114X_2 - 0.48X_3 + 0.021X_4 + 0.26X_1X_2 - 1.33X_1X_3 - 0.080X_1X_4 - 0.42X_2X_3 - 0.107X_2X_4 + 0.036X_3X_4 + 0.35X_1^2 + 0.16X_2^2 + 0.75X_3^2 + 0.077X_4$$

Equation 2.10

Table 2.9 ANOVA for response surface quadratic model analysis of variance table (partial sum of squares-type III) for the resolution

Source	Sum of squares	Df	Mean square	F value	P-value Prob > F
Model	58.54	14	4.18	14.75	< 0.0001
X_1	3.53	1	3.53	12.44	0.0030
X_2	0.023	1	0.023	0.022	0.9955
X_3	5.44	1	5.44	19.18	0.0005
X_4	0.010	1	0.010	0.037	0.8509
X_1X_2	1.04	1	1.04	3.68	0.0743
X_1X_3	28.29	1	28.29	99.80	< 0.0001
X_1X_4	0.10	1	0.10	0.36	0.5559
X_2X_3	2.77	1	2.77	9.78	0.0069
X_2X_4	0.16	1	0.16	0.58	0.4600
X_3X_4	0.020	1	0.020	0.072	0.7923
X_1^2	3.43	1	3.43	12.11	0.0034
X_2^2	0.74	1	0.74	2.62	0.1267
X_3^2	15.32	1	15.32	54.05	< 0.0001
X_4^2	0.16	1	0.16	0.58	0.4582
Residuals	4.25	15	0.28		
Pure error	0.035	5	0.026		
Cor total	62.79	29			

Values in red indicate significant independent variables

The data reveal that buffer composition (X_1) and quadratic factors X_1^2 and X_3^2 had a significant and positive effect on peak resolution whereas variables pH (X_3), and linear X_1X_3 and X_2X_3 had a significant and antagonistic effect on resolution. The data reveal that an increase in buffer content leads to a better resolution. This is expected, since water is more polar than ACN therefore increasing the buffer (aqueous) content in the mobile phase will result in non-polar analytes such as MTZ and ODZ to be attracted to the non-polar stationary phase and be retained longer. MTZ and ODZ exhibited longer retention times with increased

buffer content leading to adequate resolution between the compounds Equation 2.10 reveals that buffer composition has a synergistic effect and pH has an antagonistic effect on the resolution. This means that an increase in buffer composition and a decrease in pH result in an increase in resolution.

2.7.3.4.2 Response Surface Model Plots for Resolution

Figure 2.12 depicts a 2D contour plot and Figure 2.13 a 3D response surface plot that describe the impact of buffer content and pH on the resolution between MTZ and ODZ. From Equation 2.10 the negative value of the coefficient for factor X_3 (pH) suggests that resolution significantly improved with a decrease in buffer pH. The contour plot suggests that at high pH values > 5.5 and low buffer content i.e. 50-60% v/v there is a slight improvement in peak resolution. However at lower pH values between 4 and 5 and high buffer content i.e. >60% v/v there is a significant increase in the resolution factor to values >4 that may be due to the use of pH values >5 as the retention time of ODZ was not drastically affected by pH changes, unlike the retention time for MTZ. Therefore ODZ did not move to the same extent as MTZ resulting in poor resolution between the peaks. It was also observed that in some of the experimental runs performed using a buffer of pH 6 that ODZ produced a double peak while in others runs it did not. This inconsistency may be due to the fact that ODZ is hydrolysed above pH 5.5 to 6 to form an epoxide via intramolecular nucleophilic attack following opening of the epoxide to produce a diol [236]. It has also been reported that during HPLC analysis of ODZ using pH > 5.5 to 6, a double peak of ODZ was observed [237]. The 3D response surface plot (Figure 2.13) revealed that at high buffer content and low pH (pH <5) peak resolution is optimised. At high pH values and low buffer content the resolution factor does not increase significantly since the retention time of ODZ does not change significantly above pH 5 while that of MTZ is significantly increased resulting in poor separation of the two peaks.

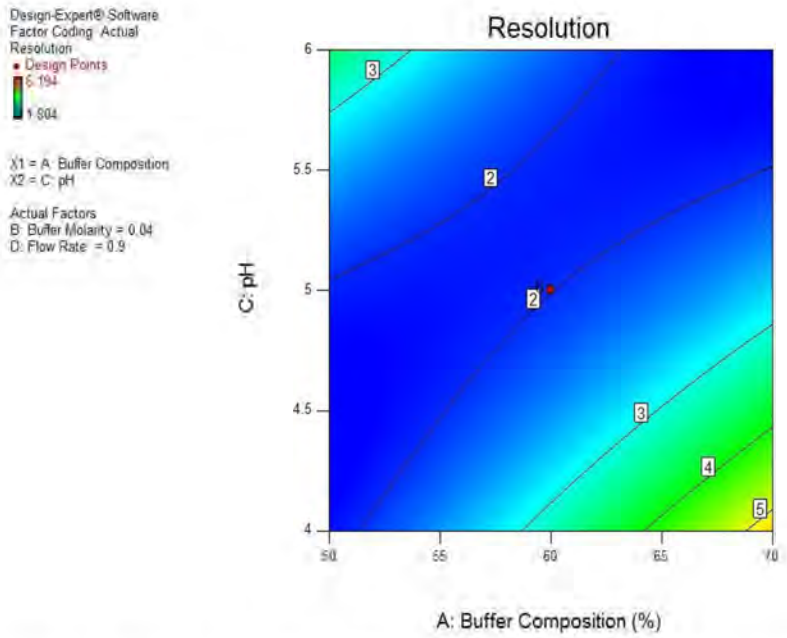

Figure 2.12 Contour plot depicting the impact effect of changes in pH and buffer content on peak resolution

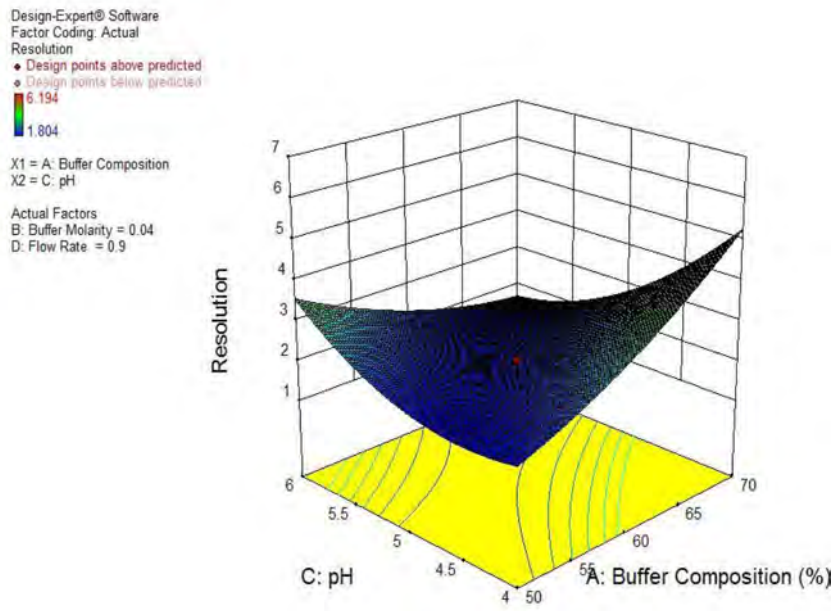

Figure 2.13 3D response surface plot depicting the impact of pH and buffer content on peak resolution

2.7.3.5 Evaluation of Model Adequacy for peak tailing of MTZ

The values for the factors assessed to determine the model adequacy for peak tailing are summarised in Table 2.10. The % for coefficient of variation was < 10%, adequate precision > 4 and the difference between the predicted and adjusted R^2 was < 0.2. The model F-value

of 11.49 indicates that there is only a 0.01% chance that an F-value this large could occur due to noise. All parameters considered for determining adequacy of the model revealed that the quadratic model that was selected was appropriate to navigate the design space for this separation.

Table 2.10 Summary of model adequacy parameters and values for peak tailing of MTZ

Parameter	Value	Parameter	Value
Standard deviation	0.14	R-Squared	0.9147
Mean	1.24	Adjusted R-Squared	0.8351
% Coefficient of variation	9.08	Predicted R-Squared	0.6410
F-Value	11.49	Adequate precision	13.161

2.7.3.5.1 Residual analysis for peak tailing of MTZ

The normal plot of residuals and plot of residuals vs predicted responses for peak tailing of MTZ are depicted in Figures 2.14 and 2.15 respectively. Points on the normal plot of residuals fall on a straight line while points on the residuals vs predicted responses plot are scattered therefore it can be concluded that the model is adequate to navigate the design space.

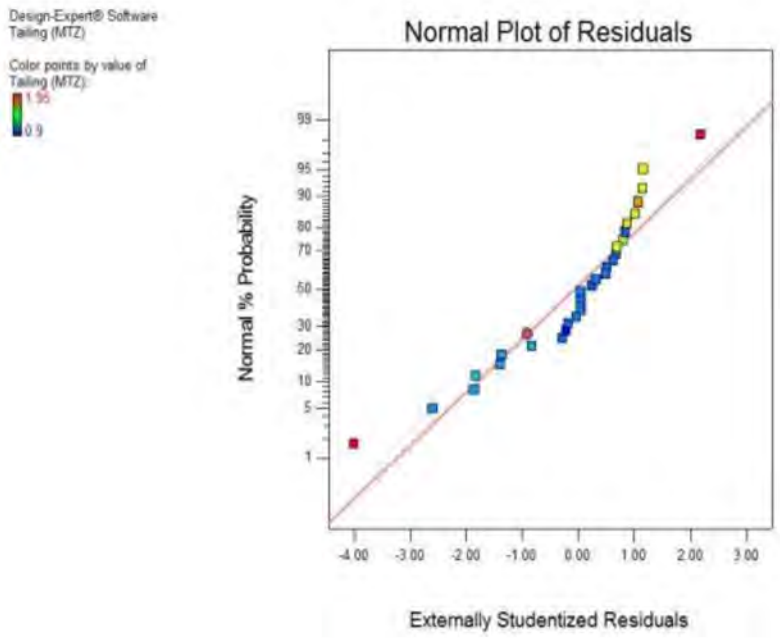

Figure 2.14 Normal probability plot of residuals for peak tailing of MTZ

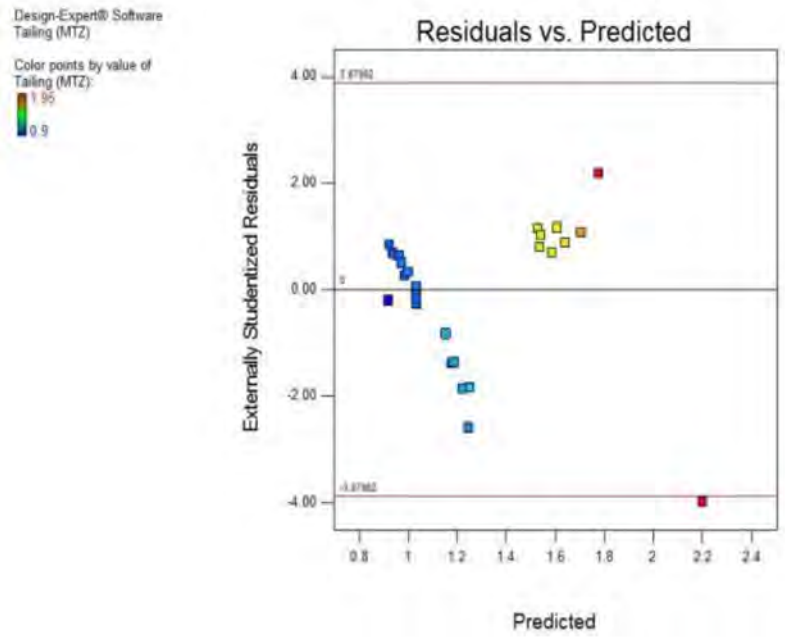

Figure 2.15 Residual versus predicted response plot for peak tailing of MTZ

2.7.3.5.2 Box-Cox Plot for Transformations for peak tailing of MTZ

The Box-Cox plot for peak tailing is depicted in Figure 2.16 and reveals that no transformation is required since the value for $\lambda=1$ and that the data does not deviate from normality.

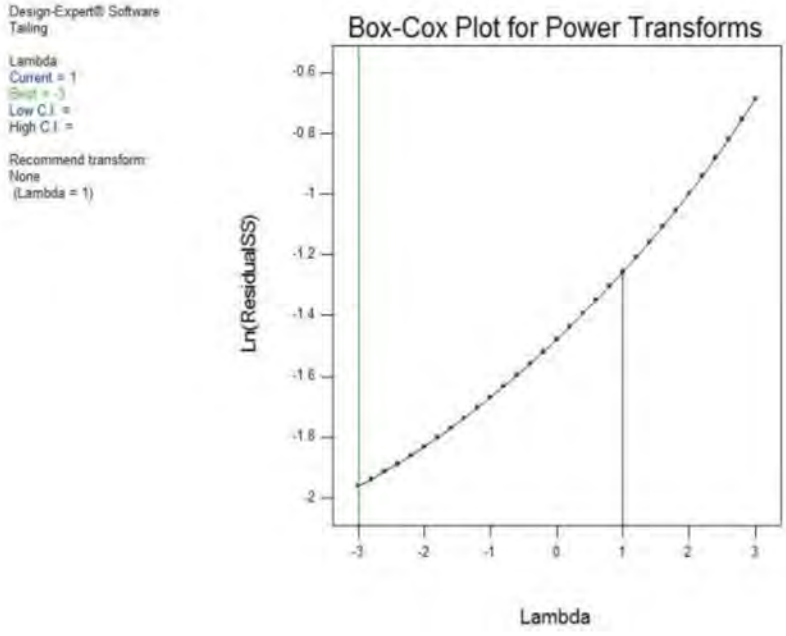

Figure 2.16 Box-Cox plot for peak tailing of MTZ.

2.7.3.6 ANOVA for Tailing of MTZ

2.7.3.6.1 Significant Factors Affecting MTZ peak tailing

ANOVA results for the factors that significantly affect peak tailing of MTZ are listed in Table 2.11. Model terms with a p-value < 0.05 are significant. The relationship between independent variables and peak tailing is mathematically described using Equation 2.11.

Table 2.11 ANOVA results for the response surface quadratic model (partial sum of squares-type III) for MTZ peak tailing

Source	Sum of squares	Df	Mean square	F value	P-value Prob > F
Model	3.05	14	0.22	11.49	<0.0001
X_1	0.384	1	0.384	0.41	0.5335
X_2	0.013	1	0.013	0.66	0.4277
X_3	2.46	1	2.46	129.92	<0.0001
X_4	0.092	1	0.092	0.097	0.7599
X_1X_2	0.381	1	0.381	0.40	0.5348
X_1X_3	0.262	1	0.262	0.28	0.6063
X_1X_4	0.070	1	0.070	0.074	0.7891
X_2X_3	0.032	1	0.032	1.66	0.2170
X_2X_4	0.093	1	0.093	0.027	0.8724
X_3X_4	0.112	1	0.112	0.12	0.7350
X_1^2	0.057	1	0.057	3.00	0.1039
X_2^2	0.048	1	0.048	2.52	0.1330
X_3^2	0.48	1	0.48	25.11	0.0002
X_4^2	0.051	1	0.051	2.68	0.1226
Residuals	0.28	15	0.019		
Pure error	0.134	5	0.027		
Cor total	3.34	29			

Values in red indicate significant independent variables

$$Y_4 = 1.03 + 0.018X_1 - 0.023X_2 + 0.32X_3 + 0.436X_4 - 0.022X_1X_2 + 0.018X_1X_3 + 0.4668X_1X_4 - 0.044X_2X_3 - 0.280X_2X_4 + 0.012X_3X_4 + 0.046X_1^2 + 0.042X_2^2 + 0.13X_3^2 + 0.043X_4^2$$

Equation 2.11

The data reveal that the only significant factor that affects peak tailing of MTZ is the pH of the buffer. The equation reveals that pH has a positive effect on peak tailing of MTZ. In other words, peak tailing increases with buffer pH. MTZ is a basic compound that interacts strongly with free silanols on the surface of the silica of the stationary phase [25,116]. The free silanol groups become ionised at high pH and ion exchange with basic analytes, such as MTZ, result in peak tailing [126,238]. This phenomenon is known as the silanol effect. In order to minimise peak tailing of basic analytes, the adjustment of mobile phase pH is an option. Using low pH of ≤ 4 results in suppression of free silanol groups [182,238].

2.7.3.6.2 Response Surface Model Plots for peak tailing

Figure 2.17 is a contour plot in which the effect of pH and buffer content on peak tailing of MTZ is depicted. It is evident that an increase in pH results in an increase in tailing and that a tailing factor of ≤ 1 was achieved using a buffer pH values 4. The relationship between pH and peak tailing is also illustrated in a 3D response surface plot (Figure 2.18). The almost straight lines in Figure 2.17 indicate that peak tailing is not affected by buffer composition and the 3D plot (Figure 2.18) suggests that buffer molarity does not affect peak tailing of MTZ.

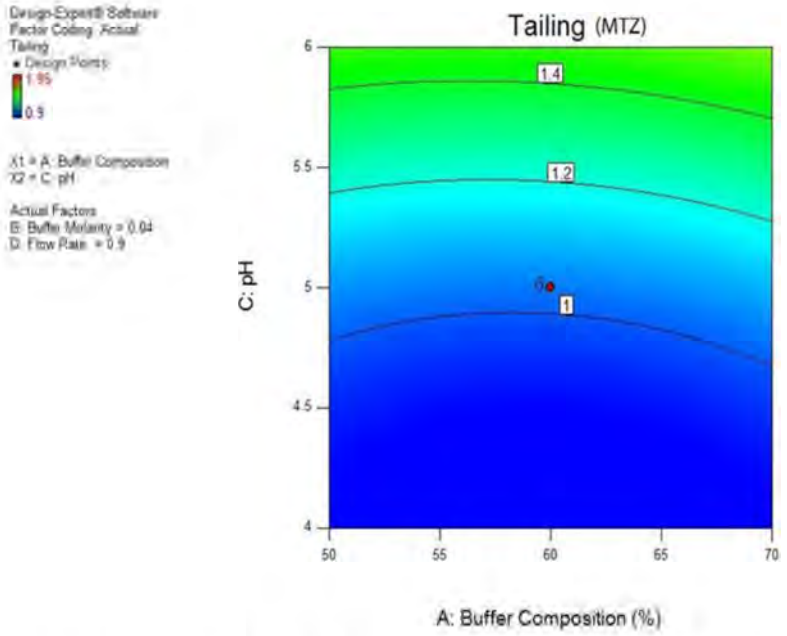

Figure 2.17 Contour plot depicting the effect of changes in buffer pH and content on peak tailing of MTZ

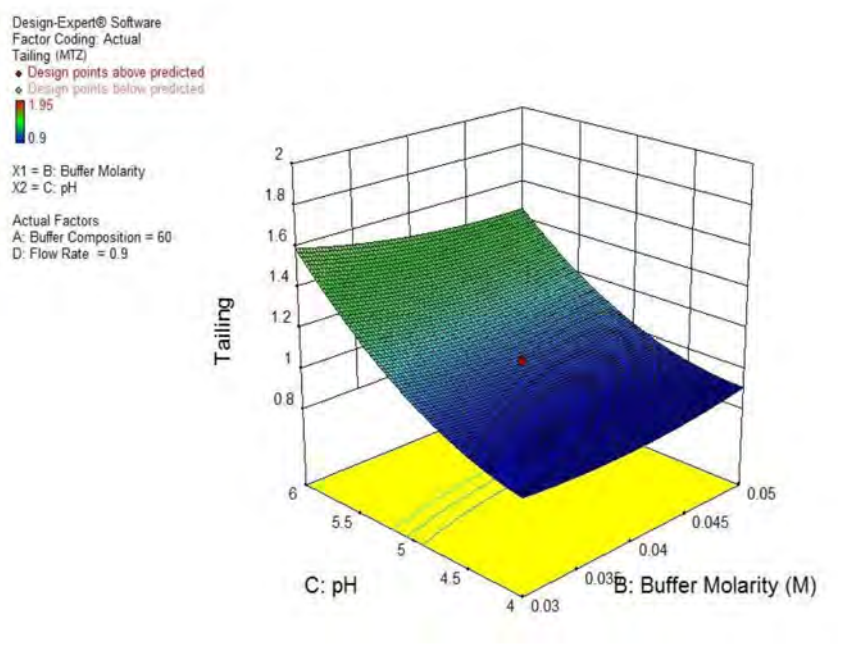

Figure 2.18 3D response surface plot depicting the impact of buffer molarity and pH on peak tailing of MTZ.

2.7.4 Validation of experimental design

Following evaluation of the effects of factors such as buffer pH, buffer content and flow rate on the retention time, peak shape and resolution of MTZ, optimal chromatographic conditions were selected using a numerical optimisation process with the aid of Design Expert software. The experimental conditions that generated a desirability value of 1 were identified. The optimised conditions were then used throughout HPLC method development and validation and are summarised in Table 2.12.

Table 2.12 Optimised chromatographic conditions for the analysis of MTZ

Parameter	Optimised condition
HPLC system	Waters® Alliance Model 2695
Detector	Waters® Model 2489 UV/Vis Detector
Column dimensions	Macherey-Nagel Nucleosil®, C8 250mm x 4mm i.d x 10µm column
Mobile phase composition	0.04M KH_2PO_4 buffer (pH=4) and ACN in a 81:19 % v/v ratio
Mode	Isocratic
Flow rate	1 ml/min
Column temperature	25°C
Detection	317 nm
Injection Volume	10 µl
Column back pressure	1200 psi

Use of the optimised chromatographic conditions resulted in a separation in which the retention time of MTZ and ODZ were 5.12 and 9.14 minutes respectively, with a resolution factor of 8.11. A typical chromatogram of the separation of a standard solution of MTZ

(120µg/ml) and ODZ (60µg/ml) is depicted in Figure 2.19. The experimental design model was validated by comparing predicted and the actual experimental values using calculated residuals and percentage error. The predicted retention times of MTZ and ODZ, peak tailing and the resolution factor, in addition to the calculated residual and percent prediction error are summarised in Table 2.13.

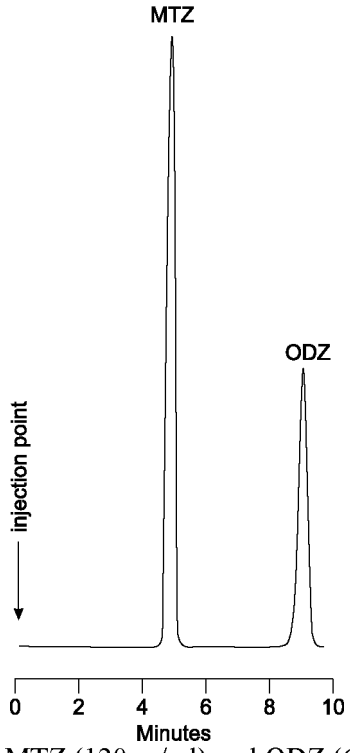

Figure 2.19 Typical chromatogram of MTZ (120µg/ml) and ODZ (60µg/ml)

Table 2.13 Validation parameters and comparison of predicted and actual responses

Response	Predicted	Actual	Residuals	% Prediction error
Retention time of MTZ	4.85	5.12	0.27	5.27
Retention time of ODZ	8.85	9.14	0.29	3.17
Resolution	7.70	8.11	0.41	5.05
Peak tailing of MTZ	1.2	0.92	0.28	3.04

The percent prediction error between predicted and actual retention times were 5.27 and 3.17 for MTZ and ODZ, respectively while the percent error for the resolution factor was 5.05%. It can be concluded that the models were reasonably accurate, particularly for peak tailing and retention time of ODZ that had a percent error < 5%. Slightly lower prediction errors may have been possible had transformation of the data been performed, however the responses observed were within limits and an adequate separation was achieved.

2.8 METHOD VALIDATION

The objective of validation of an analytical procedure or method is to confirm that the procedure used for a specific test is suitable for its intended use [239,240]. Method validation is achieved through laboratory studies and is part of the overall validation process that includes software and instrument validation and system suitability testing [121,241,242]. The pharmaceutical industry relies on the precision and accuracy of analytical instruments and methods to generate valid and reliable data for research, development, manufacture and quality control and a validated method instils confidence that methods will generate data of acceptable quality [242]. Validation is also used to establish the limits of variability for the conditions required to perform and use an analytical method [166,239]. A number of guidelines and standard procedures for analytical method validation have been published by the International Conference on Harmonisation (ICH) and the United States Food and Drug Administration (FDA) [41,167,241,243].

A new or modified analytical method should undergo a validation process in order to ensure that the results produced are reliable and reproducible when used by different operators using the same equipment in the same or a different laboratory [244]. The parameters assessed during method validation include linearity, range, accuracy, precision, selectivity, reproducibility and the limits of quantitation (LOQ) and detection (LOD) [239,241,245].

2.8.1 Linearity and range

The linearity of an analytical method describes the ability of the method to produce test results that are directly, or by a well-defined mathematical transformation, proportional to the concentration of the analyte in samples over a specific range [246,247]. Linearity is usually expressed in terms of variance around the slope of a regression line and the range of the analytical method is defined as the interval between and including the upper and lower concentration levels of the analyte that have been determined with acceptable precision, accuracy and linearity [145,239,246].

Linearity was determined using least squares linear regression analysis and establishing an equation for the line for a range of concentrations. The correlation coefficient (R^2) of the least squares linear regression line is a measure of linearity and should be between 0.98 and 1.00 or at least be > 0.999 [138,145]. A correlation coefficient of 1 represents a perfect fit of experimental data points to the regression line [248]. The closer the value is to unity, the more linear the line and therefore the response of the analytical method [115,245]. The ICH

guidelines state in order to establish linearity a minimum of 5 concentrations must be investigated [241].

Linearity was performed by repeated measurements (n=5) of seven calibration standard solutions containing MTZ and 60 µg/ml ODZ. The calibration standard solutions were prepared as described in §2.4.3 and injected in ascending order of concentration *viz.*, 0.4, 5, 20, 40, 80, 100, 120 µg/ml of MTZ.

The peak area ratios (PAR) of MTZ to ODZ were calculated and a calibration curve of PAR versus concentration plotted (Figure 2.20). Least squares linear regression analysis was performed on the data to establish whether a correlation could be established between the response and analyte concentrations. The equation for the best-fit least squares regression line was y = 0.0225x - 0.0079 with a correlation coefficient (R^2) of 0.9999. The y-intercept should be < 2% of the response or close to zero in order to establish the accuracy and linearity. The R^2 value ≥ 0.999 is an indication of linearity between sample concentrations and PAR [135,145,244]. The R^2 value of 0.9999 and the y-intercept of 0.0079 satisfied the criteria for linearity and a direct response-concentration relationship was established for the calibration curve.

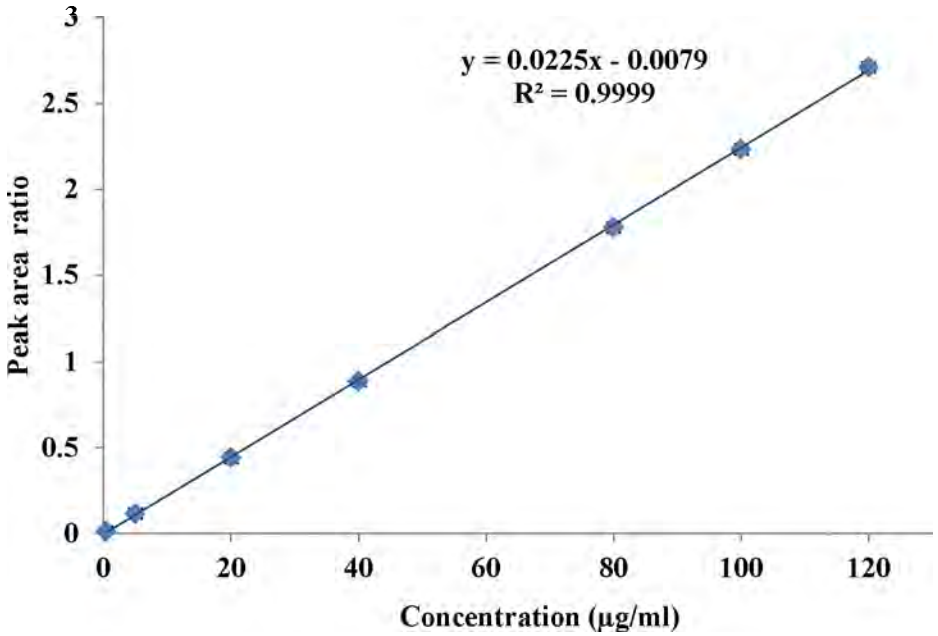

Figure 2.20 Typical calibration curve for MTZ over the concentration range 0.4 – 120 µg/mL (n = 5).

2.8.2 Precision

The precision of an analytical method is the degree of agreement between individual results when the procedure is applied repeatedly to multiple testing of an homogeneous sample [246]. It is a measure of the degree of reproducibility or repeatability of the analytical method used under defined operating conditions [167,244]. Precision is expressed as the percent relative standard deviation (RSD) for a statistically defined number of samples [244,249]. According to the ICH guidelines, precision should be performed at three different levels viz., repeatability, intermediate precision and reproducibility [241].

2.8.2.1 Repeatability

Repeatability, also known as intra-assay precision, of an analytical method is performed to evaluate variability in experimental conditions over a short period of time [246,250]. It is evaluated by the same analyst in the same laboratory using the same conditions over a short time interval such as for example within the same day [249,250].

ICH guidelines state that repeatability should be assessed using a minimum of nine determinations covering the specified range for the procedure, for example at three concentration levels in replicate (n=3) of each concentration tested [241].

Repeatability was established using three concentrations, low (10 µg/ml), medium (60 µg/ml) and high (110 µg/ml) that were within the calibration curve and analysing a minimum of five replicates (n=5) for each concentration. The percent RSD and standard deviation was calculated for each sample. For an assay method, the % RSD should be ≤ 1%. For intra-assay precision the % RSD should be ≤ 2%, whereas for impurity assays, the intra-assay precision should be ≤ 10% [244]. The results of repeatability for the three concentrations and calibration curve summarised in Table 2.14 and 2.15 respectively indicate that the method is repeatable and the % RSD values for all concentrations was < 2%.

Table 2.14 Summary of repeatability results for 10, 60 and 110 µg/ml

Theoretical concentration µg/ml	Actual concentration µg/ml	Mean area ratio MTZ/ODZ (n=5)	Standard deviation	%RSD
10	10.099	0.2193	0.0003	0.0012
60	59.099	1.3201	0.0181	0.0137
110	109.20	2.4474	0.0013	0.0544

Table 2.15 Summary of repeatability results for calibration curve in the range 0.4-120 µg/ml

Theoretical concentration µg/ml	Actual concentration µg/ml	Mean area ratio MTZ/ODZ (n=5)	Standard deviation	%RSD
0.4	0.3871	0.0008	0.0226	0.3751
5	5.3234	0.1119	0.0319	0.0423
20	19.834	0.4384	0.0003	0.0692
40	39.586	0.8828	0.0005	0.0537
80	59.023	1.7771	0.0011	0.0614
100	79.333	2.2315	0.0012	0.0530
120	99.527	2.7104	0.0021	0.0760

2.8.2.2 Intermediate precision

Intermediate precision is also known as inter-day precision and the extent to which it is established is dependent on the circumstances under which the method is intended to be used [241]. The ICH guidelines recommend that typical variations to be studied may be on different days, with different analysts and equipment and it is not necessary to consider these individually [241]. Intermediate precision is a consequence of within-lab variations that occur due to random events. When determining intermediate precision, experimental design should be used so that the effects, if any of the individual variables can be monitored [241,244,251]. Three solutions of MTZ at low (10 µg/ml), medium (60 µg/ml) and high (110 µg/ml) concentrations and internal standard (60 µg/ml) were analysed in triplicate (n=3) on three consecutive days using the same analytical equipment. The results of intermediate precision studies is summarised in Table 2.16 and the results of these studies reveal that there are no significant deviations in concentration for the samples analysed. All % RSD values were < 2% indicating that the analytical method is precise on a day-to-day basis.

Table 2.16 Summary s of intermediate precision results

Day	Theoretical concentration µg/ml	Mean actual concentration µg/ml (n=3)	Standard deviation	%RSD
Day 1	10	10.066	0.0002	0.2264
	60	59.343	0.0004	0.0921
	110	108.35	0.0002	0.0615
Day 2	10	10.126	0.0005	0.0817
	60	59.189	0.0012	0.0267
	110	109.05	0.0015	0.0098
Day 3	10	10.098	0.0003	0.0012
	60	59.099	0.0181	0.0138
	110	109.20	0.0013	0.0540

2.8.2.3 Reproducibility

Reproducibility of an analytical method is the ability of a method to produce precise results when used in more than one laboratory by different analysts and is a measure of between laboratory precision [241,245,246]. Reproducibility was not assessed in these studies as all analyses were performed by the same analyst, using the same equipment in the same laboratory for the duration of these studies.

2.8.3 Accuracy

The accuracy of the analytical method is a measure of the closeness of test results produced by the method to the true value for the sample and is an indication of the closeness of experimental values to the theoretical values that is dependent on inherent error that may be associated with an analytical method [246,252]. Accuracy is normally assessed following the establishment of the precision, linearity and specificity of an analytical method [241,253]. Accuracy may be determined by analysing samples to which a known amount of analyte has been added [150].

To establish the accuracy of an analytical method the ICH guidelines recommend that a minimum of nine analyses should be performed at a minimum of three concentrations viz., low (10 µg/ml), medium (60 µg/ml) and high (110 µg/ml) that cover the range of the method [241]. The solutions were prepared as previously described in §2.4.3 and analysed in replicate (n = 5). Accuracy can be established by analysing % RSD, % recovery and % bias data [245,252]. A % RSD limit of ≤ 5% and % bias of ≤ 5% was set in our laboratory as the limits for establishing acceptable accuracy of this method. The bias of a method is the difference between the mean value and true value for a sample and is used to determine the influence of an analyst on the performance of an analytical method [251,252]. The % recovery and % bias were calculated using equations 2.12 and 2.13 respectively.

$$\% \text{ Recovery} = \frac{\text{actual concentration}}{\text{theoretical concentration}} \text{ X } 100 \qquad \textit{Equation 2.12}$$

$$\% \text{ Bias} = \frac{true\ value - measured\ value}{True\ value} \text{ X } 100 \qquad \textit{Equation 2.13}$$

A summary of the results of accuracy studies is listed in Table 2.17 and indicate that the method is accurate as all % RSD and % Bias values were < 5%.

Table 2.17 Summary of accuracy results

Theoretical concentration µg/ml	Mean actual concentration µg/ml (n=5)	Standard deviation	%Recovery	%RSD	%Bias
10	10.084	0.0335	100.84	0.0019	-0.8400
60	59.843	0.0002	99.739	0.0147	0.2613
110	109.79	0.0014	99.739	0.0544	0.1893

2.8.4 Selectivity

An analytical method is selective if a response that is distinguishable for the analyte of interest in the presence of any other extraneous detectable components is produced [240,249]. Most chromatographic methods produce responses for the analyte of interest and extraneous components [251]. The selectivity of an analytical method ensures that the analyte of interest is well resolved from components that may be present in a formulation or sample matrix [240].

The selectivity of the analytical method was established by analysing commercially available Flagyl® 200 mg and 400 mg tablets using the RP-HPLC method developed and optimised in these studies. Twenty tablets were crushed in a mortar and pestle and an amount of powder equivalent to 200 mg and 400 mg MTZ was weighed and quantitatively transferred into separate 250 ml A-grade volumetric flasks and made up to volume using a solution of water and ACN in a 81:19% v/v ratio. The mixture was sonicated for 15 minutes and then diluted to with the water: ACN solution to produce a solution of final concentration of 100 µg/ml. This solution was then filtered through a 0.45µm HVLP Millipore® filter membrane prior to HPLC analysis.

The average MTZ content was 98.9% - 100.3% of the label claim for the two products tested and the results are summarised in Table 2.18 in which the % recovery and corresponding % RSD values are reported and were < 5% in all cases revealing that the method is selective and accurate.

Table 2.18 Assay results for commercially available products

Product	Label claim mg	Amount of MTZ ± SD mg	% Recovery	%RSD
Flagyl® 200	200 mg	197.80±0.0023	98.9	0.1188
Flagyl® 400	400 mg	401.20±0.0025	100.3	0.1254

2.8.5 Limits of quantitation (LOQ) and detection (LOD)

The limit of quantitation (LOQ) or lower limit of quantitation (LLOQ) is the lowest concentration of an analyte that can be accurately quantitated with the acceptable precision and accuracy for an analytical method [240,246,249]. The LOD is defined as the lowest concentration of an analyte of interest that can be detected, but not necessarily quantitated, using the defined experimental conditions [240,246]. The ICH guidelines recommend a number of approaches to establish the LOQ and LOD of methods that are based on visual evaluation, signal–to-noise ratio and standard deviation and slope of the response. Five potential concentrations viz., 0.2, 0.4, 0.6, 0.8, 1.0 µg/ml were tested to establish the LOQ of the method. The LOQ was identified using a limit for precision of ≤ 5% RSD. By convention the LOD was calculated as one third of the LOQ [254].

The lowest concentration of analyte that resulted in a response with a % RSD of < 5% following multiple injections was considered the LOQ and since a solution of 0.2 µg/ml MTZ exhibited a % RSD of 6.91% and the 0.4 µg/ml solution a % RSD of 1.77% the LOQ was established as 0.4 µg/ml. The LOD was then defined as 0.13 µg/ml. A summary of the data used to establish the LOQ and LOD is listed in Table 2.19

Table 2.19 LOQ and LOD results

Concentration µg/ml	Mean area MTZ/ODZ (n=5)	SD	%RSD
0.2	0.0038	0.0003	6.9120
0.4	0.0078	0.0001	1.7737
0.6	0.0128	0.0174	0.2020
0.8	0.0168	0.0342	0.3015
1.0	0.0213	0.0456	0.3185

2.9 FORCED DEGRADATION STUDIES

2.9.1 Introduction

Analytical methods are intended to be stability indicating in order for an analytical method to differentiate between the analyte of interest and degradation products produced during forced degradation studies or related substances [255,256]. Force degradation studies are also known as stress tests and are undertaken during the development of a drug candidate and product to provide an understanding of the intrinsic long term stability of a drug [257–259]. It is vital that degradation product(s) do not interfere with quantitation of the analyte of interest. Forced degradation studies are required to demonstrate the specificity of stability indicating methods [255,260].

2.9.2 Methods

Forced degradation studies were performed in acidic, basic, oxidative, light and elevated temperature conditions and any possible degradation products may be qualitatively and/or quantitatively reported. All degradation studies were performed in solutions and only in the solid state under dry heat conditions. Approximately 10 mg of MTZ was accurately weighed and transferred into 100 ml A-grade volumetric flasks and dissolved in the relevant medium, made up to volume to yield a solution at 100 µg/ml. The internal standard solution was prepared as described in § 2.4.3 and added to the sample immediately prior to HPLC analysis.

2.9.2.1 Temperature

The ICH guidelines recommend that the effect of temperature on a drug substance must be conducted over 10°C increments and to determine if MTZ degrades at elevated temperatures five separate 100 µg/ml samples were prepared as described in § 2.4.3. The samples were exposed to different temperature conditions (50°C - 90°C) maintained using a Colora® Model NB34980 Ultra-Thermostat water bath (Colora®, Lorch, Germany) for eight hours. Aliquots (1 ml) were removed prior to refluxing and every hour for 8 hours after refluxing commenced. A 0.5 ml aliquot of the internal standard solution was added to each sample prior to HPLC analysis. All samples refluxed below 80°C appeared to be stable however at 90°C MTZ degraded with a 22% loss of the peak area without the appearance of additional peaks in the chromatogram. A summary of observations made during analysis of each sample at the different temperatures is listed in Table 2.20. Chromatograms for samples at temperature ranges 50-80°C for time 0 and after refluxing for 8 hours are shown in Figure 2.21 and 2.22 respectively. From the chromatograms it can be observed that there is negligible change in the peak area when MTZ is refluxed up to 8 hours between 50°C-80°C. The chromatograms for the sample at 90°C for time 0 and after refluxing for 8 hours is shown in Figure 2.23, from the chromatograms it can be observed that there is a decrease in the peak area of MTZ at 90°C after refluxing for 8 hours.

Table 2.20 Summary of the effect of temperature on MTZ solutions

Temperature °C	Time Hours	Observations
50	8	MTZ peak resolved at 5.16, negligible change in peak area
60	8	MTZ peak resolved at 5.18, negligible change in peak area
70	8	MTZ peak resolved at 5.17, negligible change in peak area
80	8	MTZ peak resolved at 5.17, negligible change in peak area
90	8	MTZ peak resolved at 5.18, 22% decrease in peak area but no extra peaks observed

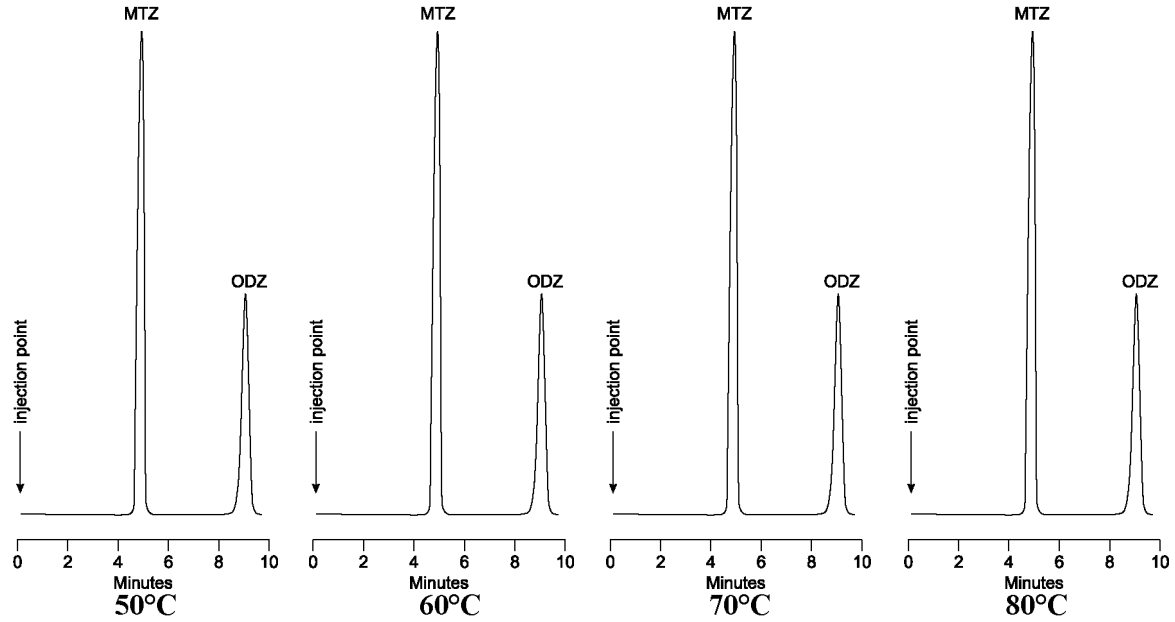

Figure 2.21 Chromatograms at 50°C, 60°C,70°C and 80°C for time 0

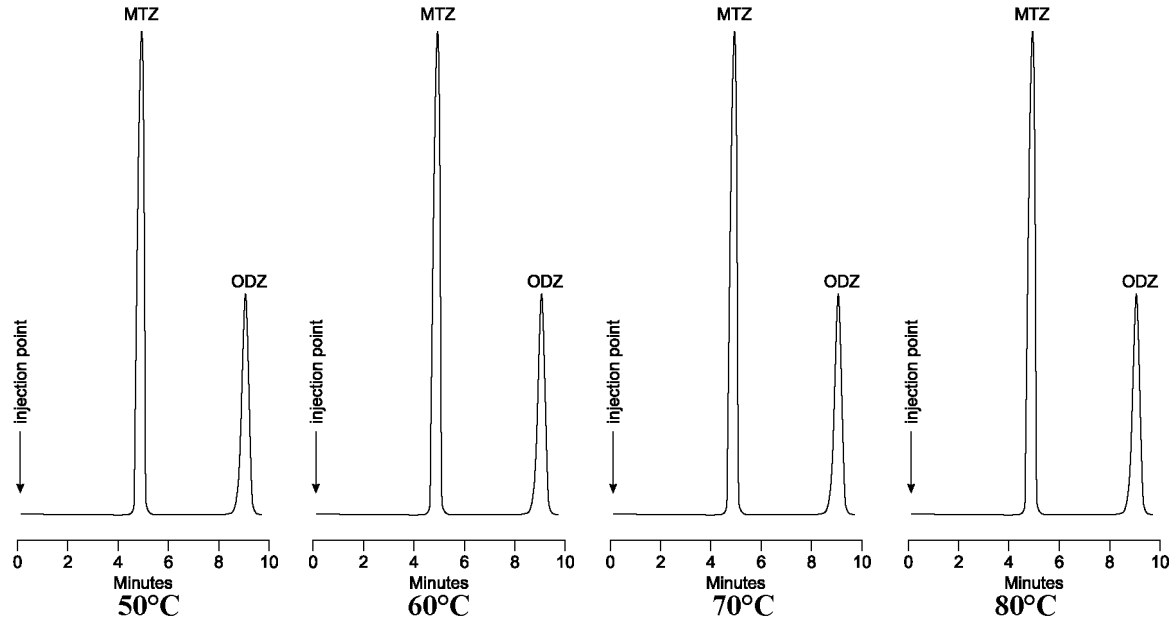

Figure 2.22 Chromatograms at 50°C, 60°C,70°C and 80°C after refluxing for 8 hours

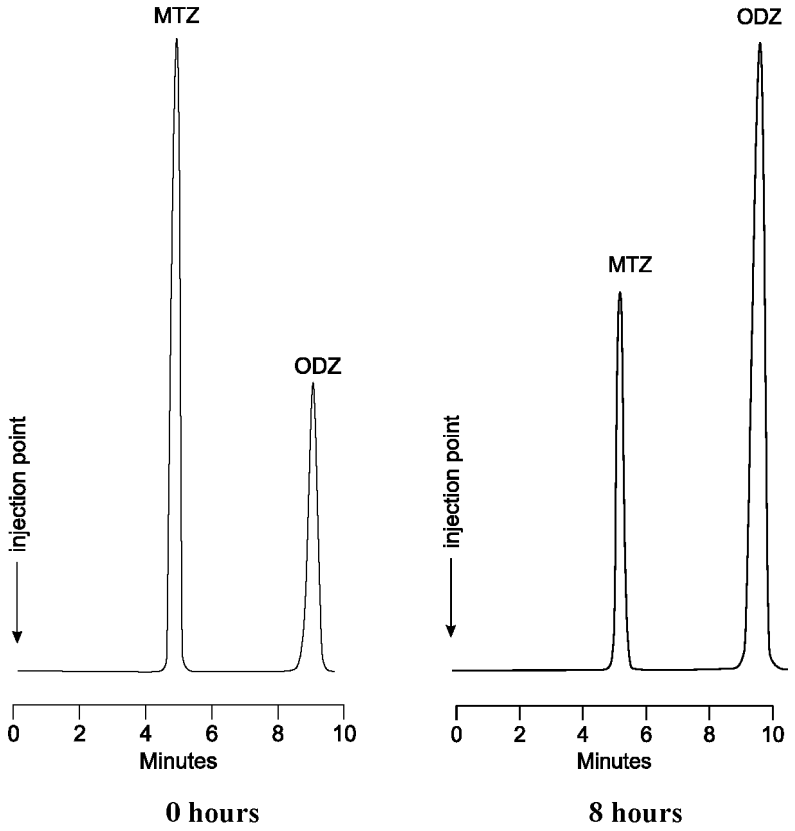

Figure 2.23 Chromatograms at 90°C for time 0 and after refluxing for 8 hours

2.9.2.2 Acidic hydrolysis

A 100 µg/ml sample of MTZ was prepared using 0.1M HCL and the solution was refluxed at 80 °C for 8 hours. Aliquots of solution (1 ml) were removed prior to refluxing and every hour after refluxing had commenced and a 0.5 ml aliquot of internal standard solution added to each sample prior to HPLC analysis.

Approximately 20% of MTZ has been reported to degrade when the compound is exposed to 0.1M HCL for 12 hours at 80°C with no additional degradation peaks formed [49]. This is consistent with other studies which reported that under acidic conditions MTZ was relatively stable with only a slight loss of MTZ with no appearance of degradation peaks [261]. These reports suggest that MTZ degrades to a low molecular weight compound as no degradation peaks have been observed during LC-MS studies [49]. MTZ was found to degrade by approximately 18±0.08% in 0.1M HCL after refluxing at 80 °C for 8 hours and no peaks attributed to degradation peaks were observed for the duration of the studies, this finding is similar to that in the reported literature [49,261]. A typical chromatogram of MTZ following exposure to acidic conditions at time 0 and after refluxing for 8 hours is depicted in Figure 2.24.

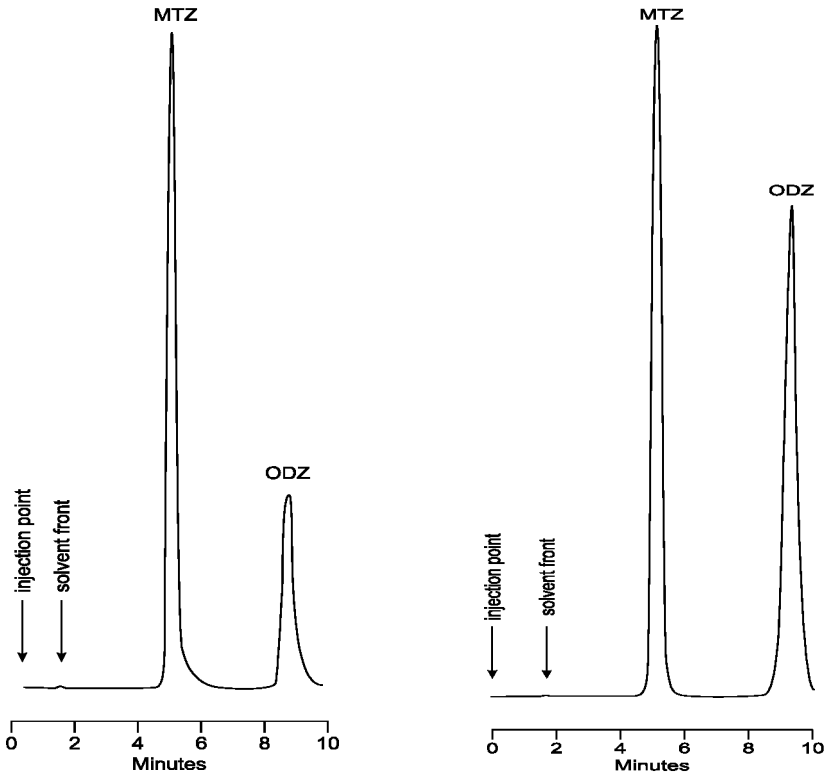

Figure 2.24 Typical chromatogram of MTZ following exposure to 0.1M HCL for time 0 and 8 h at 80°C

2.9.2.3 Alkali hydrolysis

A 100 µg/ml solution of MTZ was prepared using 0.1M NaOH and was refluxed at 80°C for 1 hour. Aliquots of solution (1 ml) were removed prior to refluxing and an hour after refluxing had commenced. A 0.5 ml aliquot of internal standard solution was added to each sample prior to HPLC analysis.

MTZ decomposes in alkali conditions to produce acetic acid and ammonia and 95% MTZ degrades following exposure to 0.1M NaOH at 80°C [262]. The degradation product formed during hydrolysis elutes at a retention time of 2 minutes [49,262]. MTZ degraded significantly to the extent of 98 ± 0.13% in 0.1M NaOH after only 1 hour of refluxing at 80 °C; this observation is therefore similar to the one reported in literature [49,262]. Additional peaks A and B were observed and eluted at 1.4 and 3.7 minutes respectively therefore alkali degradation was assumed to have occurred. A typical chromatogram of MTZ following exposure to 0.1M NaOH at time 0 and 1 hour of refluxing at 80°C is depicted in Figure 2.25.

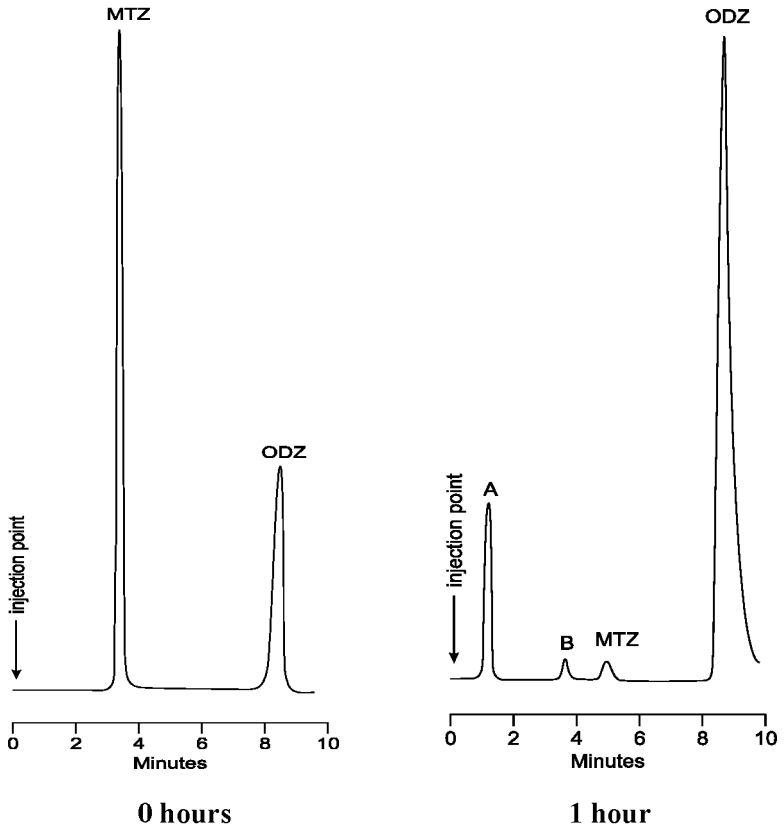

Figure 2.25 Typical chromatogram of MTZ following exposure to 0.1M NaOH for time 0 and 1 hour at 80°C

2.9.2.4 Oxidative degradation

A 100 µg/ml sample of MTZ was prepared using 10% v/v H_2O_2 and the solution was refluxed at 80°C for 1 hour. Aliquots of solution (1ml) were removed prior to refluxing and 1 hour after refluxing had commenced. A 0.5 ml aliquot of the internal standard solution was added to each sample prior to HPLC analysis. HPLC analysis revealed that MTZ degraded by approximately 83% after exposure to oxidative conditions for 1 hour. A typical chromatogram of MTZ at time 0 hours and possible degradation products formed after one hour of refluxing with H_2O_2 at 80°C is depicted in Figure 2.26. Four extra peaks C, D, E and F are clearly depicted in the chromatogram for the sample refluxed at 80°C after 1 hour. These extra peaks may be attributed to possible degradants of MTZ. It was reported that MTZ undergoes negligible degradation when exposed to 3% v/v H_2O_2 for 6 hours at room temperature but degrades to an extent of 30% when exposed to 30% v/v H_2O_2 for 48 hours at room temperature [49]. The negligible degradation that was reported could be due to the fact that a lower concentration, 3% v/v of H_2O_2 at room temperature was used as compared to the 10% v/v used at 80°C in this study. In addition 30% degradation of MTZ reported was still

lower than that found in this study, this may be due to higher temperature of 80°C used in this study as compared to the room temperature.

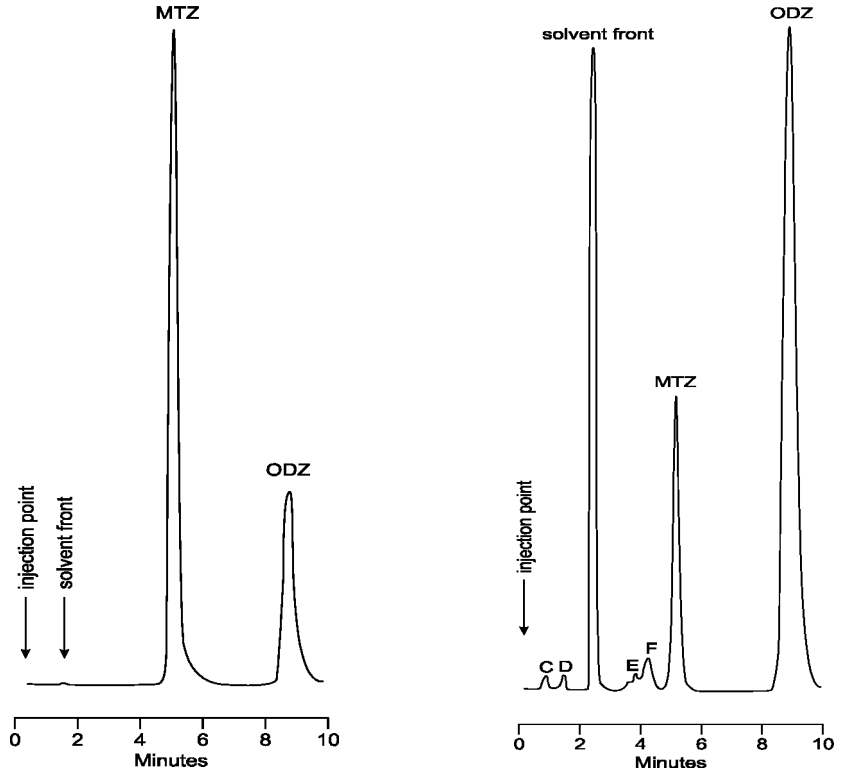

Figure 2.26 Typical chromatogram of MTZ following exposure to 0.1M NaOH for time 0 and 1 hour at 80°C

2.9.2.5 Photolysis

A 100 µg/ml solution of MTZ was prepared in water and exposed to UV and visible radiation using an Atlas SUNTEST® CPS+ (Lisengericht, Germany) cabinet for 24 hours. The lamp was set at 500W/m^2 at a temperature of 40°C. Aliquots of solution (1ml) were removed and added to 0.5ml internal standard solution prior to HPLC analysis.

The analysis of MTZ following exposure to light revealed that MTZ is photo-labile and typical chromatograms of MTZ at time 0 and following 24 hours exposure to light are depicted in Figure 2.27. Three extra peaks attributed to degradation peaks G, H and I were observed on the chromatogram following exposure to light after 24 hours. It has been reported that a solution of MTZ in water degrades up to 90% following exposure to sunlight for 12 days with the presence of three additional but minor peaks in chromatograms [49].

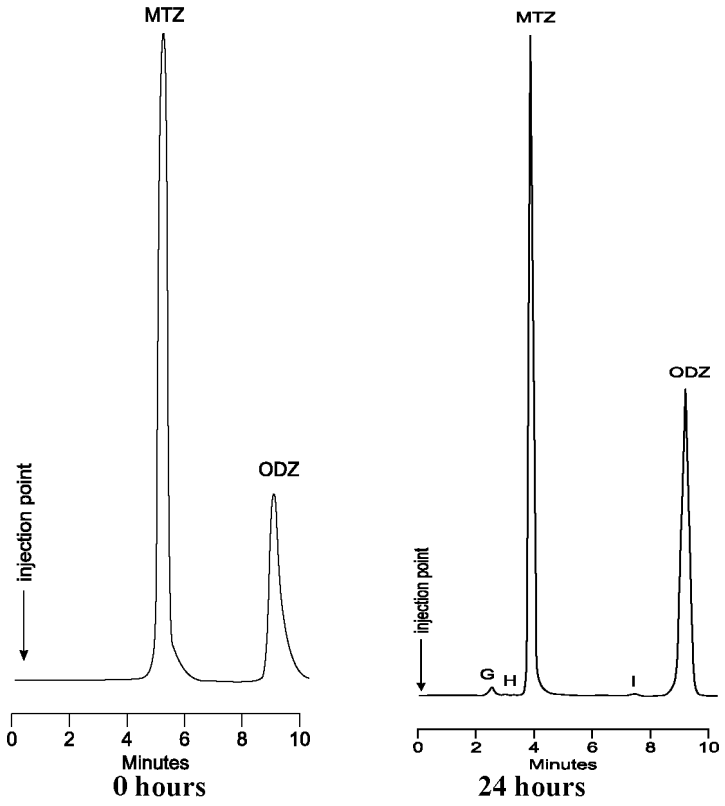

Figure 2.27 Typical chromatogram of MTZ at time 0 hours and following exposure to UV radiation for 24 hour

2.9.2.6 Dry heat

To evaluate thermal degradation of MTZ, 20mg of MTZ was spread as a thin layer of powder on a watch glass and placed in an oven (Gallenkamp®, Loughborough UK) for 8 hours at 100 °C, after which 10mg of the powder was diluted with mobile phase in a 100ml A-grade volumetric flask and analysed by HPLC. MTZ did not appear to degrade when exposed to 100°C for 8 hours in the solid state as there were no additional peaks observed in the chromatogram after heating at 100°C for 8 hours. A typical chromatogram of MTZ at time 0 and following 8 hours exposure is depicted in Figure 2.28. It has been reported that MTZ does not undergo thermal stress, negligible degradation is observed when MTZ was heated at 50°C for three months [49,51,261] hence these findings are similar to those reported in literature.

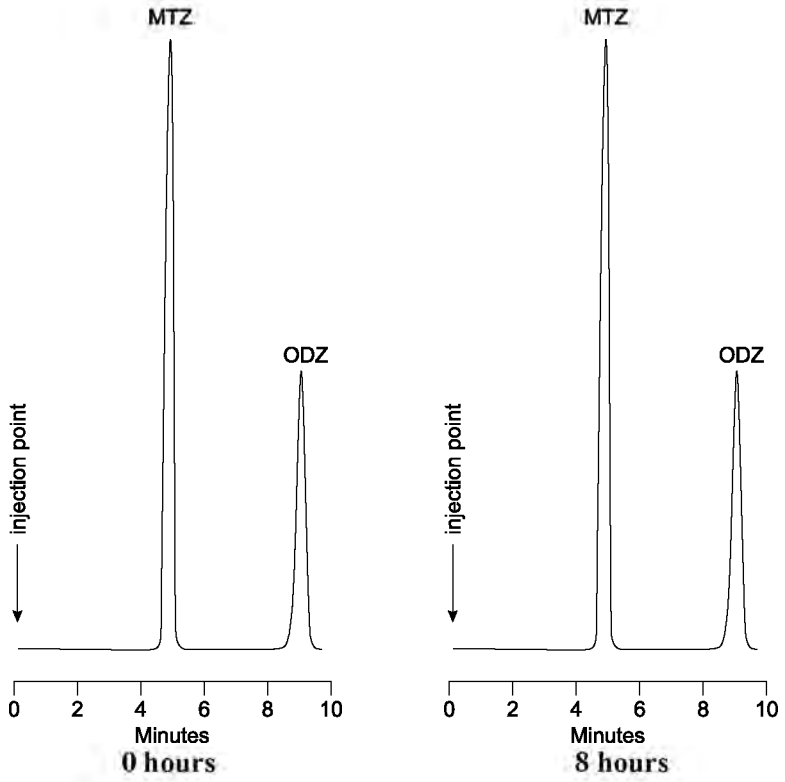

Figure 2.28 Typical chromatogram of MTZ at time 0 and following exposure to dry heat at 100°C for 8 hours.

2.10 CONCLUSIONS

The use of an appropriate and validated analytical technique is important for the generation of reliable data following analysis of raw materials and pharmaceutical products. A suitable analytical method must ensure that the compound of interest is well resolved and free from interference from excipients used in the formulation, the internal standard and/or potential degradation products.

A rapid, simple, precise, accurate and selective RP-HPLC method for the quantitation of MTZ has been successfully developed, optimised and validated. RSM was used for method optimisation to establish optimum chromatographic conditions for the separation of MTZ and the internal standard, ODZ. The amount of buffer, pH and flow rate was found to affect the retention time of MTZ and ODZ significantly, whereas buffer content and pH had a significant effect on the resolution between MTZ and ODZ peaks.

The separation using optimised conditions produced sharp and well resolved symmetrical peaks with retention times of approximately 5 and 9.14 minutes for MTZ and ODZ, respectively. The residual and percent errors for predicted responses and actual responses

prove that the model used was accurate and appropriate to navigate the design space for this method.

The method was found to be linear over the range 0.4 -120 µg/ml with a correlation coefficient of 0.999 and can be used for the analysis of MTZ in bulk and pharmaceutical dosage forms. The method was stability indicating as MTZ was well resolved from possible degradation peaks. The compound was more stable in 0.1M HCL when compared to 0.1M NaOH and H_2O_2.

This method was found to be selective and accurate for MTZ analysis in pharmaceutical dosage forms as no interfering peaks were observed during the analysis of commercially available Flagyl® tablets. This method is therefore suitable for use in formulation development studies.

This method is much simpler than most methods reported in literature as it only makes use of one type of buffer and organic solvent while most methods published make use of either more than one buffer or more than one organic solvent in the mobile phase. This method makes use of an internal standard as compared to some published methods that do not use an internal standard thus making this method more accurate and precise. The benefit of the present methodology is that it is less expensive and time consuming as it only makes use of a single buffer and organic solvent. Further the use of ODZ as an internal standard is advantageous as ODZ is a 5-nitroimidazole that has similar physical and chemical properties to MTZ. The use of an internal standard also improves the accuracy and precision of chromatographic methods of analysis.

CHAPTER THREE

PREFORMULATION STUDIES

3.1 INTRODUCTION

Pharmaceutical dosage forms are comprised of mixtures of a number of excipients included in a formulation to aid the manufacturing process, enhance drug delivery to the systemic circulation, ensure long term stability and improve patient adherence [263–265]. Each excipient has a primary function and some secondary functions but when used together may produce an optimal pharmaceutical dosage form [266]. The choice of excipient depends on the type of the dosage form to be produced, the physico-chemical and mechanical properties of the active pharmaceutical ingredient (API) and targeted delivery profiles [267]. In order to determine the effect of excipient(s) on formulation performance a series of tests or studies must be undertaken with individual excipients and in combination with the API. These studies are preformulation studies [268]. Prior to formulating a dosage form the physico-chemical properties of an API(s) and potential excipients should be known so as to ensure appropriate preformulation studies that have a vital role to play in anticipating formulation problems are conducted [269]. Preformulation studies emerged in the late 1950s as a result of a shift in emphasis in the industrial pharmaceutical product development process and the need for development of quality, safe and effective dosage forms [270,271].

3.2 SELECTION OF PHARMACEUTICAL EXCIPIENTS

The ICH guidelines state that excipients should be selected with caution as the quality of material may vary from batch to batch and different suppliers [272]. Excipients should be physiologically inert, non-toxic and stable with no evidence of drug-excipient incompatibility [273,274]. The physico-chemical properties of MTZ were reported in Chapter One and in this chapter the physico-chemical properties of excipients and compatibility studies with MTZ and the excipients will be discussed. A summary of the excipients investigated with their trade names, respective sources and primary use are listed in Table 3.1.

Excipient	Source	Use
Ammonio Methacrylate (Eudragit® RS PO)	Evonik® Röhm GmbH, Pharma Polymers, Darmstadt, Germany	Release rate controlling polymer, film coating agent
HPMC (Methocel® K15M)	Colorcon® LTD, Dartford, Kent, England	Release rate controlling polymer
MCC (Avicel® PH102)	FMC® Biopolymer, USA	Filler, diluent

Table 3.1 Excipients evaluated in preformulation studies

3.2.1 Hydroxypropyl methylcellulose (HPMC)

HPMC is an odourless white or off-white fibrous or granular powder. It is partly O-methylated and O-(2-hydroxypropylated) cellulose with the chemical name cellulose hydroxypropyl methyl ether [275]. It is a methyl and hydroxypropyl mixed ether of cellulose that contains different numbers of methoxy and hydroxypropyl functional groups [276].

HPMC is widely used in oral, ophthalmic, nasal and topical formulations [275,278]. It is a common excipient in matrix formulations and the high viscosity grades are used to retard release of drug from matrices [275,279]. HPMC is used in amounts of 10-80% w/w in tablets and capsules and as a binder in oral dosage forms at lower levels or in liquid oral and topical dosage forms as a suspending agent [275,280]. It has bio-adhesive properties and the non-ionic nature of the polymer is advantageous as it minimises the potential for interaction and results in formulations that exhibit pH independent performance [277,281].

On contact with aqueous media HPMC swells and the gel that is formed is an important characteristic for sustained release drug delivery and has an impact on the release kinetics of drug dispersed in the matrix [282]. HPMC exhibits good compression and swelling properties and has the capacity to accommodate high levels of API and these additional properties make it suitable for sustained release formulations. It is available in a number of different grades that vary in viscosity and degree of substitution [275]. [275,277].The solubility of an API is a crucial property when determining the viscosity grade of HPMC to use in a formulation. MTZ is sparingly soluble in aqueous media therefore, the use of low and high viscosity grades of HPMC was investigated. The trade name for HPMC polymer that was used in used in this study is Methocel®.

Two different grades of Methocel® were used in this study, Methocel® K100M and Methocel® K15M. The different grades are distinguished by use of a number that indicates the viscosity of a 2% w/w aqueous solution of the polymer at 20°C. Methocel® K15M has a

nominal viscosity of 15000 mPa s and Methocel® K100M a nominal viscosity of 100000 mPa s [275]. Changes in viscosity have been reported to have an effect on the API release and encapsulation efficiency of microcapsules [453,456, 473].

3.2.2 Polymethacrylate and methacrylic acid ester

Polymethacrylates are synthetic polymers that are cationic or anionic derivatives of dimethylaminoethyl methacrylates, methacrylic acid, and methacrylic acid esters in different ratios [275]. Several different types of polymethacrylate polymers are available for drug delivery and are in the form of a dry powder, aqueous dispersions or organic solutions [283]. Three types of copolymers forms exist viz., Type A, B and C that differ in terms of the methacrylic acid content and viscosity in solution [284]. Type A copolymers are ammonio methacrylate copolymer derivatives that contain ethyl acrylate, methyl methacrylate, and trimethylammonioethyl methacrylate chloride in a ratio of 1:2:0.2 [275,285].

Type B differs to Type A only in ratio content of 1:2:0.1. Type C is an aqueous dispersion of ethyl acrylate copolymer and methyl methacrylate and contains suitable surface active agents [275]. Eudragit polymers can also be classified according to their gastric solubility i.e. gastro-soluble, gastro-resistant (entero-soluble) and gastric insoluble but permeable classes. Different grades of each type of polymer exist. For example Eudragit® L and RL are Type A polymers, Eudragit® S and RS are Type B polymers and Eudragit® L30 and D-55 are Type C polymers [275,286,287]. The typical molecular weight of the polymers is ≥100 000 [275]. Polymethacrylate polymers are used mainly for oral capsule and tablet film coating agents [288]. Depending on the choice of polymer used in a formulation, different rates of release and solubility characteristics of the drug is possible.

Eudragit® RS PO is comprised of poly(ethyl acrylate, methyl methacrylate, trimethylammonioethyl methacrylate chloride) copolymers in a ratio of 1:2:0.1 [284]. This grade of Eudragit polymer is gastro-insoluble but permeable This polymer exhibits sustained release profiles and contains ammonium functional groups existing as salts making it permeable to water [289,290]. The degree of permeability depends on the proportion of ammonium groups in the polymer [290]. Eudragit® RS PO has been used in many gastric-retentive dosage forms for sustained release formulations as it forms permeable water insoluble film coats [275,291–295].

3.2.3 Microcrystalline cellulose (MCC)

Microcrystalline cellulose is purified, partially depolymerised cellulose that is commercially available in a number of different particle sizes and moisture grades that exhibit different properties and are used for different applications [296,297]. It is a white odourless, tasteless crystalline powder and is commonly used in the manufacture of pharmaceutical formulations [298].The primary function is as a diluent for oral tablet and capsule formulations but it has also been used as a binder in wet granulation and direct compression tablets. MCC also exhibits lubricant and disintegrant properties [275]. Avicel® PH 102 (FMC Biopolymer® USA) was used in these studies as it exhibits good flow properties. It has a true density of 1.420-1.460 g/cm^3, a nominal particle size of 100 μm and a moisture content of ≤ 5% [275,299].

3.3 DRUG-EXCIPIENT COMPATIBILITY STUDIES

Drug-excipient compatibility studies are an important component of preformulation studies for all dosage forms [300,301]. Most excipients are selected on the basis of empirical approaches [302]. The API is in direct contact with the excipients in a dosage form and whilst excipients are generally pharmacologically inert, they can and often do interact with an API with a negative impact on drug product stability [300,303,304]. Drug-excipient compatibility studies are used as a basis for selection of potential excipients for inclusion in formulations for pharmaceutical products [305].

Formulation scientists have evaluated a variety of thermal and non-thermal techniques for use in the identification of suitable excipients for use in dosage forms [300,306]. Advanced analytical instrumentation is now available to facilitate identification of potential excipient induced instability [300,302,306]. Excipient(s) that exhibit incompatibility with an API can therefore be rejected early in the development process and rejected from use in formulation studies [306]. To date there is no universally accepted protocol for evaluating the compatibility of an API with potential excipients [306]. However there have been a number of reports over the last decade that highlight the use of analytical tools for drug-excipient incompatibility studies [306,307]. Examples of thermal analytical techniques that are frequently used for such purposes include differential scanning calorimetry (DSC), thermogravimetric analysis (TGA), isothermal microcalorimetry and hot stage microscopy [306,308,309]. Non-thermal analytical methods include X-ray powder diffraction (XRD),

Fourier Transform Infrared Spectroscopy (FTIR), Scanning Electron Microscopy (SEM) and HPLC [306,308,310,311]. These techniques are different in the manner they generate data, the degree of thermal or mechanical stress applied and the amount of sample required [306]. Some of the techniques commonly used and the information that can be derived from these tests is summarised in Table 3.2.

Table 3.2 Techniques used to assess drug-excipient compatibility

Technique	Measurement	Use of information
Differential Scanning Calorimetry (DSC)	Measure of the temperature and heat flow associated with a materials transition as a function of time and temperature	Physico-chemical compatibility between API and excipient. Characterisation of polymorphs
Thermogravimetric analysis (TGA)	Weight changes of a sample as it is heated, cooled or held at a constant temperature	Physicochemical compatibility of API and excipient. Stoichiometry of solvates
Chromatographic analysis e.g. HPLC	Chemical interaction between sample and the stationary and mobile phase	Purity of the sample and drug-excipient compatibility
X-Ray Diffraction (XRD)	Scattering of X-rays by solid material	Characterisation of crystalline materials
Scanning Electron Microscopy (SEM)	Magnified appearance of a sample	Particle size and morphology
Fourier Transform Infrared Spectroscopy (FTIR)	Different functional groups in a molecule absorb at different frequencies	Characterisation of functional groups , drug-excipient compatibility
Hot Stage Microscopy	Magnified appearance of a sample	Study solid state transition

3.4 DRUG-EXCIPIENT INTERACTIONS

The exact mechanism by which drug-excipient interactions occur is not clear however there are a vast number of well documented interactions that have been reported [306,312–314].

Drug-excipient interactions may be beneficial or detrimental and are classified as physical or chemical interactions [264,306,315].

3.4.1 Physical interactions

Physical interactions are common but difficult to identify and these interactions are normally observed during manufacture [300,316]. Physical interactions include complexation, adsorption, and solid dispersion [308,317,318]. Complexation occurs when a complexing agent binds to an API and in some cases insoluble complexes may occur which may result in slow dissolution and reduced absorption of an API(s) [300,306,318]. However, complexing agents are used to enhance performance. For example cyclodextrin is used to improve the bioavailability of poorly water soluble drugs [306,319]. Adsorption of an API by an excipient may be detrimental. By way of example cetyl pyridinium chloride cations adsorb onto the surface of magnesium stearate resulting in a reduction in the antibacterial activity of the preservative since the compound is not available for dissolution [315,318,320]. Solid dispersions may increase the dissolution and bioavailability of hydrophobic drugs and the dissolution of drugs such as piroxicam, norfloxacin and ibuprofen improve when formulated in solid dispersions with polyethelyne glycol [263,321–324].

3.4.2 Chemical interactions

Chemical interactions are detrimental to the stability and performance of a product as they often result in the formation of unstable molecules and/or degradation products [315]. Drugs with ester, amide and lactone functional groups are susceptible to hydrolytic degradation [325]. For example stearate salts such as magnesium stearate should not be used as a tablet lubricant if an API is susceptible to hydrolysis via an ion catalysed reaction process [306,326]. Oxidative degradation is more complex when compared to hydrolysis and involves the removal of an electro-positive atom, radical or addition of an electronegative moiety [306,325]. A good approach to ensuring stability is to avoid excipients that contain oxidative species such as peroxide and fumed metal oxides such as silica. Polyethylene glycols and povidone contain organic peroxides that precipitate degradation of compounds susceptible to oxidation [285,302,306]. Hartauer *et al.,* reported that peroxide impurities found in povidone resulted in the degradation of raloxifene hydrochloride [327]. Aldehyde-amine addition is the cause of incompatibility between excipients that contain reducing sugars and drugs with amine groups and include lactose and dextrose [315,328]. The aldehyde-amine formation results in the formation of a Schiff base that further cyclises to form a glycosamine followed by Amadori rearrangement [306]. This is also known as a

Maillard reaction and is observed in a large number of incompatibility reactions between excipients and API [315].

3.5 SCANNING ELECTRON MICROSCOPY (SEM)

Scanning Electron Microscopy generates images by scanning a sample with a beam of electrons [329]. Interactions between the electrons and sample results in signals that have information about the topography and composition of the surface of a sample [330].

Gaining knowledge of the particle size and shape of a material are an important aspect of preformulation studies as the size and shape of materials, can and often do have an effect on the bulk properties of a powder. Differences and or variations in the size distribution and shape of a powder also affect the flow properties of a powder and may have a significant effect on the manufacturing process [331,332]. The particle size and shape of materials was determined using a Tescan, SEM (Vega LMU, Czechoslovakia Republic) and the surface morphology of MTZ and potential excipients visualised. The particle size was measured using image analysis software (Olympus®, Tokyo, Japan)The powder material was loaded onto a carbon stub and sputter coated with gold under vacuum for 15 minutes using a sputter-coater (Balzers Union Ltd, Balzers, Lichtenstein). The coated samples were then visualised using a Model TS 5136 LM Vega® Tescan SEM (Tescan, Vega LMU, Czechoslovakia) at a voltage of 20 kV. The particle shape of each of the excipients used in these studies is depicted in Figure 3.1I, II, III and IV.

The SEM micrographs in which the particle size of MTZ is reported are depicted in Figure 3.2 I, II, III and IV and a summary of the particle size distribution of MTZ and excipients is listed in Table 3.3.

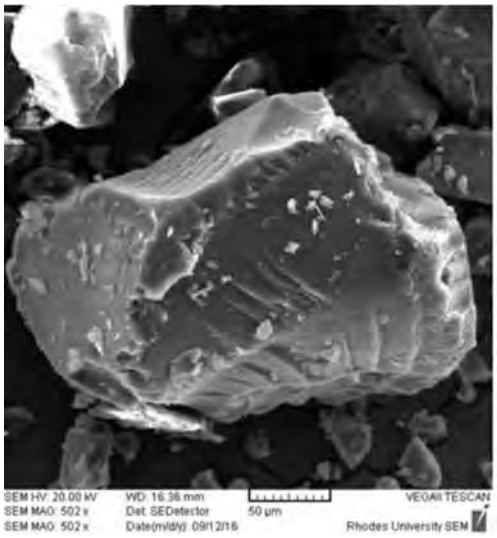

I

II

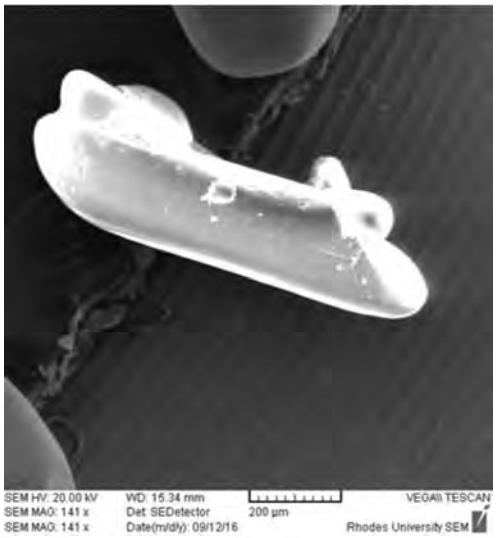

III

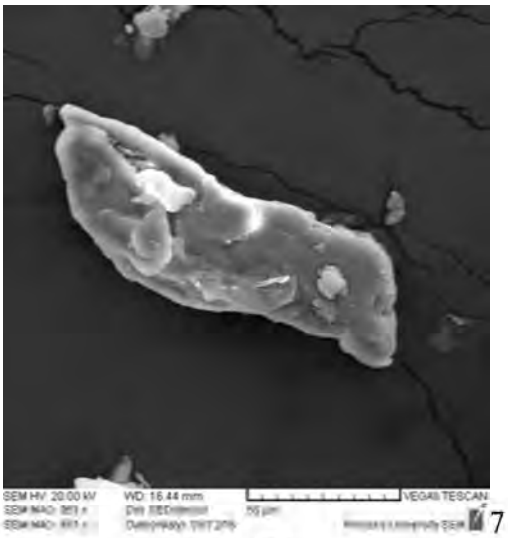

IV

Figure 3.1 Typical SEM micrographs of the particle morphology of (I) Eudragit® RS PO, (II) Avicel® PH 102, (III) MTZ and (IV) Methocel® K15M (IV)

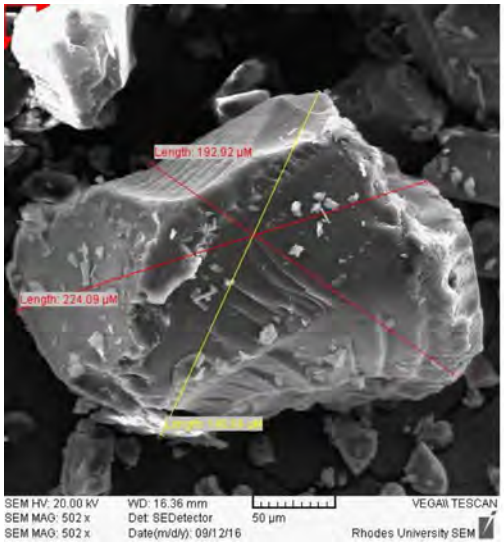

I II

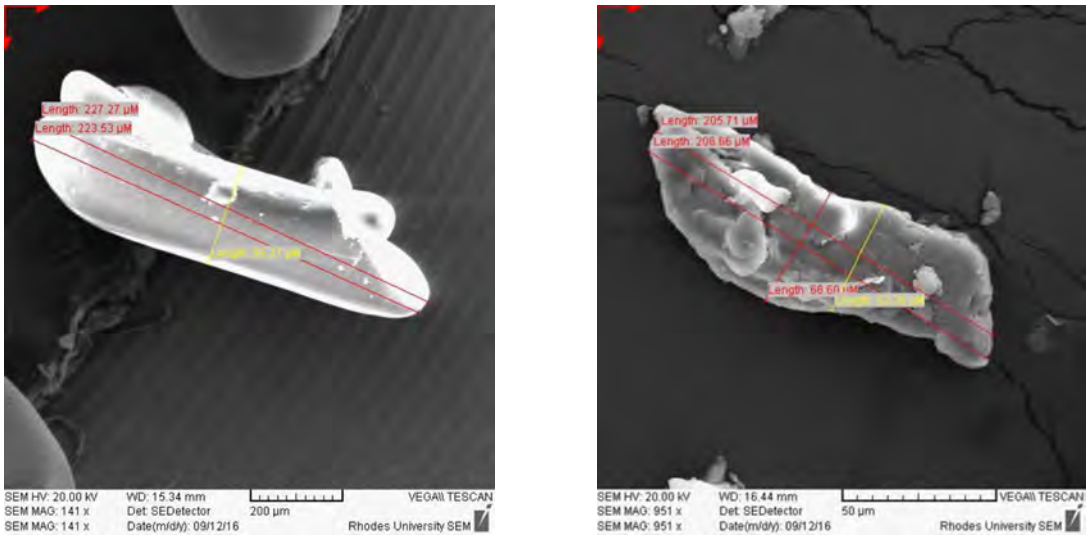

III IV

Figure 3.2 SEM micrographs depicting the particle size of (I) Eudragit® RS PO, (II) Avicel® PH 102, (III) MTZ and (IV) Methocel® K15M

Table 3.3 Summary of the particle size distribution of MTZ and excipients

Material	Particle Size Range (µm)
Eudragit®RS PO	197-224
Avicel® PH 102	190-224
Metronidazole	141-227
Methocel® K15M	199-206

The SEM image of Eudragit® RS PO particles depicted in Figure 3.1 (I) reveals that the particles are sub-angular with low sphericity. Avicel® PH 102 (Figure 3.1 II) particles are angular with no sphericity and MTZ (Figure 3.1(III)) are prism or polyhedral shaped particles. Methocel® K15M (Figure 3.1 IV) particles occur as angular like flakes with low sphericity. The data reveal that most excipients had a wide particle size distribution with highly variable particle size and poor sphericity suggesting the potential for poor powder flow. Poor sphericity means that there is a likelihood of poor flow and non-uniformity. Therefore sieving of the excipients and MTZ to ensure a uniform particle size distribution was considered appropriate for the manufacturing process.

3.6 FOURIER TRANSFORM INFRARED SPECTROSCOPY (FTIR)

Infrared spectroscopy makes use of the fact that many molecules absorb infrared radiation at frequencies that are a characteristic of their chemical structure and is based on the absorption of infrared radiation by molecules due to vibrational states of particular functional groups in a molecule [333,334]. FTIR is used to study the molecular structure of compounds and pharmaceutical product(s) [334]. FTIR is a specific type of infrared spectrophotometry and an infrared spectrum is a plot of infrared light intensity or %T versus wave number cm^{-1} [335]. FTIR is used to reveal potential interactions at a molecular level as specific functional groups vibrate at specific frequencies [306].

A Spectrum 100 FTIR spectrophotometer (Perkin-Elmer® Pty Ltd, Beaconsfield, England) was used to generate infrared spectra of potential excipients individually and in 1:1 mixtures of API and the excipient. The mixtures were prepared by physically mixing the components in a mortar and pestle. A small amount of each powder or powder blend was placed on a diamond crystal and a force of approximately 100 N was applied before analysis over the wavelength range 4000-650 cm^{-1} over 4 scans at a resolution of 4 cm^{-1}. The FTIR spectra for MTZ alone and in combination with each 1:1 mixture with an excipient are depicted in Figures 3.3-3.9. The FTIR spectrum for MTZ depicted in Figure 3.3 reveals the presence of characteristic bands at frequencies of 3211.61cm^{-1} due to an O-H stretch and at 3100.17 cm^{-1} due to C=CH and C-H stretching. The peaks observed at 1354.42 cm^{-1} and 1534.03cm^{-1} correspond to nitro functional group vibration [21,37]. Further peaks at 1073.32cm^{-1} and 825.15cm^{-1}, are due to C-O and C-N stretching, respectively [21,36,38].

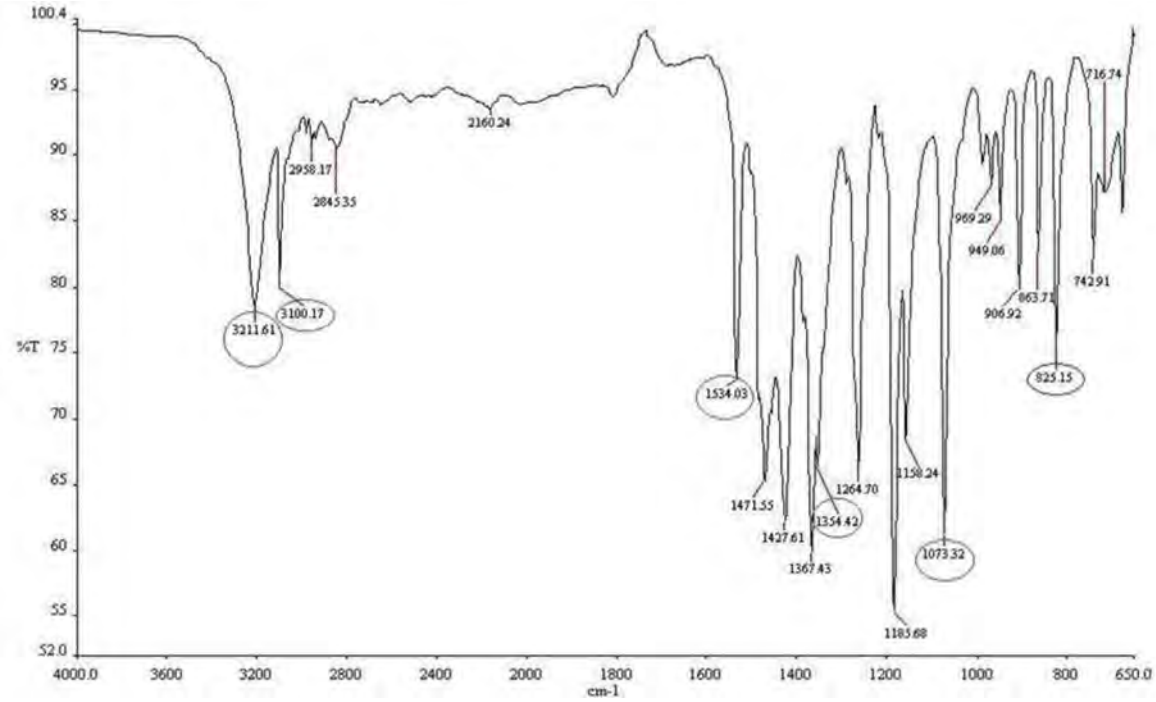

Figure 3.3 FTIR spectrum for MTZ

The spectrum generated for Eudragit® RS PO depicted in Figure 3.4 reveals the presence of an absorption band at a frequency of 1143.45 cm^{-1} due to ester groups and a peak at 1723.20 cm^{-1} due to a C=O ester vibration [336,337]. The peaks at 1236.44 cm^{-1} and 1446.59 cm^{-1} are due to C-O stretching and CH_3 bending respectively [338].

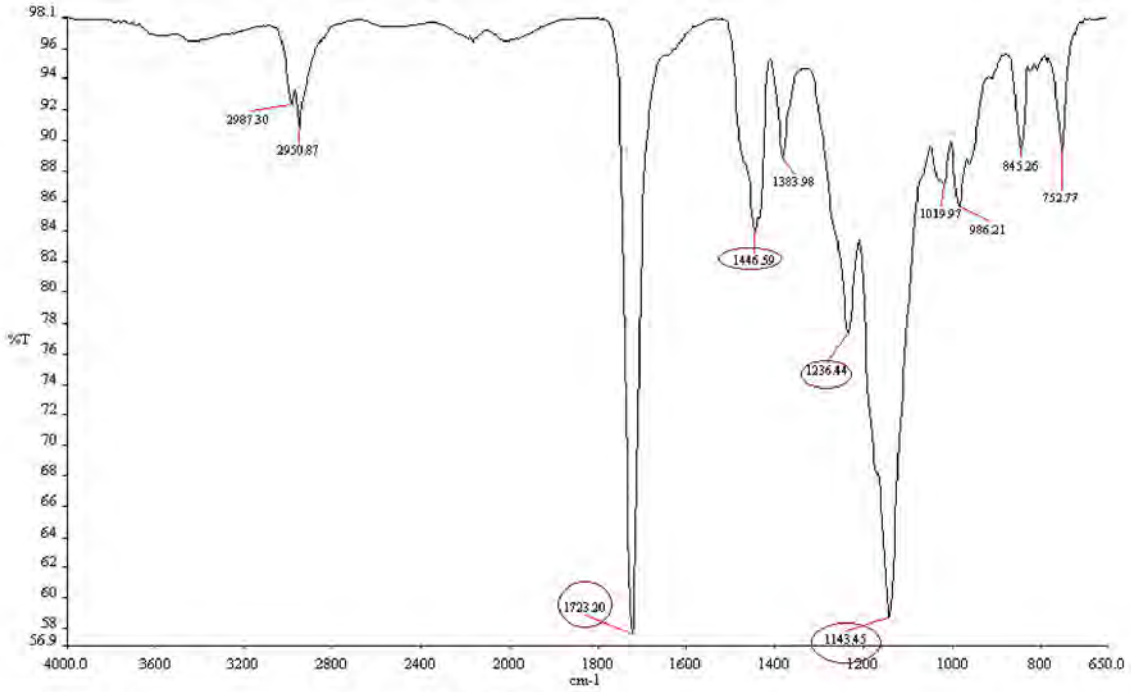

Figure 3.4 FTIR spectrum for Eudragit® RS PO

The spectrum for a binary mixture of Eudragit® RS PO and MTZ is depicted in Figure 3.5 reveals that intensity of peaks at 3210.12 cm^{-1},3100.11 cm^{-1} and 1073.98 cm^{-1} from MTZ were reduced in intensity due to the dilution effect due to mixing. All other peaks for MTZ and Eudragit® RS PO were observed in the spectrum of the binary mixture and no new additional peaks were observed. A slight change in the frequency of vibrations for the binary mixture was evident and this may be attributed to hydrogen bonding between MTZ and the excipient rather than a consequence of a chemical interaction.

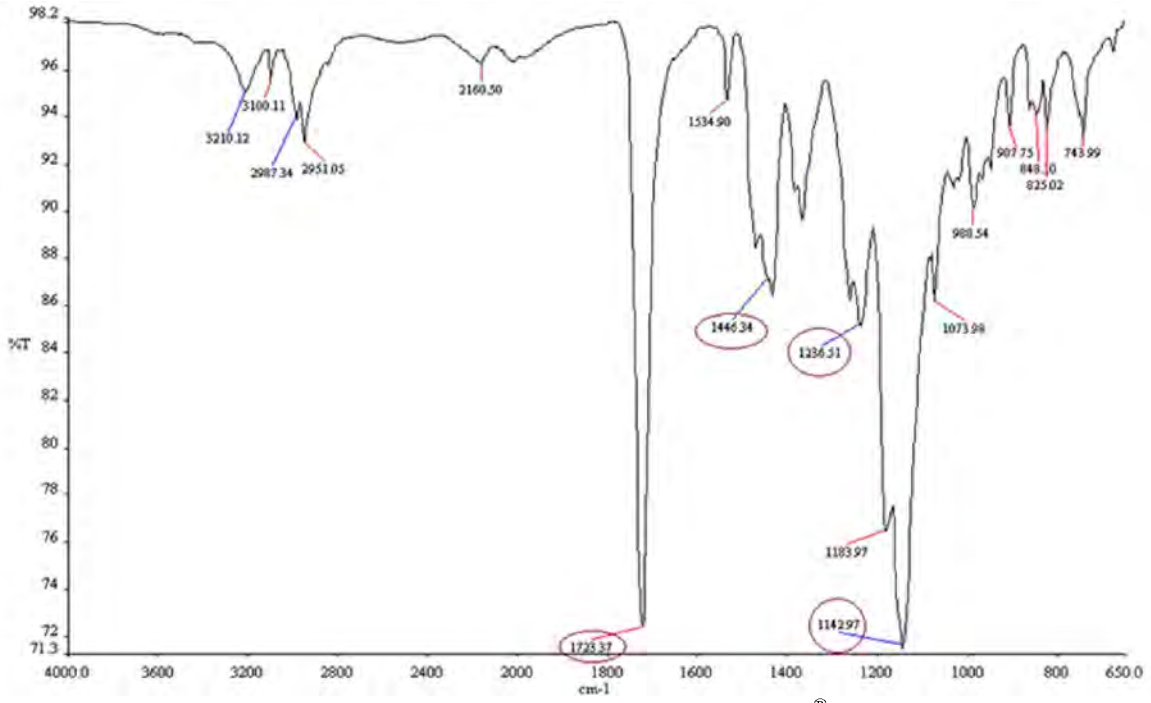

Figure 3.5 FTIR spectrum for a 1:1 binary mixture of MTZ and Eudragit® RS PO

The FTIR spectrum for Methocel® K15M is depicted in Figure 3.6 and the absorption bands at 3408.30 cm^{-1} and 2897.07 cm^{-1} are due to an OH and alkane stretch, respectively [339]. The peaks at frequencies of 1453.47 cm^{-1} and 1372.81 cm^{-1} are due to methyl C-H bending and stretching and the peak at 1051.23 cm^{-1} is due to an aliphatic C-O stretch [339,340].

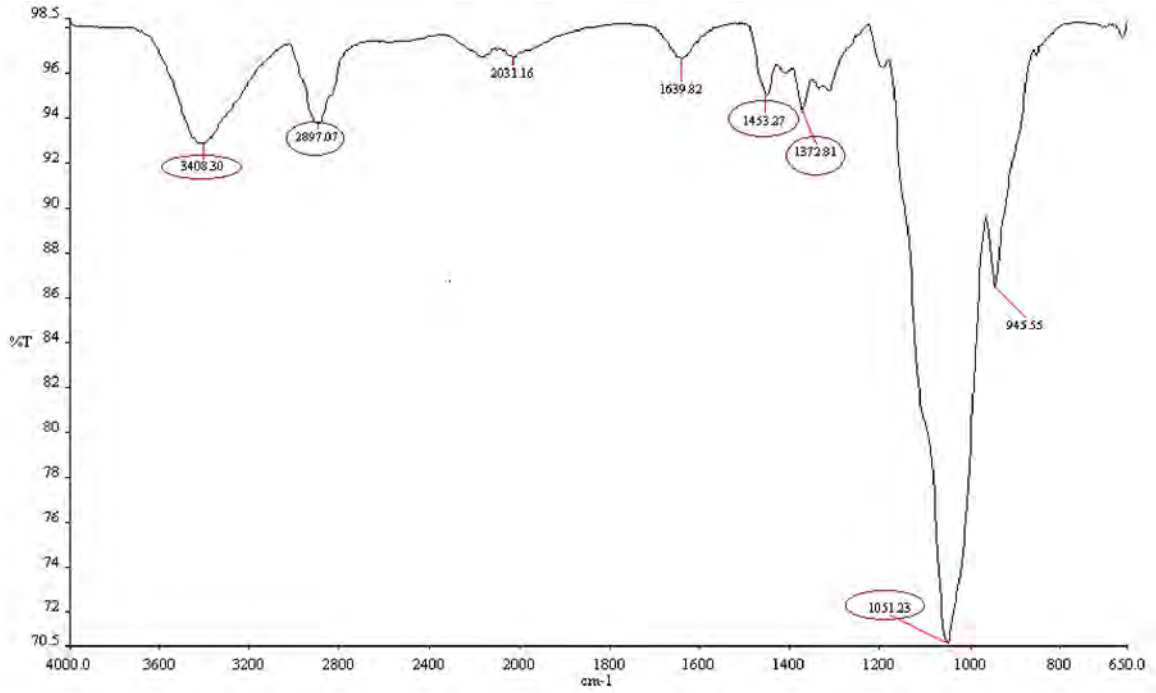

Figure 3.6 FTIR spectrum for Methocel® K15M

The spectrum of the binary mixture of MTZ and Methocel® K15M is depicted in Figure 3.7 and it is clear that the intensities of peaks at 3407.59 cm^{-1} and 2891.13 cm^{-1} are due to Methocel® K15M and are reduced in intensity due to the dilution effect of mixing the compounds in a 1:1 ratio. The peak at 1072.19 cm^{-1} in the binary mixture is quite broad and may be due to the fact that both MTZ and Methocel®K15M exhibit a C-O stretch in individual spectra. The spectrum for MTZ exhibits a peak at 1073.32 cm^{-1} and Methocel® K15M at 1051.23 cm^{-1} due to the C-O stretch and therefore a broad peak is observed in the spectrum for the binary mixture. All other peaks for MTZ and Methocel® K15M were observed in the spectrum for the binary mixture suggesting potential compatibility between these compounds.

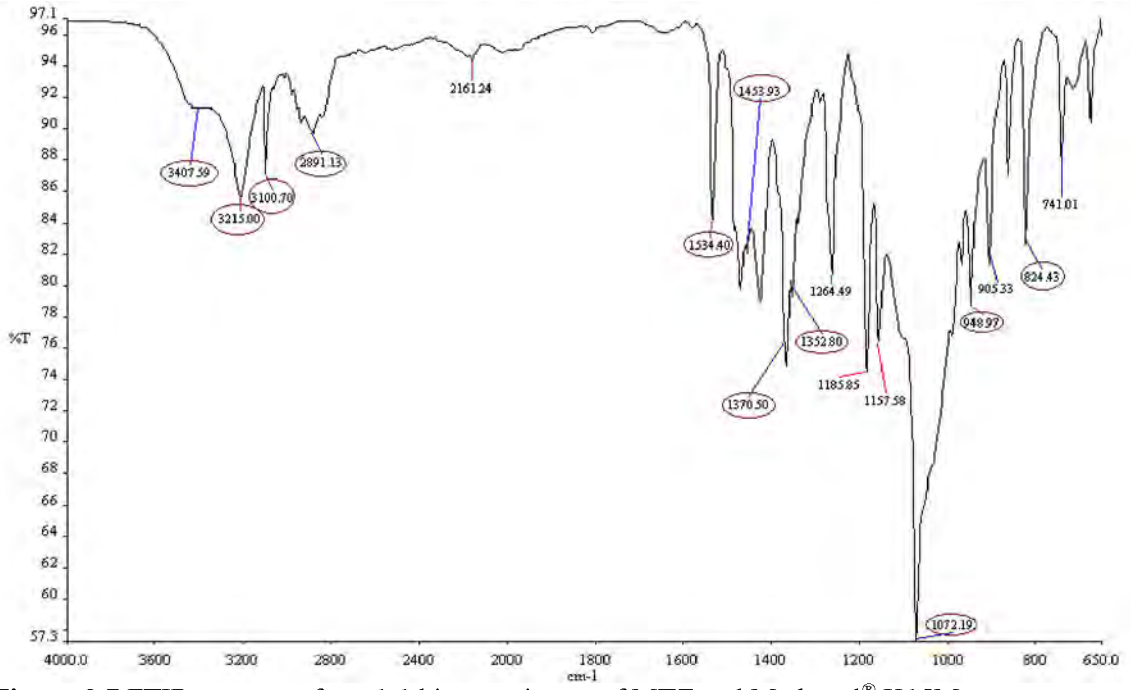

Figure 3.7 FTIR spectrum for a 1:1 binary mixture of MTZ and Methocel® K15M

The FTIR spectrum for Avicel® PH 102 is depicted in Figure 3.8 and the absorption bands at 3332.93 cm^{-1} and 2891.83 cm^{-1} are attributed to stretching of OH and symmetric stretching vibrations of CH, respectively [341] . The peaks at 1428.12 cm^{-1} and 1159.71 cm^{-1} are due to CH deformation of CH_2 and C-C stretching of the cellulose ether . The peaks at 1107.95 cm^{-1} and 1053.40 cm^{-1} are due to a C-H stretch [341].

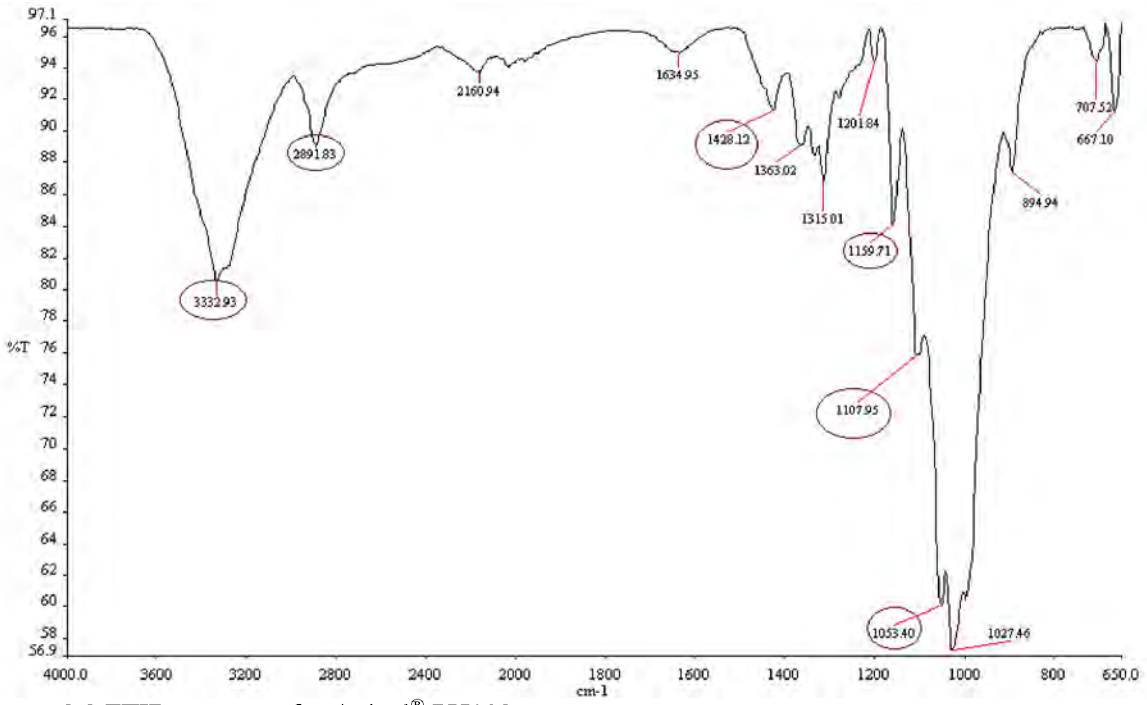

Figure 3.8 FTIR spectrum for Avicel® PH102

The spectrum of a binary mixture of MTZ and Avicel® PH 102 is depicted in Figure 3.9 and all relevant peaks for MTZ and Avicel® PH 102 were observed in the spectrum for the binary mixture.

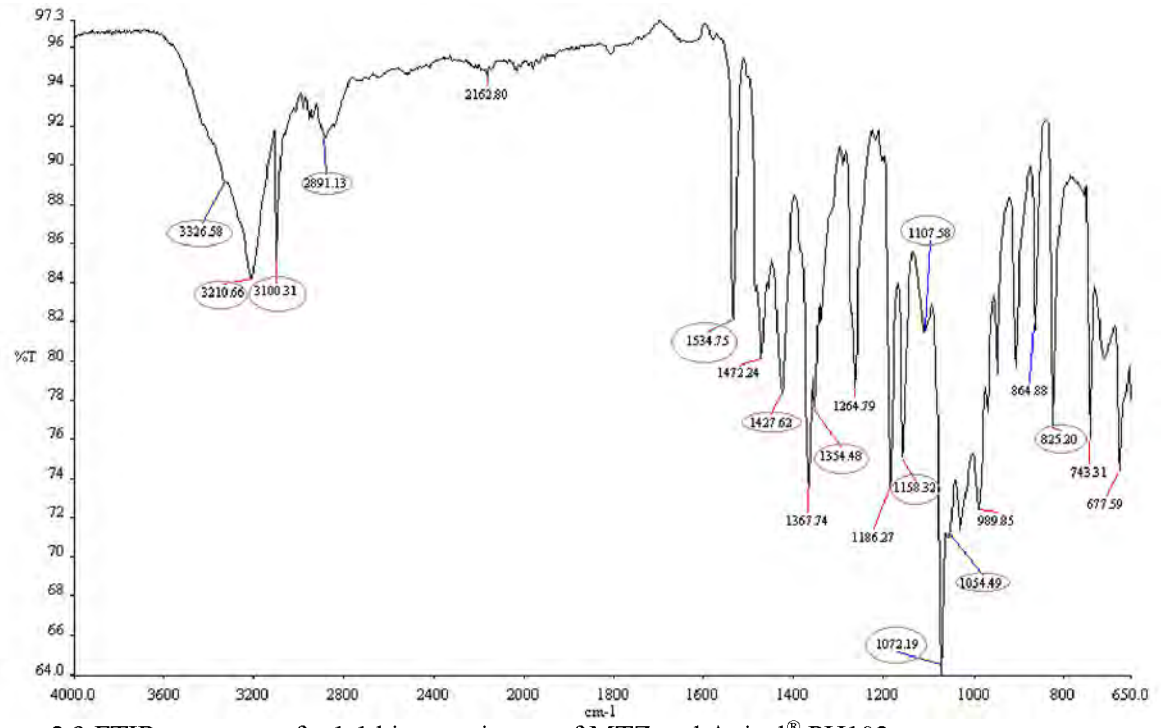

Figure 3.9 FTIR spectrum of a 1:1 binary mixture of MTZ and Avicel® PH102

The FTIR spectra for all binary mixtures revealed the presence of all absorption bands for MTZ and each of the excipients. No new or additional peaks were observed, however a slight shift in the frequencies of vibration were evident for all binary mixtures and may be attributed to hydrogen bonding between MTZ and the excipient.

3.7 DIFFERENTIAL SCANNING CALORIMETRY (DSC)

Calorimetry is a technique used to measure thermal properties of materials in order to establish a correlation between temperature and the physical properties of materials and is the only direct approach for the determination of the enthalpy of a specific process [342]. Caloric measurements have been undertaken since the 18th century and a number of types of calorimeters are available for use of which DSC is a modern and popular approach and used today [343]. DSC is a thermal analysis approach that measures changes in the physical properties of a sample as temperature is altered over time [343]. DSC measures temperature and heat flow associated with transition of materials transition as a function of time and temperature [344]. As the temperature changes the instrument measures the quantity of heat radiated or absorbed by a sample based on the temperature difference between the sample and

a reference material [342]. The sample is enclosed in an aluminium pan and the reference is usually an empty pan. Heat energy is simultaneously applied to the sample and reference pans at a linear heating rate and the difference in energy required to match the temperatures of the sample and reference is the excess amount of heat absorbed for endothermic or released for exothermic events from the sample [343,345]. DSC has been used for a number of applications including analysis of polymers and plastics, food, glasses, ceramics, pharmaceuticals, proteins and nanoscience [343]. DSC is a useful tool in the pharmaceutical industry and permits rapid evaluation of possible incompatibilities between potential formulation components and API [346]. Changes in temperature and relative humidity that occur during processing and storage of pharmaceuticals and changes in the solid state may have a considerable effect on activity, toxicity and stability of compounds [346,347]. Modelling of such conditions is therefore of high importance and changes in individual substances and mixtures can reveal potential and unexpected phenomena [347].

DSC scanning was performed using a Model DSC 6 (Perkin Elmer®, Norwalk, USA) and the scans were generated between 30-445°C at a heating rate of 10°C/min with a nitrogen flow rate of 20 ml/min and a sealed aluminium pan as the reference. The data was analysed using Pyris 6000 software (Perkin Elmer®, Johannesburg, South Africa). The mixtures were prepared by physically mixing the components in a mortar and pestle. Approximately 2.5-5 mg powder to be tested and 1:1 binary mixtures of MTZ and excipients were weighed directly into DSC aluminium pans, sealed and analysed and the resultant thermograms are depicted in Figures 3.10-3.16. The DSC thermogram for MTZ depicted in Figure 3.10 reveals a melting endotherm at 163.67 °C with an enthalpy or ΔH of 210.5630 J/g and a broad endotherm at 252.91 °C with a ΔH of 7.6603 J/g. These data are in close agreement with previously reported DSC information [21,42].

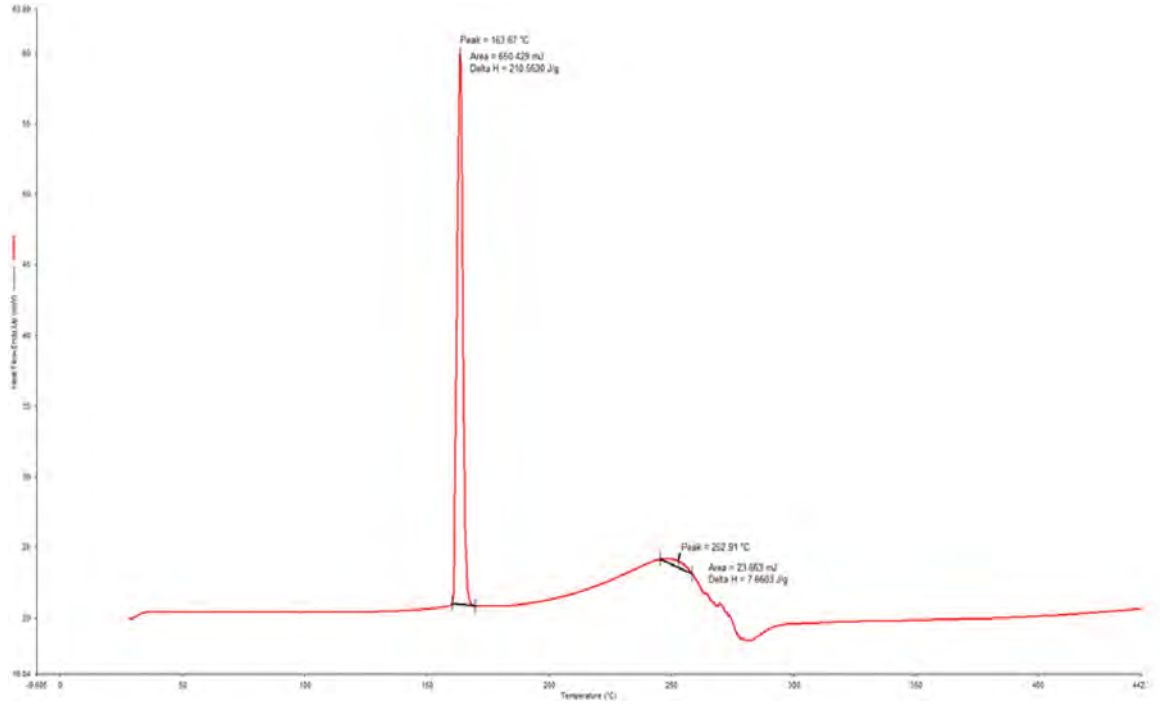

Figure 3.10 DSC thermogram for MTZ

The DSC thermograms for Eudragit® RS PO alone and the 1:1 binary mixture of MTZ and Eudragit® RS PO are depicted in Figures 3.11 and 3.12. No significant enthalpy changes were observed for Eudragit® RS PO until approximately 390°C where an endotherm at 393.23 °C with ΔH of 410.9740 J/g was observed.

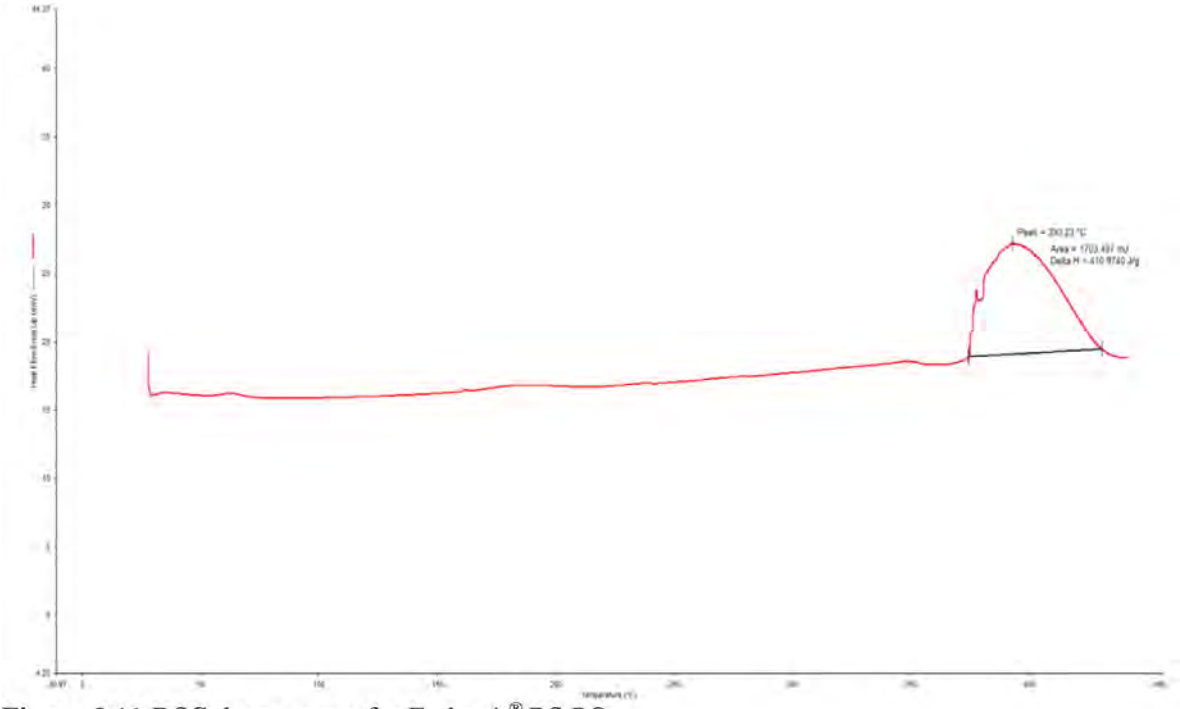

Figure 3.11 DSC thermogram for Eudragit® RS PO

The thermogram for the 1:1 binary mixture of MTZ and Eudragit® RS PO is depicted in Figure 3.12 and all relevant endotherms for MTZ and Eudragit® RS PO were observed in the thermogram for the mixture suggesting that there are no interactions between Eudragit® RS PO and MTZ and thus Eudragit ® RS PO is compatible with MTZ.

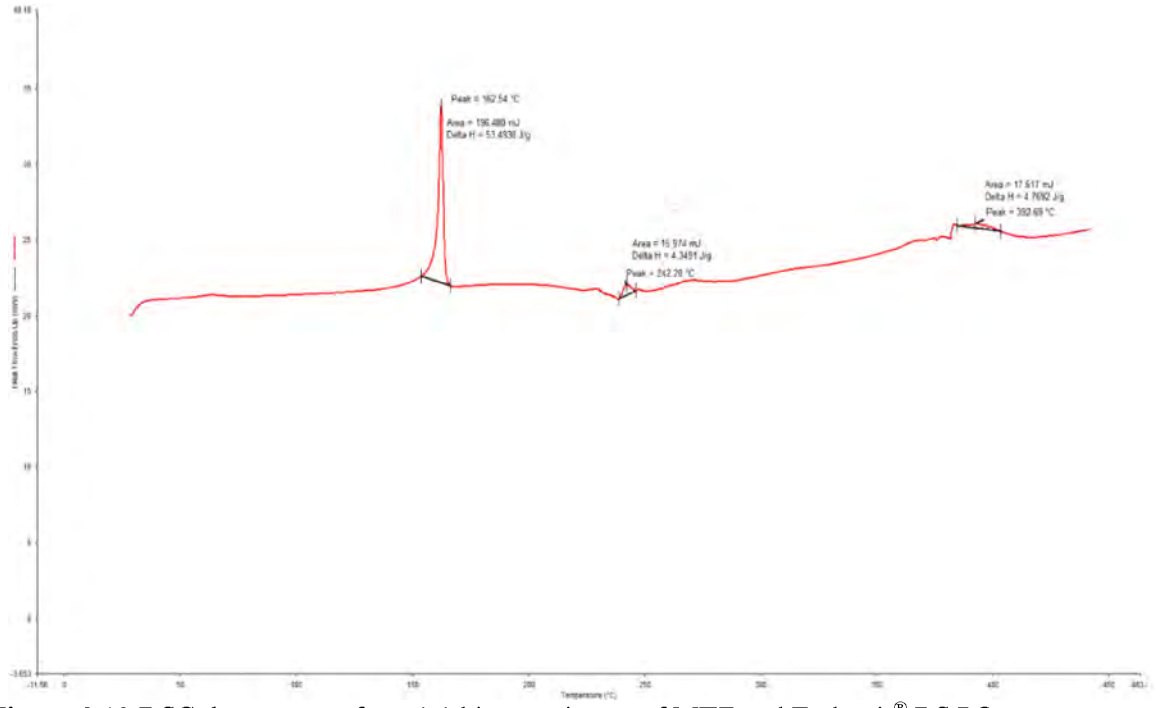

Figure 3.12 DSC thermogram for a 1:1 binary mixture of MTZ and Eudragit® RS PO

The DSC thermograms for Methocel® K15M and a 1:1 binary mixture of MTZ and Methocel® K15M are depicted in Figures 3.13 and 3.14. The thermogram for Methocel® K15M shows a melting endotherm at 53.90 °C with ΔH of 81.8871 J/g that is in close agreement with a previously reported melting point [348].

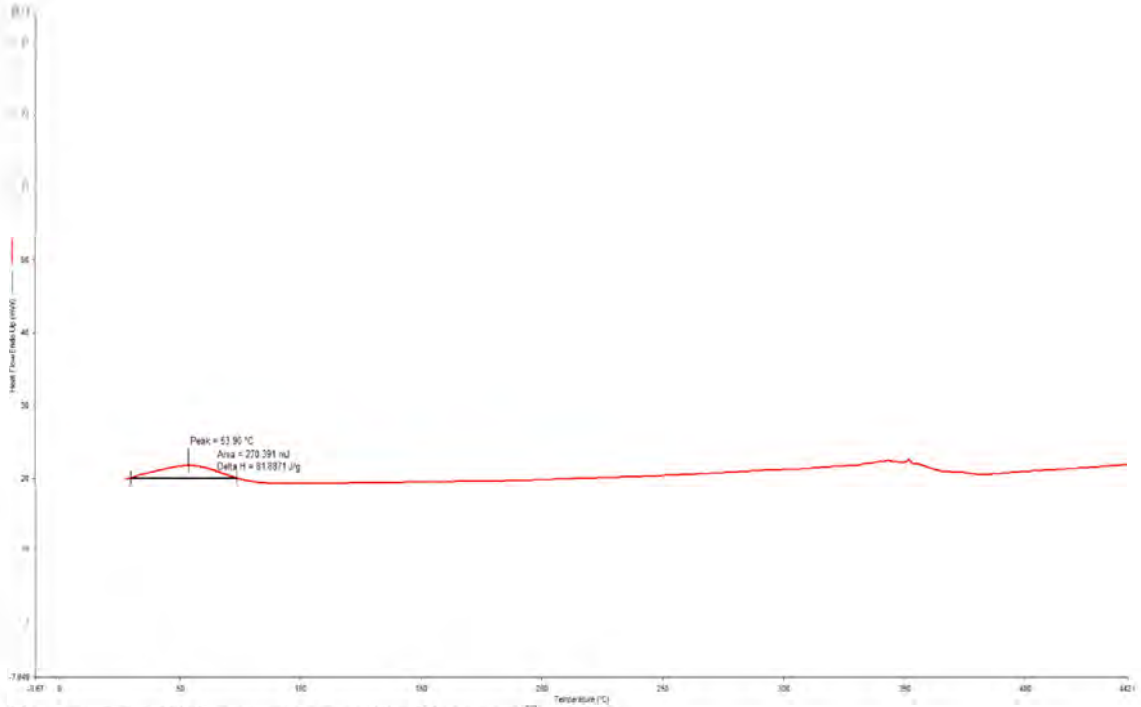

Figure 3.13 DSC thermogram for Methocel® K15M

The DSC thermogram for the binary mixture of MTZ and Methocel® K15M reveals endothermic peaks for MTZ and Methocel® K15M suggesting compatibility between the compounds.

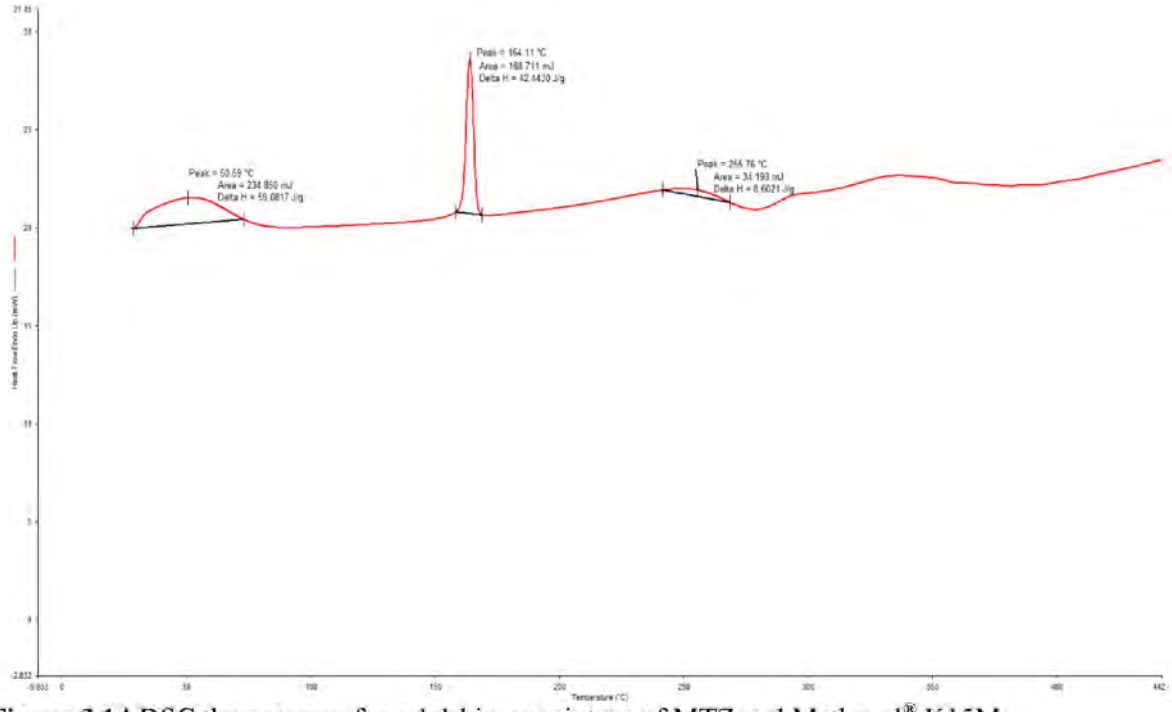

Figure 3.14 DSC thermogram for a 1:1 binary mixture of MTZ and Methocel® K15M

The DSC thermograms for Avicel® PH 102 and a 1:1 binary mixture of MTZ and Avicel® PH 102 are depicted in Figures 3.15 and 3.16. The DSC thermogram for Avicel® PH 102

revealed no significant enthalpy changes until approximately 349 °C where a melting endotherm was observed at 349.23 °C with a ΔH of 469.1047 J/g.

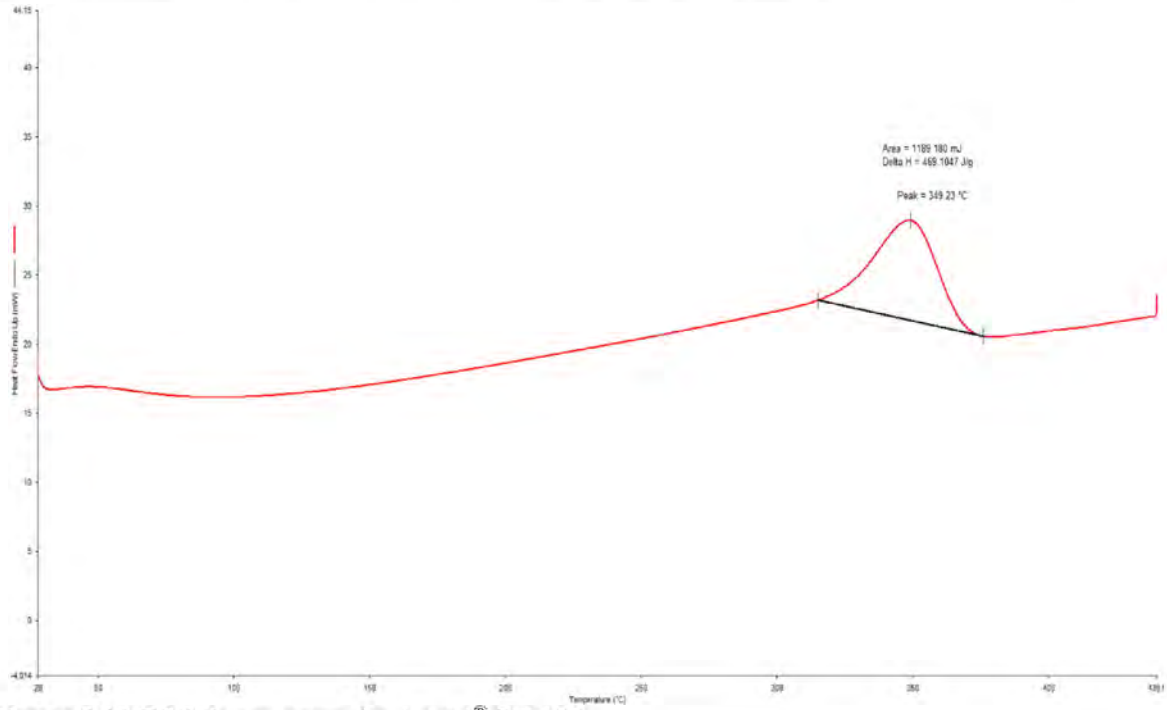

Figure 3.15 DSC thermogram for Avicel® PH 102

The DSC thermogram for the 1:1 binary mixture of MTZ and Avicel® PH 102 revealed the presence of both endotherms for MTZ and an endotherm for Avicel® PH 102.

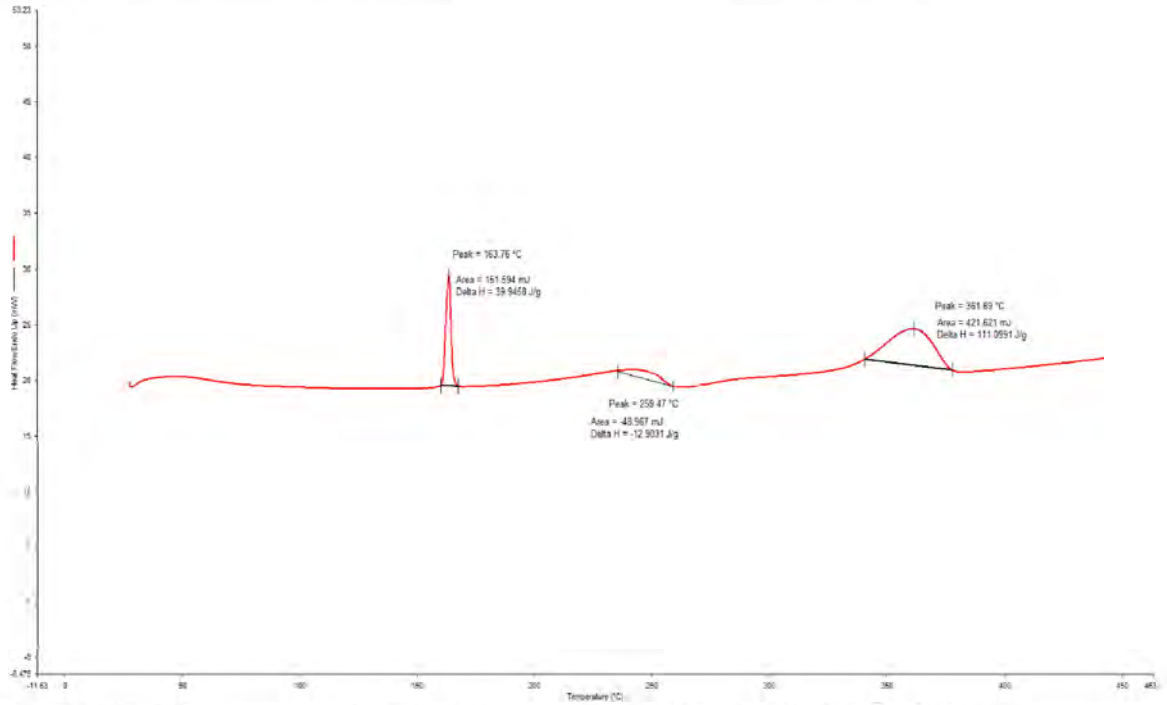

Figure 3.16 DSC thermogram for a 1:1 binary mixture of MTZ and Avicel® PH 102

The DSC study of binary mixtures of API and excipients revealed that no potential interactions are likely between MTZ and the excipients, however real time studies should be conducted to ensure that this is indeed the case.

3.8 X-RAY DIFFRACTION (XRD)

Approximately 95% of all solid materials are crystalline in nature and can be classified based on the manner in which particles occupy the crystal lattice and the type of intermolecular forces that hold the lattice together [349,350]. When a crystalline material is exposed to X-rays a diffraction pattern results. Crystalline substances act as a three-dimensional diffraction grating for X-rays that are of a wavelength similar to the spacing planes of the crystal lattice. XRD is a rapid analytical technique that is used to identify crystalline materials in addition to providing information about the dimensions of the unit cell [351]. The XRD pattern is regarded as a fingerprint for a substance and is useful for the characterisation and identification of polycrystalline phases [349]. X-ray radiation is a form of energy that travels as electromagnetic waves and as the rays pass through matter electrons in the molecule oscillate at the same frequency as the incoming radiation [350]. Destructive interference occurs when combined waves are out of phase with a result that no energy will leave the sample. If the atoms are in an organised plane, as with crystalline materials, constructive interference will occur and the resultant planes will be in phase and produce a well-defined X-ray beam that when emitted from the sample does so at characteristic angles based on the spaces between the atoms in the lattice. The diffraction pattern is obtained by plotting angular positions versus intensity of response [349,350,352].

The mixtures were prepared by physically mixing the components in a mortar and pestle. XRD studies of MTZ, individual excipients and 1:1 mixtures of MTZ and excipients were generated. X-ray powder diffraction patterns were generated at 22 °C using a Bruker D8 Discover X-ray diffractometer (Bruker AXS, Karlsruhe, Bundesland, Germany) with a proportional counter and Cu-K radiation of 1.5405 Å. Data was collected in the 2θ angle range of 10° to 100° at a scanning rate of 1° min^{-1}. The filter time constant and the slit width was 2.5 s per step and 6.0 mm, respectively. Samples were placed on a silicon wafer slide and were analysed and interpreted using XRD commander and EVA DIFFRAC.SUITE™ software (Bruker- AXS GmbH, Karlsruhe, Bundesland, Germany). The XRD diffractograms for all samples are depicted in Figures 3.17 - 3.23.

The XRD patterns for MTZ and Eudragit® RS PO are depicted in Figures 3.17 and 3.18 respectively and revealed the presence of characteristic peaks at 29.50° and 33.59° for MTZ and 14.96° for Eudragit® RS PO. The data suggests that MTZ is crystalline as the diffractograms in Figure 3.17 exhibited sharp high intensity peaks in the XRD pattern. The XRD pattern for Eudragit® RS PO (Figure 3.18) reveals the presence of a broad peak at 14.96° with low intensity indicating that Eudragit® RS PO is amorphous.

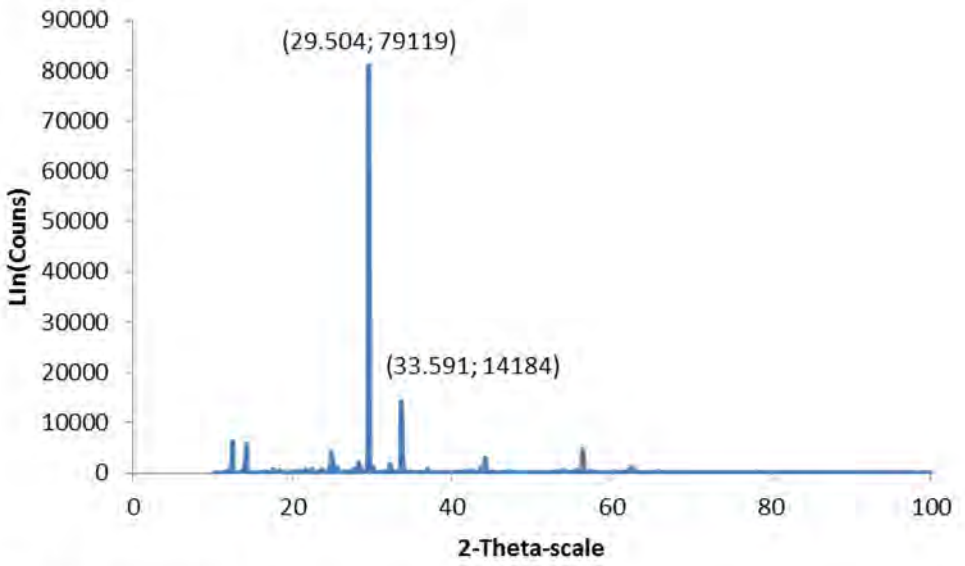

Figure 3.17 XRD pattern for MTZ

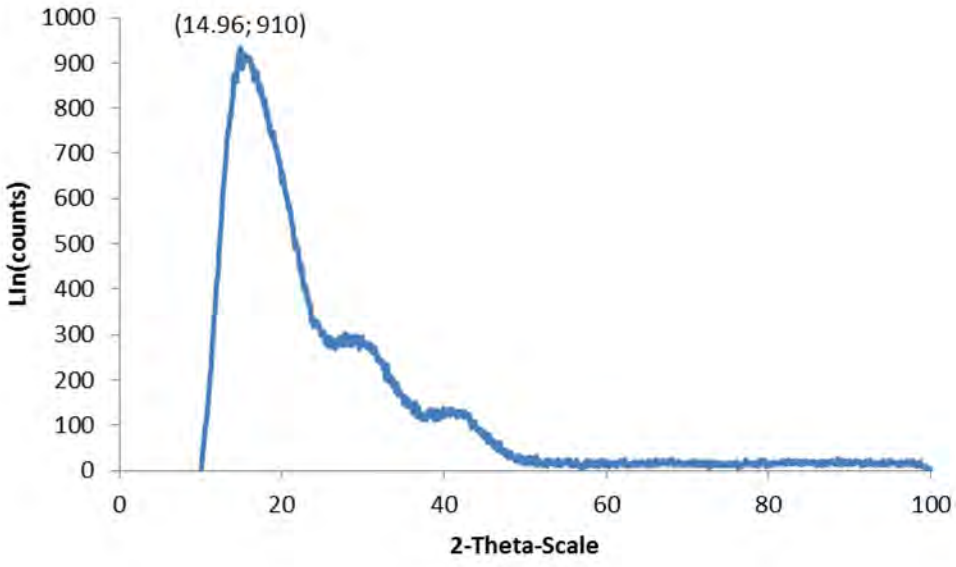

Figure 3.18 XRD pattern for Eudragit® RS PO

The XRD pattern for the 1:1 binary mixture of MTZ and Eudragit® RS PO is depicted in Figure 3.19. The reduction in the intensity of MTZ peaks in the 1:1 binary mixture could be due to dilution effect of mixing in a 1:1 ratio.

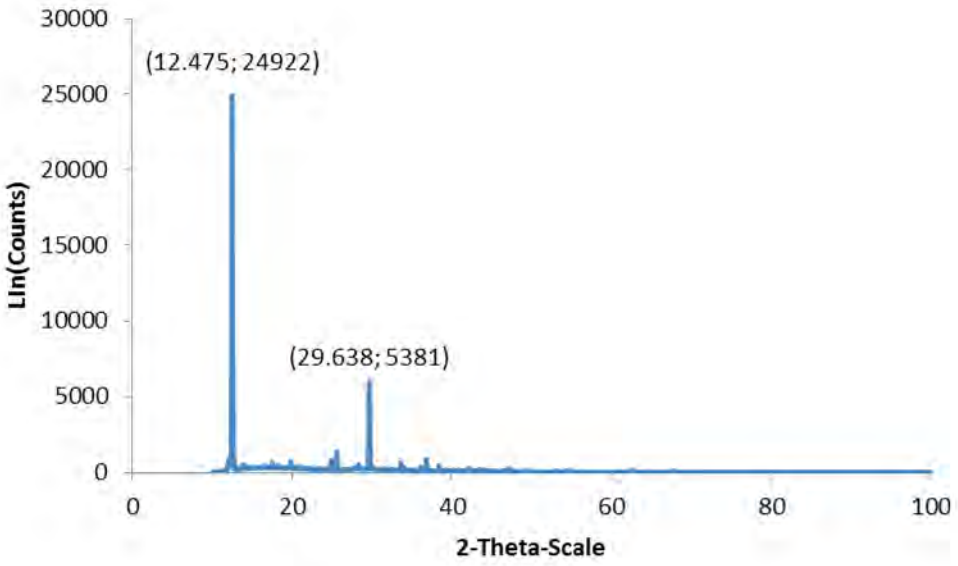

Figure 3.19 XRD pattern for a 1:1 binary mixture of MTZ and Eudragit® RS PO

The XRD patterns for Methocel® K15M and a 1:1 binary mixture of MTZ and Methocel® K15M are depicted in Figures 3.20 and 3.21 respectively. The XRD pattern for Methocel® K15M reveals the presence of a broad peak at 19.76° with a low intensity indicating the material is amorphous.

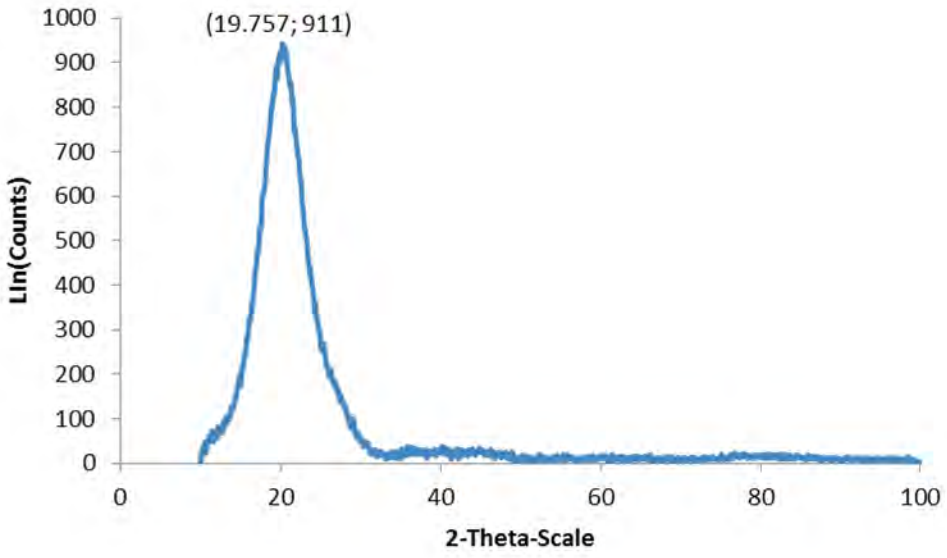

Figure 3.20 XRD pattern for Methocel® K15M

The XRD pattern for the 1:1 binary mixture of MTZ and Methocel® K15M reveals that the intensities of the peaks for MTZ are reduced and the peaks had slightly shifted. The reduction in intensity and slight shift of the peaks could be due to the dilution effect of mixing in a 1:1 ratio. A slight shift of the peaks may be attributed to hydrogen bonding rather than a chemical interaction.

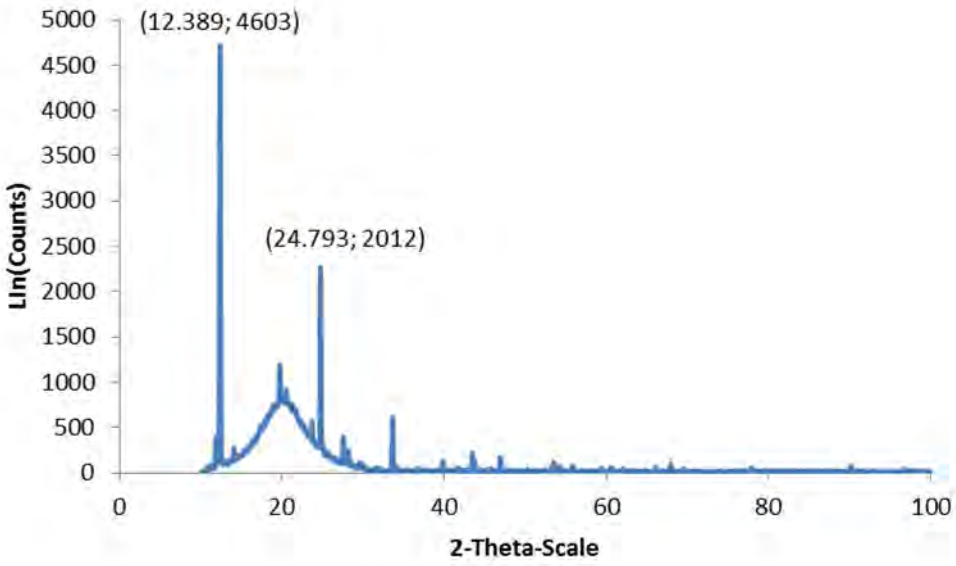

Figure 3.21 XRD pattern for a 1:1 binary mixture of MTZ and Methocel® K15M

The XRD patterns for Avicel® PH 102 and a 1:1 binary mixture of MTZ and Avicel® PH 102 are depicted in Figures 3.22 and 3.23 respectively. The XRD pattern for Avicel® PH 102 reveals the presence of a peak at 22.62° and 34.74° and the peaks are sharp and exhibit high intensities indicating that Avicel® PH 102 is crystalline.

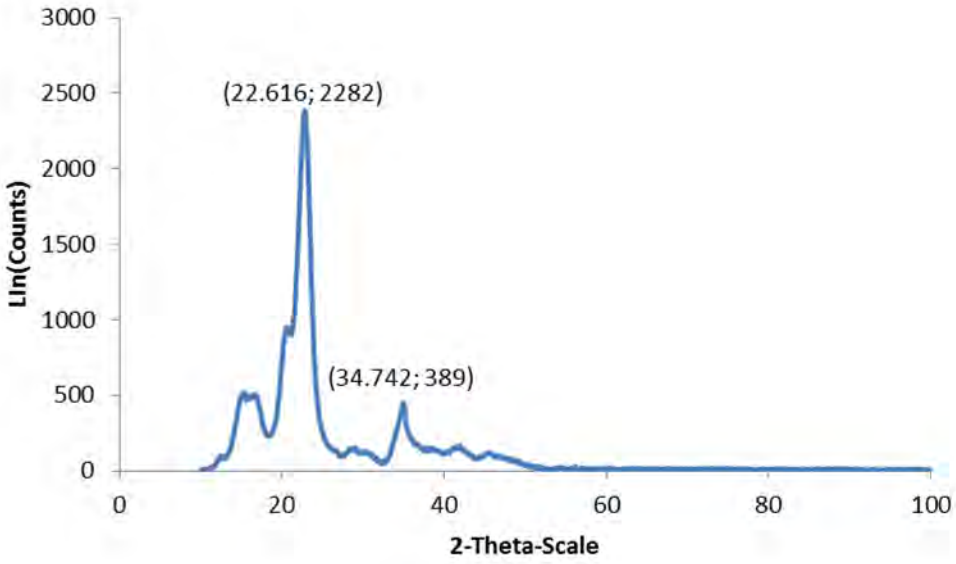

Figure 3.22 XRD pattern for Avicel® PH 102

The XRD pattern for the 1:1 binary mixture of MTZ and Avicel® PH 102 (Figure 3.23) reveal the presence of four characteristic sharp high intensity peaks at 12.46°, 14.04°, 25.56° and 27.62° indicating that both MTZ and Avicel® PH 102 exist as crystalline materials in the mixture. This means that the crystallinity of MTZ was not reduced by Avicel® PH 102 as the peaks showed high intensities.

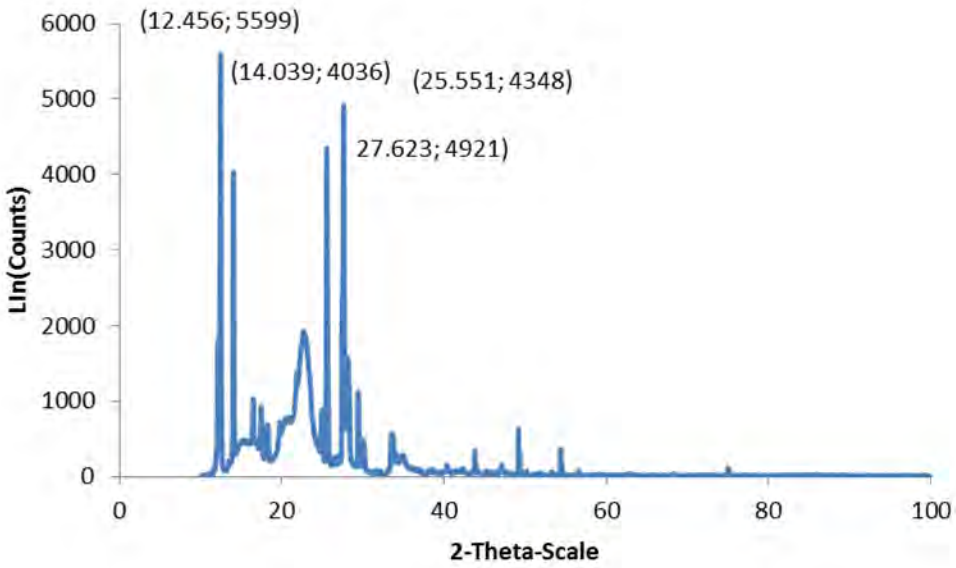

Figure 3.23 XRD pattern for a 1:1 binary mixture of MTZ and Avicel® PH 102

3.9 CONCLUSIONS

In order to undertake successful formulation processes, it is important to select appropriate excipients to ensure that a desirable high quality dosage form can be produced. Interactions between an API and pharmaceutical excipients must be identified early during product development studies to maximise the opportunity to produce quality formulations.

SEM studies revealed that MTZ and excipients exhibited a wide variation in particle size and therefore sieving of excipients and MTZ was undertaken to maintain a more uniform particle size distribution. SEM studies indicate that size reduction may also be done to ensure particles are the same size.

Infrared spectroscopic studies indicate that no interaction between MTZ and the excipients tested was likely as the major peaks for MTZ and each of the excipients were present in the 1:1 binary mixtures of MTZ and each excipient. The slight shifts observed in the absorption bands for the binary mixtures were not considered as significant and was attributed to hydrogen bonding between MTZ and individual excipients and not due to an undesirable chemical interaction.

Differential scanning calorimetry studies revealed that there were no potential interactions between MTZ and individual excipients when exposed to temperatures between 30°C and 445°C and a melting endotherm for MTZ was observed in all thermograms of 1:1 binary mixtures .

The data from XRD studies for MTZ and Avicel® PH 102 revealed the presence of sharp distinct peaks of high intensity indicating the materials are crystalline. The XRD patterns for MTZ in combination with Methocel® K15M showed a slight shift in MTZ peaks which may be attributed to hydrogen bonding and a reduction in peak intensity for MTZ which can be attributed to a dilution effect of mixing in a 1:1 ratio, however the FTIR and DSC studies indicate that there was no evidence of incompatibility between MTZ and Methocel® K15M.

The theoretical basis for DSC and FTIR analysis for the study of possible drug-excipient interactions has been applied to MTZ and three potential excipients and the results reveal that the probability of detrimental interactions between MTZ and the selected excipients is low although real time studies may be required to rule out potential incompatibility reactions. The data generated from these studies clearly indicate that the excipients considered for use are compatible with MTZ and were suitable for use in formulation development studies.

CHAPTER FOUR

FORMULATION DEVELOPMENT AND ASSESSMENT OF METRONIDAZOLE MICROCAPSULES

4.1 INTRODUCTION

Developing products for new chemical entities (NCE) can be a challenging, time consuming, and expensive process [353,354]. In addition, lead times for market access for NCE are often prolonged. Therefore there is increasing emphasis on developing and improving drug delivery systems for well-known therapeutic molecules [353,354].

A number of studies relating to the use of controlled release formulations to improve clinical benefits of well-known compounds have been conducted [355–360]. The advantages of controlled release formulations over conventional delivery approaches include an increased duration of therapeutic activity, reduction in the occurrence of drug-related adverse effects and the achievement and maintenance of optimal plasma concentrations [353]. In addition, these formulations are more convenient to immediate release dosage forms as they may reduce frequency of administration leading to less complex dosing schedules and improving patient adherence [353,354,361].

Even though controlled release dosage forms exhibit advantages, there are disadvantages such as, for example, if the integrity of the dosage form is compromised the entire dose may be released at once and the patient may be exposed to toxic API levels due to dose dumping [353]. In addition, once administered, API release from the dosage form cannot be stopped [353,362]. Furthermore, the cost of formulating controlled release dosage forms is generally more expensive when compared to formulating conventional dosage forms [353,362].

Two examples of modified release dosage forms include sustained and delayed release formulations [353]. Sustained release formulations release only a portion of the dose immediately following administration and the remaining dose over a period of time [353]. By contrast, delayed release formulations are designed to delay API release until the dosage form reaches a specific target area of in the gastro-intestinal tract prior to delivering the payload [283,353].

4.2 MICROENCAPSULATION

4.2.1 Overview

Microencapsulation is a technology approach in which solid, liquid or gaseous API are encapsulated using a polymeric material for the purposes of protecting that API from the surrounding environment [363]. The API is located in the core and the coating polymeric material forms the outer shell [363]. Microcapsules are minute heterogeneous carriers that are generally spherical in shape when the payload is a liquid and irregularly shaped when the payload is solid [364]. The microencapsulation process originated in 1930s, when a clean substitute for carbon paper and carbon ribbons was needed by the business machines industry and was first introduced in 1950s when pressure sensitive dye microcapsules for the manufacture of carbonless copying paper were commercialised [365]. Carbonless copy paper is still produced using this approach and many microcapsule products have been developed since then [363]. Microencapsulation has been applied in the pharmaceutical, cosmetic, food additive and biotechnology industries [366]. The term 'microparticle' refers to a particle with a diameter of 1-1000 μm irrespective of the interior or exterior structure [367]. In contrast the term 'microcapsule' refers to a spherical particle with size ranging between 50 nm and 2 mm containing a core substance surrounded by a material distinctly different from the core that may be solid, liquid or gas [367]. A microsphere specifically refers to spherical microparticles. The terminology used to define micro-particulate formulations is inconsistent,

however, and many researchers use these terms interchangeably [367]. The term 'capsule' implies a core located in a shell structure. However, the term microcapsule encompasses not only membrane enclosed particles, but also dispersions in solid matrices that lack a distinctive external wall phase [367]. Microcapsules typically range in between 2 and 2000 μm that distinguishes them from smaller nanoparticles or nanocapsules [367].

Microcapsules are normally spherical in shape, however irregularly shaped particles do occur as the morphology of the microcapsules is, in part, dependent on the core material and process by which the shell forms. Microcapsules can be classified as mononuclear, multinuclear and matrix type microcapsules [368,369]. The different morphologies of microcapsules are schematically depicted in Figure 4.1 [369].

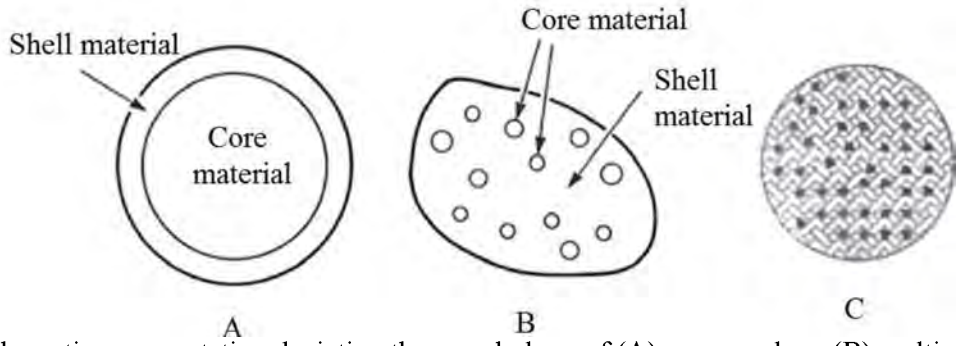

Figure 4.1 Schematic representation depicting the morphology of (A) mononuclear, (B) multinuclear and (C) matrix microcapsules[369]

Mononuclear microcapsules consist of a continuous shell around a continuous core and are also known as continuous core-shell microcapsules that exhibit spherical geometry [369]. Multinuclear microcapsules are also known as polynuclear microcapsules and exhibit an irregular shape as they contain small droplets or particles of core material; many cores are sometimes contained within a shell [369–371]. In matrix microcapsules the core is distributed homogeneously throughout the shell material [370].

Microencapsulation has been extensively studied by the pharmaceutical industry and research institutes [372]. Microencapsulation of pharmaceuticals was first investigated in 1931 when microspheres were developed and produced using coacervation. The pharmaceutical industry has used this approach to produce a number of dosage forms including tablets, capsules, powders and parenterals [367,372]. The use of microcapsules is to control rate of API absorption as the rate of release of the active from a dosage form can be controlled. Controlled release dosage forms can be designed to sustain, prolong or delay release and microencapsulated API in polymeric carriers can be used to manipulate and

control API release precisely as desired [367,372]. The organoleptic properties of API such as taste and odour can be masked using microencapsulation. Compounds such as diclofenac sodium, enoxin and paracetamol have been successfully taste-masked using this approach [371,373,374]. The successful microencapsulation of acetylsalicylic acid in order to control release and reduce adverse side effects such as gastric irritation has been reported [375]. A summary of the applications of microencapsulation for API(s) is summarised in Table 4.1.

Table 4.1 Reasons for microencapsulation of compounds[372,376,377]

Reasons for microencapsulation of API(s)
Controlled API release
Masking organoleptic properties of API
Protection of API from moisture, heat and light
Prevent API incompatibility
Reduce gastric irritation of API
Safe handling of toxic materials
Targeted API release
Easy handling of powder like materials

4.2.2 Microencapsulation approaches

A number of approaches have been reported for the microencapsulation of compounds and can be grouped into three categories viz., chemical, physico-chemical and physico-mechanical techniques [377].

4.2.2.1 Chemical

The chemical approach to microencapsulation makes use of chemical reactions during microsphere formation involving monomeric and/or prepolymeric starting materials [363]. Chemical microencapsulation is based on polymerisation or poly condensation mechanisms and interfacial and/or *in situ* polymerisation are the most common approaches used [363,377]. Interfacial polymerisation involves capsule shell formation at or on the surface(s) of particles by polymerisation of reactive monomers [378]. A monomer is dissolved in the liquid core material and subsequently dispersed in an aqueous phase containing a dispersing agent [378,379]. The use of interfacial polymerisation for the encapsulation of di-ammonium hydrogen phosphate by a polyurethane-urea membrane has been reported [380]. *In situ*

polymerisation is similar to interfacial polymerisation however no reactive agents are added to the core in this process and polymerisation occurs only in the continuous phase [377].

4.2.2.2 Physico-chemical

Physico-chemical approaches to microencapsulation include rapid expansion of supercritical fluids, simple, complex coacervation approaches[377,378]. Coacervation is a process in which partial desolvation of a homogeneous polymer solution in the polymer rich phase, known as the coacervate and a polymer poor phase or coacervation medium [377,381]. Two methods for coacervation viz., simple and complex have been used and the mechanism of microcapsule formation is similar for both methods, however the phase separation step is different [381]. For simple coacervation a desolvation agent is added to precipitate phase separation, whereas for complex coacervation, complexation between two oppositely charged polymers occurs [382].

The use of supercritical fluids for encapsulation is another example of a physico-chemical technique [377,383]. Supercritical fluids are highly compressed gasses such as CO_2, alkanes and nitrous oxide [384]. Three common methods that make use of supercritical fluids for encapsulation are rapid expansion of supercritical solution, particles from gas-saturated solution and gas anti-solvent approaches [377,382,385].

4.2.2.3 Physico-mechanical

Physico-mechanical approaches to microencapsulation include spray drying and congealing, fluidised bed technology and solvent evaporation [377,386]. Microencapsulation by spray drying and congealing is a low cost commercial process in which core particles are dispersed in a polymer solution after which the solution is sprayed into a hot chamber [369,387]. Microcapsules formed using this approach are either polynuclear or matrix type capsules. When using fluidised bed technology liquid coating material is sprayed onto particles and rapid evaporation of the solvent results in the formation of an outer layer on the surface of the particles [363,377]. Different types of fluid-bed coaters such as top, bottom and tangential spray patterns exist [377]. A number of methods using solvent evaporation have been reported for the encapsulation of MTZ and solvent evaporation was used to encapsulate MTZ in these studies [388–392].

4.3 SOLVENT EVAPORATION

There are different approaches to manufacturing microcapsules using solvent evaporation and the choice of technique that ensures efficient encapsulation of an API is, in part, dependent on the hydrophilicity or hydrophobicity of the API [377]. The use of an oil in water (o/w) method is reserved for encapsulation of water insoluble compounds [393]. The o/w solvent evaporation approach often results in low encapsulation efficiencies for water soluble APIs as these compounds tend to partition out of the dispersed phase into the continuous aqueous phase [394]. To overcome this challenge o/o, w/o/w, w/o/o and modified w/o/w emulsion techniques have been proposed for use [394,395].

The o/o solvent evaporation approach was used as the preferred method of encapsulation of MTZ for these studies as it requires ambient temperatures and mild emulsification techniques. The technique involves the use of three phases viz., a core, coating material and a liquid manufacturing vehicle (LMV) [377]. The API to be encapsulated is the core and the coating material is polymeric material whilst the LMV is an aqueous solvent or continuous phase [393].

The initial step in the process requires dissolving polymeric materials in a volatile immiscible organic solvent to produce a coating solution in which the core material is dissolved or dispersed. The organic solvent containing the API and polymers should not be soluble in the LMV. The organic solution is added to the LMV and the mixture agitated [377,393]. Emulsification of the organic or dispersed phase in the continuous phase occurs as the organic solvent is extracted from the dispersed phase into the continuous phase as solvent evaporation occurs and droplets of the dispersed phase subsequently transform into solid particles [393] . Free flowing particles are harvested by filtration and residual solvents that may be present in the microspheres are removed by drying [393,395–397].

The dispersed phase contains the API, polymer and organic solvent and the choice of the polymer depends on the targeted rate of release [398]. In many cases a combination of polymers are necessary to achieve the specific rate of release [397]. The polymers used may be biodegradable or biocompatible. Examples of polymers used include albumin, dextrin, alginic acid, chitosan, ethylcellulose, hydroxylpropyl cellulose, hydroxypropyl methycellulose and poly (lactic acid) [399].The API to polymer ratio has a significant effect on encapsulation efficiency and release rate. Increasing the amount of polymer used resulted

in better coating of API particles, whereas decreasing API to polymer ratios revealed an increase in entrapment efficiencies and slower release rates [400].

The amount of polymer used was varied in these studies in order to assess the effect of polymer concentration on MTZ release rates and encapsulation efficiency. The solvent should be highly volatile, have a low boiling point, exhibit low toxicity and dissolve the polymer(s) to be used [393]. Solvents commonly used for solvent evaporation microencapsulation include acetone, ethyl acetate, chloroform and dichloromethane [395]. Acetone was selected as the solvent due to its low boiling point and ability to form turbid viscous solutions with Methocel® K15M and dissolve Eudragit® RS PO [275]. The volume of the continuous phase is usually larger than that of the dispersed phase and often contains a surfactant [393]. The surfactant is a tension-active agent used to facilitate the dispersion of one phase in an immiscible liquid. In addition the surfactant stabilizes the emulsion and reduces the surface tension of the continuous phase. Liquid paraffin was used as the continuous phase with Span® 80 included as a surfactant [393].

Additional components that may be added to the dispersed phase include co-solvents and/or porosity generators [393,401]. Co-solvents are added to enhance the solubility of an API not totally soluble in a single solvent, in the dispersed phase and examples include methanol and ethanol [393,395]. Porosity generators or porosigens or porogens are used to ensure pores are generated in the surfaces of microspheres to increase the degradation rate of polymers to release rapid dissolution rates for encapsulated API. In addition an antifoaming agent such as dimethicone, oleyl alcohol and simethicone may be added to the continuous phase when high agitation rates are required as foaming may interfere with polymer deposition and microsphere formation [275,393]. The rate of solvent evaporation can be increased using elevated temperatures. Drawbacks include, however, a decrease in total mass recovered, a shift in size distribution and a reduction in encapsulation efficiency [393,397,402]. Consequently the temperature used should not denature the API or result in boiling of the solvent [393].

4.4 PROPOSED FORMULATION

4.4.1 Background

The oral route of administration is convenient and extensively used as solid oral dosage forms are relatively cheap to produce, easy to store and transport, are convenient to use and may

enhance patient adherence when compared to medicines administered via other delivery routes [403,404].

Helicobacter pylori is a most common bacterial infection and primary pathogen causing gastritis, gastroduodenal ulcer formation and gastric cancer disease [3,405]. The clinical eradication rate of *Helicobacter pylori* is low due to instability of antibiotics at low pH, low concentrations of API in deep gastric mucosal tissues and short gastric residence time of many antibiotics [3,406,407]. Several factors influence gastric retention of API(s) including physiological and pharmaceutical factors [3]. Gastric emptying time is a key physiological factor that influences gastric retention of API(s) and diseases such as chronic renal failure and diabetes can delay gastric emptying time [408,409]. Variability in gastric emptying times may lead to incomplete API release from dosage forms resulting in reduced therapeutic efficacy [3].

Prolonging the gastric residence time of an API is a logical approach to overcoming these challenges and site-specific gastric-retentive dosage forms are one approach [3,410]. Extensive research has been undertaken in respect of gastric-retentive dosage forms for a number of API(s), including those used to treat *Helicobacter pylori.* The recommended treatment regimen for *Helicobacter pylori* is triple combination therapy that includes a proton pump inhibitor and any two of antimicrobial compounds clarithromycin, amoxicillin or MTZ [16,17]. MTZ is a relatively cheap well known compound and was used to manufacture gastric-retentive microcapsules in these studies.

Gastric-retentive dosage forms are designed to remain in the stomach for extended periods of time following oral administration and are useful for delivering compounds that are active in the stomach such as misroprostol, are unstable in the intestinal or colonic environment including MTZ and captopril or API(s) that exhibit poor solubility at high pH such as diazepam and verapamil hydrochloride [6,411–413].

4.4.2 Approaches to gastric-retentive dosage forms for API delivery

Gastric retention can be achieved using different approaches and research into gastric-retentive API delivery systems has resulted in the development of floating, bioadhesive, expandable and magnetic systems [3,414–417]. All approaches are able to prolong the gastric residence time of API and improve the therapeutic efficacy and outcomes. A schematic of the different approaches of gastric retention is depicted in Figure 4.2 [5,418].

Figure 4.2 Schematic depicting approaches to gastric retention including (A) floating, (B) bioadhesive, , (C) expandable and (D) magnetic systems [5,418].

4.4.2.1 Floating technologies

Floating drug delivery systems were initially described in 1968 and are low density systems that float on the surface of gastric contents, increasing gastric retention time and bioavailability [6,419–421]. Floating drug delivery system retains low density and high buoyancy when compared to the contents of the stomach, provide an adequate barrier to protect API from gastric acid secretions and release the API in a controlled or sustained manner [3,422,423]. Hydrophilic matrices have been used to manufacture floating systems and these matrices adsorb water, swell, have a low density and float on the surface of gastric fluids [3,424]. Hydrodynamically balanced systems (HBS), gas generating and low density systems are the common approaches to formulating intra-gastric floating systems [425,426]. Excipients that have been used to produce HBS include hydroxypropyl methylcellulose (HPMC), sodium carboxymethylcellulose and alginic acid [3,413,427]. By way of example, HPMC hydrates and swells to form a gel barrier with low density resulting in the dosage form floating with release controlled by the swollen gel layer [3,6,421]. Gas generating systems achieve buoyancy through gas generation, an example of which is CO_2 from the reaction between sodium bicarbonate in acid solution[3,428]. Low density systems are manufactured using low density materials such as empty hard gelatin capsules, polystyrene foams and pop-rice grains that entrap oil or air [3,411,429,430]. Over the past decade emulsification solvent evaporation for the manufacture of low density systems has gained popularity and a number of studies have applied solvent evaporation manufacture to the encapsulation of antimicrobial compounds such as MTZ, tetracycline and amoxicillin [3,431–434].

4.4.2.2 Bioadhesive technologies

Bioadhesive dosage forms stick to mucosal surfaces via a number of mechanisms as formulations are made of a mucous coating or adhesive polymer [295]. Bioadhesive polymers

are classified as anionic such as alginate and pectin, cationic such as chitosan and neutral such as polyethylene glycol materials [6,435,436]. Following administration of a dosage form, it dissolves in gastric fluids and adheres to mucosal tissues to prolong gastric residence time of the API [3]. The adhesive mechanisms may be explained using electronic, adsorption, wetting and diffusion theory [437,438]. These dosage forms are challenging to develop and retain due to the turnover of gastric mucosa tissues. Promising results have nonetheless been reported [3].

4.4.2.3 Expandable technologies

A dosage form in the stomach will withstand gastric transit if it is bigger than the pyloric sphincter. However the dosage form should be small enough to swallow and not cause gastric obstruction. Expandable drug delivery technologies should be small for ease of swallowing and expand once in contact with gastric fluids as gastric emptying and residence time are affected by the size of the dosage form in the stomach [6,412,416,418]. The systems should control API release and reduce in size following API release so as tofacilitate safe elimination of the system [3]. Superporous hydrogels are an example of a material used to produce these systems and are pH and temperature sensitive with a high swelling capacity and swell rapidly on hydration [3,439,440].

4.4.2.4 Magnetic technologies

Magnetic systems are comprised of two (2) components viz., the pharmaceutical aspect or dosage form containing a small internal magnet and an external magnet [5,410]. Following administration of the pharmaceutical component, the external magnet is placed over the abdomen, near the stomach and through magnetic attractive forces is retained in that region [5]. An increase in plasma concentrations of acyclovir administered in the form of magnetic tablets has been reported [441]. The disadvantage of this system is the requirement of an external device, which may decrease patient adherence due to inconvenience [6,442]. The external magnet must be carefully and precisely located so as to ensure that API is released at the appropriate site and to avoid patient discomfort [5,6,442].

4.4.3 Rationale

The clinical effectiveness of MTZ for the treatment of *Helicobacter pylori* is well documented [443,444]. The elimination half-life of MTZ is approximately 8 hours and typical dosage regimens for the treatment of *Helicobacter pylori* infections requires administration of MTZ every 8 to 12 hours [16,52]. MTZ is unstable in the colonic

environment, acts locally in the stomach and is therefore a potential candidate for inclusion in oral controlled gastric-retentive delivery systems [3]. The development of gastric-retentive dosage forms is an approach to increasing gastric residence time of MTZ thereby improving the eradication rate of *Helicobacter pylori i*nfections [6]. Oral sustained delivery of MTZ permits slow release of the MTZ over time at a desired rate facilitating a reduction in the frequency of administration and improving adherence. Floating microspheres based on non-effervescent approaches are gastric-retentive technologies [445]. A non-effervescent HBS approach using two different grades of HPMC (Methocel®) was used to manufacture floating microspheres containing MTZ. Non-effervescent drug delivery systems are prepared using gel forming or highly swellable cellulose polymer derivatives such as HPMC, polyacrylates or carbopol [445,446]. HPMC forms a gel when in contact with gastric fluids and has a bulk density < 1 g/ml in the gastric environment [445]. As HPMC swells it entraps air and buoyancy is achieved in these dosage forms [445,446]. HBS is an approach in which one or more highly swellable cellulose based hydrocolloid such as HPMC is used. HPMC forms a colloidal barrier around the gel surface and the swollen polymer entraps air maintaining buoyancy [447]. The successful formulation and manufacture of gastric-retentive floating microspheres of API using HPMC have been reported as the polymer controls release and confers buoyancy to dosage forms [448–456].

4.5 EXPERIMENTAL

4.5.1 Materials

MTZ powder was purchased from China Skyrun Industrial (Tsim Sha Tsui, Hongkong). Methocel®(K100M and K15M were donated Colorcon® Ltd (Dartford, Kent, England). Avicel®PH102 was donated by FMC® Biopolymer, USA. Eudragit® RS PO was donated by Evonik® Röhm GmbH, Pharma Polymers. Span® 80 was purchased from Sigma Aldrich (St Louis, Missouri, USA). Liquid paraffin was supplied by ADC Laboratories (Durban, South Africa) and acetone AR was purchased from Associated Chemical Enterprises (Southdale, South Africa). *n*-Hexane was acquired from Burdick and Jackson Laboratories (Michigan, USA). Chemicals were used as received without further purification.

4.5.2 Method of manufacture

Microcapsules were manufactured using emulsification and solvent evaporation using the approach described by Khamanga *et al*., [457] and depicted in Figure 4.3.

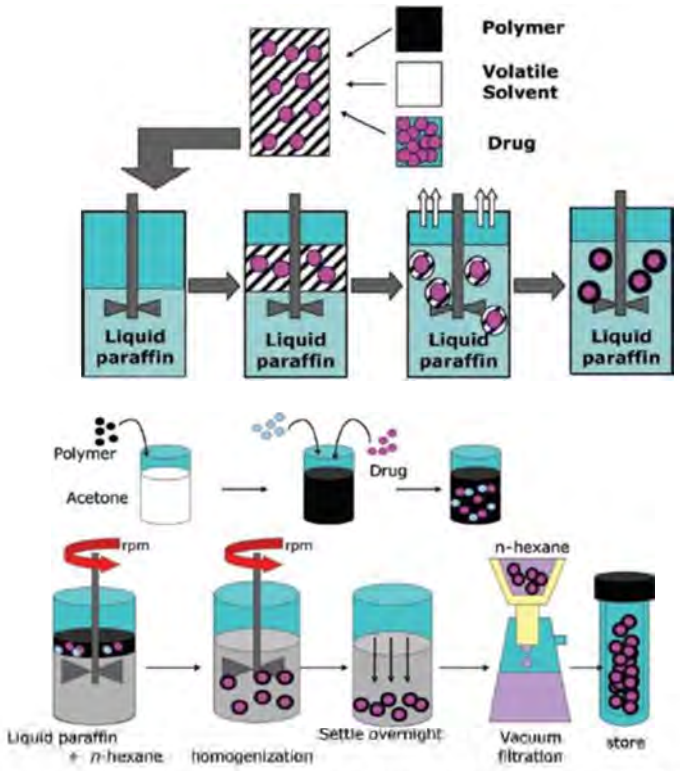

Figure 4.3 Schematic depicting the steps involved in the solvent evaporation manufacture of microcapsules[457]

Different amounts of the polymers, Avicel® PH102 and MTZ were weighed using a Mettler® Model AE163 top-loading analytical balance (Zurich, Switzerland). The polymers and Avicel® PH102 were dispersed in 20 ml acetone and then1 g MTZ was added and dispersed in the polymer solution. Light liquid paraffin (120 ml) containing 1% v/v Span 80 was poured into a 400ml beaker and agitated with a four-blade "butterfly" propeller of 50 mm diameter linked to a homogeniser (Virtis Company, New York, USA) to produce a homogenous oily phase. The acetone solution containing the polymers, Avicel® PH102 and MTZ was then poured into the oily continuous phase. The volume of the liquid paraffin, acetone and Span 80 were constant for all batches of product made in this study. Following two hours of agitation, 10 ml n-hexane was added to harden the microcapsules and stirring continued for a further 5-7 hours. The microcapsules were collected using a Buchner funnel and were washed 2-3 times with 50 ml n-hexane to remove any residual liquid paraffin. The microcapsules were then dried in an oven (Gallenkamp®, Loughborough UK) at 25°C for 24 hours and transferred to airtight amber coloured glass bottles.

4.5.3 Formulation Composition

The composition of preliminary formulations used viz., MTZ-001- MTZ-007 are listed in Table 4.2.

Table 4.2 Preliminary formulation composition

Batch	MTZ g	Methocel® K100M g	Methocel® K15M g	Eudragit® RS PO g	Avicel® PH102 g	Homogenisation speed rpm	Time hrs
MTZ-001	1.00	2.00	-	1.00	0.25	500	5
MTZ-002	1.00	1.00	-	1.00	1.25	500	5
MTZ-003	1.00	-	2.00	1.00	0.25	500	5
MTZ-004	1.00	-	1.00	1.00	1.25	500	5
MTZ-005	1.00	-	1.00	1.50	0.75	500	5
MTZ-006	1.00	-	1.00	1.50	0.75	500	6
MTZ-007	1.00	-	1.00	1.50	0.75	1500	6

rpm= revolutions per minute

Preliminary studies were undertaken using two different viscosity grades of Methocel® viz., Methocel®K100M and Methocel®K15M and Eudragit® RS PO in different quantities. Processing variables such as homogenisation speed and time were varied. Avicel® PH102 was used as a diluent and the amount used was modified to ensure each batch was a constant weight of 4.25 g. Preliminary formulations are manufactured to identify factors that may have an impact on a product response or attribute. Preliminary formulations were manufactured and assessed in terms of *in vitro* release, yield, encapsulation efficiency, morphology, and percentage buoyancy. The target was to minimise the amount of MTZ released at 0.5 hour and this range was set between 0-15%, have approximately < 30% MTZ released after 2 hours and maximise MTZ released at 12 hours and this target was set to be > 85% up to 100% MTZ released. Targets to maximise buoyancy, yield and encapsulation efficiency were set to be > 50% up to 100%. The target particle size was set at 2-2000µm.

4.6 EVALUATION OF MICROCAPSULES

4.6.1 Encapsulation efficiency (EE)

The EE was determined using the approach reported by Khamanga *et al.,* [457]. The microcapsules were crushed and powdered using a mortar and pestle and an aliquot of powder equivalent to 10 mg MTZ was accurately weighed and dissolved in 100 ml of a mixture of water and ACN in an 81:19 % v/v ratio and sonicated for 60 minutes. The solution was then filtered through an HVLP Durapore® 0.45µm membrane filter (Millipore®, Bedford, MA, USA) prior to analysis using a validated HPLC method to determine the MTZ content of

microcapsules. The EE was calculated using Equation 4.1 and is reported as a percentage [457]. The encapsulation efficiency was assessed in triplicate.

$$\% \text{ EE} = \frac{Actual\ drug\ loading}{Theoretical\ drug\ loading} \text{x}100 \qquad \textit{Equation 4.1}$$

4.6.2 Buoyancy

The buoyancy was determined using previously reported approaches [453,458]. A Hanson Model No 73-100-104 USP Apparatus 2 (Hanson Research, Chatsworth, CA, USA) was used to carry out buoyancy studies. Approximately 100 mg of microcapsules were weighed and placed in 900 ml 0.1 M HCL and the medium was agitated with a paddle rotating at 100 rpm for 12 hours. The fractions that remained afloat and that had settled were harvested separately and then dried and weighed. The buoyancy reported as a percentage was calculated using Equation 4.2 [294,448,453]. Buoyancy studies were done in triplicate.

$$\% \text{ Buoyancy} = \frac{Q_f}{Q_f + Q_s} \qquad \textit{Equation 4.2}$$

Where,

Q_f = weight of floating microcapsules
Q_s = weight of settled microcapsules

4.6.3 Yield

The yield or amount of microspheres produced from each formulation was established by weighing the product and calculating the percent yield using Equation 4.3 [459].

$$\% \text{ Yield} = \frac{The\ amount\ of\ microspheres\ obtained\ (g)}{Theoretical\ amount\ (g)} \text{x}100 \qquad \textit{Equation 4.3}$$

4.6.4 *In vitro* release

In vitro release studies were performed using a Hanson Model No 73-100-104 USP Apparatus 1 (Hanson Research, Chatsworth, CA, USA) coupled with an Autoplus™ Multifill™ and Maximiser Syringe Fraction Collector purchased from the same source. MTZ release monitoring was performed using a modified USP Apparatus I in which a glass basket

was used for *in vitro* release studies [460]. A dialysis tubing cellulose membrane with an average width of 25 mm and an average diameter of 16 mm with a molecular weight cut-off to approximately 14,000 daltons was soaked overnight in 600 ml 0.1M HCL. The dialysis membrane was then attached to the lower end of a glass tube and used in place of stainless steel baskets. Microcapsules were packed into size 000 capsules and the capsules then placed into the glass tubes with 2ml dissolution medium. The dialysis tubing was tied to the glass tube with the aid of elastic bands to prevent leakage and the glass tube attached to the shaft of the dissolution apparatus. All formulations were subjected to *in vitro* dissolution testing using 900 ml of 0.1M HCL as the dissolution medium. The studies were conducted over 12 hours at a speed of 100 rpm and samples were taken at 0.5, 1, 2, 4, 6, 8, 10 and 12 hours. The sample volume was 5ml and an equivalent amount of fluid was replaced. The amount of MTZ released at each time point was determined and used to generate cumulative percentage MTZ released profiles.

4.6.5 Scanning electron microscopy (SEM)

The mean particle size and surface morphology of the microcapsules was investigated using SEM (Tescan, VEGA LMU, Czechoslovakia Republic). The particle size was measured in triplicate using image analysis software (Olympus®, Tokyo, Japan). The microcapsules were mounted onto a double-sized carbon stub placed on a sample disc carrier of 3 mm height and 10 mm diameter and coated with gold for 15 minutes under vacuum (0.25 Torr) with a sputter coater (Balzers, Union Ltd, Balzers, Lichtenstein). The images were generated using a 20 kV electron beam.

4.7 RESULTS AND DISCUSSION

4.7.1 Encapsulation efficiency (EE)

The encapsulation efficiency for formulations MTZ-001 - MTZ-007 ranged between 68.54 - 78.63% which was found to be within the set target range and are summarised in Table 4.3.

Table 4.3 Mean encapsulation efficiency for formulations MTZ-001 - MTZ-007

Batch	Mean encapsulation efficiency % ± SD (n=3)
MTZ-001	78.63 ± 3.38
MTZ-002	72.02 ± 1.55
MTZ-003	77.21 ± 2.64
MTZ-004	70.65 ± 2.77
MTZ-005	71.32 ± 0.83
MTZ-006	70.89 ± 2.84
MTZ-007	68.54 ± 1.86

An increase in the amount of rate controlling polymer used viz., Methocel® K15M and Methocel® K100M revealed that the EE increased. For example, formulations MTZ-001 and MTZ-003 exhibited higher encapsulation efficiency when compared to formulations MTZ-002 and MTZ-004. Furthermore, slightly higher encapsulation efficiencies were observed when Methocel® K100M was used, however this increase in encapsulation efficiency for the highv iscosity grade polymer was not significant. It has been reported that an increase in polymer concentration leads to an increase in the viscosity of the dispersed phase resulting in higher encapsulation efficiency [453,456]. The increase in viscosity of the dispersed phase reduces the migration of MTZ into the continuous phase resulting in higher encapsulation efficiencies [458].

4.7.2 Buoyancy

The microcapsules were designed to achieve *in vitro* buoyancy based on using HBS technology in which the hydrocolloid, in this case HPMC (Methocel®) swells when in contact with gastric fluids and forms a colloidal gel barrier around capsule surface [445–447]. The air trapped by the swollen polymer results in a density < 1 g/ml and confers buoyancy to the microcapsules [445,449]. The percent buoyancy for formulations MTZ-001-MTZ-007 ranged between 56.75% - 61.89% and were found to be within the set target range, the data are summarised in Table 4.4. The percent buoyancy was greater for formulations in which the levels of both viscosity grade Methocel® polymers was high. For example when Methocel® K15M content was decreased from 2g to 1g there was an approximate decrease buoyancy of 3 % from 61.89 to 57.45%. Studies have reported that an increase in the percent buoyancy is attributed to an increase in Methocel® polymer concentration [449–451,454–456,458,461] as the greater the polymer content the more air can be entrapped air resulting in greater buoyancy [449,451,456,462,463].

Table 4.4 Mean percentage buoyancy for formulations MTZ-001 - MTZ-007

Batch	**Mean percentage Buoyancy % ± SD (n=3)**
MTZ-001	61.47 ± 2.88
MTZ-002	56.75 ± 4.01
MTZ-003	61.89 ± 1.89
MTZ-004	57.45 ± 3.65
MTZ-005	57.10 ± 2.26
MTZ-006	57.49 ± 2.75
MTZ-007	56.74 ± 1.62

4.7.3 Yield

The percentage yield following the manufacture of microcapsules using preliminary formulation compositions ranged between 91.45 to 96.47% (Table 4.5) and it is clear that polymer type or polymer level has little impact on the yield. However, an approximately 9% decrease in yield was observed when the homogenisation speed was increased from 500 rpm (MTZ-006) to 1500 rpm (MTZ-007). An increase in the homogenisation speed when using solvent evaporation imparts greater energy to the emulsion system with the potential for frequent breakage of microparticles as they form thereby reducing the yield [464].

Table 4.5 Mean yield for formulations MTZ-001 - MTZ-007

Batch	Mean Yield ± SD (n=3) %
MTZ-001	95.12 ± 2.08
MTZ-002	96.45 ± 2.28
MTZ-003	96.47 ± 2.63
MTZ-004	94.67 ± 2.03
MTZ-005	95.75 ± 2.69
MTZ-006	96.42 ± 3.17
MTZ-007	91.45 ± 2.54

4.7.4 Scanning Electron Microscopy (SEM)

The mean particle size and surface morphology of the microcapsules was determined using SEM and revealed that most microcapsules were spherical in shape. The mean particle size of the microcapsules is summarised in Table 4.6. The particle size ranged between 61.01µm-653.33 µm and hence was within the target range that was set.

Table 4.6 Mean size of microcapsules

Batch	Mean Size ± SD (n=3) µm
MTZ-001	653.33 ± 3.64
MTZ-002	599.52 ± 1.84
MTZ-003	494.09 ± 4.15
MTZ-004	491.73 ± 4.47
MTZ-005	421.20 ± 4.37
MTZ-006	386.60 ± 2.21
MTZ-007	61.010 ± 3.62

The change in particle size observed for formulations MTZ-005 and MTZ-006 from approximately 420 µm to 380 µm may be due to an increase in homogenisation time as short homogenisation times result in the formation of larger particles due to the incomplete

diffusion of the organic solvent through the interface of oil droplets prior to hardening, resulting in large particle production [465,466].

A significant change in particle size was observed for formulations MTZ-006 and MTZ-007 and an increase in homogenisation speed from 500 to 1500 rpm resulted in an approximate 6 times decrease in particle size. On the basis of published data, high homogenisation speeds result in the production of smaller microspheres and conversely lower speeds result in the production of particles of larger size [467,468]. The droplet size of the dispersed phase is larger at low agitation speed resulting in production of larger particles [402,469]. In contrast at high homogenisation speeds the high shear stress imparted reduces the viscosity of the emulsion facilitating the formation of particles that are smaller in size [470].

The SEM micrographs of microcapsules produced using formulations MTZ-001- MTZ-007 are depicted in Figure 4.4 and 4.5. The majority of the microcapsules produced had a rough surface with only formulations MTZ-003 and MTZ-004 exhibiting a smooth surface. The presence of MTZ on the surface of on some microcapsules was observed in some micrographs, for example formulation MTZ-002 and MTZ-007 and may be due to poor encapsulation of the MTZ.

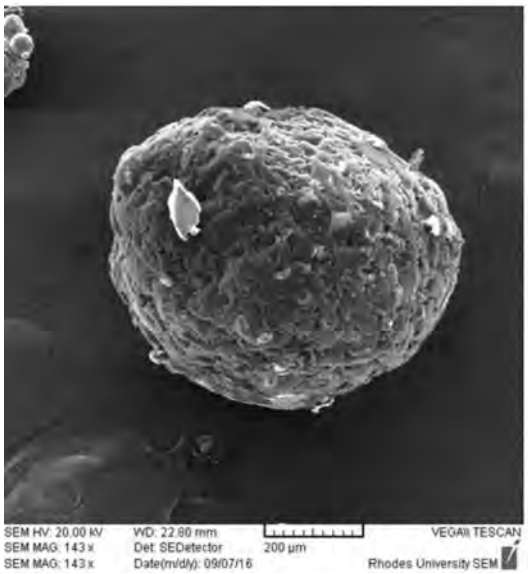

MTZ-001

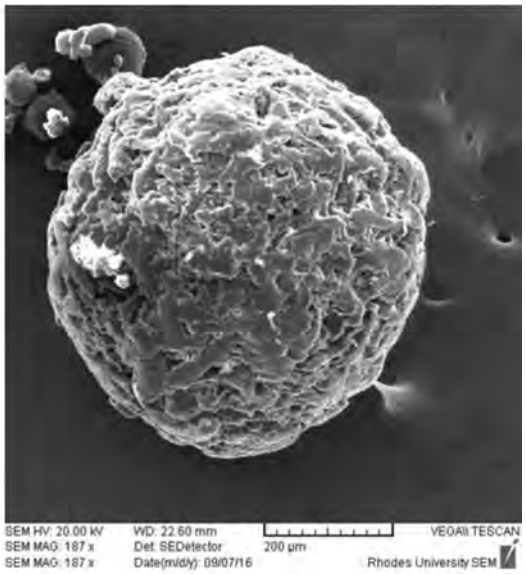

MTZ-002

MTZ-003

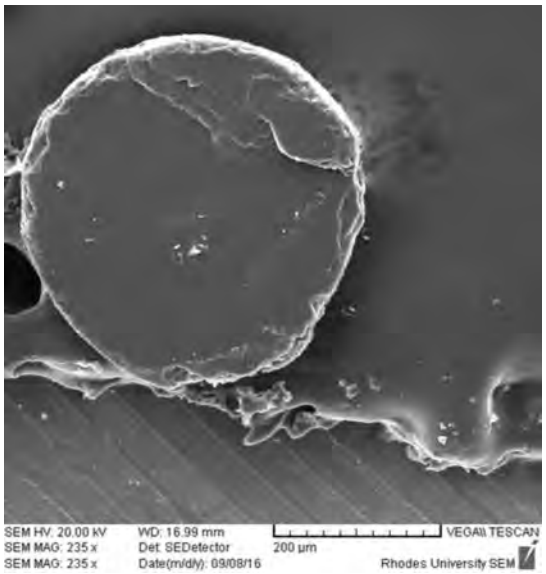

MTZ-004

Figure 4.4SEM micrographs depicting the morphology of microcapsules produced using formulations MTZ-001-MTZ-004

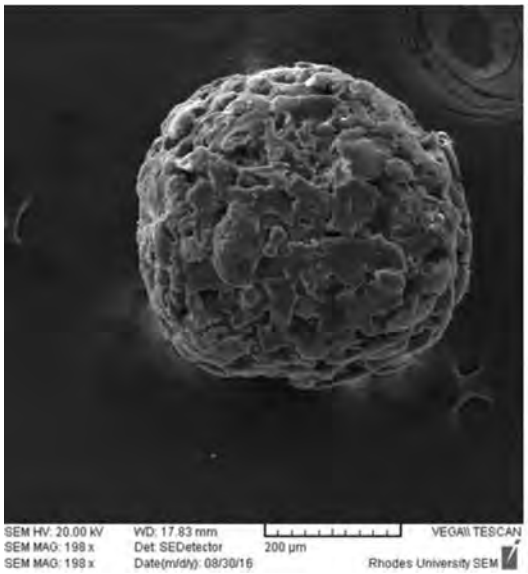

MTZ-005

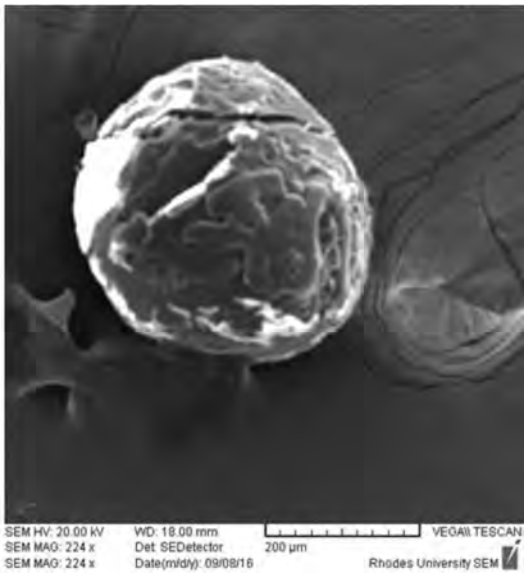

MTZ-006

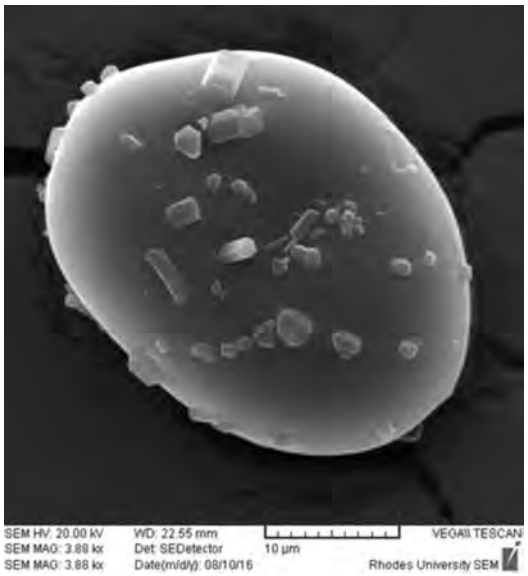

MTZ-007

Figure 4.5 SEM micrographs depicting the morphology of microcapsules produced using formulations MTZ-005-MTZ-007

4.7.5 *In Vitro* release

A summary of the cumulative % MTZ released at 0.5, 2 and 12 hours from preliminary formulations is listed in Table 4.7 and the *in vitro* release profile for formulations MTZ-001-MTZ-007 are depicted in Figures 4.6 - 4.12 respectively. Three replicates were tested for *in vitro* release studies.

Table 4.7 Mean cumulative percent MTZ released at 0.5, 2 and 12 hours (±SD, n=3)

Batch	0.5 hours %	2 hours %	12 hours %
MTZ-001	2.762 ±0.92	19.31 ± 1.70	70.60 ± 1.81
MTZ-002	6.605 ± 1.89	23.33 ±2.47	74.64 ±1.50
MTZ-003	4.452 ± 0.24	25.24 ± 1.75	77.31 ±1.66
MTZ-004	8.460 ± 2.06	32.03 ±2.52	83.42 ± 1.49
MTZ-005	9.391 ± 2.75	26.62 ± 2.97	80.96 ± 2.71
MTZ-006	10.42 ±2.13	27.77 ± 1.82	81.31 ± 2.10
MTZ-007	11.69 ± 1.71	33.87 ± 2.52	86.92 ± 3.46

Formulation MTZ-001 included 2g Methocel®K100M as the rate controlling polymer and the *in vitro* release profile for formulation MTZ-001 depicted in Figure 4.6 reveals that 19.31%, MTZ had been released at 2 hours and only 70.60% MTZ was released after 12 hours of dissolution testing. The incomplete release of MTZ from formulation MTZ-001 was below 85% the target set for minimum release at 12 hours and the formulation was therefore considered unsuitable, yet provided a useful starting point for the development of better formulations.

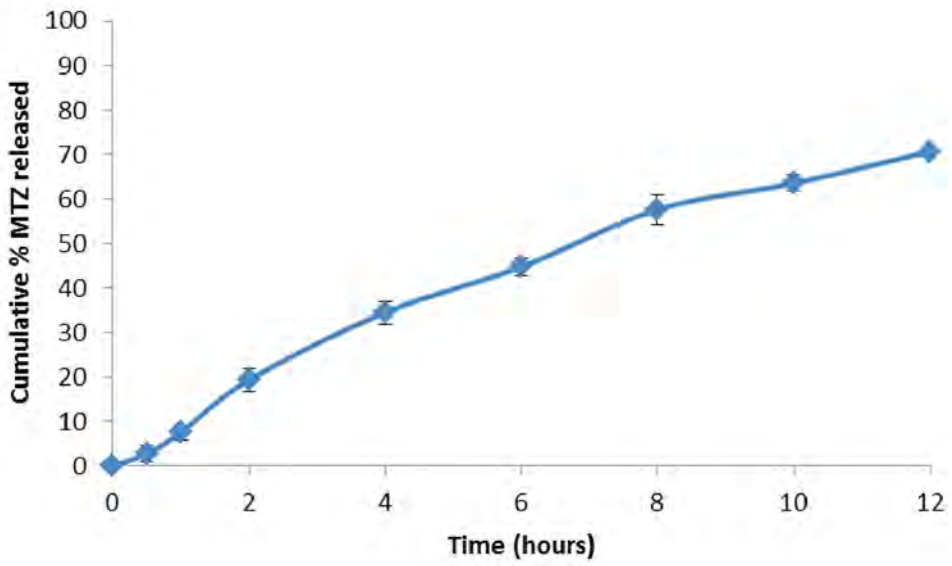

Figure 4.6 Dissolution profile for MTZ from batch MTZ-001

Formulation MTZ-002 was manufactured using 1 g Methocel® K100M and the release profile depicted in Figure 4.7 reveals that the cumulative % MTZ released after 2 and 12 hours was 23.33% and 74.64% respectively, indicating that decreasing the rate controlling polymer content resulted in an increase in the amount of MTZ released. Although there was a significant increase in the percent MTZ released from formulation MTZ-002, the total release was below the target value of 85% and therefore a lower viscosity grade polymer was included in subsequent formulation compositions. It has been reported that an increase in the amount of HPMC used results in a decrease in the rate of API release from dosage forms [471] as high levels of polymer result in an increased thickness and viscosity of the gel layer that surrounds the microcapsule when in contact with gastric fluids leading to an increase in the diffusional path length and reduction in API release rates [456,472].

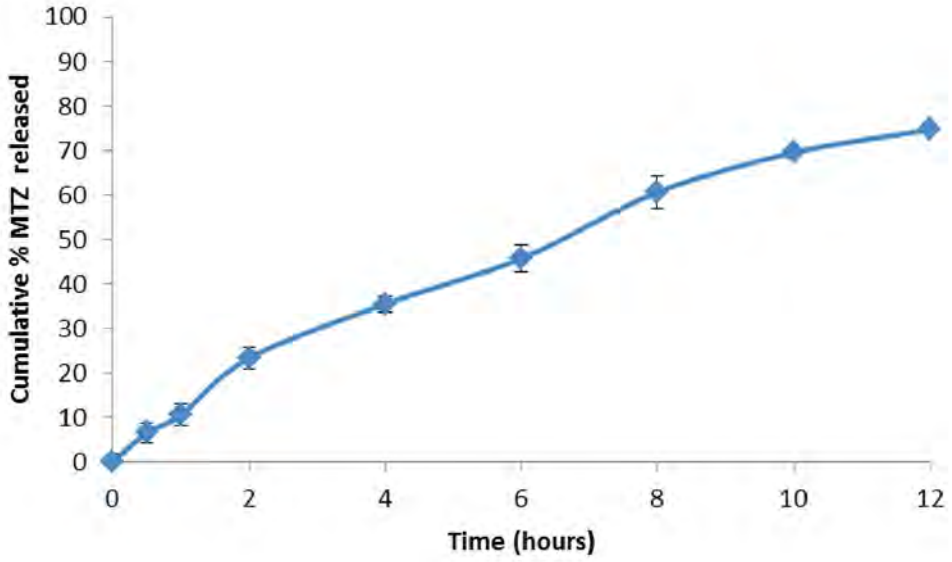

Figure 4.7 Dissolution profile for MTZ from batch MTZ-002

Formulation MTZ-003 was manufactured using 2g Methocel® K15M and the release profile depicted in Figure 4.8 reveals that MTZ release had increased significantly when compared to formulations MTZ-001 and MTZ-002 in which Methocel® K100M had been included.

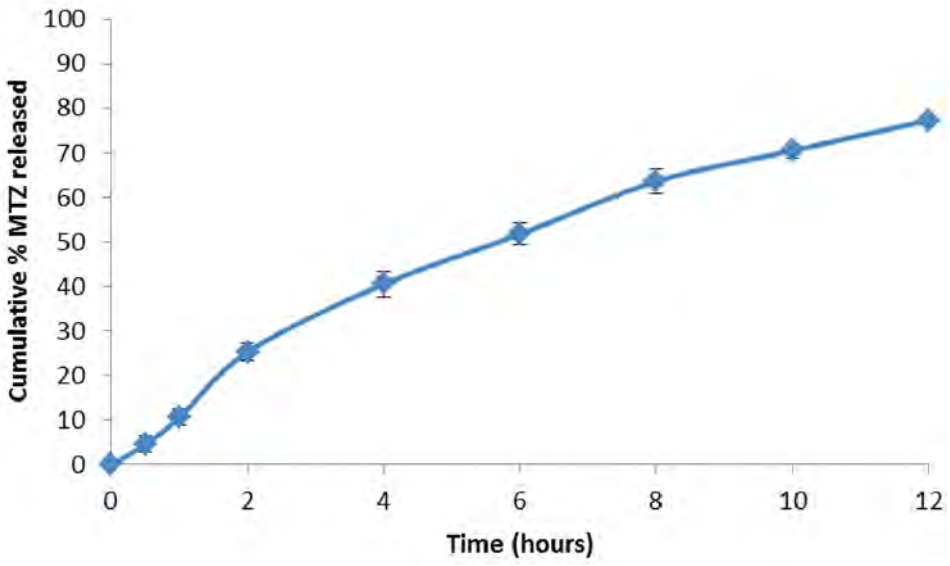

Figure 4.8 Dissolution profile for MTZ from batch MTZ-003

A 2% solution of Methocel® K15M has a nominal viscosity of 15000 mPa s and Methocel® K100M a nominal viscosity of 100000 mPa s [275]. Approximately 77% MTZ was released at the end of 12 hours from formulation MTZ-003 and Methocel® K15M was considered a better polymer than Methocel® K100M in terms of total MTZ released at 12 hours. Furthermore < 30% MTZ was released in 2 hours. The large difference in nominal viscosity between the two polymers results in a significant change in *in vitro* release and higher viscosity grades of Methocel® lead to a slower rates of MTZ release [456,473]. High viscosity grade polymers produce a thicker gel layer following hydration inducing greater chain entanglement resulting in retardation of MTZ release [473].

Formulation MTZ-004 was manufactured with a reduced amount of Methocel® K15M as an attempt to further increase the % MTZ released at 12 hours while still ensuring sustained release of the compound. The release profile for MTZ release from formulation MTZ-004 is depicted in Figure 4.9.

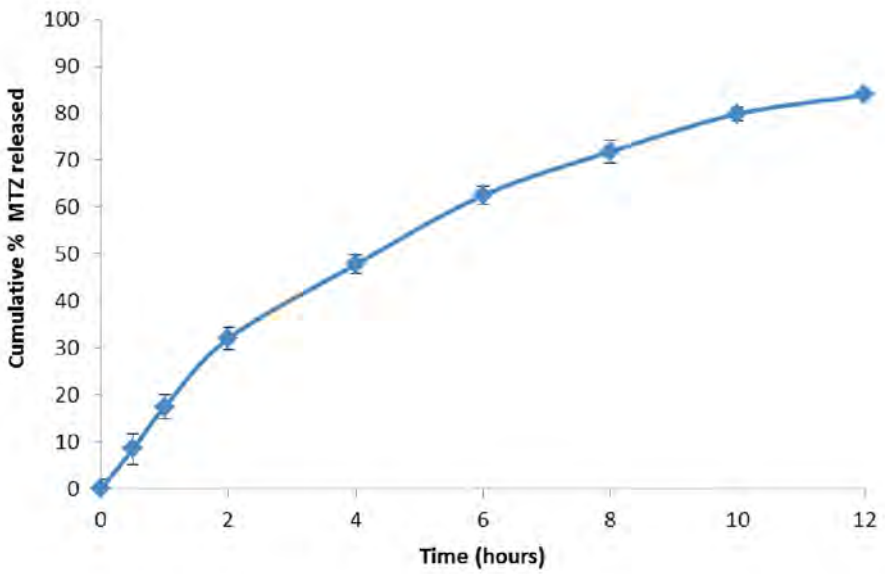

Figure 4.9 Dissolution profile for MTZ from batch MTZ-004

From the release profile depicted in Figure 4.9 it is evident that 32.03% and 83.42% MTZ was released at 2 and 12 hours respectively and that the decrease in Methocel K15M content in formulation MTZ-004 resulted in an increase in the amount of MTZ released. Higher proportions of polymer lead to an increase in the viscosity and diffusional path length resulting in a decrease in rate of diffusion of MTZ with a reduction in MTZ release rates [474].

Formulation MTZ-005 was manufactured with an increased amount of Eudragit® RS PO (1.5g) whilst keeping the other component levels constant. The dissolution profile depicted in Figure 4.10 reveals that MTZ release from formulation MTZ-005 is slightly lower with a % MTZ released of 80.96% at 12 hours when compared to MTZ release from formulation MTZ-004. This may be due to the increased level of Eudragit® RS PO which may further sustain the release of MTZ.

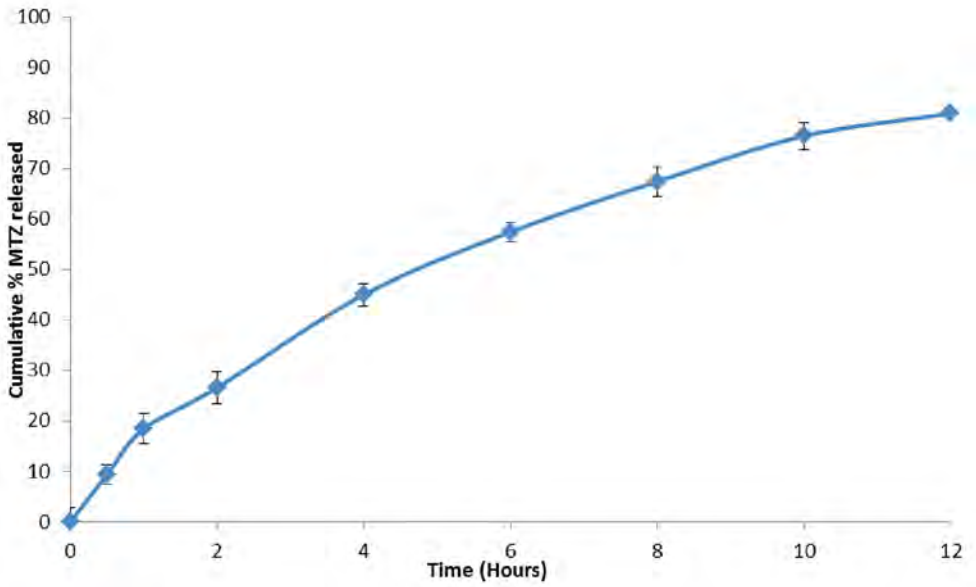

Figure 4.10 Dissolution profile for MTZ from batch MTZ-005

Formulation MTZ-006 was manufactured using the same formulation composition as Formulation MTZ-005 with the homogenisation time being increased to 6 hours. The cumulative % MTZ released from formulation MTZ-006 after 12 hours (Figure 4.11) was similar to that observed for formulation MTZ-005, suggesting that even though the increase in homogenisation time may reduce the particle size of the microcapsules produced, homogenisation time does not have a significant impact on MTZ release from the dosage form.

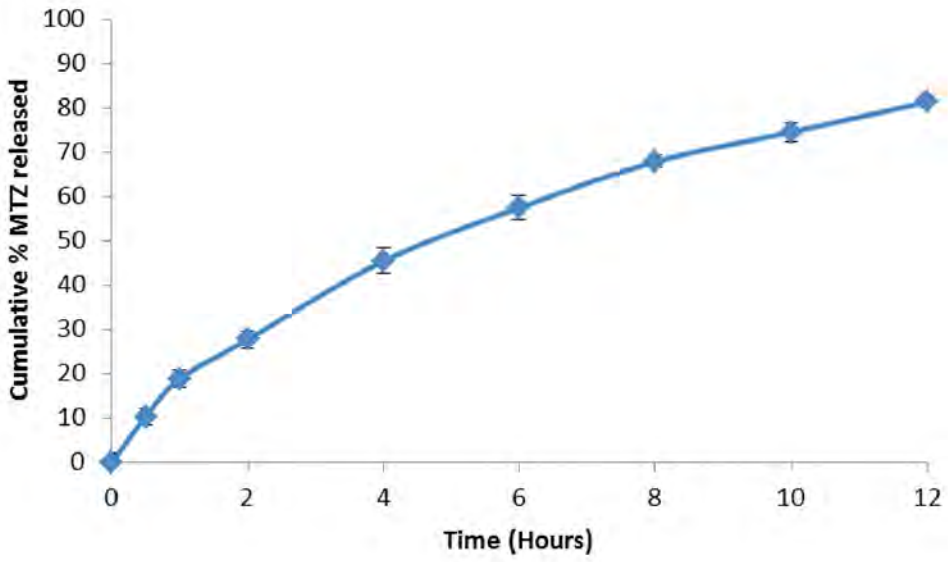

Figure 4.11 Dissolution profile for MTZ from batch MTZ-006

Formulation MTZ-007 was manufactured using the same composition and homogenisation time as formulation MTZ-006, however the homogenisation speed was increased to 1500 rpm. The release profile depicted in Figure 4.12 reveals that the % MTZ released was approximately 86% at 12 hours.

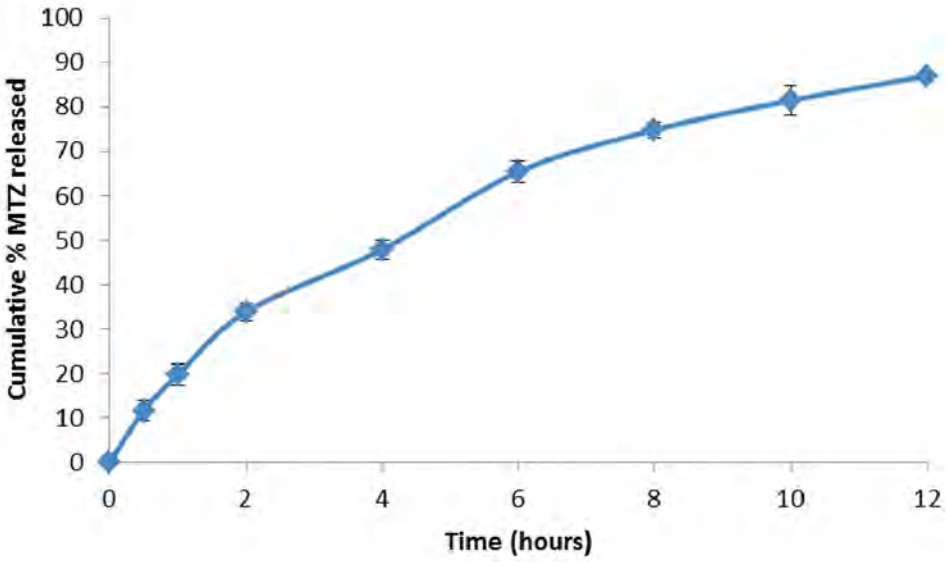

Figure 4.12 Dissolution profile for MTZ from batch MTZ-007

It can be concluded that an increase in homogenisation speed resulted in an increase % MTZ released that may be attributed to the impact of homogenisation speed on the size of the microcapsules produced [464]. Microcapsules of smaller size will exhibit a large surface area-to-volume ratio than large sized microcapsules with a more rapid rate of flux of API leaving micro particles per mass of formulation resulting in the higher % MTZ released [464,475].

4.8 CONCLUSIONS

A gastric-retentive formulation containing MTZ was manufactured in an attempt to increase the gastric residence time of MTZ and to ensure sustained release of MTZ for enhancing therapeutic outcomes when treating *Helicobacter pylori* infections. A gastric-retentive site specific delivery technology would improve eradication rates of *Helicobacter pylori* and advance treatment options for patients. The solvent evaporation method was used to manufacture gastric-retentive microparticles using a non-effervescent approach to ensure floating microspheres were produced using Methocel® as a rate retarding polymer. Methocel® swells to form colloidal gel barriers and entrap air that confers buoyancy to these dosage forms, whilst also controlling the rate of MTZ release from the dosage form. The preliminary

formulations were assessed in terms of encapsulation efficiency, buoyancy, yield, morphology and MTZ release.

Higher encapsulation efficiencies were observed when using high viscosity grade Methocel® K100M than when the lower viscosity grade Methocel® K15M was used. However, the use of Methocel® K100M even at low levels reduced the amount of MTZ released significantly and a maximum of approximately 70% release could be achieved at 12 hours.

The encapsulation efficiency also decreased, irrespective of the grade used, when lower levels of the rate controlling polymer were included in the formulation. The buoyancy increased with an increase in polymer concentration for both viscosity grades as more air was entrapped in a thicker gel layer on hydration due to increased amount of Methocel® present. The values for encapsulation efficiency, buoyancy, yield and particle size obtained for all the preliminary formulations were all within the range that was set as the target. The results obtained from the preliminary studies are useful in determining a narrower target range for percent MTZ release, encapsulation efficiency, buoyancy, yield and particle size in the formulation optimisation studies.

The results of *in vitro* release testing indicate that the Methocel® grade has an influence on the extent of MTZ release. Methocel® K15M was selected for use in formulation development activities as *in vitro* release studies revealed dosage forms could be produced that would ensure > 85% MTZ could be released at 12 hours. In order to improve the encapsulation efficiency when using Methocel® K15M additional experiments were undertaken to establish the combined effect of different levels of two polymers viz., Methocel® K15M and Eudragit® RS PO, homogenisation time and speed on product attributes. The preliminary studies were performed using the 'change one factor at a time' approach and therefore the effect of combinations of factors on the responses monitored could not be observed. On an individual basis it can be concluded that the amount of Methocel®K15M and Eudragit® RS PO used, homogenisation speed and time are all significant formulation and process variables that require further investigation and must be evaluated during the optimisation process to produce MTZ containing gastric-retentive microcapsules.

CHAPTER FIVE

FORMULATION OPTIMISATION AND MATHEMATICAL MODELLING OF METRONIDAZOLE RELEASE

5.1 INTRODUCTION

Response Surface Methodology (RSM) has been commonly used for the design and optimisation of different pharmaceutical formulations with a minimum number of experiments [357,476–480]. RSM can be used to identify factors or combinations of factors or input variables that result in an optimum response or output [190,481]. Other areas of application of RSM include screening a large number of factors in order to identify variables that may have a significant impact on a critical quality attribute (CQA) or output [190,482]. The traditional univariate approach to problem solving is time consuming, labour intensive and is based on an assumption that interaction between factors does not occur [483]. RSM simplifies experimental responses by establishing mathematical relationships between input variables and resultant responses using fewer experiments and is therefore cost-effective and efficient as fewer resources and staff are required during formulation development and process optimisation activities [190,481,484].

The objective of these studies was to use RSM to investigate the impact of formulation variables on *in vitro* release of MTZ from the gastric-retentive sustained release microcapsules described in Chapter 4. These studies were also performed to identify combinations and amount of excipient and processing parameters to be used to produce an optimised product. The effect of defined input variables on responses such as encapsulation efficiency, % buoyancy and % yield were also investigated.

5.2 EXPERIMENTAL

5.2.1 Materials and methods

The materials and methods used are listed and described in § 4.5.1 and 4.5.2.

5.2.2 Experimental design

A RSM approach using a Central Composite Design (CCD) was used for these studies key input variables investigated included the Methocel® K15M (X_1) and Eudragit® RS PO (X_2) content, homogenisation speed (X_3) and homogenisation time in hours (X_4).. Each factor was studied at 3 levels *viz*., low (-1), medium (0) and high (+1) and the cumulative percent MTZ released at 0.5 hours (Y_1), 2 hours (Y_2), 6 hours (Y_3), 12 hours (Y_4), encapsulation efficiency

(Y_5), percent buoyancy (Y_6), yield (Y_7) and microcapsule size (Y_8) were the CQA or response variables monitored . The levels of each input factor, coded and actual for the CCD as well as the constraints for the responses are listed in Table 5.1 and the experiments that were performed are listed in Table 5.2. The experiments were performed in a randomised manner so as to reduce the potential of uncontrolled factors to introduce bias to the responses. Design Expert® Version 8.0.2 (Stat-Ease Inc., Minneapolis, USA) statistical software was used for data analysis and to predict levels of input variables that would result in the desired responses. Fisher's statistical test for Analysis of Variance (ANOVA) for the response surface model was used to determine the significance of each factor investigated.

Table 5.1 Translation of the coded levels used for the CCD

Factor	**Level**		
Independent	-1	0	+1
Methocel® K15M (X_1) g	1.00	1.25	1.5
Eudragit® RS PO (X_2) g	1.00	1.25	1.5
Homogenisation speed (X_3) r.p.m	500	1000	1500
Homogenisation time (X_4) hours	5	6	7
Response factors	**Constraints**		
MTZ released after hour (Y_1)	0-15% (minimise)		
MTZ released after 12 hours (Y_4)	>85%(maximise)		
Encapsulation efficiency (Y_5)	>70% (maximise)		
Buoyancy(Y_6)	>50% (maximise)		
Yield (Y_7)	>90% (maximise)		
Microcapsule size (Y_8)	2-2000μm (in range)		

Table 5.2 Actual experimental conditions generated for CCD

Formulation batch number	Experimental run number	Standard run	Methocel® K15M g	Eudragit® RS PO g	Homogenisation speed rpm	Homogenisation time hours
MTZ-008	1	28	1.25	1.25	1000	6
MTZ-009	2	29	1.25	1.25	1000	6
MTZ-010	3	15	1.00	1.50	1500	7
MTZ-011	4	9	1.00	1.00	500	7
MTZ-012	5	12	1.50	1.50	500	7
MTZ-013	6	6	1.50	1.00	1500	5
MTZ-014	7	7	1.00	1.50	1500	5
MTZ-015	8	1	1.00	1.00	500	5
MTZ-016	9	30	1.25	1.25	1000	6
MTZ-017	10	16	1.50	1.50	1500	7
MTZ-018	11	21	1.25	1.25	500	6
MTZ-019	12	11	1.00	1.50	500	7
MTZ-020	13	25	1.25	1.25	1000	6
MTZ-021	14	10	1.50	1.00	500	7
MTZ-022	15	20	1.25	1.50	1000	6
MTZ-023	16	23	1.25	1.25	1000	5
MTZ-024	17	26	1.25	1.25	1000	6
MTZ-025	18	27	1.25	1.25	1000	6
MTZ-026	19	2	1.50	1.00	500	5
MTZ-027	20	4	1.50	1.50	500	5
MZT-028	21	14	1.50	1.00	1500	7
MTZ-029	22	8	1.50	1.50	1500	5
MTZ-030	23	24	1.25	1.25	1000	7
MTZ-031	24	19	1.25	1.00	1000	6
MTZ-032	25	3	1.00	1.50	500	5
MTZ-033	26	17	1.00	1.25	1000	6
MTZ-034	27	22	1.25	1.25	1500	6
MTZ-035	28	13	1.00	1.00	1500	7
MTZ-036	29	5	1.00	1.00	1500	5
MTZ-037	30	18	1.50	1.25	1000	6

5.2.3 Evaluation of sustained release MTZ microcapsules

All formulations were evaluated in terms of the parameters described in § 4.6. Following identification of an optimised formulation composition the product was manufactured and placed into stability chambers for stability testing for 30 days.

5.2.4 Stability testing

The optimised microcapsules were manufactured and placed on short-term stability testing for 30 days. The microcapsules were stored in amber glass bottles and placed in Model KBF-240 Binder® climate chambers (Binder GmbH® Ltd, München, Germany) maintained at 25°C/ 60 %RH and 40°C/ 75 %RH. The *in vitro* release profile, buoyancy and encapsulation efficiency of the microcapsules were monitored during stability assessment.

5.3 MATHEMATICAL MODELLING OF MTZ RELEASE

5.3.1 Overview

Mathematical models have been used extensively to provide information relating to the mechanisms that govern release of an API from a dosage form [485–489]. These models can also be used to establish mass transport mechanisms that occur in modified-release dosage forms [490]. Mathematical models that have been used to characterise dissolution profiles include zero order, first order, Higuchi, Hixon-Crowell and Korsmeyer-Peppas models [485,491,492]. Mathematical modelling provides information on the effect of geometry of pharmaceutical dosage form on the release kinetics of an API [485].

5.3.2 Zero-order model

The zero-order model describes ideal release kinetics required to achieve prolonged pharmacological effects [487]. This model is suitable for describing transport from non-disintegrating modified release dosage forms [493]. Examples of such dosage forms include coated, osmotic, some transdermal and matrix tablet technologies that contain poorly soluble API [487]. The zero-order model is used to describe release profiles for which the amount of API released per unit time is constant [487,491]. A mathematical description of a zero-order model is reported in Equation 5.1 [490].

$$Q_t = Q_0 + K_0 t \qquad \textit{Equation 5.1}$$

Where,

Q_t = Amount of API dissolved at time t
Q_0 = Initial amount of API in the solution at t
K_0 =Zero-order release rate constant
t= Time

5.3.3 First-order model

First-order kinetic models are used to describe dissolution from porous matrices containing water-soluble API [485,494]. The amount of API released from the matrix is proportional to the amount of API remaining in the core therefore the rate of release of API declines over time as the amount of API remaining in the dosage form diminishes [487]. This model is therefore used to describe release from systems in which the release rate is concentration dependent [495]. A mathematical description of a first-order kinetic model is reported in Equation 5.2 [490]

$$In\ Q_t = In\ Q_0 + K_0 t \qquad \textit{Equation 5.2}$$

Where,

Q_t = the amount of API released at time = t
Q_0 = the initial amount of API in solution at t=0
K_0 = the first-order release rate constant
t = time

5.3.4 Higuchi Model

The Higuchi model can be used to describe diffusional release from solid or semi-solid matrices such as ointments or polymeric based systems containing water-soluble or poorly water-soluble API [487,496]. Higuchi described drug release as a diffusional process based on Fick's law of diffusion [497,498]. The Higuchi model assumes that the initial concentration of the API within the dosage form is much higher than the solubility of the API as this assumption provides the basis for justifying the presence of a pseudo-state when deriving the Higuchi equation [317,487,496,499,500]. The model also assumes that suspended drug particles are finely divided and are significantly smaller in diameter than the thickness of the system and that the diffusivity of the API is constant when sink conditions are maintained during dissolution testing [485,487,496]. A mathematical expression of the Higuchi model is shown in Equation 5.3 [490]

$$Q_t = K_H t^{1/2}$$ ***Equation 5.3***

Where,

Q_t = Cumulative absolute amount of API released at time t
K_H = Constant reflecting the design variables of the dosage form
t = time

5.3.5 Hixon-Crowell model

The Hixon-Crowell model describes API release from dosage forms that exhibit a change in diameter and surface area during dissolution testing [492,501]. The model is applied to dosage forms in which dissolution occurs in planes that are parallel to the surfaces of the dosage form [245,502]. The assumption is that the dimensions of the dosage form diminish proportionally while the geometrical shape is retained over time [502]. The mathematical expression of the Hixon- Crowell model is shown in Equation 5.4 [490].

$$W_0^{1/2} - W_t^{1/3} = K_s t$$ ***Equation 5.4***

Where,

W_0 = Initial amount of API in the dosage form
W_t = Amount of APi remaining in the dosage form at time t
K_S = Constant incorporating the surface to volume relationship
t = time

5.3.6 Korsmeyer – Peppas model

The Kosmeyer-Peppas model is a simple, semi-empirical model that can be used to analyse API release from dosage forms [503]. The model describes the relationship between API release and time by means of an exponential function and is known as the power law (Equation 5.5) [490]. The power law describes API release from polymeric systems that may liberate API by more than one mechanism and is only applied to dissolution data for up to 60% release [504,505].

$$\frac{Q_t}{Q_\infty} = kt^n \qquad \textit{Equation 5.5}$$

Where,

Q_t = Absolute cumulative amount of API released at time t
Q_∞ = Absolute cumulative amount of API released at infinite time
k = A constant incorporating structural and geometric characteristics
t =Time
n = Release exponent

The value of the release exponent, n is used to describe the mechanism of release of API from polymeric matrices of different geometry [487,490,496]. The value of the release exponent is categorised as a function of the swelling behaviour of and relaxation rate at the swelling front between the gel layer and the glassy core of a hydrophilic polymeric matrix [505]. Specific values for n correspond to different mechanisms of release that occur from specific geometries of dosage form. A summary of the relationship between release exponents and the mechanism of API transport in thin films, spheres and cylinder shaped dosage forms is summarised in Table 5.3 [487,490,496].

Table 5.3 Relationship between release exponent n and mechanism of API transport[490]

Release exponent (n)			Rate as a function of time*	Drug transport mechanism
Thin films	Cylinder	Sphere		
0.5	0.45	0.43	$t^{-0.5}$	Fickian diffusion
$0.5 < n < 1.0$	$0.45 < n < 0.89$	$0.43 < n < 0.85$	t^{n-1}	Anomalous transport
1.0	0.89	0.85	Zero-order release	Case II transport
>1.0			t^{n-1}	Super Case II transport

*Applies to thin films

Drug release form polymeric matrices described using Equation 5.5 may occur by one of the four mechanisms summarised in Table 5.3 *viz.* Fickian diffusion, anomalous diffusion, Case II and super Case II transport [492]. Values for n =0.5 indicate that API release from the polymeric system occurs by a Fickian diffusion process through a thin film according to Ficks 2nd law of diffusion [496,506,507]. Case II transport occurs when API release from the delivery system is controlled by swelling and is time-independent [496,508]. Values for n ranging between 0.5 and 1 correspond to anomalous or non-Fickian transport mechanisms indicating that API release function of multiple mechanisms at the same time [496,509,510]. Anomalous transport occurs when the release of API deviates from Ficks law and when mass transfer of the API is a function of diffusion and swelling [511,512].

5.3.7 Approaches for selecting the best-fit model

Various approaches can be used to establish the best-fit mathematical model that describes dissolution or API release data [487,513]. The best-fit model can be established by comparing the correlation coefficient R^2 following fitting of data to different mathematical models. The model that results in the highest R^2 value can be regarded as the best-fit model [487,513]. Other approaches for determining the best-fit model involve calculation of Akaike's Information Criterion (AIC), sum of squares residuals (SSR) and mean square residuals (MSR) [487]. The model that best described the *in vitro* release of MTZ from the gastric-retentive sustained release microcapsules was identified by selecting the model that generated the highest R^2 value.

5.4 RESULTS AND DISCUSSION

5.4.1 Central Composite Design

Design Expert® statistical software was used to generate mathematical models that best described the relationship between independent input variables and the responses monitored. The individual linear effects of input variables on responses are denoted using terms X_1, X_2, X_3 and X_4, whereas interactive effects are denoted by terms such as X_1X_2 as they contain more than one factor. Quadratic factors are denoted by the presence of coefficients with high order terms such as X_1^2 for example. The relative influence of input variables on responses was determined by evaluating the sign adjacent to each coefficient. A positive sign indicates a synergistic effect whereas a negative sign is indicative of an antagonistic effect. The mathematical equations generated for all the responses using coded factors are listed as Equations 5.6 – 5.11.

$\mathbf{Y_1} = 52.07 - 97.88X_1 - 19.49X_2 + 48.23X_3 - 13.97X_4 + 0.70X_1X_2 - 0.73X_1X_3 + 9.57X_1X_4 + 32.98X_2X_3 + 13.23X_2X_4 + 24.67X_3X_4 + 118.35X_1^2 + 96.45X_2^2 + 13.56X_3^2 - 52.82X_4^2$ ***Equation 5.6***

$\mathbf{Y_4} = 84.39 - 1.75X_1 - 0.076X_2 + 0.97X_3 - 0.019X_4 - 1.56\ X_1X_2 - 0.13X_1X_3 - 0.038X_1X_4 + 0.35X_2X_3 + 0.23X_2X_4 + 0.051X_3X_4 - 0.64X_1^2 - 0.42X_2^2 - 0.16\ X_3^2 - 1.15X_4^2$ ***Equation 5.7***

$\mathbf{Y_5} = 72.71 + 0.91X_1 + 0.34X_2 - 1.63X_3 + 0.23X_4 + 0.016\ X_1X_2 - 0.59X_1X_3 - 0.22X_1X_4 + 0.28X_2X_3 - 0.061X_2X_4 + 0.099X_3X_4 - 1.16X_1^2 - 0.20X_2^2 - 0.73\ X_3^2 + 0.87X_4^2$ ***Equation 5.8***

$\mathbf{Y_6} = 58.73 + 2.03X_1 - 0.20X_2 - 0.37X_3 - 0.12X_4$ ***Equation 5.9***

$\mathbf{Y_7} = 95.45 + 0.21X_1 - 0.10X_2 - 1.92X_3 + 0.20X_4 - 0.11\ X_1X_2 - 0.074X_1X_3 - 0.26\ X_1X_4 + 0.13X_2X_3 + 0.54X_2X_4 - 0.42X_3X_4 - 0.28X_1^2 + 1.50X_2^2 - 2.22\ X_3^2 - 0.96X_4^2$ ***Equation 5.10***

$\mathbf{Y_8} = 188.83 - 0.75X_1 + 5.86X_2 - 142.46X_3 - 32.26X_4 - 7.50X_1X_2 - 0.26X_1X_3 + 1.53X_1X_4 - 1.90X_2X_3 + 0.50X_2X_4 + 19.59X_3X_4$

Equation 5.11

ANOVA was used to determine the quality of mathematical modelling and to establish the significance of impact of input variables on responses. The mean least squares linear regression method was used to identify the mathematical model that was best described the data for each response monitored. The experimental data was fitted to linear, two factor interaction (2FI), quadratic and cubic polynomial models for all responses. Results for all cubic models were regarded as 'aliased' since the CCD lacked the unique design points required for all terms of the cubic polynomial to be accurately determined [231].

By way of example this discussion will focus on the model for MTZ released at 0.5 hours (Y_1) and 12 hours (Y_4), encapsulation efficiency (Y_5), buoyancy (Y_6), yield (Y_7) and microcapsule size (Y_8). For completeness the response surface plots, normal probability plots of residuals, plots of standardised residuals versus predicted values and Box-Cox plots for the remaining responses are reported in Appendix III. A summary of the responses for Y_1, Y_4, Y_5 - Y_8, for batches MTZ-008 – MTZ-037 for experimental runs CCD 1 to CCD 30 are listed in Table 5.4. The *in vitro* release profiles for these batches are shown in batch summary records that are reported in Appendix 2.

Table 5.4 Summary of responses batches MTZ008 – MTZ-037 (± SD, n=3)

Batch	Y_1 %	Y_4 %	Y_5 %	Y_6 %	Y_7 %	Y_8 µm
MTZ-008	5.60 ± 2.00	84.60 ± 3.33	73.70 ± 2.79	58.34 ± 2.21	96.94 ± 2.17	199.71 ± 3.21
MTZ-009	3.70 ± 0.83	84.90 ± 2.07	72.51 ± 2.65	58.45 ± 1.98	96.47 ± 1.75	233.80 ± 2.72
MTZ-010	10.69 ± 4.82	86.92 ± 1.63	70.81 ± 2.09	56.42 ± 1.67	91.76 ± 1.65	43.960 ±0.78
MTZ-011	9.60 ±2.89	81.60 ± 2.12	71.97 ± 2.27	57.15 ± 3.05	94.88 ± 2.17	280.67 ±1.86
MTZ-012	4.60 ± 1.15	77.60 ± 1.20	74.90 ± 1.39	60.55 ± 1.02	95.71 ± 1.08	303.93 ± 3.73
MTZ-013	7.20 ± 1.60	82.73 ± 8.21	69.77 ± 1.54	61.52 ± 1.76	92.82 ± 1.15	61.910 ± 2.26
MTZ-014	10.1 ± 3.43	85.92 ± 2.58	70.11 ± 3.06	56.55 ± 1.79	90.24 ± 1.97	70.670 ± 2.26
MTZ-015	10.0 ± 2.19	80.60 ± 3.55	70.93 ± 1.58	57.13 ± 2.13	94.76 ± 2.06	349.11 ± 2.57
MTZ-016	3.71 ± 1.59	83.50 ± 2.86	72.91 ± 1.19	58.22 ± 1.99	96.94 ± 2.16	191.75 ± 4.15
MTZ-017	9.34 ± 4.12	81.26 ± 1.94	71.29 ± 2.53	60.15 ± 1.30	92.18 ± 4.81	38.740 ±2.54
MTZ-018	2.66 ± 0.71	83.19 ± 2.86	73.58 ± 1.66	59.60 ± 0.96	94.71 ± 3.02	332.24 ±2.56
MTZ-019	8.19 ± 2.29	83.92 ± 3.00	71.79 ± 2.02	57.45 ± 2.67	96.76 ± 0.50	279.05 ± 2.07
MTZ-020	3.80 ± 1.51	84.90 ± 2.27	73.41 ± 1.99	59.21 ± 1.19	94.12 ±2.10	190.86 ± 3.62
MTZ-021	6.77 ± 1.75	81.58 ± 2.82	74.25 ± 2.56	62.54 ± 0.94	96.94 ± 2.14	267.89 ±4.56
MTZ-022	7.19 ± 2.96	83.14 ± 2.51	71.12 ± 2.28	58.54 ± 2.21	96.94 ± 1.72	181.55 ± 357
MTZ-023	3.33 ±0.30	84.71 ± 1.74	72.57 ± 2.03	58.46 ± 1.99	93.76 ± 2.53	244.43 ±1.68
MTZ-024	3.63 ± 0.76	84.77 ± 2.17	73.35 ± 2.01	57.51 ± 1.68	94.35 ± 2.74	175.92 ± 3.21
MTZ-025	3.70 ± 1.59	83.00 ± 2.12	74.49 ± 3.04	58.40 ± 23.0	96.47 ± 2.65	180.94 ± 2.53
MTZ-026	7.38 ± 1.02	81.81 ± 2.09	74.49 ± 1.89	61.88 ± 1.11	96.47 ± 1.98	402.22 ±1.10
MTZ-027	2.60 ± 0.17	77.60 ± 1.63	75.03 ± 2.29	60.56 ± 1.89	94.12 ±2.07	357.27 ± 2.08
MTZ-028	7.38 ± 2.03	81.81 ± 2.01	69.59 ± 2.04	59.55 ± 0.94	90.01 ±1.42	35.670 ± 0.43
MTZ-029	6.19 ± 2.05	79.23 ± 1.36	70.89 ± 2.17	61.56 ± 2.09	92.12 ± 3.16	54.090 ± 5.80
MTZ-030	3.70 ± 0.37	82.00 ± 3.42	73.4 ± 1.95	58.55 ± 1.90	94.35 ± 2.02	146.76 ± 2.38
MTZ-031	8.11 ± 2.21	85.04 ± 1.52	72.7 ± 1.96	57.54 ± 1.34	96.09 ± 1.29	168.89 ± 3.05
MTZ-032	8.89 ± 2.06	83.92 ± 2.18	71.59 ± 2.75	55.90 ± 2.37	94.11 ±2.14	653.33 ±3.17
MTZ-033	9.69 ± 1.36	86.12 ± 0.85	70.46 ± 1.74	58.55 ± 1.97	95.49 ± 0.77	165.21 ±4.50
MTZ-034	7.61 ±2.01	85.60 ± 1.03	69.14 ± 2.01	56.50 ± 0.93	90.88 ± 1.98	45.490 ± 0.85
MTZ-035	10.60 ± 2.05	84.60 ± 0.99	69.59 ± 1.65	56.45 ± 1.75	91.47 ± 1.06	31.120 ± 5.21
MTZ-036	9.78 ± 0.76	83.11 ± 1.18	68.06 ± 2.51	57.45 ± 2.54	92.23 ± 1.28	47.590± 0.04
MTZ-037	5.60 ± 2.00	80.60 ± 1.02	71.42 ± 1.73	61.20 ± 2.12	94.47 ± 2.00	153.35 ±3.48

5.4.1.1 MTZ released at 0.5 hours (Y_1)

5.4.1.1.1 Verification and evaluation of the model for percent MTZ released at 0.5 hours

A summary of statistics used to determine the most suitable model for percent MTZ released at 0.5 hours (Y_1) are summarised in Table 5.5. The quadratic model was the most suitable model for response Y_1 as the Prob > F value was < 0.05 indicating that the model is significant and does not show significant lack of fit. From equation 5.6 the negative signs for input variables Methocel® K15M (X_1) and Eudragit® RS PO (X_2) reveal that Methocel® K15M and Eudragit® RS PO have an antagonistic effect on the percent MTZ released at 0.5 hour while homogenisation speed (X_3) has a synergistic effect on response Y_1 as there is positive sign adjacent to term X_3. This means that an increase in the amount of Methocel® K15M and Eudragit® RS PO result in a decrease in percent MTZ released at 0.5 hour and an increase in homogenisation speed results in an increase in percent MTZ released at 0.5 hour.

Table 5.5 Summary of sequential model for sum of squares and lack of fit tests for percent MTZ released at 0.5 hours

Sequential model of sum of squares						
Source	**Sum of squares**	**DF**	**Mean square**	**F-value**	**p-value Prob > F**	**Remarks**
Mean vs Total	1103.01	1	1103.01			
Linear vs Mean	333.48	4	56171.26	5.34	0.0030	
2FI vs Linear	31423.17	6	5237.19	0.43	0.8501	
Quadratic vs 2FI	315.82	4	53202.61	42.35	<0.0001	Suggested
Cubic vs Quadratic	9216.95	8	1152.12	0.84	0.5989	Aliased
Residual	9624.87	7	1374.98			
Total	496.62	30	41031.09			
Lack of fit tests						
Source	**Sum of squares**	**DF**	**Mean square**	**F- value**	**p-value Prob > F**	**Remarks**
Linear	390.48	20	13153.35	7709.50	<0.0001	
2FI	343.72	14	16545.98	9698.01	<0.0001	
Quadratic	18833.29	10	1883.33	1103.87	0.1224	Suggested
Cubic	9616.34	2	4808.17	2818.19	<0.0001	Aliased
Pure error	8.53	5	1.71			

This quadratic model had a R^2 value of 0.9614 and a predicted R^2 value of 0.8032 that are in reasonable agreement with the adjusted R^2 of 0.9253 as summarised in Table 5.6.

Table 5.6 Summary statistics for the model for percent MTZ released at 0.5 hours

Model summary statistics					
Source	**Standard deviation**	**R^2**	**Adjusted R^2**	**Predicted R^2**	**Remarks**
Linear	102.58	0.4606	0.3743	0.2425	
2FI	110.42	0.5251	0.2751	-0.5362	
Quadratic	35.44	0.9614	0.9253	0.8032	Suggested
Cubic	37.08	0.9803	0.9182	0.9182	Aliased

The quadratic model was significant for percent MTZ released at 0.5 hours (Y_1) as indicated by the model F value of 26.66 (Table 5.7). The model F-value of 26.66 implies that there is only a 0.01% chance that a value this large could occur due to noise. The data revealed that individual linear contributions by Methocel® K15M (X_1), Eudragit® RS PO (X_2) and homogenisation speed (X_3) were significant ($p < 0.05$). The cross contribution of X_2X_3, X_3X_4 and quadratic contributions of X_1^2, X_2^2 and X_4^2 also had a significant effect on percent MTZ released at 0.5 hours (Y_1). However, the p-value > 0.05 indicates that the individual contribution of homogenisation time (X_4) and cross-contributions of X_1X_2, X_1X_3, X_1X_4, X_2X_4 and quadratic contribution of X_3^2 did not have a significant effect on response Y_1. This means that an increase in the levels of Methocel® K15M and Eudragit® RS PO increase the % MTZ released at 0.5 hour. Homogenisation speed has a significant effect on % MTZ released at 0.5 hour, however homogenisation time does not significantly affect the % MTZ released at 0.5 hour. An increase in homogenisation speed increases the % MTZ released at 0.5 hour. The Prob > F for the entire model was < 0.0001 indicating that the model was significant and that the overall contribution of the terms in the model have a significant impact on percent MTZ released at 0.5 hours (Y_1).

Table 5.7 ANOVA data for the quadratic model for percent MTZ released at 0.5 hour.

Source	Sum of squares	DF	Mean Square	F-value	p-value Prob > F
Model	695.90	14	33494.19	26.66	< 0.0001
X_1	256.01	1	256.01	137.30	< 0.0001
X_2	6840.92	1	6840.92	5.45	0.0339
X_3	41872.08	1	41872.08	33.33	<0.0001
X_4	3511.77	1	3511.77	2.80	0.1152
X_1X_2	7.76	0	7.76	0.31	0.9384
X_1X_3	8.45	1	8.45	0.33	0.9357
X_1X_4	1466.61	1	14466.61	1.17	0.2970
X_2X_3	17399.85	1	17399.85	13.85	0.0020
X_2X_4	2801.87	1	2801.87	2.23	0.1560
X_3X_4	9738.63	1	9738.63	7.75	0.0139
X_1^2	36290.57	1	36290.57	28.89	<0.0001
X_2^2	24103.60	1	24.103.60	19.19	0.0005
X_3^2	476.20	1	476.20	0.38	0.5473
X_4^2	7227.25	1	7227.250	5.75	0.0299
Residual	1841.82	15	1256.12		
Lack of fit	18833.29	10	1883.33	1103.87	0.1224
Pure error	8.53	5	1.71		
Cor total	723.96	29			

Values in red indicate significant independent variables

5.4.1.1.2 Diagnostic plots for percent MTZ released at 0.5 hours

Model adequacy was also tested using a normal probability plot of residuals, a plot of standardised residuals versus predicted values and a Box-Cox plot for power transformation. The normal plot of residuals is depicted in Figure 5.1 and reveals that a majority of the residuals fall in a straight line indicating that the assumption of normality is satisfied.

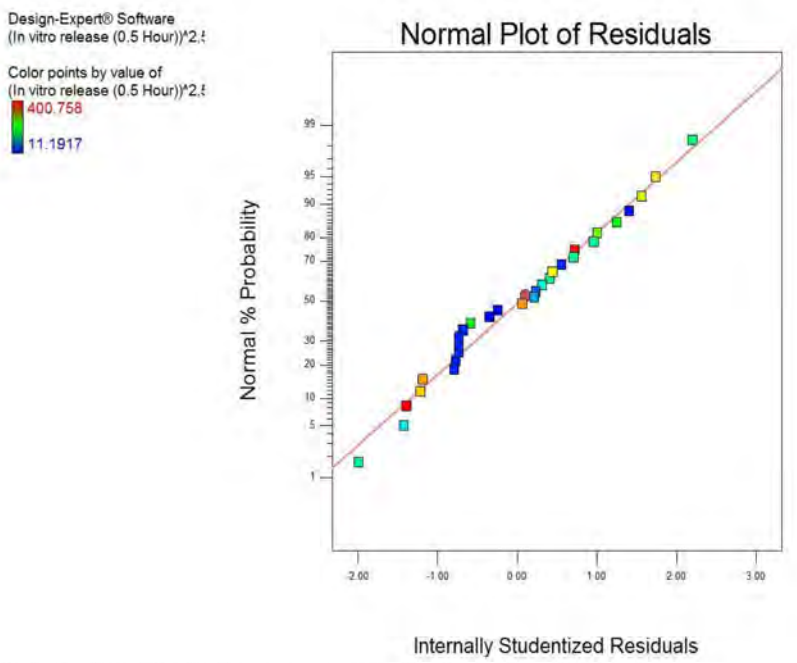

Figure 5.1 Normal plot of residuals for amount MTZ released at 0.5 hrs

The plot of residuals versus predicted values for amount of MTZ released at 0.5 hours (Y_1) is depicted in Figure 5.2 and reveals no distinct pattern as the residuals are scattered above and below zero suggesting model adequacy.

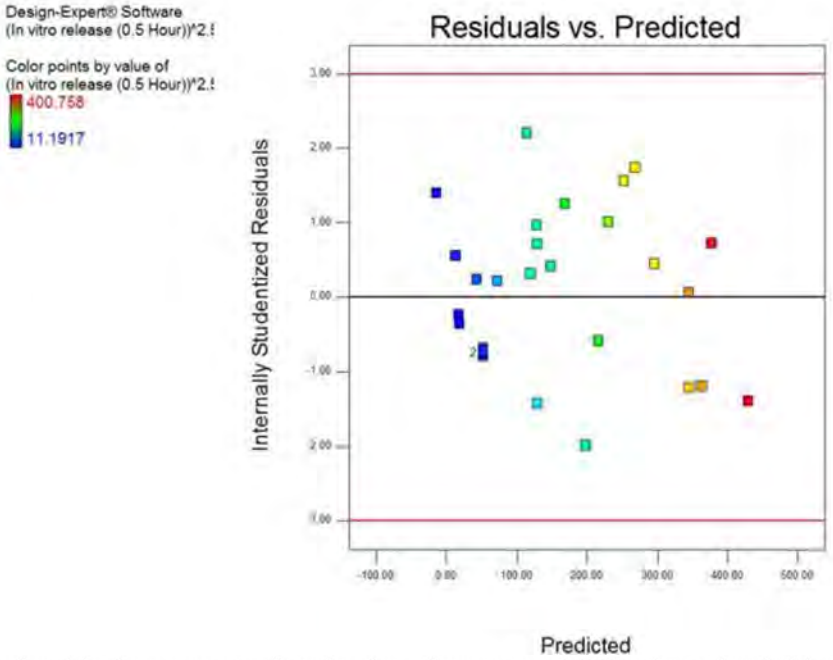

Figure 5.2 Plot of residuals versus predicted values for amount MTZ released at 0.5 hrs

Box-Cox plots prior to and following transformation are depicted in Figures 5.3 (A) and 5.3 (B) respectively. A power transformation with $\lambda = 2.53$ was recommended and all reported statistical data for response Y_1 pertained to transformed data. Box-Cox plots for transformation are useful when attempting to normalise data [514].

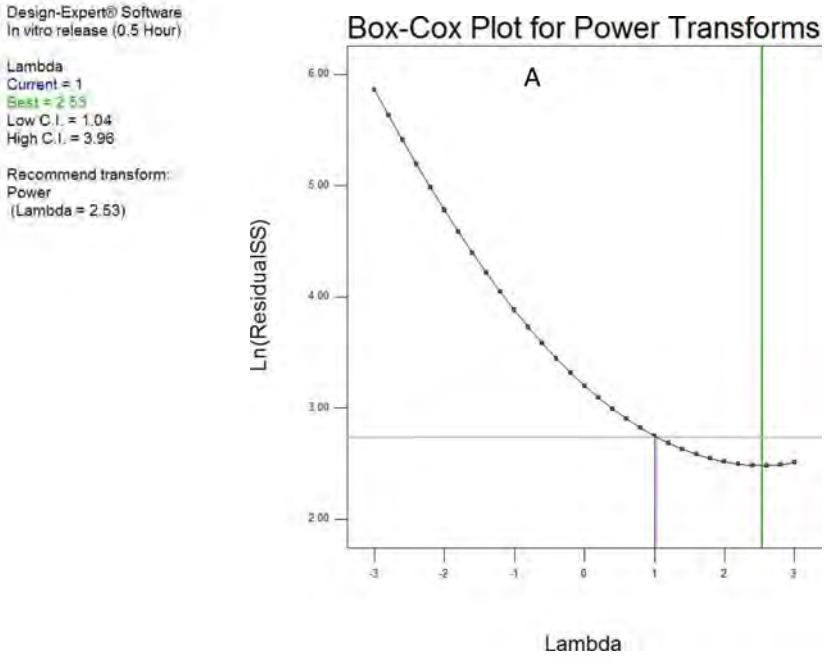

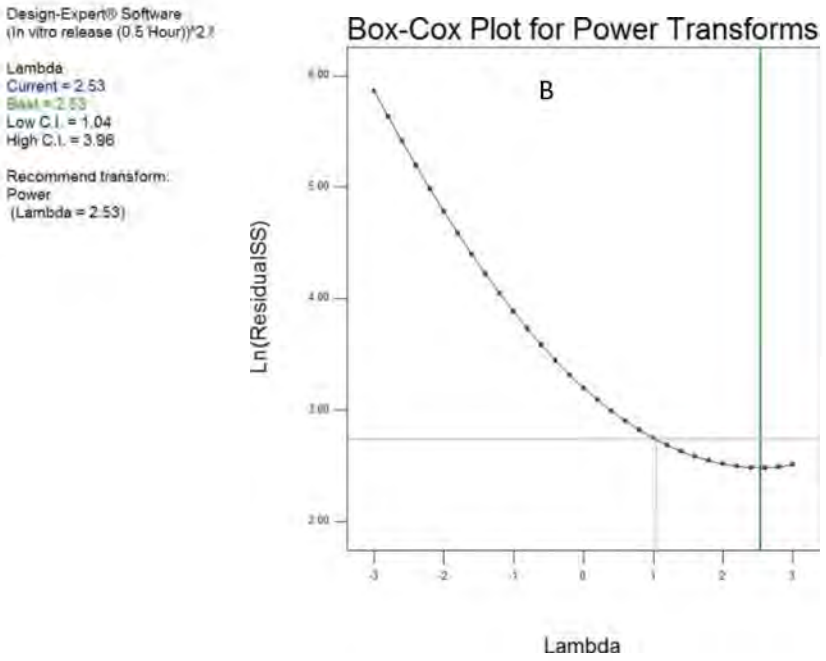

Figure 5.3 Box-Cox plots prior (A) to and following transformation (B) for amount MTZ released at 0.5 hrs

5.4.1.1.3 Response surface plots for percent MTZ released at 0.5 hour

Two dimensional contour and three-dimensional response surface plots were used to study the interactive effects of input variables on percent MTZ released at 0.5 hours (Y_1) and the contour plots for homogenisation speed versus amount of Methocel® K15M and homogenisation speed versus amount of Eudragit® RS PO are depicted in Figures 5.4 and 5.5 respectively .

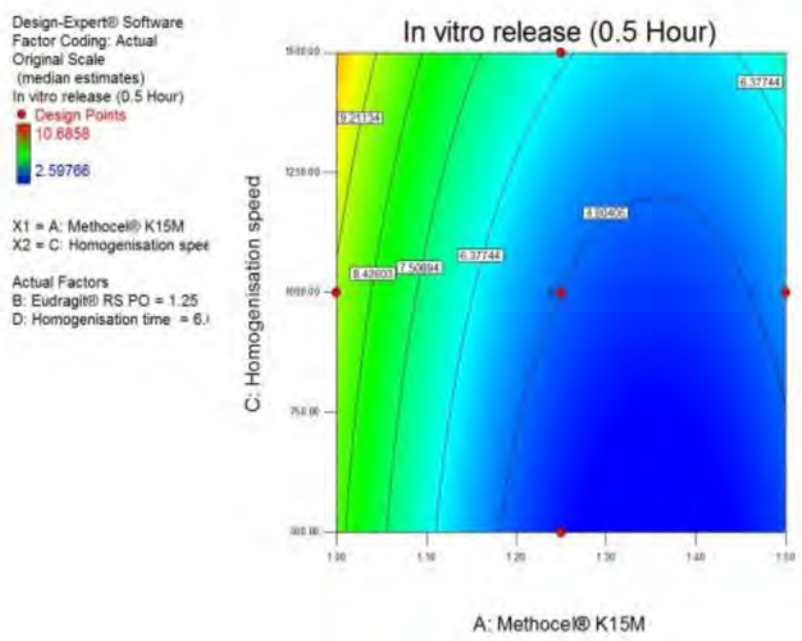

Figure 5.4 Contour plot depicting the effect of homogenisation speed and amount of Methocel® K15M on percent MTZ released at 0.5 hrs

From the contour plot depicted in Figure 5.4 it is evident that an increase in the amount of Methocel® K15M resulted in a decrease in the percent of MTZ released in the first 30 minutes of dissolution testing. The same effect was also observed for Eudragit® RS PO suggesting that the rate controlling polymers effectively slow or control the release of MTZ (Figure 5.5). When the amount of Methocel® K15M is increased an increase in the thickness and viscosity of the gel layer that forms around the microcapsules on hydration occurs, leading to an increase in the diffusional path length for MTZ and slower drug release [471,472]. These observations are in agreement with reports than an increase in the levels of HPMC used result in a decrease in the rate of drug release from dosage forms [456]. The contour plot also reveals that an increase in homogenisation speed when Methocel® K15M content ranged between 1.2 to 1.5g results in a slight increase in the % MTZ released which may be due to higher homogenisation speeds producing smaller size microcapsules leading to an increase in the rate and extent of MTZ release. The size of microcapsules decreases as

the homogenisation speed increases due to high power input thus leading to the distribution of the internal phase into smaller droplet sizes thereby producing smaller microcapsules [464]. Microcapsules with a small size have a large surface area-to-volume ratio and the rate of flux of drug from the microparticle per unit mass increases resulting in an increased rate of dissolution [475]. The Figure 5.5 shows that an increase in Eudragit RS PO results in a decrease in percent MTZ released at 0.5 hours.

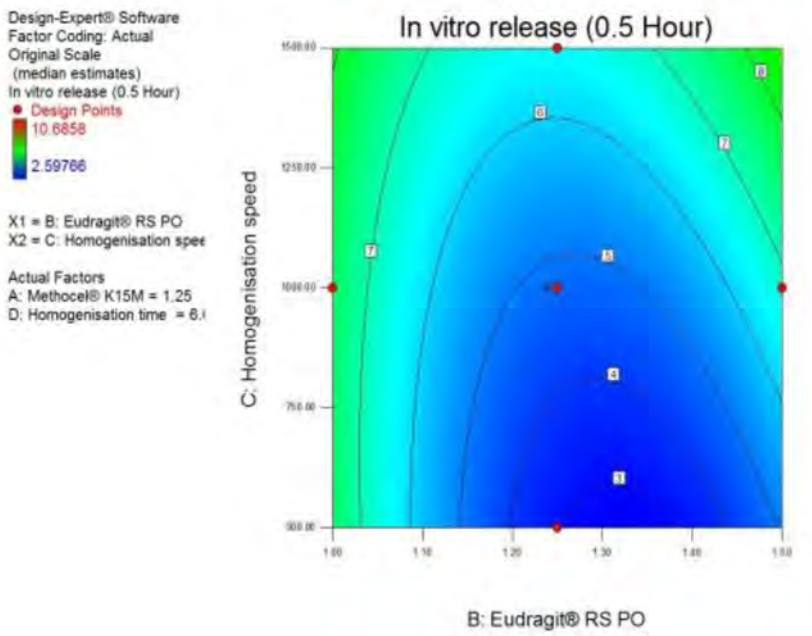

Figure 5.5 Contour plot depicting the impact of homogenisation speed and amount of Eudragit® RS PO on the amount of MTZ released at 0.5 hours

The three-dimensional (3D) response surface plots for percent released at 0.5 hours are depicted in Figures 5.6 and 5.7. The 3D plot in Figure 5.6 reveals that a decrease in Methocel® K15M content resulted in an increase in the percent MTZ released at 0.5 hours. This figure also reveals that minimal relationship between the amount of HPMC K15M and the release after 0.5 hours exist. The plot depicted in Figure 5.7 reveals that an increase in homogenisation speed resulted in an increase in the percent MTZ released at 0.5 hours, whereas an optimum for homogenisation time at 6 hours was observed to have a significant effect on MTZ released at this time.

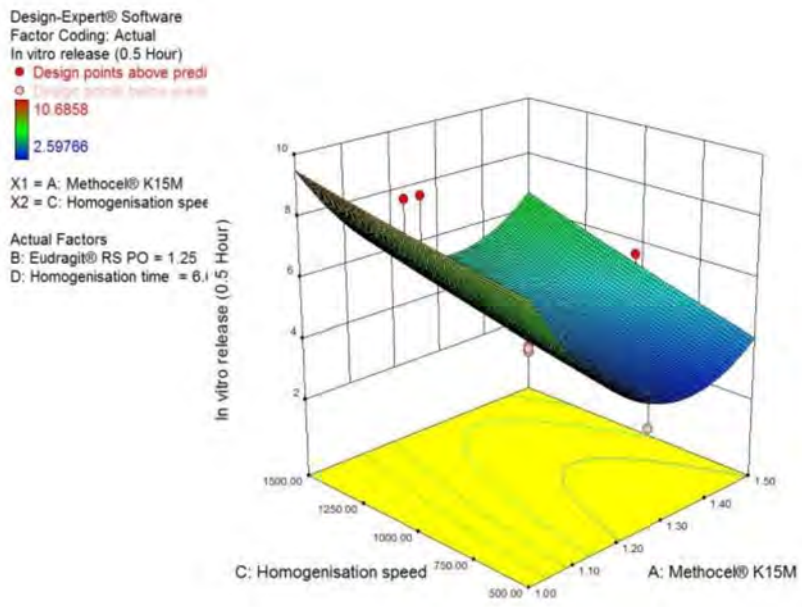

Figure 5.6 3D plot depicting the impact of homogenisation speed and amount of Methocel® K15M on the release of MTZ at 0.5 hours

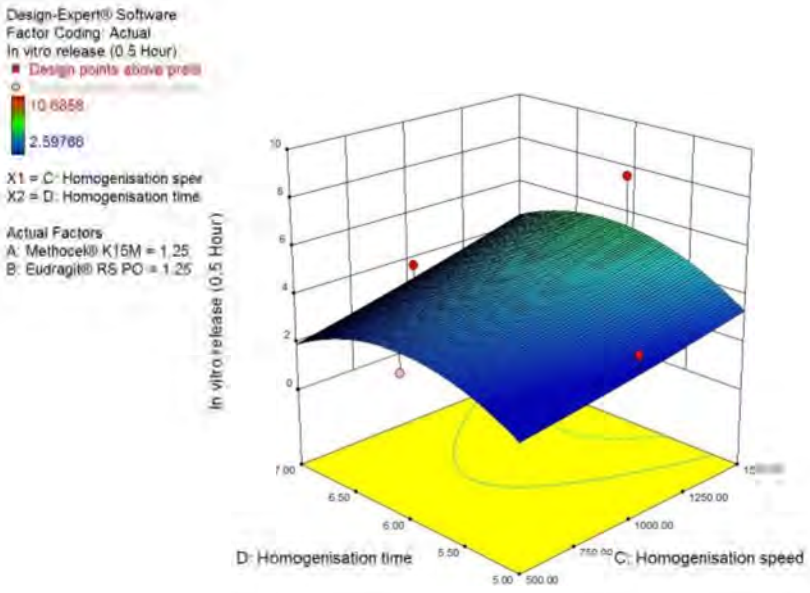

Figure 5.7 3D response surface plot depicting the impact of homogenisation time and speed on the amount of MTZ released at 0.5 hours

5.4.1.2 MTZ released at 12 hours (Y_4)

5.4.1.2.1 Verification and evaluation of the model for percent MTZ released at 12hours

A summary of statistics used to determine the best fit model for percent MTZ released at 12 hours are summarised in Table 5.8 and it is clear that a quadratic model was the best fit model for response Y_4 as the Prob > F value was < 0.05 indicating that the model was significant.

Table 5.8 Summary of sequential model of sum of squares and lack of fit tests for percent MTZ released at 12 hours

Sequential model of sum of squares						
Source	**Sum of squares**	**DF**	**Mean square**	**F-value**	**p-value Prob > F**	**Remarks**
Mean vs Total	306.47	1	306.47			
Linear vs Mean	72.19	4	18.05	4.88	0.0048	
2FI vs Linear	42.23	6	7.04	2.66	0.0480	
Quadratic vs 2FI	32.91	4	8.23	7.11	0.0020	Suggested
Cubic vs Quadratic	13.81	8	1.73	3.41	0.0616	Aliased
Residual	3.54	7	0.51			
Total	306.77	30	6890.22			
Lack of fit tests						
Source	**Sum of squares**	**DF**	**Mean square**	**F-value**	**p-value Prob > F**	**Remarks**
Linear	89.13	20	4.46	6.63	0.0226	
2FI	46.90	14	3.35	4.98	0.0431	
Quadratic	13.99	10	1.40	2.08	0.2165	Suggested
Cubic	0.18	2	0.090	0.13	0.8777	Aliased

The model summary statistics are summarised in Table 5.9 and the quadratic model has an R^2 = 0.8946. However, the predicted R^2 value of 0.5376 is not as close to the adjusted R^2 value of 0.7963 suggesting a large block effect.

Table 5.9 Model summary statistics for percent MTZ released at 12 hours

Model summary statistics					
Source	**Standard deviation**	**R^2**	**Adjusted R^2**	**Predicted R^2**	**Remarks**
Linear	1.92	0.4383	0.3485	0.1124	
2FI	1.63	0.6948	0.5341	-0.0539	
Quadratic	1.08	0.8946	0.7963	0.5376	Suggested
Cubic	0.71	0.9785	0.9109	0.8425	Aliased

Factors such as Methocel® K15M content (X_1) have a negative sign adjacent to the term in Equation 5.7 indicating that the amount of Methocel® K15M has an antagonistic effect on MTZ release, this means that a decrease in the amount of Methocel® K15M results in an increase of percent MTZ released after 12 hours. Homogenisation speed has a positive sign adjacent to its coded term X_3 in Equation 5.7 meaning that an increase in homogenisation speed results in an increase of percent MTZ released.

A summary of ANOVA results for percent MTZ released at 12 hours (Table 5.10) suggest that the quadratic model was significant as indicated by a model F value = 9.10 and a value this large implies that there is only a 0.01% chance that a Model F Value could occur due to noise. The data revealed that individual linear contributions for Methocel® K15M content (X_1) and homogenisation speed (X_3) were significant factors with $p < 0.05$. The cross contribution of X_1X_2 also had a significant effect on the release of MTZ at 12 hours. This means that Methocel® K15M and homogenisation speed significantly affect the percent MTZ released at 12 hours. An increase in the amount of Methocel® K15M results in decrease in percent MTZ released at 12 hours while an increase in homogenisation speed results in an increase in percent MTZ released at 12 hours.

In addition a combination of the two polymers Methocel® K15M and Eudragit® RS PO have a significant effect on the percent MTZ released at 12 hours. A value for $p > 0.05$ indicates that individual contributions of Eudragit® RS PO content (X_2) and homogenisation time (X_4) and the cross-contribution of terms X_1X_3, X_1X_4, X_2X_3, X_2X_4, X_3X_4 and the quadratic contribution of terms X_1^2 $X_2^2X_3^2$ and X_4^2 do not have a significant effect on the percent MTZ released at 12 hours. Eudragit® RS PO and homogenisation time did not have a significant effect on the % MTZ released after 12 hours. The Prob > F was < 0.0001 suggesting that the overall contribution of the terms in the model have a significant impact on MTZ release at 12 hours.

Table 5.10 ANOVA results for the quadratic model for percent MTZ released at 12 hours

Source	Sum of squares	DF	Mean Square	F-value	p-value Prob > F
Model	147.33	14	10.52	9.10	< 0.0001
X_1	55.19	1	55.19	47.71	< 0.0001
X_2	0.10	1	0.10	0.090	0.7680
X_3	16.89	1	16.89	14.60	0.0017
X_4	0.31	1	0.31	0.27	0.9427
X_1X_2	39.07	1	39.07	33.78	<0.0001
X_1X_3	0.27	1	0.27	0.23	0.6352
X_1X_4	0.023	1	0.023	0.020	0.8888
X_2X_3	1.97	1	1.97	1.70	0.2115
X_2X_4	0.85	1	0.85	0.74	0.4045
X_3X_4	0.042	1	0.042	0.036	0.8517
X_1^2	1.06	1	1.06	0.92	0.3530
X_2^2	0.45	1	0.45	0.39	0.5412
X_3^2	0.063	1	0.063	0.054	0.8192
X_4^2	3.43	1	3.43	2.96	0.1058
Residual	17.35	15	1.16		
Lack of fit	13.99	10	1.40	2.08	0.2165
Pure error	3.36	5	0.67		
Cor total	164.68	29			

Values in red indicate significant independent variables

5.4.1.2.2 Diagnostic plots for percent MTZ released at 0.5 hours

The normal probability plot of residuals depicted in Figure 5.8 reveals that most residuals fall on a straight line with some residuals placed slightly above or below the line loosely satisfying the assumption of normality.

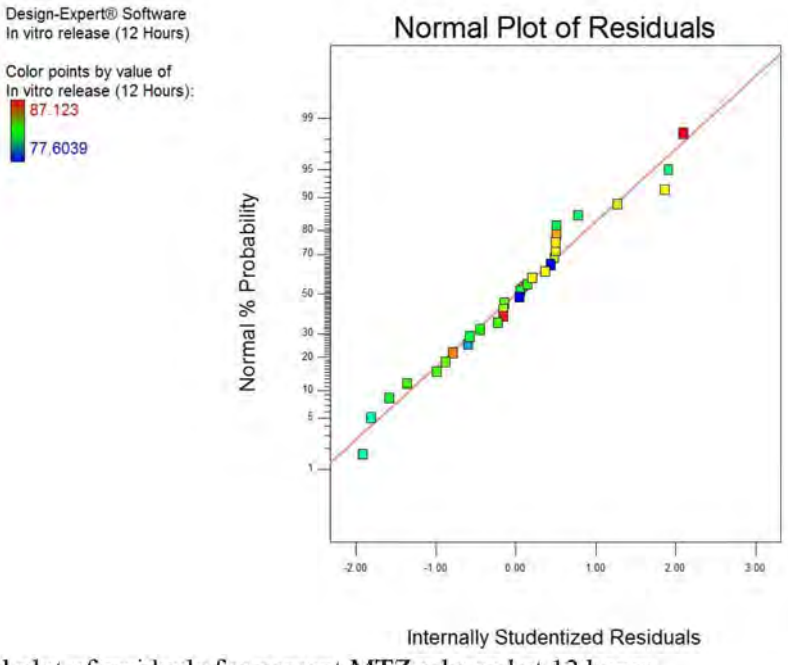

Figure 5.8 Normal plot of residuals for percent MTZ released at 12 hours

The plot of residuals versus predicted values for percent MTZ released is depicted in Figure 5.9 and as no distinct pattern exists in the plot the model is adequate.

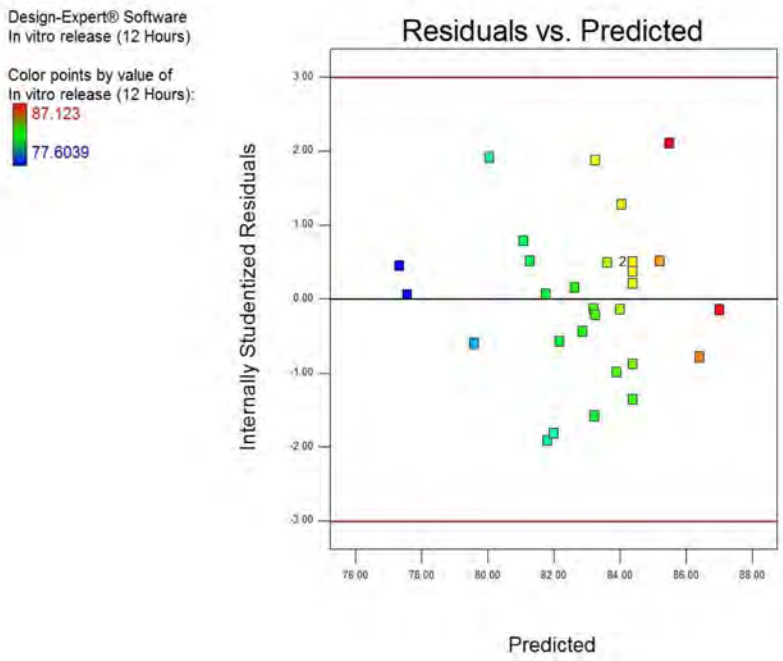

Figure 5.9 Plot of residuals versus predicted values for percent MTZ released at 12 hrs

The Box-Cox plot depicted in Figure 5.10 reveals $\lambda = 1$ and therefore no transformation of data was necessary.

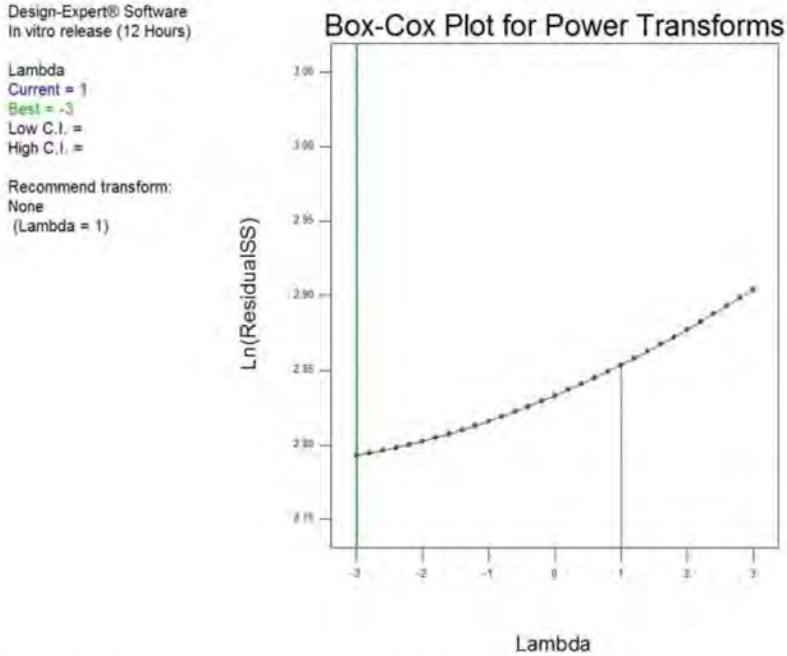

Figure 5.10 Box-Cox plot for response for amount MTZ released at 12 hrs

5.4.1.2.3 Response surface plots for percent MTZ released at 12 hours

Two dimensional contour and three-dimensional response surface plots were used to study the interactive effects of input variables on the percent MTZ released at 12 hours. The impact of amount of Methocel® K15M and homogenisation speed on the release of MTZ at 12 hours is depicted in Figure 5.11 and it is evident that an increase in Methocel® K15M content resulted in a decrease in amount of MTZ released at 12 hours whereas an increase in homogenisation speed resulted in an increase in MTZ release after 12 hours. The three-dimensional response surface plot for MTZ released at 12 hours is depicted in Figure 5.12 and reveals that an increase in MTZ release occurred at 12 hours as an increase in homogenisation speed and a decrease in the amount of Methocel® K15M is implemented.

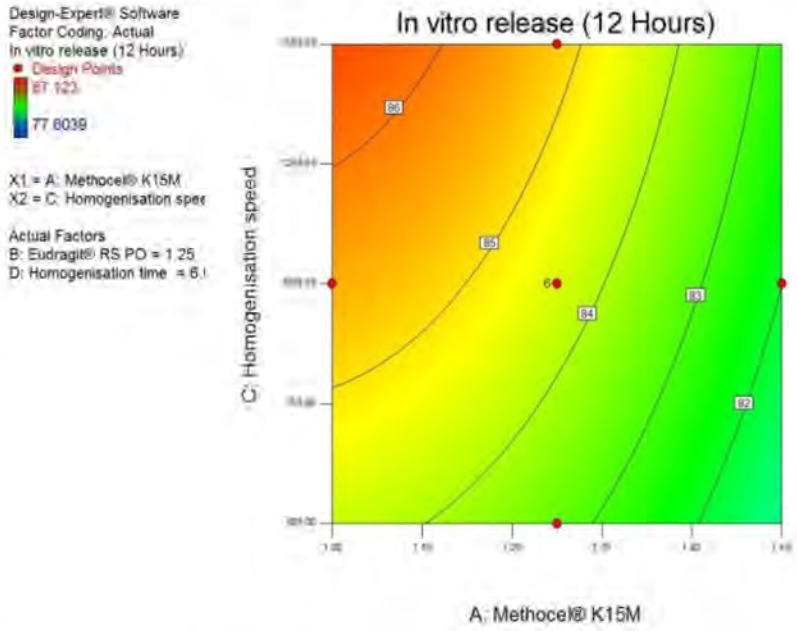

Figure 5.11 Contour plot showing the effect of homogenisation speed and amount of Methocel® K15M on amount of MTZ released at 12 hours

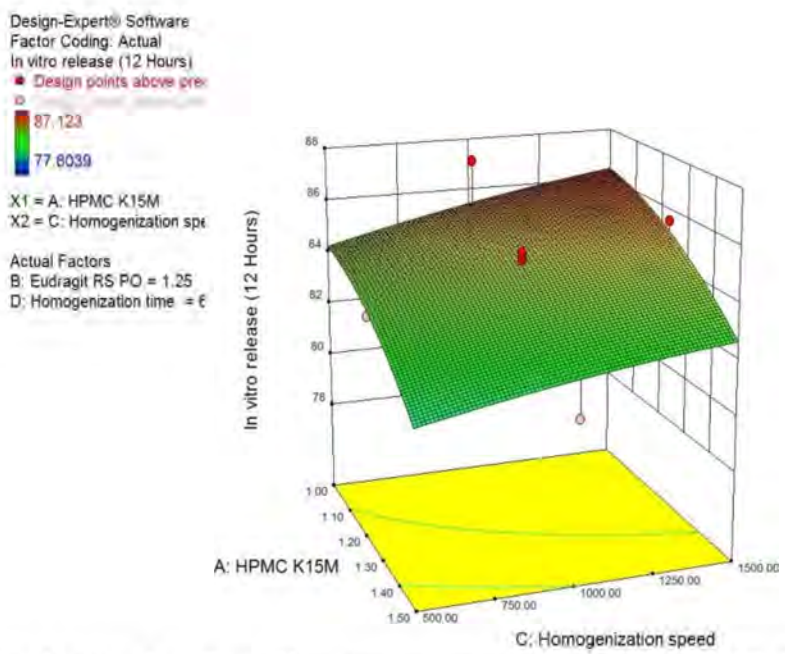

Figure 5.12 3D plot showing the effect of homogenisation speed and amount of Methocel® K15M on amount of MTZ released at 12 hours

5.4.1.3 Encapsulation efficiency (Y_5)

5.4.1.3.1 Verification and evaluation of the model for encapsulation efficiency

A quadratic model was identified as the best fit model for encapsulation efficiency and the statistical data used to establish the best fit model are summarised in Table 5.11. The mathematical equation representing the relationship for encapsulation efficiency (Equation 5.8) has positive and negative signs adjacent to the terms for Methocel® K15M content (X_1) and homogenisation speed (X_3) highlighting the synergistic effect of Methocel® K15M content and antagonistic effect of homogenisation speed on encapsulation efficiency. This means that an increase in the amount of Methocel® K15M results in an increase in the encapsulation efficiency while a decrease in the homogenisation speed results in an increase in encapsulation efficiency.

Table 5.11 Summary of sequential model of sum of squares and lack of fit tests for encapsulation efficiency

Sequential model of sum of squares						
Source	**Sum of squares**	**DF**	**Mean square**	**F- value**	**p-value Prob > F**	**Remarks**
Mean vs Total	230.63	1	230.63			
Linear vs Mean	65.46	4	16.37	12.74	<0.0001	
2FI vs Linear	7.79	6	1.30	1.01	0.4453	
Quadratic vs 2FI	13.03	4	3.26	4.33	0.0159	Suggested
Cubic vs Quadratic	4.55	8	0.57	0.59	0.7619	Aliased
Residual	6.74	7	0.96			
Total		30	5183.98			
Lack of fit tests						
Source	**Sum of squares**	**DF**	**Mean square**	**F-value**	**p-value Prob > F**	**Remarks**
Linear	30.70	20	1.53	5.38	0.0354	
2FI	22.90	14	1.64	5.73	0.0322	
Quadratic	9.87	10	0.99	3.46	0.0916	Suggested
Cubic	5.32	2	2.66	9.32	0.0206	Aliased
Pure error	1.43	5	0.29			

The Prob > F value < 0.05 indicates that the model is significant for this response. A summary of the R^2, predicted and adjusted R^2 values for the models are listed in Table 5.12.

Table 5.12 Model summary statistics for encapsulation efficiency

Model summary statistics					
Source	**Standard deviation**	**R^2**	**Adjusted R^2**	**Predicted R^2**	**Remarks**
Linear	1.13	0.6708	0.6181	005501	
2FI	1.13	0.7507	0.6195	0.4898	
Quadratic	0.87	0.8842	0.7762	0.6084	Suggested
Cubic	0.98	0.9309	0.7137	-5.5125	Aliased

The quadratic model has a R^2 value of 0.8842 and a predicted R^2 of 0.6084 that is in reasonable agreement with the adjusted R^2 of 0.7762. The ANOVA data for encapsulation efficiency are summarised in Table 5.13 and the quadratic model has an F-value of 8.18 implying that the model is significant and that there is only a 0.01% chance that the model F-value this large could occur due to noise. Linear factors for Methocel® K15M (X_1) and homogenisation speed (X_3), cross contributions of terms X_1X_3 and quadratic factors X_1^2 had a significant effect on the encapsulation efficiency. Eudragit® RS PO and homogenisation time did not have any effect on the encapsulation efficiency. The Prob > F was 0.0001 indicating that the overall contribution of the terms in the model have a significant impact on encapsulation efficiency.

Table 5.13 ANOVA for quadratic model for encapsulation efficiency

Source	Sum of squares	DF	Mean Square	F-value	p-value Prob > F
Model	86.29	14	6.16	8.18	0.0001
X_1	14.76	1	14.76	19.60	0.0005
X_2	2.13	1	2.13	2.83	0.1132
X_3	47.65	1	47.65	63.26	<0.0001
X_4	0.92	1	0.92	1.23	0.2857
X_1X_2	0.20	1	0.20	0.27	0.9421
X_1X_3	5.55	1	5.55	7.37	0.0160
X_1X_4	0.81	1	0.81	1.07	0.3173
X_2X_3	1.22	1	1.22	1.62	0.2227
X_2X_4	0.060	1	0.060	0.080	0.7809
X_3X_4	0.16	1	0.16	0.21	0.6563
X_1^2	3.46	1	3.46	4.60	0.0488
X_2^2	0.10	1	0.10	0.14	0.7150
X_3^2	1.39	1	1.39	1.84	0.1945
X_4^2	1.98	1	1.98	2.63	0.1258
Residual	11.30	15	0.75		
Lack of fit	9.87	10	0.99	3.46	0.0916
Pure error	1.43	5	0.29		
Cor total	97.58	29			

Values in red indicate significant independent variables

5.4.1.3.2 Diagnostic plots for encapsulation efficiency

The normal plot probability plot of residuals depicted in Figure 5.13 reveals that the residuals fall in a slightly S-shaped pattern and that the assumption of normality was loosely satisfied. The plot of residuals versus predicted values for encapsulation efficiency is depicted in Figure 5.14 and reveals no clear pattern in the data as residuals are scattered suggesting the data was fitted adequately by the model.

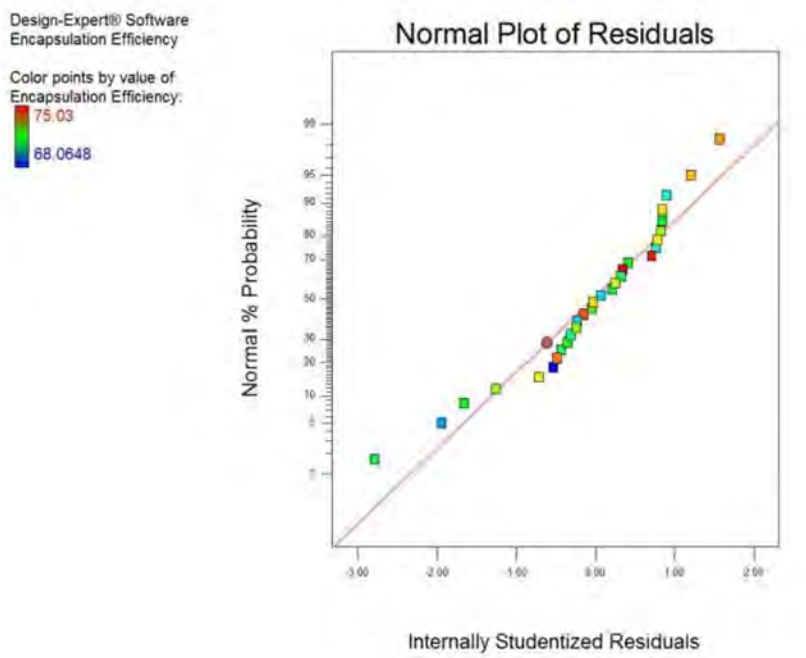

Figure 5.13 Normal plot of residuals for encapsulation efficiency

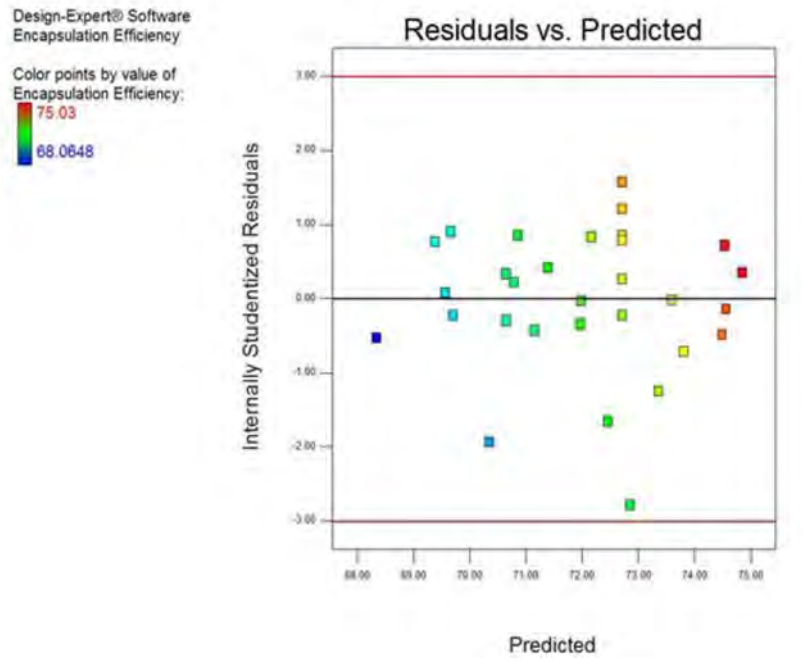

Figure 5.14 Plot of residuals versus predicted values for encapsulation efficiency

The Box-Cox plot for encapsulation efficiency is depicted in Figure 5.15 and $\lambda = 1$ indicating that no data transformation is necessary.

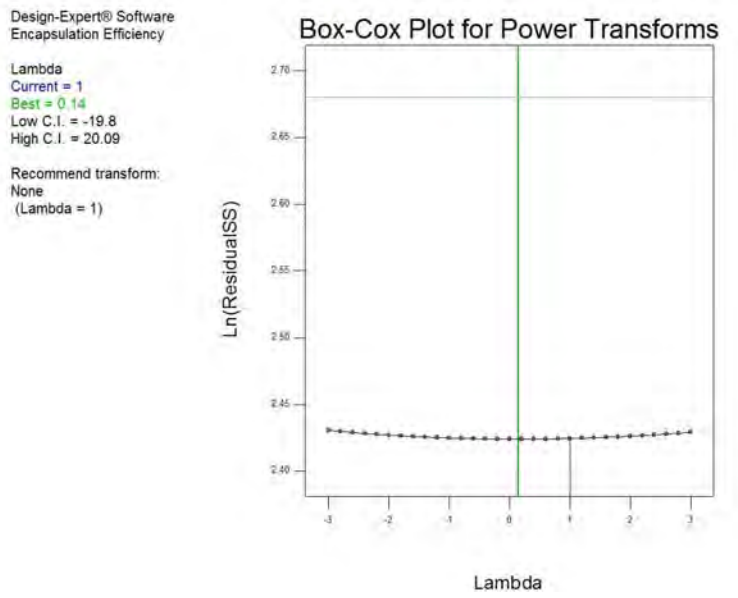

Figure 5.15 Box-Cox plot for encapsulation efficiency

5.4.1.3.3 Response surface plots for encapsulation efficiency

The two-dimensional contour plot depicted in Figure 5.16 reveals the impact of homogenisation speed and amount of Methocel® K15M on encapsulation efficiency (Y_5). The plot indicates that an increase in Methocel® K15M content results in an increase in encapsulation efficiency and an increase of the polymer content from 1.00 g to 1.20 g results in a significant increase in encapsulation efficiency when compared an increase from 1.2 to 1.5 g. This is evident from the contour lines that are close when the Methocel® K15M content is increased from 1.00 to 1.20 g and become wider between 1.20 and 1.5 g levels of Methocel® K15M. It has been reported that an increase in the amount of rate controlling polymer such as Methocel® K15M used results in an increase in encapsulation efficiency as higher Methocel® K15M levels lead to an increase in viscosity of the dispersed phase thereby reducing the migration of drug to the continuous or aqueous phase resulting in higher encapsulation efficiencies [453,456,458].

From the contour plot (Figure 5.16) it is also evident that when Methocel® K15M levels are constant such as at 1.2 g for example an increase in homogenisation speed resulted in a decrease in encapsulation efficiency. An increase in homogenisation speed when using a solvent evaporation process results in a decrease in encapsulation efficiency has been observed and reported [397,464]. The high power introduced by increasing homogenisation speeds imparts greater energy to the emulsion system resulting in frequent reduction of the microparticle sizes with a consequence of lower encapsulation efficiency [464].

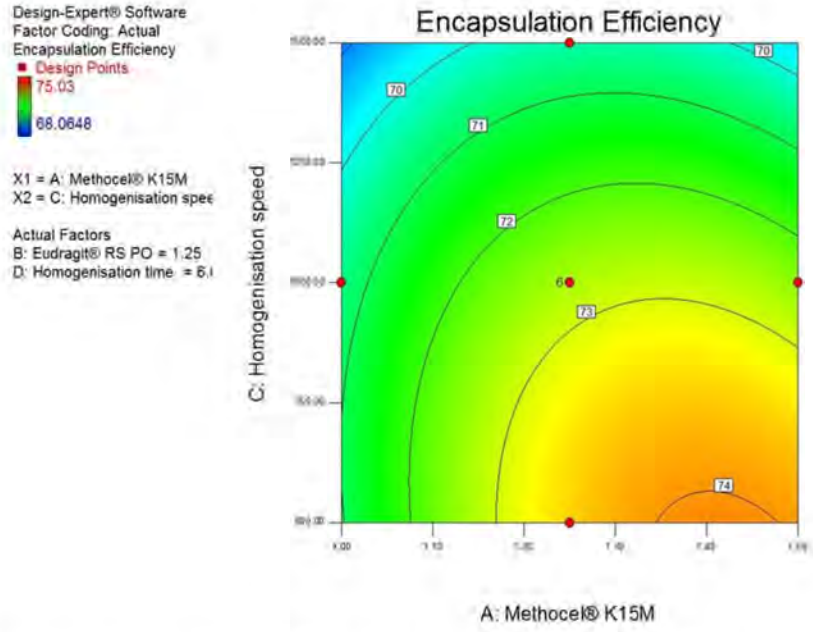

Figure 5.16 Contour plot showing the effect of homogenisation speed and amount of Methocel® K15M on encapsulation efficiency

These results are also evident in the three-dimensional response surface plot depicted in Figure 5.17 that reveals the effect of Methocel® K15M content and homogenisation speed on encapsulation efficiency (Y_5).

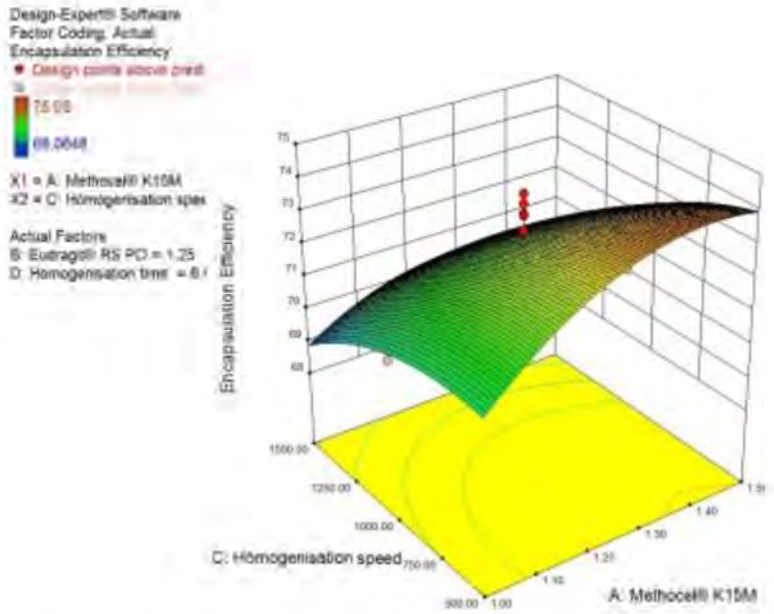

Figure 5.17 3D plot showing the effect of homogenisation speed and amount of Methocel® K15M on encapsulation efficiency

5.4.1.4 Buoyancy (Y_6)

5.4.1.4.1 Verification and evaluation of the model for buoyancy

A linear model was identified as the most suitable model to describe buoyancy and the summary of statistics used to identify the model are summarised in Table 5.14.

Table 5.14 Summary of sequential model of sum of squares and lack of fit tests for buoyancy

Sequential model of sum of squares						
Source	**Sum of squares**	**DF**	**Mean square**	**F- value**	**p-value Prob > F**	**Remarks**
Mean vs Total	175.13	1	175.13			
Linear vs Mean	77.23	4	19.31	24.53	< 0.0001	Suggested
2FI vs Linear	5.04	6	0.84	1.09	0.4030	
Quadratic vs 2FI	5.98	4	1.49	2.59	0.0794	
Cubic vs Quadratic	6.91	8	0.86	3.45	0.0600	Aliased
Residual	1.75	7	0.25			
Total	175.28	30	3938.09			
Lack of fit tests						
Source	**Sum of squares**	**DF**	**Mean square**	**F- value**	**p-value Prob > F**	**Remarks**
Linear	18.21	20	0.91	3.10	0.1064	Suggested
2FI	13.17	14	0.94	3.20	0.1024	
Quadratic	7.19	10	0.72	2.45	0.1672	
Cubic	0.28	2	0.14	0.48	0.6426	Aliased
Pure error	1.47	5	0.29			

The model was found to be significant as the Prob > F value was < 0.05. The R^2 value for linear model was 0.7969 (Table 5.15) and the predicted R^2 of 0.7091 was in reasonable agreement with the adjusted R^2 of 0.7644. From Equation 5.9 the positive sign for input variable term X_1 suggests that Methocel® K15M content has a synergistic effect on buoyancy.

Table 5.15 Model summary statistics for buoyancy

Model summary statistics					
Source	**Standard deviation**	**R^2**	**Adjusted R^2**	**Predicted R^2**	**Remarks**
Linear	0.89	0.7969	0.7644	0.7091	Suggested
2FI	0.88	0.8490	0.7695	0.6350	
Quadratic	0.76	0.9106	0.8272	0.5861	
Cubic	0.50	0.9819	0.9251	0.3393	Aliased

The linear model was established as significant for buoyancy as indicated by the model F-value of 24.53 (Table 5.16) that implies that there is only a 0.01% that a Model F Value this large could occur due to noise. The data revealed that individual linear contribution of Methocel® K15M content was the only significant factor indicated by $p < 0.05$. All other factors were not significant as p was > 0.05 in all cases. The Prob > F for the entire model

was < 0.0001 indicating that the model is significant and shows that the overall contribution of the collective terms in the model have a significant impact

Table 5.16 ANOVA for quadratic model for buoyancy

Source	Sum of squares	DF	Mean Square	F-value	p-value Prob > F
Model	77.23	4	19.31	24.53	<0.0001
X_1	73.85	1	73.85	93.80	<0.0001
X_2	0.70	1	0.70	0.89	0.3556
X_3	2.42	1	2.42	3.08	0.0916
X_4	0.26	1	0.26	0.33	0.5683
Residual	19.68	25	0.79		
Lack of fit	18.21	20	0.91	3.10	0.1064
Pure error	1.47	5	0.29		
Cor total	96.91	29			

Values in red indicate significant independent variables

5.4.1.4.2 Diagnostic plots for buoyancy

The normal plot of residuals depicted in Figure 5.18 reveals that the residuals fall roughly along a straight line, therefore the assumption of normality was satisfied.

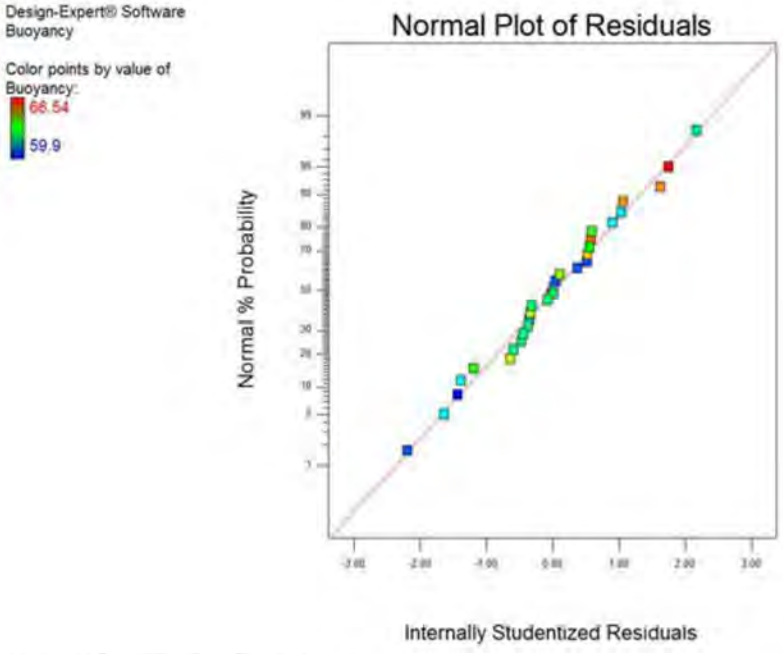

Figure 5.18 Normal plot of residuals for buoyancy

The plot of residuals versus predicted values for buoyancy is depicted in Figure 5.19 and indicates no clear pattern in the data as the residuals are scattered and do not fall outside the limit lines indicating that the data was adequately fitted to the model.

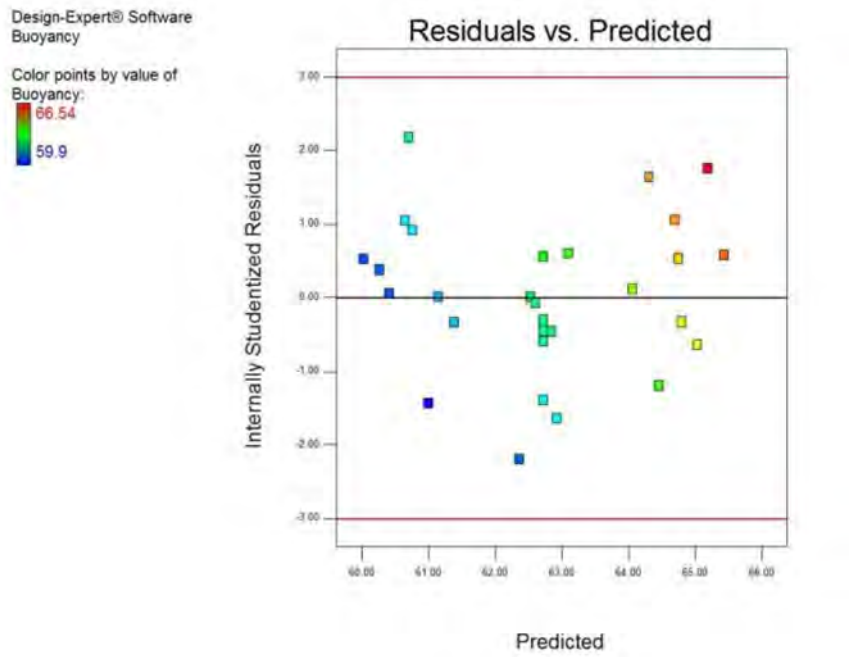

Figure 5.19 Plot of residuals versus predicted values for buoyancy

The Box-Cox plot for buoyancy is depicted in Figure 5.20 and λ =1 indicating that no transformation of the data was required.

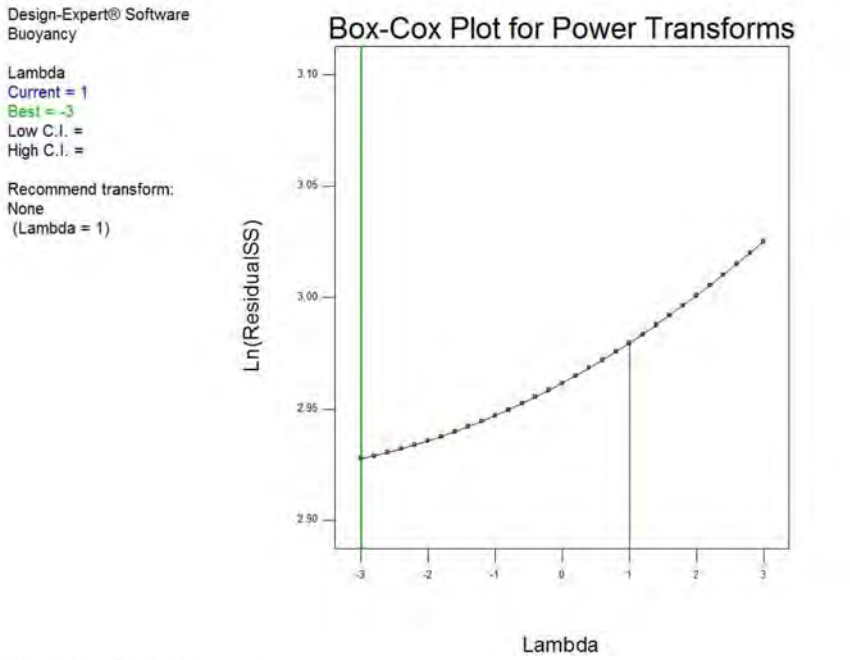

Figure 5.20 Box-Cox plot for buoyancy

5.4.1.4.3 Response surface plots for buoyancy

The two-dimensional contour plot (Figure 5.21) and 3D response surface plots (Figure 5.22) depict the impact of Eudragit® RS PO and Methocel® K15M content on the buoyancy (Y_6) of the particles. The plot reveals that an increase in Methocel® K15M content results in an increase in buoyancy and studies have shown that an increase in buoyancy due HPMC (Methocel®) content occur as a colloidal gel barrier is formed by the polymer around the gel surface and air is entrapped by the swollen polymer [445–447,449]. The air trapped by the swollen polymer imparts a density of < 1 g/ml conferring buoyancy to the dosage form due to increased levels of entrapped air [449–452,455,456,458,461].

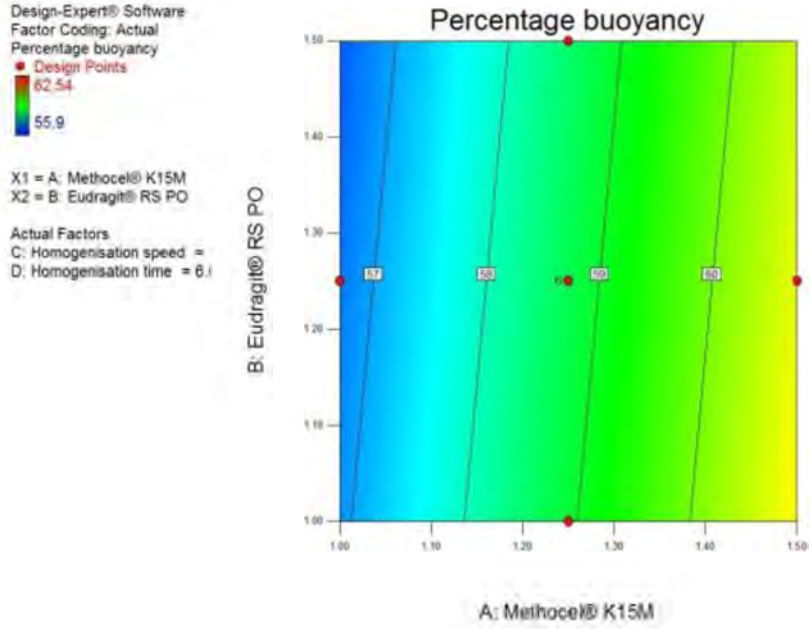

Figure 5.21 Contour plot showing the effect of the amount of Eudragit® RS PO and amount of Methocel® K15M on buoyancy

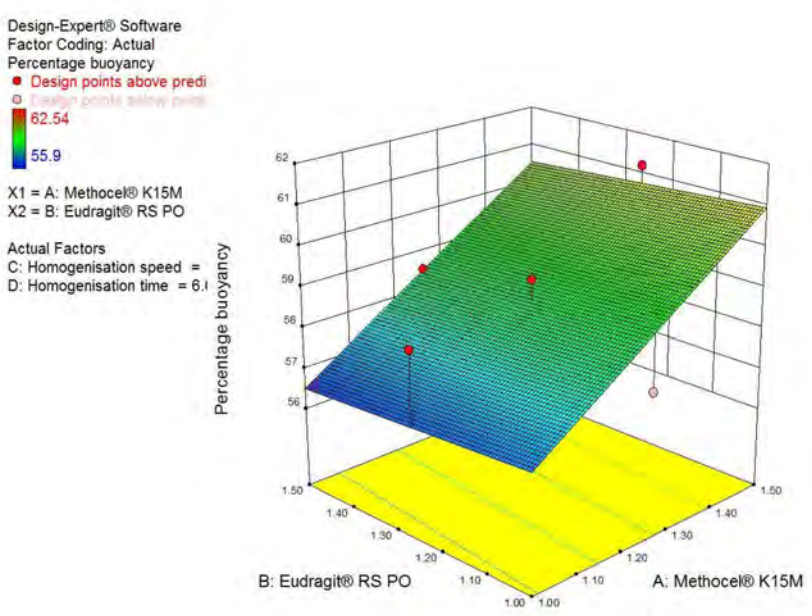

Figure 5.22 3D plot showing the effect of the amount of Eudragit® RS PO and amount of Methocel® K15M on bouayancy

5.4.1.5 Yield (Y_7)

5.4.1.5.1 Verification and evaluation of the model for response yield

A quadratic model was identified as the most suitable model for yield (Y_7) and a summary of the statistics used to identify the model is listed in Table 5.17.

Table 5.17 Summary of sequential model of sum of squares and lack of fit tests for yield

Sequential model of sum of squares						
Source	**Sum of squares**	**DF**	**Mean square**	**F- value**	**p-value Prob > F**	**Remarks**
Mean vs Total	395.67	1	395.67			
Linear vs Mean	68.34	4	17.08	6.84	0.0007	
2FI vs Linear	9.14	6	1.52	0.54	0.7691	
Quadratic vs 2FI	36.34	4	9.08	8.04	0.0011	Suggested
Cubic vs Quadratic	5.67	8	0.71	0.44	0.8640	Aliased
Residual	11.28	7	1.61			
Total	395.97	30	8891.89			
Lack of fit tests						
Source	**Sum of squares**	**DF**	**Mean square**	**F- value**	**p-value Prob > F**	**Remarks**
Linear	54.04	20	2.70	1.61	0.3145	
2FI	44.90	14	3.21	1.91	0.2450	
Quadratic	8.56	10	0.86	0.51	0.8292	Suggested
Cubic	2.89	2	1.45	0.86	0.4767	Aliased
Pure error	8.39	5	1.68			

The model was significant as a Prob > F value < 0.05 was generated. The R^2 value for the quadratic model was 0.8704 and the predicted R^2 was 0.5156 which is not in close agreement to the adjusted R^2 of 0.7494 suggesting a large block effect may be at play in the model (Table 5.18). From Equation 5.10 a negative sign is observed for the input variable homogenisation speed (X_3) indicating that homogenisation speed has an antagonistic effect on product yield.

Table 5.18 Model summary statistics for yield

Model summary statistics					
Source	**Standard deviation**	**R^2**	**Adjusted R^2**	**Predicted R^2**	**Remarks**
Linear	1.58	0.5226	0.4462	0.3462	
2FI	1.67	0.5925	0.3780	-0.0930	
Quadratic	1.06	0.8704	0.7494	0.5156	Suggested
Cubic	1.27	0.9137	0.6426	-1.9260	Aliased

The quadratic model was significant for yield as indicated by the model F-value of 7.20 (Table 5.19) that also implies there is only a 0.02% chance that a Model F-Value this large could occur due to noise. The data revealed that the homogenisation speed (X_3) and the quadratic factors X_2^2 and X_3^2 were the only significant factors as indicated by $p < 0.05$. All other factors listed in table were not significant as $p > 0.05$.

Table 5.19 ANOVA for quadratic model yield

Source	**Sum of squares**	**DF**	**Mean Square**	**F-value**	**p-value Prob > F**
Model	1113.81	14	8.13	7.20	0.0002
X_1	0.76	1	0.76	0.68	0.4241
X_2	0.19	1	0.19	0.17	0.6860
X_3	66.69	1	66.69	59.03	<0.0001
X_4	0.69	1	0.69	0.61	0.4460
X_1X_2	0.19	1	0.19	0.17	0.6840
X_1X_3	0.087	1	0.087	0.077	0.7858
X_1X_4	1.06	1	1.06	0.94	0.3482
X_2X_3	0.25	1	0.25	0.22	0.6448
X_2X_4	4.74	1	4.74	4.19	0.0585
X_3X_4	2.81	1	2.81	2.49	0.1356
X_1^2	0.20	1	0.20	0.18	0.6765
X_2^2	5.84	1	5.84	5.17	0.0381
X_3^2	12.79	1	12.79	11.32	0.0043
X_4^2	2.38	1	2.38	2.10	0.1676
Residual	16.95	15	1.13		
Lack of fit	8.56	10	0.86	0.51	0.8292
Pure error	8.39	5	1.68		
Cor total	130.76	29			

Values in red indicate significant independent variables

5.4.1.5.2 Diagnostic plots for yield

The normal probability plot of residuals depicted in Figure 5.23 reveals that the pattern for residuals is slightly S-shaped loosely satisfying the normality assumption.

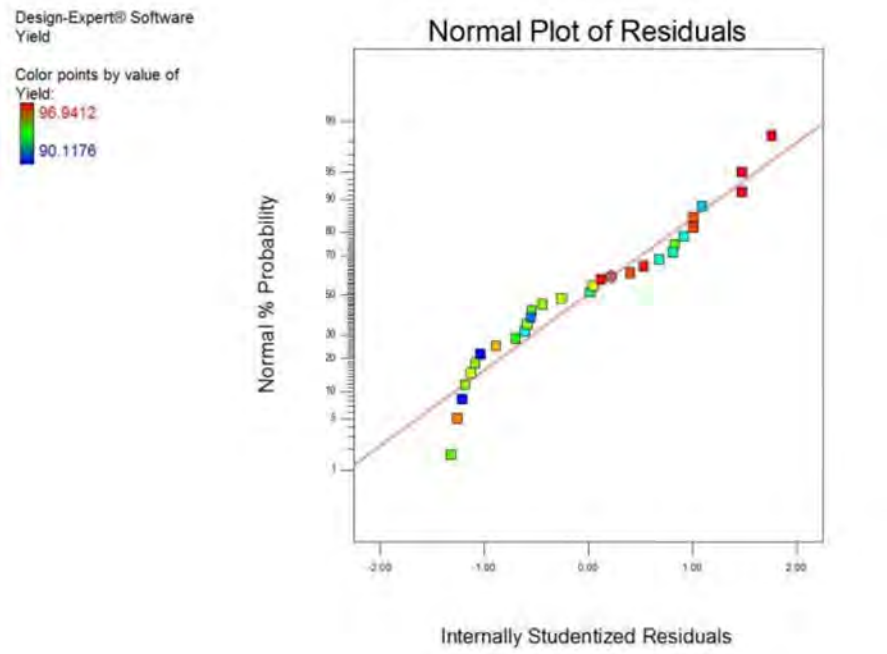

Figure 5.23 Normal plot of residuals for yield

The plot of residuals versus predicted values for yield is depicted in Figure 5.24 and reveals no clear pattern in the data and the residuals are scattered and do not fall outside the red limit lines indicating that the data are adequately fitted to the model. The Box-Cox plot for yield is depicted in Figure 5.25 with $\lambda = 1$ indicating that no data transformation was required.

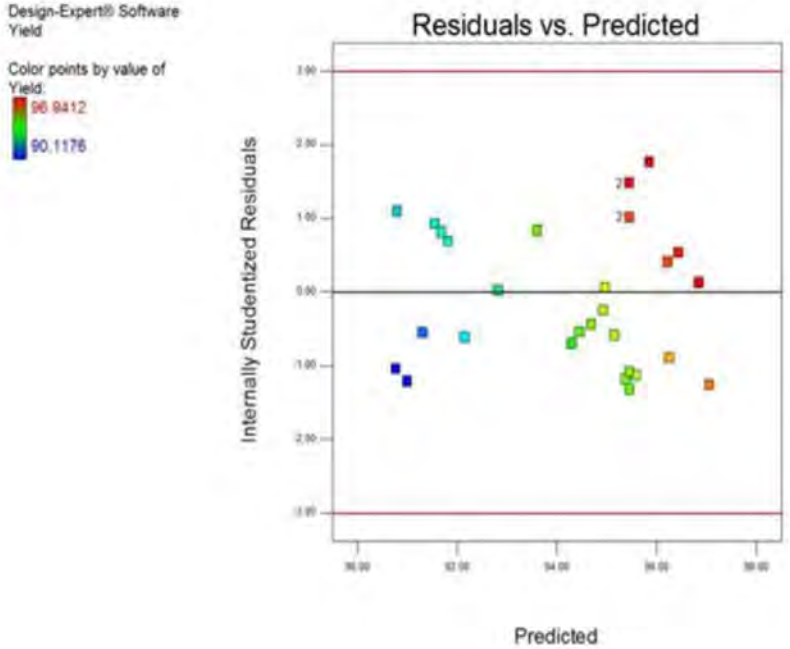

Figure 5.24 Plot of residuals versus predicted values for yield

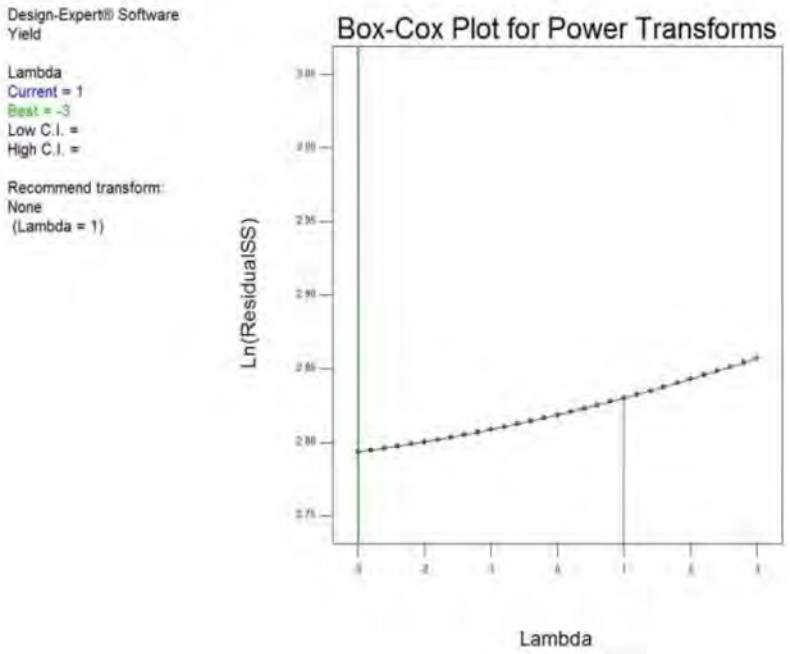

Figure 5.25 Box-Cox plot for yield

5.4.1.5.3 Response surface plots for yield

The 2D contour plot depicted in Figure 5.26 reveals the impact of homogenisation time and speed on yield (Y_7). From the shape of the contour plot it is evident that a decrease in yield

occurs at homogenisation speeds > 1000 r.p.m. The contour plot also reveals that homogenisation time does not have a significant effect on yield as indicated by almost straight contour lines. Increased stirring speed in a solvent evaporation process imparts greater energy to emulsion systems resulting in frequent disruption in microcapsule formation thereby reducing yields [464].

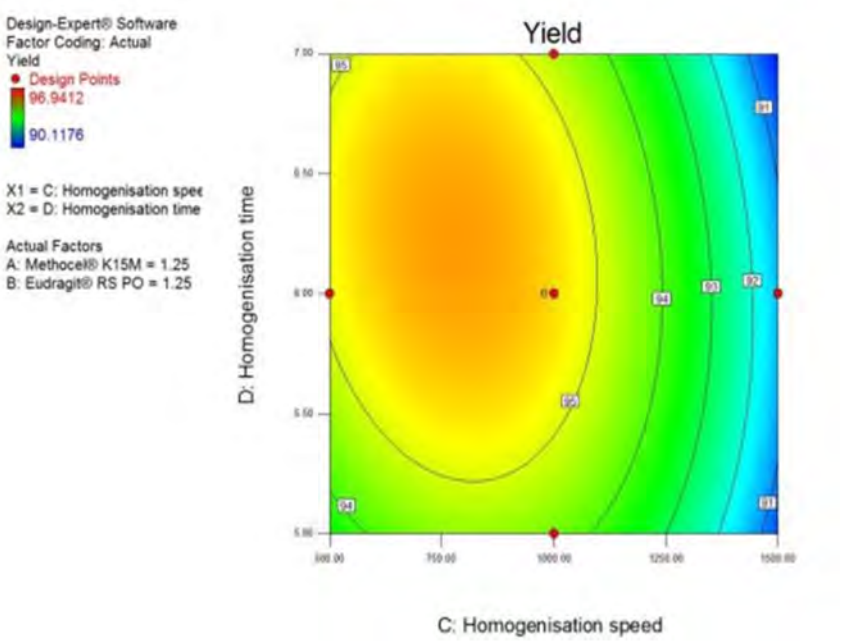

Figure 5.26 Contour plot showing the effect of homogenisation time and speed for yield

The 3D response surface plot depicted in Figure 5.27 depicts the impact of homogenisation speed and Methocel® K15M content on the yield (Y_7) and reveals that a significant decrease in yield occurs at homogenisation speeds > 1000 r.p.m whereas Methocel® K15M content has little or no effect on the yield.

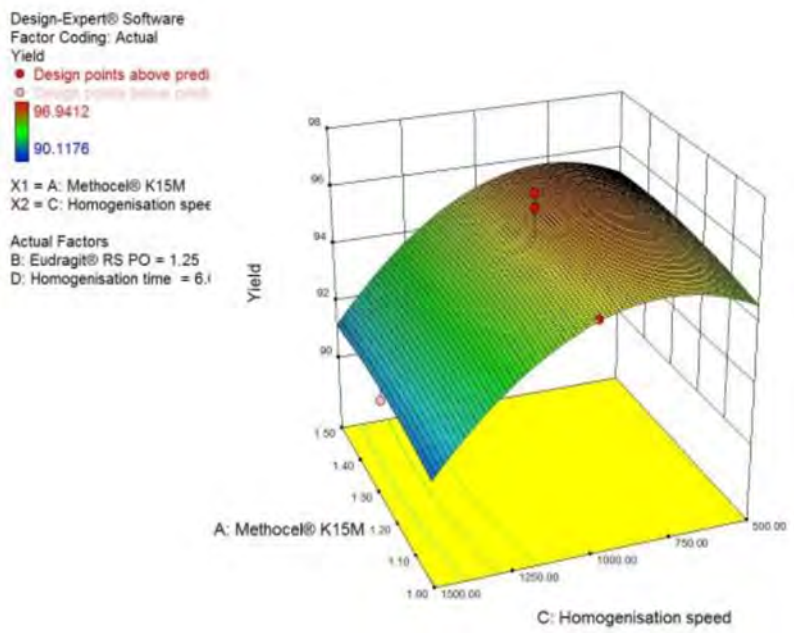

Figure 5.27 3D plot showing the effect of homogenisation speed and amount of Methocel® K15M on yield

5.4.1.6 Microcapsule size (Y_8)

5.4.1.6.1 Verification and evaluation of the model for microcapsule size

A 2 FI model was identified as the most suitable model to predict microcapsule size and the statistics used to identify the model are summarised in Table 5.20.

Table 5.20 Summary of sequential model of sum of squares and lack of fit tests for microcapsule size

Sequential model of sum of squares						
Source	**Sum of squares**	**DF**	**Mean square**	**F- value**	**p-value Prob > F**	**Remarks**
Mean vs Total	430.06	1	430.06			
Linear vs Mean	570.95	4	96171.99	153.93	< 0.0001	
2FI vs Linear	7143.37	6	1190.56	2.67	0.0474	Suggested
Quadratic vs 2FI	1568.28	4	392.07	0.85	0.5147	
Cubic vs Quadratic	2737.89	8	342.24	0.57	0.7730	Aliased
Residual	4169.80	7	595.69			
Total	591.83	30	48888.02			
Lack of fit tests						
Source	**Sum of squares**	**DF**	**Mean square**	**F- value**	**p-value Prob > F**	**Remarks**
Linear	13503.81	20	675.19	1.60	0..3186	
2FI	6360.45	14	454.32	1.07	0.5099	Suggested
Quadratic	4792.16	10	479.22	1.13	0.4734	
Cubic	2054.28	2	1027.14	2.43	0.1833	Aliased
Pure error	2115.52	5	423.10			

The model was significant with a Prob > F value < 0.05. The 2FI model exhibited a R^2 = 0.9788 and the predicted R^2 of 0.9249 is in reasonable agreement with the adjusted R^2 of

0.9677 (Table 5.21). From Equation 5.11 the negative sign for the terms for homogenisation speed and homogenisation time indicate that they have an antagonistic effect on microcapsule size.

Table 5.21 Model summary statistics for microcapsule size

Model summary statistics					
Source	**Standard deviation**	**R^2**	**Adjusted R^2**	**Predicted R^2**	**Remarks**
Linear	25.00	0.9610	0.9547	0.9382	
2FI	21.12	0.9788	0.9677	0.9249	Suggested
Quadratic	21.46	0.9827	0.9666	0.9117	
Cubic	24.41	0.9896	0.9568	0.0260	Aliased

The 2FI model was significant for microcapsule size with a model F-value of 87.83 (Table 5.22) and a model F value of 87.83 implies that there is only a 0.01% that a Model F value this large could occur due to noise. The data revealed that only homogenisation speed (X3), homogenisation time (X4) and the term X3X4 were significant variables and all other input variables had no significant effect on microcapsule size since the Prob > F value was > 0.05 for these factors.

Table 5.22 ANOVA for quadratic model for microcapsule size

Source	**Sum of squares**	**DF**	**Mean Square**	**F-value**	**p-value Prob > F**
Model	581.48	10	39183.13	87.83	<0.0001
X_1	10.11	1	10.11	0.023	0.8819
X_2	617.22	1	617.22	1.38	0.2540
X_3	542.15	1	542.15	818.93	<0.0001
X_4	18733.51	1	18733.51	41.99	<0.0001
X_1X_2	900.94	1	900.94	2.02	0.1715
X_1X_3	1.11	1	1.11	0.12	0.9608
X_1X_4	37.56	1	37.56	0.084	0.7748
X_2X_3	57.67	1	57.67	0.13	0.7232
X_2X_4	3.95	1	3.95	0.44	0.9260
X_3X_4	6142.14	1	6142.14	13.77	0.0015
Residual	8475.97	19	446.10		
Lack of fit	6360.45	14	454.32	1.07	0.5099
Pure error	2115.52	5	423.10		
Cor total	594.10	29			

Values in red indicate significant independent variables

5.4.1.6.2 Diagnostic plots for microcapsule size

The normal plot of residuals depicted in Figure 5.28 reveal that the residuals are fall roughly along a straight line with scattered points above and below the line loosely satisfying the assumption of normality.

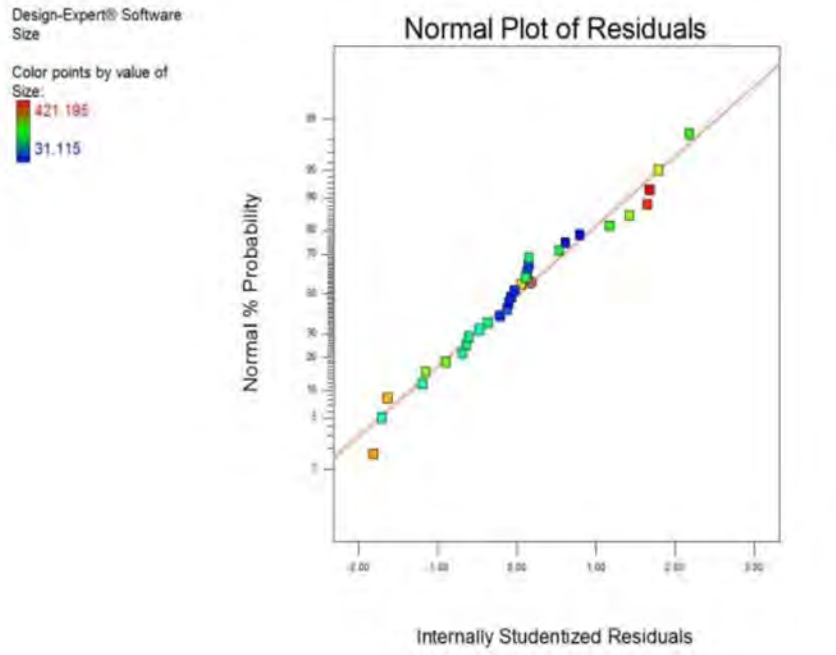

Figure 5.28 Normal plot of residuals for response microcapsule size

The plot of residuals versus predicted values for microcapsule size is depicted in Figure 5.29 and no clear pattern exists and the residuals are scattered satisfying model adequacy. The Box-Cox plot depicted in Figure 5.30 with $\lambda = 1$ indicates that no transformation of data is required

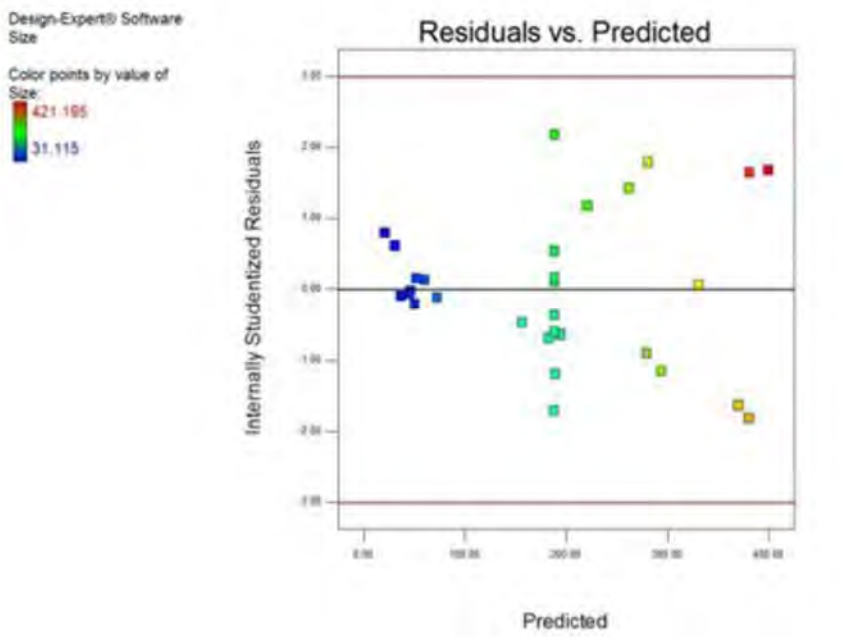

Figure 5.29 Plot of residuals versus predicted values for microcapsule size

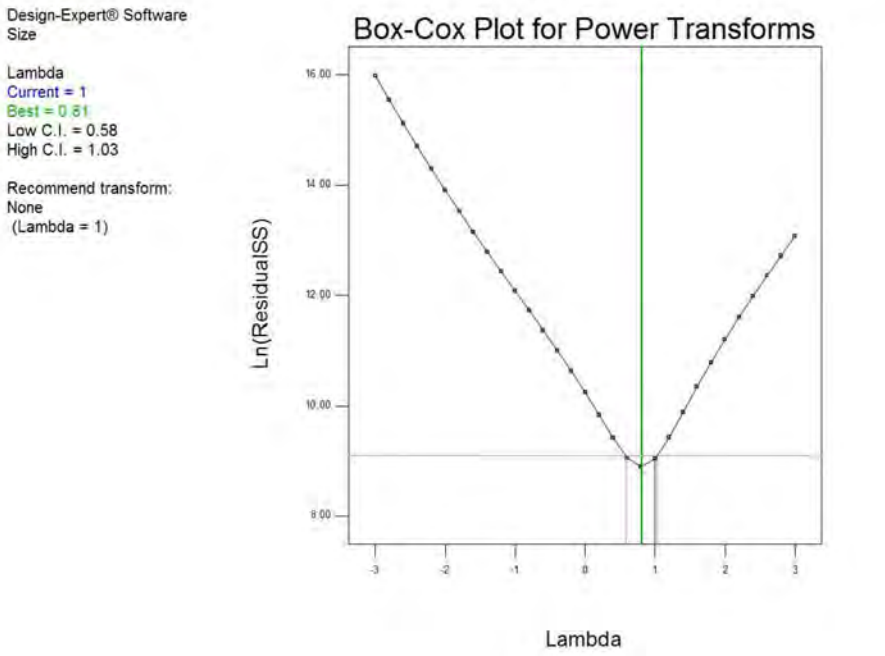

Figure 5.30 Box-Cox plot for microcapsule size

5.4.1.6.3 Response surface plots for microcapsule size

The 2D contour plot for microcapsule size is depicted in Figure 5.31 and reveals that microcapsule size decreased with an increase in homogenisation time and speed.

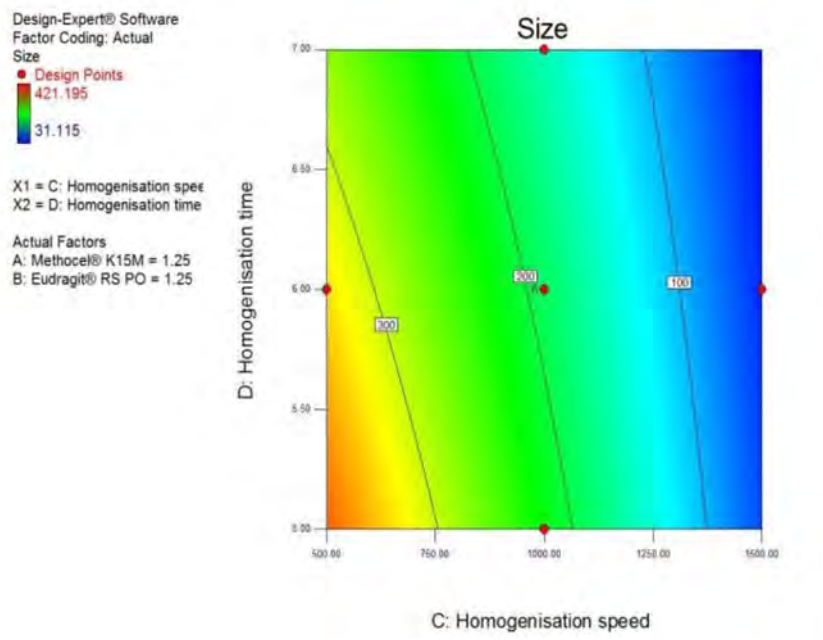

Figure 5.31 Contour plot showing the effect of homogenisation time and speed on microcapsule size

From the contour plot (Figure 5.31) it is evident that the size of the microcapsule is affected by homogenisation speed to a greater extent than homogenisation time as indicated by slanting contour lines for speed but are which are almost straight for homogenisation time. This finding is also evident in the 3D response surface plot depicted in Figure 5.32. An increase in homogenisation time resulted in a decrease in particle size as when homogenisation was performed for a short duration the diffusion of organic solvent through the interface of oil droplets may be incomplete and as droplets harden larger particles are formed [465]. When homogenisation time is increased the extent of diffusion is greater resulting in particles of smaller size [465]. At shorter homogenisation times course particles are produced due to a lower magnitude of shear stress being applied to a system whereas long homogenisation times yield small particles due to an increase in stress resulting in an increase in the energy density in the system and more efficient droplet break down [466]. As homogenisation speed increases the particle size decreases since higher shear stress reduces the viscosity of the emulsion resulting in a decrease in particle size [470].

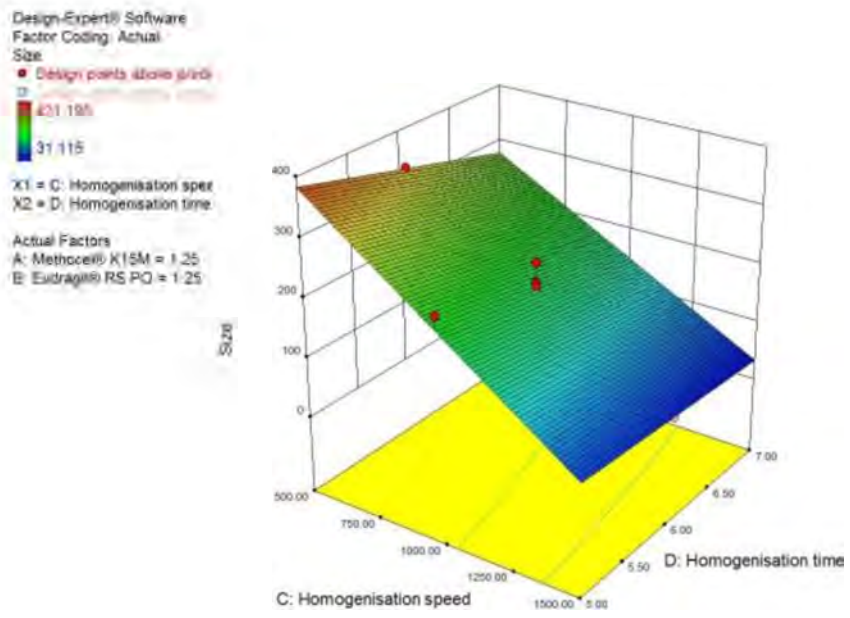

Figure 5.32 3D plot showing the effect of homogenisation speed and time on microcapsule size

5.4.2 Mathematical modelling

The release kinetics of MTZ was investigated by fitting dissolution data to a number of different mathematical models. The typical release pattern observed for formulations in which low levels of rate controlling polymer were used revealed rapid release of MTZ during the first two hours of dissolution testing. The rapid rate of MTZ release may be due to the presence of MTZ particles on the surface of the microcapsules due to poor encapsulation and that were released prior to the formation of a gel layer with sufficient mechanical strength to modulate MTZ release [515,516]. The initial high amount of MTZ released was followed by slow release of MTZ following an increase in the thickness and stability of the gel layer [517]. The increase in thickness of the gel layer can be attributed to an increase in the volume of dissolution medium entering the hydrophilic polymer layer resulting in extensive hydration and swelling thereby forming a longer diffusional path length for MTZ to traverse [516,518].

The experimental data for all 30 formulations were fitted to zero-order, first-order, Higuchi, Hixson-Crowell and the Korsmeyer-Peppas models. The model that generated the highest R^2 value was selected as the best-fit model for MTZ dissolution data. A summary of results from mathematical modelling of MTZ release for all batches MTZ-008- MTZ-037 is listed in Table 5.23, the highest R^2 values for each batch are highlighted in red. Some batches were better fitted for the Higuchi model while other batches were better fitted for the first-order model and very few batches were better fitted for the Hixon-Crowell model. The Higuchi

model and first-order model appeared to best fit the data as majority of the formulation batches had highest R^2 values for these models. The Higuchi model showed the highest R^2 values and appeared to best fit the data for 11 of the 30 batches while the first–order was the best model for 15 batches and only 4 batches showed highset R^2 values for the Hixon-Crowell model.

The Higuchi model describes diffusion controlled release from solid and/or semi solid dosage forms for water soluble and poorly water soluble compounds [487,490]. The assumptions for the Higuchi model described in Section 5.3.4 may not be valid for most modified release systems that incoperate HPMC (Methocel®) however, due to simplicity of the Higuchi model it is often used to analyse experimental release data and a number of studies have used the Higuchi model to describe the performance of HPMC-based drug delivery sytems [459,490,519,520].

The first-order model is used to describe release from systems in which the release rate is concentration dependent and the rate of release of API declines over time as the amount of API remaining in the dosage form diminishes [487,495]. In general all the models seemed to be adequate as R^2 values for all models >0.9, this is where the use of Akaike Information Criterion and other criteria may also be used to asses fitting that would obtain the best model. The Korsmeyer-Peppas model generated a release exponent of between 0.5 and 1 for all batches indicating that MTZ release from all formulations occurred by an an anomalous transport process and was a facilitated by a combination of diffusion, swelling and polymer releaxtion[490,505].

Table 5.23 Summary of release kinetic parameters following modelling of dissolution data for batches MTZ-008 – MTZ-03

Batch	Zero-order		First-order		Higuchi		Hixson-Crowell		Korsmeyer-Peppas			
	R^2	K_0	R^2	K_1	R^2	k_H	R^2	K_{HC}	R^2	k	n	Drug transport mechanism
MTZ-008	0.9611	6.8406	0.9905	0.1514	0.9960	29.3102	0.9873	0.1798	0.9517	10.287	0.9154	Anomalous
MTZ-009	0.9604	6.9611	0.9946	0.1556	0.9958	29.8355	0.9941	0.1832	0.9597	10.188	0.9230	Anomalous
MTZ-010	0.9526	6.7833	0.9948	0.1725	0.9927	29.1458	0.9938	0.2082	0.9933	18.327	0.6646	Anomalous
MTZ-011	0.9550	6.1011	0.9962	0.1360	0.9970	26.2376	0.9814	0.1739	0.9848	17.530	0.6532	Anomalous
MTZ-012	0.9496	6.5347	0.9933	0.1316	0.9914	28.1037	0.9934	0.1781	0.9782	10.683	0.8717	Anomalous
MTZ-013	0.9532	6.6438	0.9975	0.1473	0.9981	28.2324	0.9918	0.1835	0.9875	14.216	0.7561	Anomalous
MTZ-014	0.9462	6.7889	0.9920	0.1690	0.9904	29.2335	0.9935	0.2101	0.9915	17.721	0.6807	Anomalous
MTZ-015	0.9544	6.0309	0.9956	0.1337	0.9966	25.938	0.9820	0.2039	0.9870	17.840	0.6413	Anomalous
MTZ-016	0.9475	6.8869	0.9178	0.1502	0.9905	29.568	0.9971	0.1726	0.9878	10.209	0.9203	Anomalous
MTZ-017	0.9607	6.4855	0.9971	0.1405	0.9909	27.723	0.9961	0.1858	0.9946	15.381	0.7005	Anomalous
MTZ-018	0.9603	6.8726	0.9956	0.1474	0.9963	29.463	0.9907	0.1729	0.9367	8.7458	0.9934	Anomalous
MTZ-019	0.9475	6.7789	0.9918	0.1594	0.9905	29.172	0.9946	0.2023	0.9877	15.563	0.7307	Anomalous
MTZ-020	0.9603	6.9030	0.9941	0.1539	0.9985	29.094	0.9967	0.1827	0.9560	10.968	0.9078	Anomalous
MTZ-021	0.9603	6.6785	0.9963	0.1442	0.9910	28.667	0.9928	0.1887	0.9889	13.318	0.7847	Anomalous
MTZ-022	0.9603	6.6863	0.9968	0.1520	0.9952	28.746	0.9912	0.1922	0.9850	14.498	0.7566	Anomalous
MTZ-023	0.9620	6.8877	0.9919	0.1540	0.9963	29.525	0.9954	0.1815	0.9472	9.9495	0.9351	Anomalous
MTZ-024	0.9571	6.7774	0.9958	0.1462	0.9960	29.098	0.9946	0.1800	0.9553	10.322	0.9116	Anomalous
MTZ-025	0.9556	6.5399	0.9974	0.1425	0.9876	28.029	0.9913	0.1857	0.9876	14.236	0.7456	Anomalous
MTZ-026	0.9570	6.6499	0.9976	0.1315	0.9947	28.534	0.9920	0.1743	0.9603	7.9086	0.9260	Anomalous
MTZ-027	0.9456	6.2248	0.9966	0.1397	0.9925	26.842	0.9868	0.1821	0.9577	16.117	0.7022	Anomalous
MTZ-028	0.9339	6.1656	0.9923	0.1308	0.9911	26.734	0.9804	0.1769	0.9629	13.986	0.7623	Anomalous
MTZ-029	0.9534	6.6530	0.9961	0.1419	0.9946	28.600	0.9924	0.1822	0.9504	10.454	0.9013	Anomalous
MTZ-030	0.9533	6.5399	0.9977	0.1584	0.9972	28.152	0.9917	0.1904	0.9787	16.391	0.7071	Anomalous
MTZ-031	0.9554	6.6987	0.9940	0.1520	0.9920	28.729	0.9905	0.1967	0.9920	16.050	0.7079	Anomalous
MTZ-032	0.9600	6.5386	0.9975	0.1584	0.9989	28.073	0.9904	0.1911	0.9838	17.543	0.6732	Anomalous
MTZ-033	0.9525	6.6100	0.9934	0.1547	0.9970	28.413	0.9920	0.1973	0.9671	16.278	0.7138	Anomalous
MTZ-034	0.9441	6.2917	0.9921	0.1489	0.9903	27.122	0.9329	0.1907	0.9909	18.471	0.6408	Anomalous
MTZ-035	0.9268	6.2835	0.9883	0.1490	0.9844	27.256	0.9739	0.2061	0.9723	18.888	0.6481	Anomalous
MTZ-036	0.9640	6.2749	0.9936	0.1320	0.9948	26.829	0.9928	0.1650	0.9595	13.207	0.7717	Anomalous
MTZ-037	0.9339	6.1656	0.9923	0.1308	0.9911	26.734	0.9804	0.1769	0.9629	13.986	0.7623	Anomalous

5.4.3 Formulation optimisation

A numerical optimisation approach using Design Expert Version 8.0.2 (Stat-Ease Inc., Minneapolis, USA) statistical software was used to identify a formulation composition that would produce a microparticle technology with CQA and performance characteristics. The statistical software was used to set limits for composition such that the minimum amount of MTZ would be released at between 0.5 and 2 hours and a maximum or > 85% released at 12 hours. In addition the highest EE, buoyancy and yield of microcapsules were target attributes. All microcapsule formulations produced following the CCD were within this size range 2 - 2000 µm and therefore a numerical goal for the size was not specified [367]. The combination of input variables that generated the highest desirability was selected as the potential optimised formulation composition and processing parameters (Table 5.24). The batch name for optimised formulation is MTZ-038

Table 5.24 Formulation composition and process parameters for the manufacture of the optimised formulation (MTZ-038)

Process parameters	
Homogenisation speed	1000 rpm
Homogenisation time	6 hours
Formulation composition	
Ingredient	**Amount g**
MTZ	1
Methocel® K15M	1.25
Eudragit® RS PO	1.49
Avicel® PH102	0.51

The optimised formulation was manufactured and the experimental responses for this formulation were quantitatively compared to the values predicted using statistical software and the results are listed in Table 5.25

Table 5.25 Predicted and experimental responses for the optimised formulation (MTZ-038)

Response	**Predicted %**	**Mean experimental % ± SD (n=3)**	**Prediction error %**
% MTZ released at 0.5 hour	8.90	9.85 ± 2.09	10.67
% MTZ released at 2 hours	28.00	29.50 ± 2.16	5.35
% MTZ released at 6 hours	63.18	64.07 ± 1.51	1.41
% MTZ released at 12 hours	86.56	87.58 ± 1.72	1.18
Encapsulation efficiency	71.48	72.60 ±1.67	1.57
Buoyancy	57.24	58.41 ± 1.81	2.04
Yield	95.67	96.83 ± 1.51	1.2

The results indicate that the experimental data were similar to the predicted values as the majority of the responses had a prediction error of <5%. The values for % prediction error for % MTZ released at 0.5 hour and 2 hours were > 5% suggesting that the use of CCD for predicting responses is better for % MTZ released at 6 hours, % MTZ released at 12 hours, encapsulation efficiency, buoyancy and yield. The microcapsules manufactured using the optimised formula revealed an encapsulation efficiency of 72.60% (Y5), a buoyancy of 58.41% (Y6) with a yield of 96.83 (Y_7) %. The dissolution profile for the optimised formulation is depicted in Figure 5.33 and reveals that the release of MTZ is sustained over 12 hour period with 87.58% (Y_4) released at 12 hours. The *in vitro* release data was fitted to mathematical models in an attempt to establish the mechanism of MTZ release from the microcapsules. The R^2 values for the mathematical models for the optimised formulation are summarised in Table 5.26 and the data suggest that the Higuchi model best described MTZ release from the optimised formulation.

Table 5.26 Summary of mathematical model parameters for the optimised formulation (MTZ-038)

Model	R^2	k
Zero-order	0.9463	7.3164
First-order	0.9894	0.1775
Higuchi	0.9979	27.717
Hixon-Crowell	0.9957	0.2094
Korsmeyer-Peppas	0.9878	0.6815

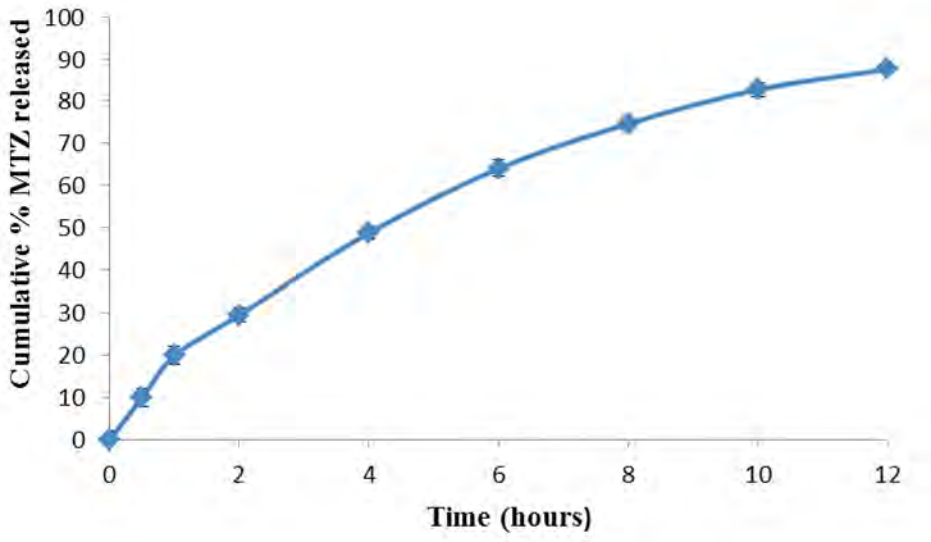

Figure 5.33 In vitro release profile for MTZ release from the optimised optimised formulation(MTZ-038)

5.4.4 STABILITY TESTING

Stability testing is an important component of the product development process and is routinely performed on API and final products at different stages of the product development timeline [255,521]. A stable formulation should maintain aesthetic appeal and elegance from the time of manufacture until administration to the patient. If the organoleptic properties of a pharmaceutical product change over time patients may lose confidence in the effectiveness and safety of medicines resulting in non-adherence [521]. In addition degradation of an API on storage may lead to the patients receiving reduced dose with a subsequent lack of clinical effectiveness [522]. The results from short term stability for the optimised product stored at 25°C/60% RH and 40°C/75% RH are summarised in Table 5.27. The cumulative percent MTZ released at 0.5 hour for the formulations stored at 25°C/60% RH and 40°C/75% RH ranged from 9.740% to 9.850% and 9.72% to 9.82% respectively over the four weeks of stability testing. The cumulative percent MTZ released at 12 hours for the formulations stored at 25°C/60% RH and 40°C/75% RH ranged from 86.80% to 87.43% and 86.50% to 87.24% respectively over the four weeks of stability testing. The encapsulation efficiency for the formulations stored at 25°C/60% RH and 40°C/75% RH ranged from 71.74% to 72.64% and 71.94% to 72.67% respectively over the four weeks of stability testing. The buoyancy for the formulations stored at 25°C/60% RH and 40°C/75% RH ranged from 57.75% to 58.24% and 57.80% to 58.27% respectively over the four weeks of stability testing. The results from the stability tests revealed that there were no significant changes in encapsulation efficiency, buoyancy and percent released of MTZ.

Table 5.27 Results from stability testing of the optimised formulation at 25°C/60% RH and 40°C/75% RH

Stability testing at 25°C/60% RH					
Response	**Day 1**	**Day 7**	**Day 14**	**Day 21**	**Day 30**
% MTZ released at 0.5 hour	9.850 ± 1.50	9.790 ± 1.52	9.740 ± 2.03	9.810± 2.48	9.750 ± 1.56
% MTZ released at 12 hours	87.43 ± 1.75	86.95 ± 1.31	86.80 ± 2.91	87.10 ± 2.43	86.89 ± 2.10
Encapsulation efficiency	72.64 ± 0.88	72.04 ± 3.05	71.74 ± 2.07	71.84 ± 1.08	72.44 ± 2.52
Buoyancy	58.24 ± 1.69	57.90 ± 2.70	57.75 ± 2.59	58.15 ± 2.51	57.89 ± 5.47
Stability testing at 40°C/75%RH					
Response	**Day 1**	**Day 7**	**Day 14**	**Day 21**	**Day 30**
% MTZ released at 0.5 hour	9.82 ±1.18	9.80 ±2.01	9.72 ± 1.58	9.80 1.18	9.77 ± 2.70
% MTZ released at 12 hours	87.24 ± 2.52	86.94 ± 3.09	86.50 ±2.66	87.12 ± 2.19	86.57 ±2.00
Encapsulation efficiency	72.67 ± 2.02	72.37 ± 2.59	71.94 ± 2.07	72.15 ± 2.06	71.97 ± 1.50
Buoyancy	58.27 ± 2.03	57.95 ± 1.51	57.80 ± 1.98	58.20 ± 1.51	57.91 ±2.14

5.5 CONCLUSIONS

Gastric-retentive sustained release MTZ microcapsules were manufactured using a solvent evaporation process. RSM was used to study the main, interactive and quadratic effects of formulation and processing variables on the *in vitro* release, encapsulation efficiency, buoyancy, yield, and microcapsule size. The RSM approach was successful and reduced the time and resources required for formulation optimisation. The results suggest that the level of Methocel® K15M, Eudragit® RS PO and homogenisation speed had a significant effect on the *in vitro* release of MTZ. An increase in the amount of Methocel® K15M and Eudragit® RS PO polymers resulted in a decrease in percent MTZ released.The amount of Methocel® K15M and homogenisation speed were found to have a significant effect on the encapsulation efficiency. It was found that an increase in the amount of Methocel® K15M and a decrease in homogenisation speed resulted in an increase in encapsulation efficiency. Buoyancy was found to be significantly affected by the amount of Methocel® K15M, an increase in the amount of Methocel® K15M resulted in an increase in buoyancy. The microcapsule size was affected by homogenisation speed and time while the yield of the microcapsules was affected by homogenisation speed only. An increase in homogenisation speed and time resulted in a decrease in microcapsule size and increase in homogenisation speed resulted in a decrease in yield.

Two dimensional and three dimensional response surface plots were used to gain further insight into the effect of independent input variables on the % MTZ released at 0.5 hour and 12 hours, encapsulation efficiency, buoyancy, yield and particle size. The prob > F value was used to determine the most suitable model for each response and ANOVA was used to determine if the model was significant. Normal probability plots, plots of residuals versus predicted and Box-Cox plots were used to determine model adequacy.

A numerical optimisation approach was used to predict a formulation composition that would result in low MTZ release initially and a maximum MTZ release at 12 hours, with a high encapsulation efficiency, yield and buoyancy. In order to validate the results from the CCD data generated experimental responses from the optimised formulation were compared to predicted responses from the model and the results reveal that the majority of predicted and experimental data were similar as the prediction error was < 5%, however two of the responses had prediction errors > 5%.

The release kinetics of MTZ from the formulations was established by fitting *in vitro* release data to mathematical models. The model that best described the data was established by identifying the highest R^2 value. The highest R^2 values were obtained when release data was fitted to the Higuchi model and first order model. Some batches were better fitted for the Higuchi model while other batches were better fitted for the first-order model. The *in vitro* release data for the optimised formulation was fitted into mathematical models and the highest R^2 value was obtained when the release data for the optimised formulation was fitted to the Higuchi model. The optimised formulation was subjected to stability testing for 30 days at 25°C/60% RH and 40°C/75% RH and no significant changes in any of the responses were observed during the 30 days stability assessment.

In conclusion a statistical experimental design approach has been successfully applied to study the effects of formulation variables on several responses and to identify a gastric-retentive formulation composition that has potential for further development and improvement. Further studies to improve this formulation would include improving the buoyancy of the microcapsules by using an effervescent approach by incorporating sodium bicarbonate in the formulation and performing dissolution studies using Simulated Gastric Fluid (SGF) to predict the in vivo release of MTZ. These studies serve as a starting point for the development of gastric-retentive sustained release formulations for API(s) that are unstable in the intestinal environment and/or may require gastric retention.

CHAPTER SIX

DEVELOPMENT AND PARTIAL VALIDATION OF A METHOD FOR THE DETERMINATION OF RESIDUAL ACETONE AND N-HEXANE USING GAS CHROMATOGRAPHY

6.1 INTRODUCTION

Organic solvents are routinely used during the synthesis of API, excipients or product formulation and manufacture [534,538,540]. The presence of solvents in the final product is undesirable due to potential toxicity or impact on the quality of API crystals, the product or result in the development of an odour and/or poor taste.

Different processes and techniques are used to remove the solvents however, residual solvents may remain in small quantities in products [534,535]. Low levels of organic solvents are also referred to as organic volatile impurities or residual solvents. In the pharmaceutical industry the determination of residual solvents in API is challenging. Following the manufacture of MTZ microcapsules, GC was used to determine residual levels of acetone and n-hexane in the product [534,536,538]. The pharmacopeial concentration limits for acetone and n-hexane is 5000 ppm and 290ppm respectively [41].

Gas chromatography (GC) was first introduced by James and Martin in the 1950s who reported the separation of volatile fatty acids by partition chromatography using a stationary phase of silicone oil/stearic acid supported on diatomaceous earth and nitrogen gas as the mobile phase [523,524]. GC has improved over the years and a vast number of different detector types and columns are available in addition to improved detection and methods of sample introduction [525,526]. GC is a standard analytical method supporting research, development and quality control for diverse application including petrochemical manufacture, environmental monitoring, food contaminant, drug residue and forensic analysis [526].

6.2 PRINCIPLES OF GC

Whilst many applications of the principle of gas chromatography all GC equipment is similar with respect to components and basic principles of operation [527]. A basic GC instrument consists of a sample injector, column, detector, carrier gas supply, flow controller and an appropriate data system/ display unit [525,527]. A schematic representation of basic GC instrumentation is depicted in Figure 6.1.

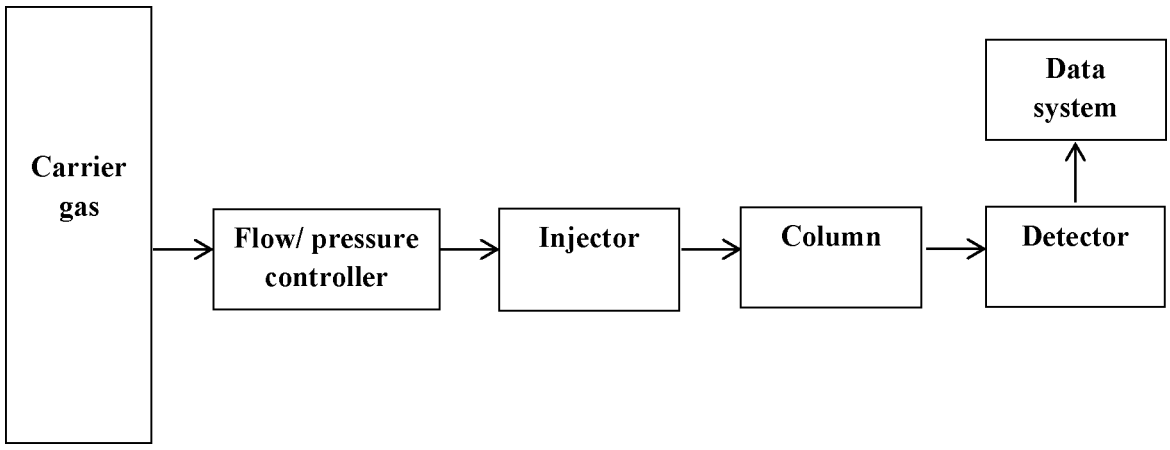

Figure 6.1 Schematic diagram of GC instrumentation

In GC the mobile phase is a carrier gas that is used to elute solutes through a column and to provide a suitable separation for the detector to measure components of the sample [524,528]. The nature of the gas is to some extent dictated by the detector used [527]. Helium, argon and nitrogen are the most commonly used carrier gasses and whilst hydrogen may be used it is not a recommended due to a potential to result in fire and/or explosions [524,526,529]. The carrier gas supply unit delivers a steady stream of the gas and with the aid of a flow rate controller that normally includes a pressure monitor and gas flow rate indicator [525,527]. Many detectors are flow sensitive and a flow rate controller maintains constant gas flow to permit a stable noise-free electrical output to be generated [527].

The sample injector may be a simple septum injector that requires a hypodermic syringe to introduce the sample directly on to the column or as complex as a high-pressure sample valve fitted with an appropriate sample loop [527]. The column ensures separation of components of a sample and is contained in a temperature controlled oven as this is where separation of components occurs [170]. Individual sample components separate as they pass through the column emerging as individual sample bands that are detected and quantified [527]. The temperature of the column controls the rate at which the components migrate through the column [527].

The detector response to a sample generates an electrical signal that is related to the concentration of the solute as it leaves the column [525]. Detectors that can be used for gas chromatographic analysis include Flame Ionisation (FID), Thermal Conductivity (TCD), Mass Spectrometer (MS) and Electron Capture Detectors (ECD) [122]. Elution time and concentration of solute are measured and a number of different display units are used to monitor and record a separation including potentiometric recorders, computer printers or for

rapid separations a cathode ray tube [525] . Modern instruments digitize detector signals and then transfer the data to a computer where it is processed and can be stored [527].

6.3 GAS CHOMATOGRAPIC METHODS FOR THE ANALYSIS OF ACETONE AND N-HEXANE

A review of published methods for GC analysis of acetone and/or n-hexane was conducted prior to the development of a method of analysis. A summary of the conditions reported for the analysis of acetone and n-hexane are listed in Tables 6.1. The majority of methods make use of FID, and hence the summaries include only methods for which FID was reported. Nitrogen and helium are the most common gasses used for the mobile phase and the retention time for acetone was approximately $\leq$ 5 minutes in most cases however, a retention time of 10 minutes was also reported. The retention time for hexane was approximately 5 to 8 minutes for most separations although retention time as long as 17.6 minutes was also reported.

Table 6.1 Summary of published GC methods for the analysis of acetone and n-hexane.

Acetone						
Sample	**Column**	**Mobile phase**	**Flow rate ml/min**	**Internal standard**	**Retention time min**	**Ref.**
Biological	Supelco®, Carbopack C 80-100 mesh, (1 m x3.17 mm I.D.)	Nitrogen	60	Oxitol	Acetone = 0.24 Oxitol = 1.96	[530]
Biological	Carbowax® CG 745 (30 m x 0.53 mm I.D.)	Nitrogen	8	N-propanol	Acetone = 1.3 N-propanol = 2.8	[531]
Biological	Varian® CPWax 57 CB (25 m x 0.25 mm I.D.)	Helium	1.5	1-propanol	Acetone = 2.02 1-propanol = 5.26	[532]
Spray dried dispersions	Stabilwax® Crossbonded (30 m × 0.32 mm I.D.)	Helium	50	-	Acetone = 4.49	[533]
API	Agilent® DB624 (30 m x 0.32 mm I.D.)	Nitrogen	1.0	-	Acetone = 10.06	[534]
API	Supelco® SPB® 624 (3 0m x 0.25 mm I.D.)	Nitrogen	1.0		Acetone- 5.23	[535]
Herbal formulation	Stabilwax® DA (60 m × 0.25 µm ID)	Helium	1.2	1-pentanol	Acetone = 4.07 1-pentanol =10.28	[536]
Hexane						
Sample	**Column**	**Mobile phase**	**Flow rate ml/min**	**Internal standard**	**Retention time min**	**Ref.**
Biological	Zebron®-1 megabore (30 m × 0.53 mm I.D.)	Nitrogen	2.5	Isooctane	N-hexane = 6.1 Isooctane = 8.0	[537]
API	Restek®-1301 (30 m x 0.53 mm I.D.)	Nitrogen	3.3	N-propanol	N-hexane = 7.9 N-propanol =8.9	[538]
API	Zebron®-624 (30 m x 0.32 mm I.D.)	Nitrogen	25	Dioxane	N-hexane = 5.3 Dioxane = 15.3	[539]
API	Restek®624 (30 m × 0.32 mm I.D.)	Nitrogen	0.5	-	N-hexane = 17.6	[540]

6.4 EXPERIMENTAL

6.4.1 Aim

The aim of these studies was to develop and validate GC methods for analysis of residual acetone and n-hexane in the optimised laboratory scale formulation.

6.4.2 Chemical and reagents

Acetone was purchased from Merck® Laboratories (Merk, Darmstadt, Germany). N-hexane HPLC grade HiPerSolv® was purchased from VWR chemicals (Leuven, Belgium). Acetophenone UniLab® was purchased from Saar Chem (Chamdor, Krugersdorp). All other chemicals were of analytical grade and no further purification was carried out.

6.4.3 Instrumentation

An Agilent model 7820A gas chromatograph (Agilent Technologies, California, USA) fitted with a FID detector was used for analysis. A Zebron® ZB WAXplus 30 m x 0.32 mm x 0.25 µm column was used for the analysis of acetone and ethanol was used as an internal standard. A DB 5 30 m x 0.32 mm x 0.25 µm column was used for analysis of n-hexane. Neither internal nor external standard was used for the analysis of n-hexane. Data acquisitions were carried out using Agilent software (Agilent Technologies, California, USA). Helium was used as a mobile phase whilst hydrogen and air were used as auxiliary FID gases.

6.4.4 Preparation of stock solutions

Stock solutions of 40000 ppm acetone (ρ = 0.791g/mL) in acetophenone were prepared by measuring 506 µl of acetone into a 10 ml A-grade volumetric flask using a 1000 µl pipette. The weight of the pipetted acetone was recorded using Mettler® Model AG135 top-loading analytical balance (Mettler®, Zurich, Switzerland) and used to adjust the calibration curve concentrations. Calibration curve concentrations were made by serial dilutions in 5 ml A-grade volumetric flasks to which the internal standard was added. Approximately 63.4 µl absolute ethanol (ρ = 0.789 g/mL) was pipetted using a 100 µl pipette and added to each 5 ml volumetric flask to make approximately 10 000 ppm internal standard concentration and acetophenone was added to the mark. Approximately 2 ml of calibration curve solutions were measured using 1000 µl pipette and transferred into clear glass vials. A 10 µl microsyringe was used to measure 1µl and manual injections were carried out in ascending order of concentrations.

Stock solutions of 4000 ppm n-hexane were made by pipetting 61.1 µl of HPLC grade *n*-hexane (ρ = 0.6548 g/mL) into 10 ml A-grade volumetric flask using a 100 µl pipette and adding acetophenone to the mark. The weight of the pipetted n-hexane was recorded using Mettler® Model AG135 top-loading analytical balance (Mettler®, Zurich, Switzerland) and used to adjust the calibration curve concentrations. The stock solution was then used to make serial dilutions for the calibration curve concentrations. The calibration curve concentrations were prepared in 5 ml A-grade volumetric flasks and made up to the mark with acetophenone. Approximately 2 ml of calibration curve solutions were measured using 1000 µl pipette and transferred into clear glass vials. A 10 µl microsyringe was used to measure 1 µl and manual injections were carried out in ascending order of concentrations.

6.5 METHOD DEVELOPMENT AND OPTIMISATION

6.5.1 Column selection

Most columns listed in Table 6.1 were not available or accessible and therefore several columns were tested to identify an appropriate phase for the analysis of acetone and hexane. N-hexane requires the use of columns with a dense stationary phase and thus it was challenging to use a single column for both n-hexane and acetone. In addition the difference in polarity between acetone and n-hexane makes it difficult to maintain the stability of both compounds in one sample.

6.5.2 Internal standard (IS) selection

A variety of internal standards were tested including ethyl acetate that eluted at 1.8 minutes which was too close to the peak for acetone and n-hexane. Pentane co-eluted close to n-hexane and butane produced a broad peak with excessive tailing at a retention time of 2.6 minutes. Heptane and ethanol were well resolved from the peaks for n-hexane and acetone, however heptane exhibited significant tailing when compared to ethanol and therefore ethanol was selected as the internal standard for the analysis of acetone. A summary of the results for internal standards and their outcome is reported in Table 6.2.

Table 6.2 Potential IS tested and chromatographic outcome

COMPOUND	RT min	COMMENTS
Ethyl acetate	1.8	Too close to acetone and n-hexane
Pentane	2.8	Co-elution with n-hexane
Butane	2.6	Broad peak with tailing
Heptane	4.6	Well resolved from n-hexane and acetone but exhibited tailing
Ethanol	5.5	Well resolved from n-hexane and acetone. Less tailing when compared to heptane. Ethanol selected as IS

RT= retention time

6.5.3 Solvent selection

A variety of solvents for preparing solutions for analysis were tested and the majority of them resulted in tailing of acetone, n-hexane and/or ethanol. Most of the solvents had a retention time greater than those of the analytes of interest due to their higher boiling point. Acetophenone caused peak fronting of ethanol however this phenomenon was minimised by reducing the amount of ethanol or by increasing the split ratio and therefore acetophenone was selected as the solvent for these studies. A summary of the results obtained when using different solvents is listed in Table 6.3.

Table 6.3 Potential solvents tested and chromatographic response

Solvent	RT min	Comments
Butanol	11.8	Tailing of n-hexane and ethanol
Pentane	4.40	Tailing of acetone
Toluene	9.80	Tailing of acetone
Acetophenone	12.88	Fronting of ethanol resolved by reducing the amount of ethanol or increasing the split ratio.

6.5.4 Resolution

The degree of separation for an adjacent peak pair is described by the resolution (Rs) and characterised by the distance between the signals relative to the signal width [541]. The resolution was calculated using Equation 6.1. A resolution factor > 2 is an indication that adequate separation has been achieved between peaks [121,133,167]. Values < 1.5 indicate poor resolution between peaks. . Resolution is dimensionless as both retention time and width are recorded in minutes. Table 6.4 summarises the resolution between all analyte peaks of interest, the resolution was found to be above 1.5 showing that there is high resolution between the compounds of interest.

$$R_S = \frac{t_{R2} - t_{R1}}{0.5(W1+W2)}$$ *Equation 6.1*

Where,

Rs = Resolution factor
t_{R1} = Retention time of first eluting peak
t_{R2} = Retention time of second eluting peak
W_1 = Width of first eluting peak at base
W_2 = Width of second eluting peak at base

Table 6.4 Resolution values between analyst of interest

Analytes	Resolution
Acetone and ethanol	44.8
Acetone and acetophenone	113
N-hexane and acetophenone	393

6.5.5 Dead volume time

The dead volume studies were carried out in order to determine if analytes of interest were retained. Dead volume time is the time required for the solute to move through the column and is the same for all solutes in a mixture [541]. The dead volume can be determined based on the Rt of three consecutive n-alkanes or other members of a homologous series [541]. The dead volume time was calculated using the retention times for pentane, heptane and n-hexane analysed under acetone and *n*-hexane chromatographic conditions. Equation 6.2 was used to calculate the dead volume time. The dead volume times were found to be 1.70 and 1.85 minutes under *n*-hexane and acetone chromatographic conditions respectively. The dead volume times for both chromatographic conditions were slightly different mainly due to the difference in mobile phase flow rate. A flow rate of 1.6 ml/min was used for acetone analysis while a flow rate of 2.2 ml/min was used for n-hexane. The dead volume times were found to be less than the retention times for all analytes of interest.

$$t_M = \frac{t_{n-pentane} \times t_{n-heptane} - t^2_{n-hexane}}{t_{n-pentane} + t_{n\,heptane} - 2 \times t_{n-hexane}}$$ *Equation 6.2*

Where,

t_M = Void volume time
t_n = Retention time

6.5.6 Optimised chromatographic conditions for acetone

Acetone was analysed using ethanol as an internal standard and He as a carrier gas at a flow rate of 1.6 ml/min. In order to increase the flow rate to 5 ml/min N_2 was added to the carrier gas. Air and H_2 were used as the detector gas at flow rates of 400 ml/min and 30 ml/min respectively. Samples (1µl) were injected at an injection temperature of 180°C. The set point temperature and detector temperature were 30°C and 250°C respectively. The average velocity of the carrier gas was 26.755 cm/sec and a split ratio of 15:1 was used to reduce peak fronting of ethanol and to improve the peak shape. The retention time for acetone, ethanol and acetophenone were 3.1, 5.5 and 15.9 ml/min respectively. Table 6.5 summarises the optimised chromatographic conditions for acetone. A typical chromatogram of the separation of acetone with ethanol as an internal standard in acetophenone is depicted in Figure 6.2(a) and a zoomed in chromatogram of acetone with ethanol Figure 6.2 (b).

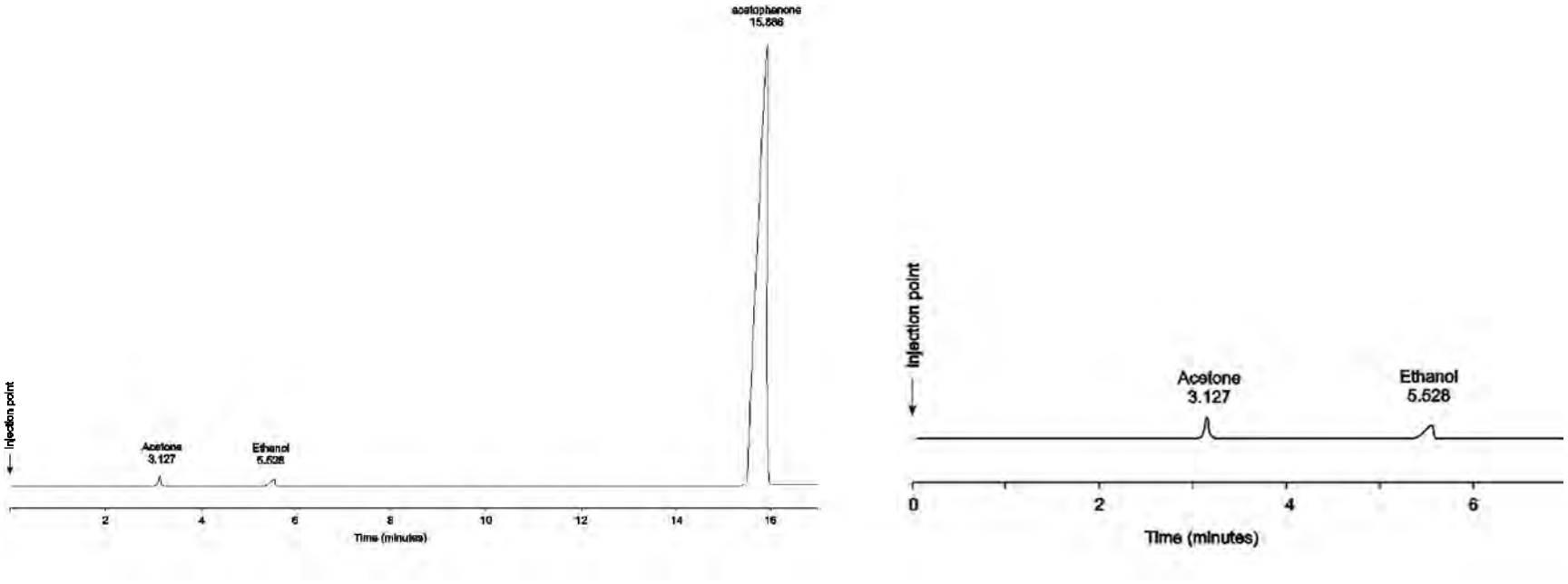

Figure 6.2 Typical chromatogram of the separation of acetone (1000 ppm)and ethanol(8000 ppm)in acetophenone (a) and a zoomed in chromatogram of acetone with ethanol (b)

6.5.7 Optimised chromatographic conditions for the analysis of n-hexane

N-hexane was analysed without use of an internal standard and with He as a carrier gas at a flow rate of 2.2 ml/min. In order to increase the flow rate to 5 ml/min N_2 was added to the carrier gas. Air and H_2 were used as the detector gas at flow rates of 400 ml/min and 30 ml/min, respectively. Samples (1µl) were injected at a temperature of injection of 170°C. The set point and detector temperatures were 40°C and 300°C respectively. The average velocity of the carrier gas was 35.216cm/sec and a split ratio of 15:1 was used to improve the peak shape. The retention time for n-hexane and acetophenone was 2.0 and 12.8 ml/min, respectively. A typical chromatogram of the separation of n-hexane in acetophenone is depicted in Figure 6.3(a) and a zoomed in chromatogram of n-hexane is depicted in Figure 6.3 (b), the optimised chromatographic conditions for n-hexane are summarised in Table 6.5.

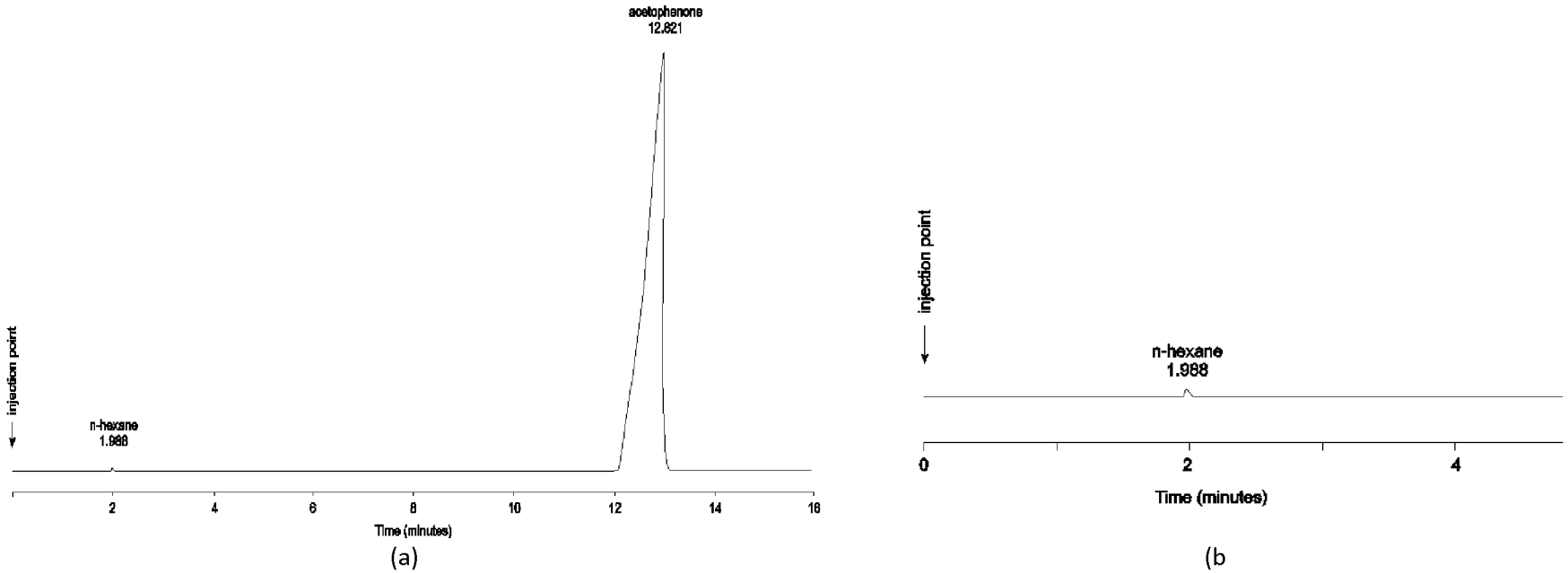

Figure 6.3 Chromatogram of n-hexane (2000ppm) in acetophenone(a) and and a zoomed in chromatogram of n-hexane (b)

Table 6.5 Optimised chromatographic conditions for acetone and n-hexane

Parameter	Acetone	n-hexane
Column	Zebron® (ZB WAXplus 30 m x 0.32 mm x 0.25 µm)	DB 5 (30 m x 0.32 mm x 0.25 µm)
Detector	FID	FID
Set point temperature (°C)	30	40
Injection temperature (°C)	180	170
Mode	split	split
Split ratio	15:1	15:1
Mobile phase (He) flow rate	1.6 ml/min	2.2 ml/min
Average velocity	26.755 cm/sec	35.216 cm/sec
Detector gas:		
H_2 flow	30 ml/min	30 ml/min
Air flow	400 ml/min	400 ml/min
Detector temperature (°C)	250	300
Make up (N_2) flow rate	5 ml/min	5 ml/min
Injection volume	1 µl	1 µl
Injection mode	Manual	Manual
Retention times (minutes)	acetone 3.1 ethanol 5.5 acetophenone (Solvent) 15.9	n-hexane 2.0 acetophenone (Solvent) 12.8

6.6 METHOD VALIDATION

6.6.1 Linearity and range

An analytical method is linear when the test results generated are proportional to the concentration of the analyte in a sample within a given range [246,247]. The ICH guidelines for method validation state and recommend that to determine linearity that a minimum of five concentrations in the analytical range be used to establish linearity [241]. Linearity was determined using least squares linear regression analysis of the calibration curve and identifying the equation for the line. The correlation coefficient (R^2) of the least squares linear regression line is a measure of linearity and should fall between 0.98 and 1.00 or be > 0.999 for linearity to prevail [138,145].

The range for the calibration curve was 608 to 12171 ppm for acetone. Stock solutions and serial dilutions of acetone in acetophenone using ethanol as an internal standard were prepared as described in §6.44. The peak area ratios (PAR) of acetone to ethanol was calculated and a calibration curve of PAR versus concentration (ppm) was plotted and is depicted in Figure 6.4. The equation for the best-fit least squares regression line for acetone was $y = 0.0002x - 0.0383$ with $R^2 = 0.9962$. The %RSD obtained for the calibration curve

points for acetone were < 2%. Table 6.6 summarizes the PAR, standard deviation and % RSD for the calibration curve points for acetone.

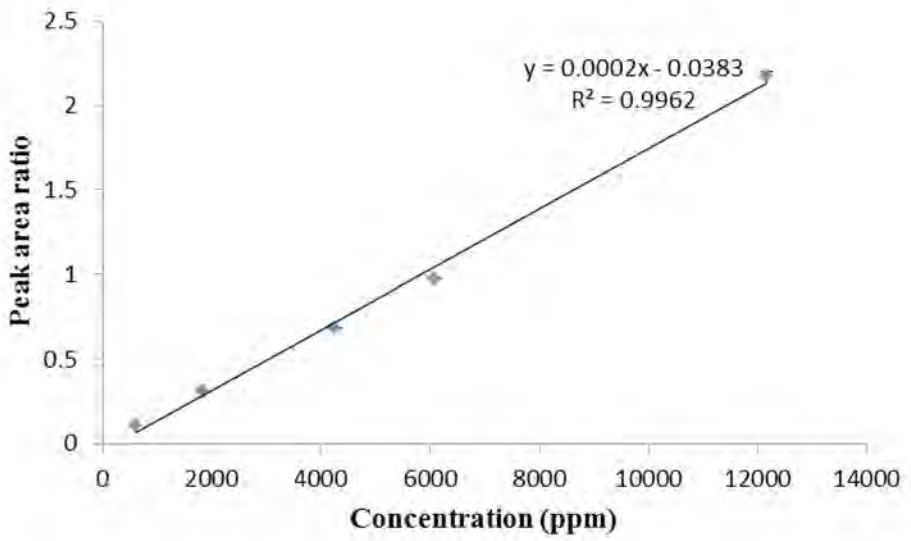

Figure 6.4 Typical calibration curve for acetone over the concentration range 608 to 12171ppm

Table 6.6 Typical summarised calibration curve data for acetone over the concentration range 608-12171ppm

Concentration (ppm)	Average PAR ± SD (n=3)	%RSD
608	0.1080 ± 0.0004	0.33
1825	0.3126 ± 0.0036	1.17
4260	0.6873 ± 0.0016	0.23
6085	0.9747 ± 0.0051	0.53
12171	2.1727 ± 0.0324	1.49

The range for the calibration curve for n-hexane was 76 to 1530 ppm. Stock solutions and serial dilutions of n-hexane in acetophenone were prepared as described in §6.4.4. The average peak area (PA) of hexane was calculated and a calibration curve of peak area (PA) versus concentration (ppm) was plotted for n-hexane and is depicted in Figure 6.5. The equation for the best-fit least squares regression line for n-hexane was y = 1.1974x -73.039 with R^2= 0.9954. The %RSD obtained for the calibration curve points for n-hexane were < 5%, the average peak area, standard deviation and % RSD values are summarised in Table 6.7

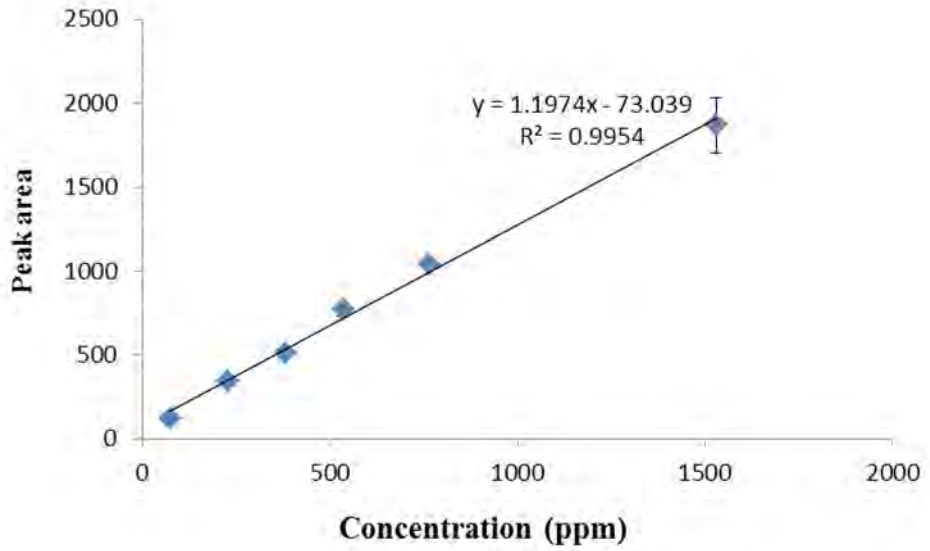

Figure 6.5 Typical calibration curve for n-hexane over the concentration range 76 -1530 ppm

Table 6.7 Typical calibration curve for n-hexane over the concentration range 76 to 1530 ppm

Concentration (ppm)	Average peak area ± SD (n=3)	%RSD
76.5	116.4779 ± 1.0394	0.89
229.5	362.0948 ± 8.8149	2.43
382.5	510.0242 ± 15.835	3.10
535.5	766.9128 ± 34.121	4.45
765.0	1040.643 ± 19.579	1.88
1530.0	1818.951 ± 47.547	2.61

6.6.2 Precision

The precision of an analytical method is a measure of the degree of agreement of individual test results when the method is applied to multiple analysis of a homogeneous sample repeatedly [246]. The precision of an analytical method measures the reproducibility or repeatability of the procedure under normal operating conditions and is usually expressed as a percent relative standard deviation or %RSD [167,244,249]. In this study intra-day and inter-day precision were established for these analyses.

6.6.2.1 Intra-day precision

Intra-day precision or repeatability and is used to evaluate the variability in experimental conditions over a short period of time. Intra-day precision is evaluated within the same laboratory under the same conditions on the same day. A solution of acetone and ethanol in acetophenone was prepared to make a solution of 4260 ppm of acetone. This solution was manually injected six times and the % RSD calculated. The results for intra-day precision for

acetone are summarized in Table 6.8 and the % RSD was 0.51 %. A solution of n-hexane in acetophenone was prepared to make a solution of 536 ppm of n-hexane. This solution was manually injected six times and the % RSD calculated. The results for the intra-day precision for n- hexane are summarized in Table 6.8 and the % RSD was 4.65 %. The intra-day studies for both acetone and n-hexane were found to have a %RSD <5% and thus the method was found to be precise.

Table 6.8 Intra-day precision data for acetone and n-hexane

Acetone	
Concentration (ppm)	4260
Mean PAR ± SD (n=3)	0.6675 ±0.0340
% RSD	0.51
Hexane	
Concentration (ppm)	536
Mean PA ± SD (n=3)	668.80 ± 31.120
% RSD	4.65

6.6.2.2 Inter-day precision

Inter-day precision or intermediate precision measures within-lab variations due to random events such as undertaken analyses on different days, by different analysts or using different equipment [241,244,251]. Acetone and ethanol were mixed with acetophenone to produce a 4260 ppm acetone solution. This solution was manually injected six times on two different days. N-Hexane was mixed with acetophenone to produce a 536 ppm n-hexane solution. This solution was manually injected six times on two different days. The results for the inter-day precision studies for acetone and n-hexane are summarized in Table 6.9. The % RSD for acetone and n-hexane were < 5%.

Table 6.9 Inter-day precision data for acetone and n-hexane

Acetone			
Day No.	**Concentration ppm**	**Mean PAR ± SD (n=3)**	**%RSD**
1	4260	0.6675 ± 0.0034	0.51
2	4260	0.6623 ±0.0063	0.95
Hexane			
Day No.	**Concentration ppm**	**Mean PA ± SD (n=3)**	**%RSD**
1	536	668.80 ± 31.111	4.65
2	536	653.60 ± 27.001	4.13

6.6.3 Limits of quantitation (LOQ) and detection (LOD)

The LOQ of an analytical method is the lowest concentration of an analyte that can be accurately quantitated with acceptable precision and accuracy [240,246,248]. The LOD is

defined as the lowest concentration of an analyte of interest that can be detected but not necessarily quantitated with the necessary precision and accuracy using the required experimental conditions [240,246]. A concentration of 912 ppm for acetone and 153 ppm for n-hexane were identified as the LOQ for these analytes. The % RSD for both compounds was < 5%. By convention the LOD was established as one third of the response for the LOQ and therefore was 304 ppm for acetone and 51 ppm for n-hexane [254]. A summary of results for the determination of LOQ for acetone and n-hexane are listed in Table 6.10.

Table 6.10 LOQ data for acetone and n-hexane

Acetone	
Concentration (ppm)	912
Mean PAR	0.1359 ± 0.0014
% RSD	1.01
Hexane	
Concentration (ppm)	153
Mean PA	192.63 ± 8.4603
% RSD	4.39

6.7 THE DETERMINATION OF RESIDUAL SOLVENTS CONTENT IN MTZ MICROCAPSULES

6.7.1 Determination of extraction efficiency for acetone

A solution of acetone in acetophenone (547 ppm) was prepared. A flow chart (Figure 6.6) summarises the extraction efficiency method for acetone. Approximately 1000 mg (n=3) of the MTZ microcapsules was accurately weighed using a Mettler® Model AE 163 analytical balance (Mettler® Inc., Zurich, Switzerland) and placed into three separate Kimax® centrifuge tubes. The acetone solution (2 ml) was added and vortexed for 30 seconds (n=3) using a Model G-560E Vortex-Gene2 mixer (Scientific Industries Inc., Bohemia, New York, USA), followed by centrifugation for 10 minutes at 250 rpm using Model HN-SII Centrifuge (Damon IEC Division, Bedfordshare, England). The process was outperformed three times until distinct layers of formulation and solvent were observed. The solvent was removed using a Pasteur pipette and placed into a 5 ml A-grade volumetric flask and was spiked with the internal standard and made up to volume with acetophenone. Approximately 2 ml of the final solution was transferred to a clear glass vial and analysed using a validated GC method. The extraction efficiency was calculated by dividing the amount extracted by the total amount of acetone and is reported as a percentage. The extraction efficiency was 56.106% ± 0.0007 with a % RSD of 0.32%. The extraction efficiency of approximately 56 % for acetone may not be considered satisfactory, however the precision of the extraction was good (%

RSD = 0.32%) suggesting that the low extraction efficiency may not be an issue for the purposes of these studies. It is evident that further studies must be undertaken to improve the extraction efficiency for acetone using this method.

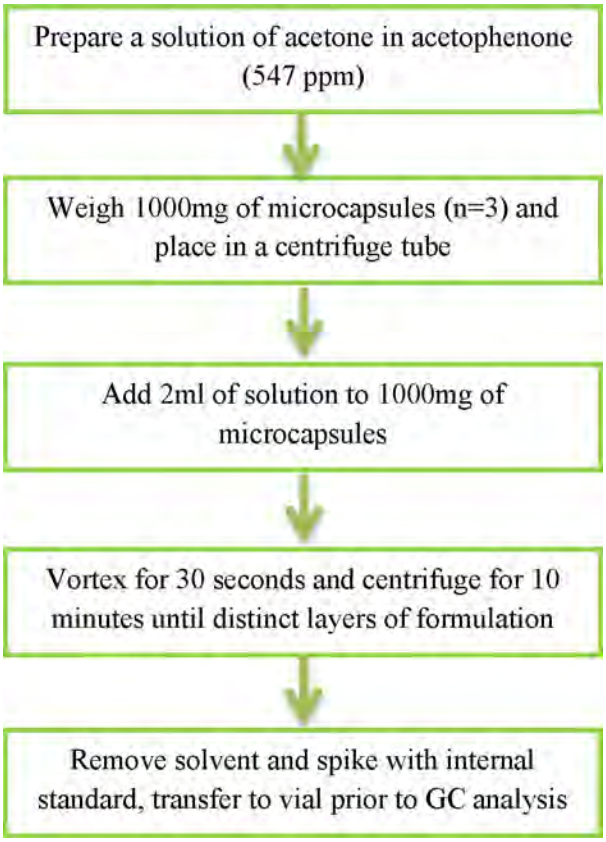

Figure 6.6 A summary of the extraction efficiency method for acetone

6.7.2 Determination of extraction efficiency for n-hexane

A solution of n-hexane in acetophenone was prepared (535 ppm). A flow chart (Figure 6.7) summarises the extraction efficiency method for n-hexane. Approximately 1000 mg (n=3) of the MTZ microcapsules was accurately weighed using a Mettler® Model AE 163 analytical balance (Mettler® Inc., Zurich, Switzerland) and placed into three separate Kimax® centrifuge tubes. The n-hexane solution (2 ml) was added and vortexed for 30 seconds (n=3) using a Model G-560E Vortex-Gene2 mixer (Scientific Industries Inc., Bohemia, New York, USA), followed by centrifuging for 10 minutes at 250 rpm using Model HN-SII Centrifuge (Damon IEC Division, Bedfordshare, England). The process was performed three times until distinct layers of formulation and solvent were observed. The solvent was removed using a Pasteur pipette and placed into a 5 ml A-grade volumetric flask. Approximately 2 ml of the final solution was transferred to a clear glass vial and analysed using a validated GC method. The extraction efficiency was calculated by dividing the amount extracted by the total amount of

n-hexane and reported as a percentage. The extraction efficiency was 55.942% ± 11.029 and the % RSD was 2.56%. The extraction efficiency for n-hexane was approximately 55 % with a % RSD of 2.56%. The extraction efficiency of 55 % for n-hexane may not be considered satisfactory, however the precision of the extraction was good (% RSD = 2.56%) suggesting that the low extraction efficiency may not be an issue for the purposes of these studies. It is evident that further studies must be undertaken to improve the extraction efficiency for n-hexane using this method.

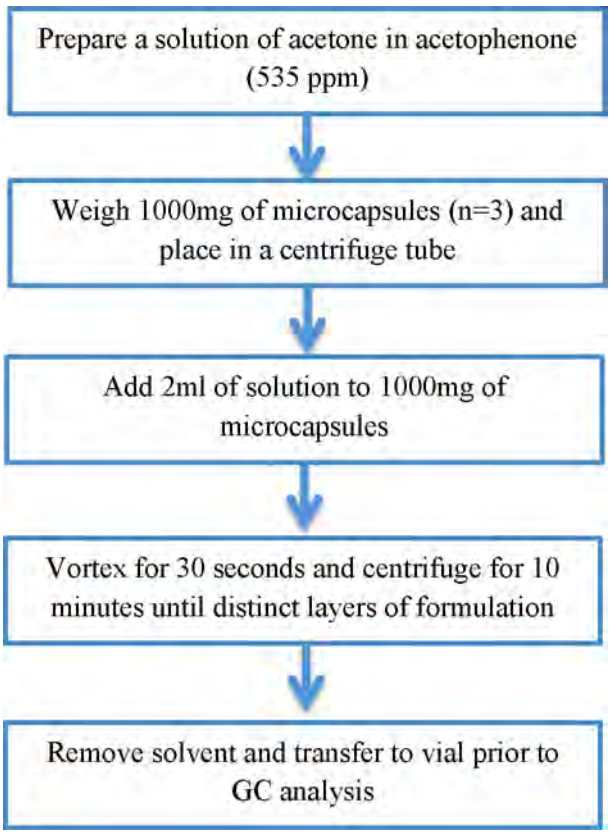

Figure 6.7 A summary of the extraction efficiency method for n-hexane

6.7.3 Microcapsule extraction for acetone

Approximately 1000 mg (n=3) of the MTZ microcapsules was accurately weighed using a Mettler® Model AE 163 analytical balance (Mettler® Inc., Zurich, Switzerland) and placed into three separate Kimax® centrifuge tubes. Acetophenone (2 ml) was added and vortexed for 30 seconds (n=3) using a Model G-560E Vortex-Gene2 mixer (Scientific Industries Inc., Bohemia, New York, USA), followed by centrifugation for 10 minutes at 250 rpm using Model HN-SII Centrifuge (Damon IEC Division, Bedfordshare, England). The process was outperformed three times until distinct layers of formulation and solvent were observed. The solvent was removed using a Pasteur pipette and placed into a 5 ml A-grade volumetric flask and was spiked with the internal standard ethanol. Approximately 2 ml of the solvent was

transferred to a clear glass vial and analysed using a validated GC method. The peak area ratio was used to calculate the amount of residual acetone in the product. The pharmacopeial concentration limit for acetone is 5000 ppm and the amount of acetone level was found to be 213.60 ppm/ g of formulation [41]. A flow chart (Figure 6.8) summarises the extraction procedure for acetone from the microcapsules

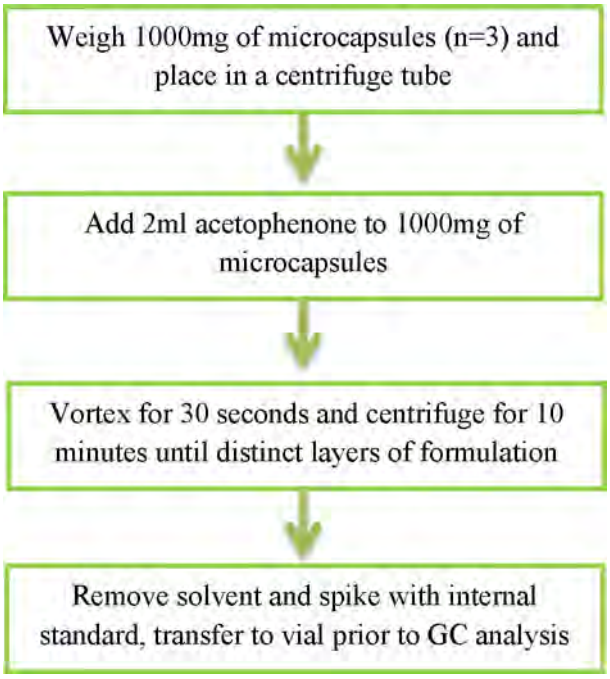

Figure 6.8 A summary of the extraction procedure for acetone from the microcapsules.

6.7.4 Microcapsule extraction for n-hexane

Approximately 1000 mg (n=3) of the MTZ microcapsules was accurately weighed using a Mettler® Model AE 163 analytical balance (Mettler® Inc., Zurich, Switzerland) and placed into three separate Kimax® centrifuge tubes. Acetophenone (2 ml) was added and vortexed for 30 seconds (n=3) using a Model G-560E Vortex-Gene2 mixer (Scientific Industries Inc., Bohemia, New York, USA), followed by centrifuging for 10 minutes at 250 rpm using Model HN-SII Centrifuge (Damon IEC Division, Bedfordshare, England). The process was performed three times until distinct layers of formulation and solvent were observed. The solvent was removed using a Pasteur pipette and placed into a 5 ml A-grade volumetric flask. Approximately 2 ml of the solvent was transferred to a clear glass vial and analysed using a validated GC method. The peak area was used to calculate the amount of residual n-hexane in the product. The pharmacopeial concentration limit for n-hexane is 290 ppm and the amount of n-hexane level was found to be 25.23 ppm/ g of formulation and is well below the limit

[41]. A flow chart (Figure 6.9) summarises the extraction procedure for n-hexane from the microcapsules

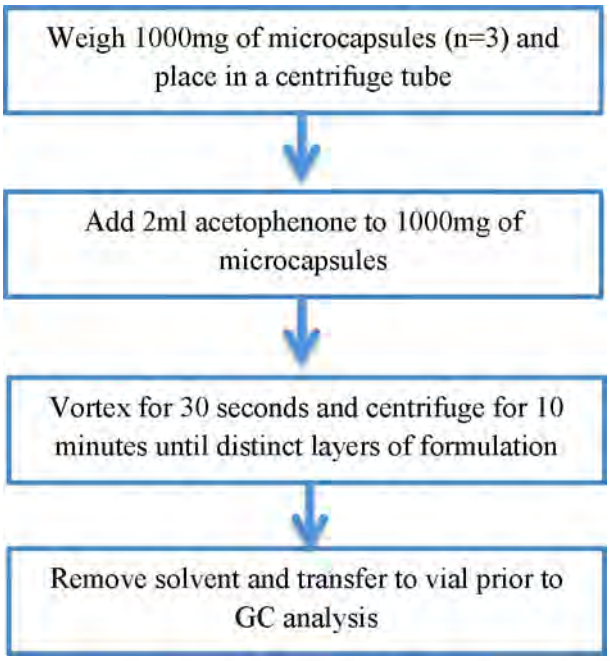

Figure 6.9 A summary of the extraction procedure for n-hexane from the microcapsules.

6.8 CONCLUSIONS

Organic solvents are commonly used during the synthesis of API, excipients and/or product manufacture. Different approaches are used to remove solvents following use however, some solvent may remain in the final product albeit in small quantities. The residual solvent may cause toxicity or undesirable effects in respect of patient treatment or product integrity. MTZ microcapsules manufacture involved the use of two solvents *viz.*, acetone and n-hexane and a GC-FID method was developed and used to quantitate residual levels of acetone and n-hexane in a batch of the optimised formulation.

The GC-FID method was developed using an empirical approach to identify solvent systems and an internal standard. Ethanol was identified and selected as the internal standard for the analysis of acetone whereas n- hexane was analysed without use of an internal standard. The samples were prepared using acetophenone as the diluent. The GC-FID method was optimised and partially validated in terms of linearity, precision, LOQ and LOD.

The microcapsules manufactured using the optimised formulation and process were prepared for analysis using acetophenone to extract residual acetone and n-hexane from the formulation. The samples were analysed using the validated GC-FID method and the amount of residual acetone and n-hexane quantitated. The residual levels of acetone and n-hexane were 213.60 ppm and 25.23 ppm per gram of formulation respectively and were well below pharmacopeial limits.

In conclusion the developed and validated GC-FID methods were successfully used for the determination and quantitation of residual acetone and n-hexane. The method found to be precise for both intra-day and inter-day studies. The methods were linear with R^2 values >0.99 and the % RSD for LOQ studies was found to be <5%. The separation using optimised conditions produced sharp and well resolved peaks for both acetone and n-hexane.

Future studies to improve the GC-FID methods include research in selecting a single column that could be used to detect both acetone and n-hexane simultaneously with the use of one internal standard and conducting a full validation study that is stability indicating.

CHAPTER SEVEN
CONCLUSIONS

Helicobacter pylori is one of the most common pathogenic bacterial infections leading to gastritis, gastro-duodenal ulcer disease and gastric cancer [3,542]. The prevalence of *Helicobacter pylori* is high in most counties, and affects 50-75% of the population globally [1]. The development of new compounds to treat *Helicobacter pylori* infections is time consuming and expensive and therefore the manufacture of formulations that can optimise the delivery of existing compounds such as MTZ used to treat the disease may be useful for eradication of disease associated with the bacterium. A combination of drugs is used to treat *Helicobacter pylori* infections however clinical eradication is poor [3]. Some reasons for this include instability of API in gastric fluids, the low concentration of therapeutic agents in the gastric mucosa and the short gastric residence time of API [1,3]. Prolonging the gastric residence time of API is one approach to overcome some of the aforementioned challenges [3]. Oral site-specific delivery systems that increase the duration of therapy at the target site may be an effective treatment option for *Helicobacter pylori* infections.

MTZ is a 5-nitroimidazole derivative that exhibits antibiotic and antiprotozoal activity, and is used in combination with other compounds for the treatment of *Helicobacter pylori* infections in peptic ulcer disease [11,12,16,110]. MTZ is almost completely absorbed following oral administration and has a bioavailability of > 90% [8,9]. MTZ is widely distributed in the biological system and has an apparent volume of distribution of 0.6-0.9 l/kg. It is a cost-effective API that exhibits good antimicrobial activity, has favourable pharmacokinetic properties and minimal side effect profile [7]. The development of a gastro-retentive sustained release MTZ formulation may be an approach to increasing the residence time of MTZ in the stomach thereby enhancing the local delivery of MTZ and improving treatment outcomes and ultimately patient adherence.

A stability indicating RP-HPLC method for the quantitation of MTZ in pharmaceutical dosage form was developed and optimised using a CCD and RSM approach. The mobile phase flow rate, buffer content, pH and molarity were variables that had to be optimised to effect an appropriate separation. The responses monitored were retention time of MTZ and ODZ, resolution and peak tailing of MTZ. Least squares linear regression was used to identify a mathematical model that best described the experimental data and ANOVA was used to establish the significance and relevance of input factors to the responses monitored.

The amount of buffer, pH and flow rate had a significant effect on the retention time of MTZ and ODZ, whereas buffer content and pH had a significant effect on resolution between MTZ and ODZ. A numerical optimisation approach was used to establish the optimum separation conditions for the RP-HPLC method. The optimised conditions produced sharp and well-resolved symmetrical peaks with retention times of approximately 5 and 9.14 minutes for MTZ and ODZ, respectively. A rapid, simple, precise, accurate and selective RP-HPLC method for the quantitation of MTZ was successfully developed, optimised and validated. The method was found to be linear over the concentration range 0.4 -120 µg/ml with a correlation coefficient of 0.999 and can be used for the analysis of MTZ in bulk API and dosage forms. The LOQ and LOD of the method were 0.4µg/ml and 0.13µg/ml respectively. Alkali and oxidative degradation studies revealed that when MTZ in solution was refluxed in 0.1 NaOH and H_2O_2 for one hour additional peaks were observed in the chromatogram and therefore degradation of MTZ was assumed to have occurred.

Preformulation studies were conducted as part preparative work required to manufacture a sustained release gastric-retentive microcapsule formulation for MTZ. SEM was used to visualize the size and shape of MTZ and the excipients used and results revealed that difference in the size and shape of the particles existed requiring size reduction prior to formulation. MTZ-excipient interactions were investigated using FTIR, DSC and XRD. FTIR and DSC studies revealed the presence of characteristic peaks in 1:1 binary mixtures of MTZ and excipients and as no additional peaks were observed indicating that MTZ was compatible with all excipients tested. XRD studies revealed a slight shift in the peak for MTZ that can be attributed to hydrogen bonding of MTZ when combined with Methocel® K15M. However the shift may also be due to the amorphous nature of Methocel® K15M and incompatibility was not confirmed using FTIR and DSC. The data generated from these studies clearly indicate that the excipients to be used are compatible with MTZ and were suitable for use in formulation development studies.

A solvent evaporation approach was used to manufacture gastric-retentive microcapsules. A non-effervescent method was used to formulate floating microcapsules with HPMC (Methocel®) that swells to form a colloidal gel barrier, entrapping air that confers buoyancy to these dosage forms. HPMC also controls the rate of MTZ release from the dosage form. All formulations were assessed in terms of encapsulation efficiency, buoyancy, yield, morphology and *in-vitro* MTZ release.

High encapsulation efficiencies were observed when the high viscosity grade Methocel® K100M was used when compared to Methocel® K15M. However the use high viscosity polymer even at low levels significantly reduced the cumulative % MTZ released and only approximately 70% of the compound was recovered after 12 hours of dissolution testing. Therefore a compromise between polymer type and content is necessary to achieve the desired performance characteristics of the formulation.

For both viscosity grades of polymer reducing the level of polymers resulted in a decrease in encapsulation efficiency. The buoyancy was found to increase with an increase in polymer concentration for both viscosity grades as more air was entrapped during swelling due to the higher level of Methocel® present

The results from *in vitro* release testing reveal, as expected that different Methocel® grades influence the *in vitro* release behaviour of MTZ. Altering the levels of Methocel® used had an influence on the rate and extent of *in vitro* release of MTZ. Methocel® K15M was selected for use based on the *in vitro* release studies as approximately 85% MTZ was released at 12 hours. In order to improve the encapsulation efficiency when using Methocel® K15M further optimization was undertaken to observe the combined effect of Methocel® K15M and Eudragit® RS PO, homogenisation time and speed on dosage form performance. Preliminary studies were performed by changing one factor at a time and therefore the effect of combination of factors on responses monitored was not easily observed. It was established that homogenisation speed and time, Methocel® K15M and Eudragit® RS PO levels had an impact on product performance and were taken into consideration when optimisation studies were performed. .

A DoE approach with CCD and RSM was used to investigate the impact of formulation variables on MTZ release, encapsulation efficiency, buoyancy and yield. Four key variables identified were the amount of Methocel® K15M and Eudrgait® RS PO included, homogenisation time and speed. Least squares linear regression was used to identify the mathematical model that best described the experimental data and ANOVA was used to analyse the significance and relevance of input variables on responses. The results indicate that the amount of Methocel® K15M used had a significant and synergistic effect on the encapsulation efficiency and buoyancy of the dosage form but an antagonistic effect on the *in vitro* release of MTZ. Homogenisation speed was also found to have a synergistic effect on *in vitro* release of MTZ and homogenisation time had an impact on microcapsule size. Two

dimensional contour and three dimensional response surface plots were used to gain further insight into the impact of input variables on the responses monitored. The release kinetics of MTZ from experimental formulations was established by fitting *in vitro* release data to several mathematical models. The model that the data were best fitted to was identified by using the value for R^2. Some batches of formulations were better fitted for the Higuchi model while other batches were better fitted for the first-order model, Higuchi model and first-order model appeared to best fit the data as majority of the formulation batches had highest R^2 values for these models. MTZ release from all formulations was a facilitated by a combination of diffusion, swelling and polymer releaxtion.

A numerical optimisation approach was used to predict a formualtion composition that would produce low initial MTZ release and a maximum release of MTZ at 12 hours, encapsulation efficiency, yield and buoyancy. In order to validate the results from the CCD experimental responses from the optimized formulation were compared to predicted responses. Results indicate that the majority of predicted and experimental results were similar as the prediction error < 5%. However the percent MTZ released at 0.5 and 2 hours had prediction errors of > 5%. Short-term stability on optimised formulations at 25°C/60% RH and 40°C/75% RH for 30 days were performed and no significant changes were observed for *in vitro* MTZ release, encapsulation efficiency and buoyancy over the 30 days stability study.

A GC-FID method was developed and validated for the quantitation of residual acetone and n-hexane in microcapsules and the method was linear and precise. Samples of microcapsules were analysed using the validated GC-FID method and the amount of residual acetone and n-hexane determined. It was established that the residual amount of acetone was 213.60 ppm/ g and n-hexane was 25.23 ppm/ g of formulation and was well below pharmacopeial limits of 5000 ppm and 290 ppm for acetone and n-hexane respectively[41].

In conclusion, sustained release gastro-retentive MTZ microcapsules with potential for further development have been developed and evaluated in these studies. The optimised formulation released 87.58% MTZ after 12 hours of dissolution testing in 0.1M HCL and had an encapsulation efficiency of 72.60%, a buoyancy of 58.41%, and a yield of 96.83 %.

Further studies to improve this formulation would include improving the buoyancy of the microcapsules by using an effervescent approach by incorporating sodium bicarbonate in the formulation. In addition conducting dissolution studies in simulated gastric fluid to get an idea of *in vivo* behaviour of the formulation would be an advantage. Future studies to

improve the GC-FID methods include research in selecting a single column that could be used to detect both acetone and n-hexane simultaneously with the use of an internal standard. In addition selecting an appropriate solvent in order to improve the extraction efficiency may also enhance the precision and accuracy of the method. This study has provided a starting point for the development of sustained release gastro-retentive formulations for API that are stable at gastric pH and for which gastric retention may improve treatment outcomes.

REFERENCES

1. M. Safavi, R. Sabourian, and A. Foroumadi, Treatment of Helicobacter pylori Infection: Current and Future Insights, *World Journal of Clinical Cases*, 4(1), 5–19, (2016).

2. T. N. A. Archampong, R. H. Asmah, E. K. Wiredu, R. K. Gyasi, K. N. Nkrumah, and K. Rajakumar, Epidemiology of Helicobacter pylori Infection in Dyspeptic Ghanaian Patients, *Pan African Medical Journal*, 20(178), 1–9, (2015).

3. S. Zhao, Y. Lv, J. Zhang, B. Wang, G. Lv, and X. Ma, Gastroretentive Drug Delivery Systems for the Treatment of Helicobacter pylori, *World Journal of Gastroenterology*, 20(28), 9321–9329, (2014).

4. S. Asnaashari, N. S. Khoei, M. H. Zarrintan, K. Adibkia, and Y. Javadzadeh, Preparation and Evaluation of Novel Metronidazole Sustained Release and Floating Matrix Tablets, *Pharmaceutical Development and Technology*, 16(4), 400–407, (2011).

5. C. M. Lopes, C. Bettencourt, A. Rossi, F. Buttini, and P. Barata, Overview on Gastroretentive Drug Delivery Systems for Improving Drug Bioavailability, *International Journal of Pharmaceutics*, 510(1), 144–158, (2016).

6. A. Kumar Nayak, R. Maji, and B. Das, Gastroretentive Drug Delivery Systems: A Review, *Asian Journal of Pharmaceutical and Clinical Research*, 3(1), 1–10, (2010).

7. S. Löfmark, C. Edlund, and C. E. Nord, Metronidazole Is Still the Drug of Choice for Treatment of Anaerobic Infections., *Clinical Infectious Diseases*, 50(1), 16–23, (2010).

8. C. R. Craig and R. E. Stitzel, Modern Pharmacology with Clinical Applications, 6th ed. Philadelphia: Lippincott Williams and Wilkins, 2004.

9. C. H. Nightingale, Antimicrobial Pharmacodynamics in Theory and Clinical Practice, 2nd ed. New York: Informa Healthcare, 2007.

10. V. Arcangelo and A. Peterson, Pharmacotherapeutics for Advanced Practice: A Practical Approach, 2nd ed. Philadelphia: Lippincott Williams and Wilkins, 2006.

11. A. Hauser, Antibiotics Basics for Clinicians: The ABCs of Choosing the Right Antibacterial Agent, 2nd ed. Philadelphia: Lippincott Williams and Wilkins, 2013.

12. T. Dougherty and M. Pucci, Antibiotic Discovery and Development, 1st ed. New York: Springer Science and Business Media, 2012.

13. J. A. Romich, Fundamentals of Pharmacology for Veterinary Technicians, 2nd ed. U.S.A: Delmar Cengage Learning, 2012.

14. V. K. Kapoor, R. Chadha, P. K. Venisetty, and S. Prasanth, Medical Significance of Nitroimidazoles: Some Recent Advances, *Journal of Scientfic and Industrial Research.*, 62(7), 659–665, (2003).

15. P. Lewis, Clinical Pharmacology in Obstetrics, 1st ed. U.S.A: Elsevier, 1983.

16. S. C. Sweetman, Martindale: The Complete Drug Reference, 33rd ed. London: Pharmaceutical Press, 2002.

17. South African Medicines Formulary, 10th ed. Pinelands, S.A: South African Medical Association,Health and Medical Publishing Group, 2012.

18. G. F. Brooks, K. C. Carroll, J. S. Butel, S. A. Morse, and T. A. Mietzner, Jawetz, Melnick and Adelberg's Medical Microbiology, 22nd ed. New York: McGraw-Hill, 2001.

19. J. W. D. McDonald, A. K. Burroughs, and B. G. Feagan, Evidence-Based Gastroenterology and Hepatology, 1st ed. U.S.A: John Wiley and Sons, 2008.

20. J. P. Menard, Antibacterial Treatment of Bacterial Vaginosis: Current and Emerging Therapies, *International Journal of Women's Health*, 3(1), 295–305, (2011).

21. L. Wearley and G. D. Anthony, Analytical Profile of Drug Substances, 5. New Jersey: Academic Press, 1976.

22. F. S. Southwick, Infectious Diseases in 30 days, 1st ed. U.S.A: McGraw Hill Professional, 2003.

23. C. Dollery, Therapeutics Drugs, 2. United Kingdom: Churchill Livingstone, 1991.

24. T. L. Lemke and D. A. Williams, Foye's Principles of Medicinal Chemistry, 7th ed. Philadelphia: Lippincott Williams and Wilkins, 2012.

25. D. G. Watson, Pharmaceutical Chemistry, 1st ed. Philadelphia: Elsevier Health Sciences, 2011.

26. J. P. Remington, D. B. Troy, and P. Beringer, Remington: The Science and Practice of Pharmacy, 21st ed. Philadelphia: Lippincott Williams and Wilkins, 2006.

27. R. Liu, Water-insoluble Drug Formulation, 2nd ed. New York: CRC Press, 2008.

28. J. J. Ramsden, Partition Coefficients of Drugs in Bilayer Lipid Membranes, *Experientia*, 49(8), 688–92, (1993).

29. S. F. Donovan and M. C. Pescatore, Method for Measuring the Logarithm of the Octanol-water Partition Coefficient by Using Short Octadecyl-poly(vinyl alcohol) High Performance Liquid Chromatography Columns, *Journal of Chromatography A*, 952(1–2), 47–61, (2002).

30. J. Ghasemi and S. Saaidpour, Quantitative Structure-property Relationship Study of N-octanol-water Partition Coefficients of Some of Diverse Drugs using Multiple Linear Regression., *Analytica Chimica Acta*, 604(2), 99–106, (2007).

31. C. F. Rediguieri, V. Porta, Nunes. T, Kamal. M, Shah. V *et al.*, Biowaiver Monographs for Immediate Release Solid Oral Dosage Forms: Metronidazole, *Journal of Pharmaceutical Sciences*, 100(5), 1618–1627, (2011).

32. N. M. Mahfouz and M. A. Hassan, Synthesis, Chemical and Enzymatic Hydrolysis, and Bioavailability Evaluation in Rabbits of Metronidazole Amino Acid Ester Prodrugs with Enhanced Water Solubility, *Journal of Pharmacy and Pharmacology*, 53(6), 841–848, (2001).

33. J. Coates, Interpretation of Infrared Spectra: A Practical Approach, 1st ed. New York: John Wiley and Sons, 2006.

34. J. L. Koenig, Spectroscopy of Polymers, 2nd ed. New York: Elsevier, 1999.

35. A. Tamba, B. Cioroiu, L. Profire, and I. Lazăr, Spectral UV and IR Determinations of New Xanthine Derivatives, *Farmacia*, 60(6), 939–946, (2012).

36. J. Mohan, Organic Spectroscopy: Principles and Applications, 2nd ed. United Kingdom: CRC Press, 2002.

37. C. G. Ţ. Anu, M. Ă. Gan, S. Braha, M. C. Popescu, and G. L. I. S. Ă, Preparation and Characterisation of Niosomes Containing Metronidazole, *Farmacia*, 61(6), 1178–1185, (2013).

38. M. K. Trivedi, S. Patil, H. Shettigar, K. Bairwa, and S. Jana, Spectroscopic Characterisation of Biofield Treated Metronidazole and Tinidazole, *Medicinal Chemistry*, 5(7), 340–344, (2015).

39. D. Breuer, Molecular Spectroscopy in the Ultraviolet and Visible Range, *The MAK-Collection for Occupational Health and Safety: Part III: Air Monitoring Methods*, 10(1), 39–53, (2007).

40. A. A. Edwards and B. D. Alexander, Organic Applications of UV-Visible Absorption Spectroscopy, 2nd ed. New York: Academic Press, 2010.

41. British Pharmacopoeia, 1. United Kingdom: The Stationery Office, 2013.

42. Kiss D, Zelkó R, N. C, and É. Z, Application of DSC and NIRS to Study the Comaptibility of Metronidazole with Different Pharmaceutical Excipients, *Journal of Thermal Analysis and Calorimetry*, 84(2), 447–451, (2006).

43. M. Y. Kraft, P. M. Kochergin, A. M. Tsyganova, and V. S. Shlikhunova, Synthesis of Metronidazole from Ethylenediamine, *Pharmaceutical Chemistry Journal*, 23(10), 861–863, (1989).

44. Z. Osman, D. Elhag, A. Suliman, and M. Almansour, A Comparative Photostability Study of Flagyrid, Metronidazole and Metrogyl Intravenous Infusion Brands Registered in Sudan, *American Journal of PharmTech Research*, 5(1), 431–442, (2015).

45. R. G. Finch, D. Greenwood, R. J. Whitley, and S. R. Norrby, Antibiotic and Chemotherapy, 9th ed. United Kingdom: Elsevier Health Sciences, 2010.

46. B Marciniec, A. Bugaj, and W. Kedziora, Kinetic Studies of the Photodegradation of Nitroimidazole Derivatives in the Solid State, *Acta Poloniae Pharmaceutica*, 52, pp.197-200, (1995).

47. A. Albini and E. Fasani, Drugs, Photochemistry and Photostability, 1st ed. United Kingdom: The Royal Society of Chemistry, 1998.

48. E. I. Karim, K. E. Ibrahim, and M. E. Adam, Studies on the Photochemical Decomposition of Metronidazole, *International Journal of Pharmaceutics*, 76(3), 261–264, (1991).

49. M. Bakshi and S. Singh, Stress Degradation Studies on Metronidazole and Development of a Validated Stability-indicating HPLC Assay Method, *Pharmaceutical Technology*, 27(10), 148, (2003).

50. R. Chadha, A. Aggarwal, J. V Jain, V. K. Kapoor, D. Thakur, and A. Sharma, Degradation Kinetics of Metronidazole and its Mutual Prodrug with Ciprofloxacin: A Calorimetric Analysis, *International Journal of Biological and Chemical Sciences*, 1(3), 197–210, (2007).

51. P. Verma, V. Namboodiry, S. Mishra, A. Bhagwat, and S. Bhoir, A Stability Indicating HPLC Method for the Determination of Metronidazole Using Ecofriendly Solvent as Mobile Phase Component, *Internation Journal of Pharmacy and Pharmaceutical Sciences*, 5(2), 496–501, (2013).

52. J. E. Bennett, R. Dolin, and M. J. Blaser, Principles and Practice of Infectious Diseases, 8th ed. New York: Elsevier Health Sciences, 2014.

53. H. B. Fung and T. L. Doan, Tinidazole: A Nitroimidazole Antiprotozoal Agent, *Clinical Therapeutics*, 27(12), 1859–1884, (2005).

54. D. Mayers, Antimicrobial Drug Resistance: Mechanisms of Drug Resistance, 1st ed. New York: Springer Science and Business Media, 2009.

55. K. Brophy, Clinical Drug Therapy for Canadian Practice, 2nd ed. Philadelphia: Lippincott Williams and Wilkins, 2010.

56. R. A. Cawson and E. W. Odell, Cawson's Essentials of Oral Pathology and Oral Medicine, 8th ed. London: Churchill Livingstone, 2008.

57. A. Galbraith, S. Bullock, E. Manias, B. Hunt, and A. Richards, Fundamentals of Pharmacology : An Applied Approach for Nursing and Health, 2nd ed. United Kingdom: Routledge, 2015.

58. R. Berkow, The Merck Manual, 19th ed. New Jersey: Merck Sharp and Dohme Research Laboratories, 2011.

59. C. R. Mahon, D. C. Lehman, and G. Manuselis, Textbook of Diagnostic Microbiology, 5th ed. Missouri: Elsevier, 2014.

60. J. Sun, Z. Deng, and A. Yan, Bacterial Multidrug Efflux Pumps: Mechanisms, Physiology and Pharmacological Exploitations, *Biochemical and Biophysical Research Communications*, 453(2), 254–267, (2014).

61. F. Mégraud, Helicobacter pylori Antibiotic Resistance: Prevalence, Importance, and Advances in Testing, *Gut*, 53(9), 1374–84, (2004).

62. P. A. Heasman, Restorative Dentistry, Paediatric Dentistry and Orthodontics, 2nd ed. Philadelphia: Elsevier, 2008.

63. F. J. Hughes, Clinical Problem Solving in Periodontology and Implantology, 1st ed. Philadelphia: Churchill Livingstone Elsevier, 2013.

64. T. M. Woo and M. V. Robinson, Pharmacotherapeutics for Advanced Practice Nurse Prescribers, 4th ed. Philadelphia: F.A. Davis Company, 2015.

65. National Department of Health, Standard Treatment Guidelines And Essential Medicines List for South Africa: Hospital Level Adults, 3rd ed. South Africa: National Department of Health, 2012.

66. R. A. Helms, Textbook of Therapeutics: Drug and Disease Management., 8th ed. Philadelphia: Lippincott Williams and Wilkins, 2006.

67. National Department of Health, Sexually Transmitted Infections Management Guidelines. South Africa, 2015.

68. P. N. Karamanakos, Thomas.C, Pappas. P, Boumba. V, M. Malamas *et al.*, Pharmaceutical Agents Known to Produce Disulfiram-like Reaction: Effects on Hepatic Ethanol Metabolism and Brain Monoamines, *International Journal of Toxicology*, 26(5), 423–432, (2007).

69. J. Griffin and P. D'Arcy, A Manual of Adverse Drug Interactions, 5th ed. New York: Elsevier, 1997.

70. M. C. Brucker and T. L. King, Pharmacology for Women's Health, 2nd ed. U.S.A: Jones and Bartlett Publishers, 2015.

71. L. Turner, Daily Drug Use, 9th ed. Cape Town: Tincture Press, 2010.

72. O. Eradiri, F. Jamali, and A. B. Thomson, Interaction of Metronidazole with Phenobarbital, Cimetidine, Prednisone, and Sulfasalazine in Crohn's Disease, *Biopharmaceutics and Drug Disposition*, 9(2), 219–227, (1988).

73. C. Marcucci, Hutchens. M, Wittwer. E, Weingarten.T, Sprung.J *et al.*, A Case Approach to Perioperative Drug Interactions, 1st ed. New York: Springer, 2015.

74. R. C. Dart, Medical Toxicology, 3rd ed. Philadelphia: Lippincott Williams and Wilkins, 2004.

75. D. E. Golan, Principles of Pharmacology: The Pathophysiologic Basis of Drug Therapy, 2nd ed. Philadelphia: Lippincott Williams and Wilkins, 2008.

76. S. L. Gorbach, J. G. Bartlett, and N. R. Blacklow, Infectious Diseases, 3rd ed. Philadelphia: Lippincott Williams and Wilkins, 2004.

77. J. E. Sykes, Canine and Feline Infectious Diseases, 1st ed. Missouri: Elsevier, 2013.

78. M. S. Ebadi and M. S. Ebadi, Desk Reference of Clinical Pharmacology, 2nd ed. London: CRC Press, 2008.

79. J. L. Vincent, Textbook of Critical Care., 6th ed. Missouri: Elsevier, 2011.

80. R. J. Hamilton, Tarascon Pharmacopoeia 2016: Desk Reference Edition., 16th ed. U.S.A: Jones and Bartlett Learning, 2015.

81. J. Moini, Fundamental Pharmacology for Pharmacy Technicians, 2nd ed. Austrialia: Cengage Learning, 2015.

82. M. Courtenay and M. Griffiths, Medication Safety: An Essential Guide, 1st ed. United Kingdom: Cambridge University Press, 2010.

83. R. Woodrow, B. J. Colbert, and D. M. Smith, Essentials of Pharmacology for Health Professions, 7th ed. Austrialia: Cengage Learning, 2014.

84. D. Silverstein and K. Hopper, Small Animal Critical Care Medicine, 2nd ed. Missouri: Elsevier Health Sciences, 2008.

85. M. W. Edmunds, M. S. Mayhew, and S. M. Setter, Pharmacology for the Primary Care Provider, 4th ed. Missouri: Elsevier, 2013.

86. R. A. Lehne and L. Rosenthal, Pharmacology for Nursing Care, 8th ed. Missouri: Elsevier Health Sciences, 2014.

87. R. L. Sweet and R. S. Gibbs, Infectious Diseases of the Female Genital Tract, 5th ed., Philadelphia: Lippincott Williams and Wilkins, 2012, 204–206.

88. S. F. McKay-Moffat, Disability in Pregnancy and Childbirth, 1st ed. Missouri: Elsevier Health Sciences, 2007.

89. L. L. Lilley, S. R. Collins, and J. S. Snyder, Pharmacology and the Nursing Process, 8th ed. Missouri: Elsevier Health Sciences, 2015.

90. P. Burtin, A. Taddio, O. Ariburnu, T. R. Einarson, and G. Koren, Safety of Metronidazole in Pregnancy: A Meta-analysis, *American Journal of Obstetrics and Gynecology*, 172(2), 525–529, (1995).

91. C. Koss, Investgations of Metronidazole use During Pregnancy and Adverse Birth Outcomes, *Antimicrobial Agents and Chemotherapy*, 56(9), 4800–4805, (2012).

92. Z. Kazy, E. Puhó, and A. E. Czeizel, Teratogenic Potential of Vaginal Metronidazole Treatment During Pregnancy, *European Journal of Obstetrics Gynecology and Reproductive Biology*, 123(2), 174–178, (2005).

93. M. Hochadel, Mosby's Drug Reference for Health Professions, 5th ed. Missouri: Elsevier Health Sciences, 2012.

94. A. Lee, S. Inch, and D. Finnigan, Therapeutics in Pregnancy and Lactation, 1st ed. Oxfordshire: Radcliffe Publishing, 2000.

95. N. Washington, C. Washington, and C. Wilson, Physiological Pharmaceutics: Barriers to Drug Absorption, 2nd ed. London: Taylor and Francis, 2001.

96. E. M. Scholar and W. B. Pratt, The Antimicrobial Drugs, 2nd ed. New York: Oxford University Press, 2000.

97. R. Jewell, Metronidazole, 1st ed. New York: Elsevier, 2007.

98. J. M. Ritter, L. D. Lewis, T. G. Mant, and F. Albert, A Textbook of Clinical Pharmacology and Therapeutics, 5th ed. London: CRC Press, 2008.

99. S. Faro, Sexually Transmitted Diseases in Women, 1st ed. Philadelphia: Lippincott Williams and Wilkins, 2003.

100. B. G. Katzung, Katzung - Basic and Clinical Pharmacology, 12th ed. U.S.A: The McGraw-Hill, 2012.

101. R. G. Ouellette and J. A. Joyce, Pharmacology for Nurse Anesthesiology, 1st ed. Massachusetts: Jones and Bartlett Learning, 2011.

102. J. Rello, Infectious Diseases in Critical Care, 2nd ed. New York: Springer Science and Business Media, 2007.

103. D. L. Snyder, J. Roberts, and E. Friedman, Handbook of Pharmacology of Aging, 2nd ed. U.S.A: CRC Press, 1996.

104. V. Alagarsamy, Textbook of Medicinal Chemistry, 2nd ed. India: Elsevier, 2012.

105. M. L. Grayson and A. Kucers, Kucers' the Use of Antibiotics a Clinical Review of Antibacterial, Antifungal, Antiparasitic and Antiviral Drugs, 6th ed. U.S.A: Taylor and Francis, 2010.

106. S. S. Long, L. K. Pickering, and C. G. Prober, Principles and Practice of Pediatric Infectious Disease, 4th ed. Philadelphia: Elsevier Health Sciences, 2012.

107. S. B. Ainsworth, Neonatal Formulary: Drug Use in Pregnancy and the First Year of Life, 7th ed. United Kingdom: John Wiley and Sons, 2010.

108. T. N. A. Archampong, R. H. Asmah, E. K. Wiredu, R. K. Gyasi, and K. N. Nkrumah, Factors Associated with Gastro-duodenal Disease in Patients Undergoing Upper GI Endoscopy at the Korle-Bu Teaching Hospital, Accra, Ghana, *African Health Sciences*, 16(2), 611–619, (2016).

109. L. H. Eusebi, R. M. Zagari, and F. Bazzoli, Epidemiology of Helicobacter pylori Infection, *Helicobacter*, 19(1), 1–5, (2014).

110. J. H. Kim and D. Y. Cheung, Must-have Knowledge About the Helicobacter pylori-Negative Gastric Cancer, *Gut and Liver*, 10(2), 157–159, (2016).

111. S. Davis, Eradication of Helicobacter pylori, *South African Family Practice*, 56(3), 1–4, (2014).

112. J. C. Yang, C. W. Lu, and C. J. Lin, Treatment of Helicobacter pylori Infection: Current Status and Future Concepts, *World Journal of Gastroenterology*, 20(18), 5283–5293, (2014).

113. O. McPolin, An Introduction to HPLC for Pharmaceutical Analysis, 1st ed. United Kingdom: Mourne Training Services, 2009.

114. R. L. Wixom and C. W. Gerhke, Chromatography: A Science of Discovery, 1st ed. New Jersey: John Wiley and Sons, 2011.

115. L. R. Snyder, J. J. Kirkland, and J. W. Dolan, Introduction to Modern Liquid Chromatography, 3rd ed. New Jersey: John Wiley and Sons, 2011.

116. M. Dong, Modern HPLC for Practicing Scientists, 1st ed. Massachusetts: John Wiley and Sons, 2006.

117. A. Braithwaite and J. F. Smith, Chromatographic Methods, 5th ed. London: Kluwer Academic Publishers, 1999.

118. R. Cooper and G. Nicola, Natural Products Chemistry: Sources, Separations, and Structures, 1st ed. Florida: CRC Press, 2014.

119. D. Kealey and P. J. Haines, Instant Notes in Analytical Chemistry, 1st ed. United Kingdom: BIOS Scientific Publishers Limited, 2002.

120. T. G. Venkateshwaran and J. T. Stewart, Determination of Metronidazole in Vaginal Tissue by High Performance Liquid Chromatography Using Solid Phase Extraction, *Journal of Chromatography B*, 672(2), 300–304, (1995).

121. United States Pharmacopoeia-National Formulary (USP-28/NF-23). Rockville: United States Pharmacopoeial Convention, 2005.

122. C. A. Burtis, C. A. Burtis, D. E. Bruns, B. G. Sawyer, and N. W. Tietz, Tietz Fundamentals of Clinical Chemistry and Molecular Diagnostics, 7th ed. Missouri: Elsevier, 2015.

123. M. M. Houck, Forensic Chemistry, 1st ed. London: Elsevier, 2015.

124. L. M. L. Nollet, Food Analysis by HPLC, 2nd ed. New York: Marcel Dekker, 2000.

125. K. Cabrera, Applications of Silica-based Monolithic HPLC Columns, *Journal of Separation Science*, 27(10–11), 843–52, (2004).

126. D. Corradini, Handbook of HPLC, 2nd ed. New York: CRC Press, 2011.

127. B. Abdul and R. Hassan, HPLC Uses and Importance in the Pharmaceutical Analysis and Industrial Field, *Pharmaceutica Analytica Acta*, 3(3), 1–2, (2012).

128. W. J. Tilstone, K. A. Savage, and L. A. Clark, Forensic Science: An Encyclopedia of History, Methods, and Techniques, 1st ed. California: ABC-CLIO, 2006.

129. S. Bayne and M. Carlin, Forensic Applications of High Performance Liquid Chromatography, 1st ed., Florida: CRC Press, 2010, 213–215.

130. M. W. Hajnos and J. Sherma, High Performance Liquid Chromatography in Phytochemical Analysis, 1st ed. New York: CRC Press, 2011.

131. M. C. McMaster, HPLC, A Practical User's Guide, 2nd ed. New Jersey: John Wiley and Sons, 2007.

132. B. M. Ham and A. Maham, Analytical Chemistry: A Chemist and Laboratory Technician's Toolkit, 1st ed. New Jersey: John Wiley and Sons, 2015.

133. S. Ahuja and M. Dong, Handbook of Pharmaceutical Analysis by HPLC, 1st ed. London: Elsevier, 2005.

134. T. Sirard, Fundamentals of HPLC. Waters Corporation, 2012.

135. S. Y. Gabhe, K. R. Mahadik, S. E. Potawale, and A. B. Thati, Development and Validation of Chromatographic Methods for Simultaneous Quantification of Drugs in Bulk and in their Formulations : HPLC and HPTLC Techniques, 1st ed. Hamburg: Anchor Academic Publishing, 2015.

136. B. Sivasankar, Bioseparations: Principles and Techniques, 1st ed. New Delhi: Prentice-Hall of India, 2005.

137. K. Valkó, Separation Methods in Drug Synthesis and Purification, 1st ed. Amsterdam: Elsevier, 2000.

138. Y. Kazakevich and R. Lobrutto, HPLC for Pharmaceutical Scientists. New Jersey: John Wiley and Sons, 2007.

139. K. Wilson and J. Walker, Principles and Techniques of Biochemistry and Molecular Biology, 7th ed.7. Cambridge: Cambridge University Press, 2010.

140. R. F. Venn, Principles and Practice of Bioanalysis, 1st ed. London: Taylor and Francis, 2000.

141. P. R. Brown, E. Grushka, and S. M. Lunte, Advances in Chromatography, 43. New Jersey: Marcel Dekker, 2004.

142. B. Levine, Principles of Forensic Toxicology, 2nd ed. Washington: AACC Press, 2003.

143. P. K. Mukherjee, Evidence-based Validation of Herbal Medicine, 1st ed. Amsterdam: Elsevier, 2015.

144. V. R. Meyer, Practical High-Performance Liquid Chromatography. New York: John Wiley and Sons, 2010.

145. J. Cazes, Encyclopedia of Chromatography, 2nd ed. New York: CRC Press, 2005.

146. H. J. Issaq, A Century of Separation Science, 1st ed. New York: Marcel Dekker, 2002.

147. R. Freitag, Modern Advances in Chromatography, 1st ed.76. New York: Springer-Verlag Berlin Heidelberg, 2002.

148. J. Khan, T. J. Kennedy, and D. R. Christian, Basic Principles of Forensic Chemistry, 1st ed. New York: Springer Science and Business Media, 2012.

149. S. S. Nielsen, Food Analysis, 4th ed. New Jersey: Springer Science and Business Media, 2010.

150. G. D. Watson, Pharmaceutical Analysis: A Textbook for Pharmacy Students and

Pharmaceutical Chemists, 4th ed. United Kingdom: Elsevier Health Sciences, 2014.

151. Y. Picó, Food Toxicants Analysis: Techniques, Strategies, and Developments, 1st ed. London: Elsevier, 2007.

152. E. Oltean, Development and Validation of RP-HPLC Method for the Quantition Studies of Metronidazole in Tablet and Powdered Dosage Forms., *Veterinary Drug*, 5(2), 71–73, (2011).

153. Y. Kumar, P. Sivaprasad, and A. Kumar, RP-HPLC Method Development and Validation for Simulatneous Quantitative Estimation of Metronidazole and Nalidixic Acid in Tablets, *International Journal of Pharmaceutical Sciences*, 7(2), 367–371, (2015).

154. M. Kubodera, T. Tokumura, and Y. MacHida, Determination of Metronidazole in a Rat Stomach by HPLC for Obtaining Basic Data of the Eradication Therapy of Helicobacter pylori, *Journal of Pharmaceutical Analysis*, 2(5), 378–381, (2012).

155. N. H. Binhashim, S. N. Alvi, and M. M. Hammami, A Validated Reversed Phase HPLC Assay for the Determination of Metronidazole in Human Plasma, *World Journal Of Pharmacy and Pharmaceutical Sciences*, 3(12), 32–41, (2014).

156. M. Silva, S. Schramm, E. Kano, E. Koono, V. Porta, and C. Serra, Development and Validation of a HPLC-MS-MS Method for Quantification of Metronidazole in Human Plasma., *Journal of Chromatographic Science*, 47(9), 781–784, (2009).

157. A. Cemal, A. O. Sibel, S. Zuhre, and C. Semsettin, Simulatneous Determination of Metronidazole and Miconazole in Pharmaceutical Dosage Forms by RP-HPLC, *Il Farmaco*, 57(1), 953–957, (2000).

158. K. R. Danano, S. M. Hiradeve, A. V Kasture, and P. G. Yeole, RP-HPLC Simultaneous Estimation of Metronidazole and Diloxanide Furoate in Combination, *International Journal of Pharmacy and Life Sciences*, 1(2), 82–85, (2010).

159. G. Lunn and N. R. Schmuff, HPLC Methods for Pharmaceutical Analysis, 26(4). U.S.A: John Wiley and Sons, 1998.

160. E. Jaber, G. Neda, and H. Hamed, A Rapid and Sensitive HPLC Method for the Analysis of Metronidazole in Human Plasma: Application to Single Dose Pharmacokinetic and Bioequivalence Studies, *DARU Journal of Pharmaceutical Sciences*, 14(1), 15–21, (2006).

161. E. Lundanes, L. Reubsaet, and T. Greibrokk, Chromatography: Basic Principles, Sample Preparations and Related Methods, 1st ed. New York: John Wiley and Sons, 2013.

162. Z. Alhalabi, M. Al-khayat, and S. Haidar, Separation and Assay of Antiprotozoal Imidazole Derivatives (metronidazole, tinidazole and secinidazole) by RP-HPLC, *International Journal of Pharmaceutical Sciences Review and Research*, 13(1), 13–18, (2012).

163. 1 Essam Ezzeldin and T. M. El-Nahhas, New Analytical Method for the Determination of Metronidazole in Human Plasma: Application to Bioequivalence Study, *Tropical Journal of Pharmaceutical Research*, 11(5), 799–805, (2012).

164. C. Akay, S. A. Özkan, Z. Şentürk, and Ş. Cevheroğlu, Simultaneous Determination of Metronidazole and Miconazole in Pharmaceutical Dosage Forms by RP-HPLC, *Farmaco*, 57(11), 953–957, (2003).

165. D. Corradini, Handbook of HPLC, 2nd ed. CRC Press, 2016.

166. L. R. Snyder, J. J. Kirkland, and J. L. Glach, Practical HPLC Method Development, 2nd ed. New York: John Wiley and Sons, 1997.

167. Food and Drug Administration: Reviewer Guidance: Validation of Chromatographic Methods, Centre for Drug Evaluation and Research (CDER), U.S.A, (1994).

168. Z. Pápai and T. L. Pap, Analysis of Peak symmetry in Chromatography., *Journal of Chromatography A*, 953(1–2), 31–38, (2002).

169. D. Song and J. Wang, Modified Resolution Factor for Asymmetrical Peaks in Chromatographic Separation, *Journal of Pharmaceutical and Biomedical Analysis*, 32(6), 1105–1112, (2003).

170. E. F. Barry and R. L. Grob, Columns for Gas Chromatography: Performance and Selection, 1st ed. New Jersey: John Wiley and Sons, 2007.

171. W. J. Lough and I. W. Wainer, High Performance Liquid Chromatography: Fundamental Principles and Practice, 1st ed. London: CRC Press, 1996.

172. S. Ahuja and H. Rasmussen, HPLC method development for pharmaceuticals, 1st ed. Amsterdam: Academic Press, 2007.

173. C. H. Chan, C. H. Chia, and S. Thomas, Physical Chemistry of Macromolecules: Macro to Nanoscales, 1st ed. New Jersey: Apple Academic Press, 2014.

174. I. F. Uchegbu, Fundamentals of Pharmaceutical Nanoscience, 1st ed. New York: Springer Science and Business Media, 2013.

175. J. C. J. Bart, Additives in Polymers: Industrial Analysis and Applications, 1st ed. United Kingdom: John Wiley and Sons, 2005.

176. R. J. Flanagan, A. Taylor, I. Watson, and R. Whelpton, Fundamentals of Analytical Toxicology, 3rd ed. United Kingdom: John Wiley and Sons, 2015.

177. J. K. Swadesh, HPLC: Practical and Industrial Applications, 2nd ed. New York: CRC Press, 2000.

178. K. M. Usher, S. W. Hansen, J. S. Amoo, A. P. Bernstein, and M. E. P. McNally, Precision of Internal Standard and External Standard Methods in High Performance Liquid Chromatography (HPLC), *Recent Developments in HPLC and UPLC*, 33(4), 1–10, (2015).

179. S. Kromidas, HPLC Made to Measure: A Practical Handbook for Optimisation, 1st ed. United Kingdom: John Wiley and Sons, 2008.

180. R. Ohtaka, M. Maeda, T.Iwagami, T.Ueda, Y. Kimura *et al.*, Precision of Internal Standard Method in HPLC Analysis, *Yakugaku Zasshi*, 123(5), 349–355, (2003).

181. P. G. Wang, Monolithic Chromatography and its Modern Applications, 1st ed. United Kingdom: ILM Publications, 2010.

182. S. C. Moldoveanu and V. David, Essentials in Modern HPLC Separations, 1st ed. U.S.A: Newnes, 2012.

183. V. R. Meyer, Pitfalls and Errors of HPLC in Pictures, 3rd ed. New York: John Wiley and Sons, 2013.

184. T. Tuzimski and J. Sherma, High Performance Liquid Chromatography in Pesticide Residue Analysis, 109. Florida: CRC Press, 2015.

185. P. R. Loconto, Trace Environmental Quantitative Analysis: Principles, Techniques and Applications, 2nd ed. London: CRC Press, 2005.

186. H. R. Irving and C. Gehring, Plant Signaling Peptides, 1st ed. New York: Springer Science and Business Media, 2012.

187. E. Heftmann, Fundamentals and Applications of Chromatography and Related Differential Migration Methods, 69. New York: Elsevier, 2004.

188. E. Lennart, Design of Experiments: Principles and Applications, 3rd ed. Sweden: MKS Umetrics AB, 2008.

189. N. Torrealday, L. González, R. M. Alonso, R. M. Jiménez, and E. Ortiz Lastra, Experimental Design Approach for the Optimisation of a HPLC-Fluorimetric Method for the Quantitation of the Angiotensin II Receptor Antagonist Telmisartan in Urine, *Journal of Pharmaceutical and Biomedical Analysis*, 32(4–5), 847–857, (2003).

190. G. A. Lewis, D. Mathieu, and R. Phan-Tan-Luu, Pharmaceutical Experimental Design, 1st ed. New York: CRC Press, 1998.

191. T. P. Ryan, Modern Experimental Design, 1st ed. New York: Wiley-Interscience, 2007.

192. R. H. Myers, D. C. Montgomery, and C. M. Anderson-Cook, Response Surface Methodology: Process and Product Optimisation Using Designed Experiments, 4th ed. New Jersey: John Wiley and Sons, 2016.

193. W. M. Amir, M. Shafiq, and K. Mokhtar, Simple Response Surface Methodology Using RSREG (SAS), *Journal of Modern Applied Statistical Methods*, 15(1), 855–867, (2016).

194. H. Pham, Springer Handbook of Engineering Statistics, 1st ed. London: Springer Science and Business Media, 2006.

195. R. N. Das, Robust Response Surfaces, Regression, and Positive Data Analyses, 1st ed. Florida: CRC Press, 2014.

196. P. R. Nelson, M. Coffin, and K. A. F. Copeland, Introductory Statistics for Engineering Experimentation, 1st ed. U.S.A: Academic Press, 2003.

197. M. Ben-Daya, S. O. Duffuaa, and A. Raouf, Maintenance, Modeling and Optimisation, 1st ed. New York: Springer Science and Business Media, 2000.

198. A. I. Khuri and S. Mukhopadhyay, Response Surface Methodology, *Wiley Interdisciplinary Reviews: Computational Statistics*, 2(2), 128–149, (2010).

199. M. C. Gacula, Design and Analysis of Sensory Optimisation., 1st ed. U.S.A: John Wiley and Sons, 2008.

200. T. A. Reddy, Applied Data Analysis and Modeling for Energy Engineers and Scientists, 1st ed. New York: Springer Science and Business Media, 2011.

201. M. Dutka, M. Ditaranto, and T. Løvås, Application of a Central Composite Design for the Study of NO x Emission Performance of a Low NO x Burner, *Energies*, 8(1), 3606–3627, (2015).

202. B. Oyejola and J. Nwanya, Selecting the Right Central Composite Design, *International Journal of Statistics and Applications*, 5(1), 21–30, (2015).

203. A. O. Beringhs, M. Dalmina, T. B. Creczynski-Pasa, and D. Sonaglio, Response Surface Methodology IV-optimal Design Applied to the Performance Improvement of an RP-HPLC-UV Method for the Quantification of Phenolic Acids in Cecropia glaziovii products, *Brazilian Journal of Pharmacognosy*, 25(5), 513–521, (2015).

204. R. N. Dash, H. Mohammed, and T. Humaira, An Integrated Taguchi and Response Surface Methodological Approach for the Optimisation of an HPLC Method to Determine Glimepiride in a Supersaturatable Self-Nanoemulsifying Formulation, *Saudi Pharmaceutical Journal*, 24(1), 92–103, (2016).

205. P. D. Kalariya, D. Namdev, R. Srinivas, and S. Gananadhamu, Application of Experimental Design and Response Surface Technique for Selecting the Optimum RP-HPLC Conditions for the Determination of Moxifloxacin HCl and Ketorolac Tromethamine in Eye Drops, *Journal of Saudi Chemical Society*, 1(1), 1–10, (2014).

206. S. M. Khamanga and R. B. Walker, The Use of Experimental Design in the Development of an HPLC-ECD Method with Electrochemical Detection for the Analysis of Captopril, *Talanta*, 83(3), 1037–1049, (2011).

207. E. Klein and S. Rivera, A Review of Criteria Functions and Response Surface Methodology for the Optimisation of Analytical Scale HPLC Separations, *Journal of Liquid Chromatography and Related Technologies*, 23(14), 2097–2121, (2000).

208. M. Bezerra, R. Santelli, E. Oliveira, L. Villar, and L. Escaleira, Response Surface Methodology as a Tool for Optimisation in Analytical Chemistry, *Talanta*, 76(1), 965–977, (2008).

209. P. Sahu and C. Patro, Application of Chemometric Response Surface Methodology in Development and Optimisation of a RP-HPLC Method for the Separation of Metaxalone and its Base Hydrolytic Impurities, *Journal of Liquid Chromatography and Related Technologies*, 13(17), 2444–2464, (2014).

210. A. Owezarek, L. Kuzma, H. Wysokinska, and A. Olszewska, Application of Response Surface Methodology for Optimisation of Simulataneous UHPLC-PDA Determination of Oleanolic and Ursolic Acids and Standardisation of Ericaaeae Medicinal Plants, *Applied Sciences*, 6(244), 1–16, (2016).

211. Y. Chen, P. Tsai, and P. Wu, Optimisation and Validation of High Performance Chromatographic Condition for Simultaneous Determination of Adapalene and Benzoyl Peroxide by Response Surface Methodology, *PloS One*, 10(3), 1–9, (2015).

212. Russel V. Lenth, Response Surface Methods in R, Using RSM, *Journal of Statistical Software*, 32(7), 1–17, (2009).

213. D. B. Hibbert, Experimental Design in Chromatorgraphy: A Tutorial Review, *Journal of Chromatography B*, 910(1), 2–13, (2012).

214. L. Xie and D. Huang, Advanced Engineering and Technology, 1st ed. New York: CRC Press, 2014.

215. M. Y. Noordin, V. C. Venkatesh, S. Sharif, S. Elting, and A. Abdullah, Application of Response Surface Methodology in Describing the Performance of Coated Carbide Tools when Turning AISI 1045 Steel, *Journal of Materials Processing Technology*, 145(1), 46–58, (2004).

216. M. P. Oakes and M. Ji, Quantitative Methods in Corpus-Based Translation Studies: A Practical Guide to Descriptive Translation Research., 1st ed. U.S.A: John Benjamins Pub. Co, 2012.

217. J. F. Faraway, Linear Models with R, 1st ed. New York: CRC Press, 2004.

218. J. K. Sharma, Business Statistics, 2nd ed. India: Dorling Kindersley, 2012.

219. P. Barmpalexis, F. I. Kanaze, and E. Georgarakis, Developing and Optimizing a Validated Isocratic Reversed Phase High Performance Liquid Chromatography Separation of Nimodipine and Impurities in Tablets Using Experimental Design Methodology, *Journal of Pharmaceutical and Biomedical Analysis*, 49(5), 1192–1202, (2009).

220. F. L. Romano, G. M. B. Ambrosano, M. B. B. de A. Magnani, and D. F. Nouer, Analysis of the Coefficient of Variation in Shear and Tensile Bond Strength Tests, *Journal of Applied Oral Science*, 13(3), 243–246, (2005).

221. A. Malakahmad and S. Y. Chuan, Application of Response Surface Methodology to Optimise Coagulation Flocculation Treatment of Anaerobically Digested Palm Oil Mill Effluent Using Alum, *Desalination and Water Treatment*, 51(34–36), 6729–6735, (2016).

222. U. Rajamanickam, M. Krishnaswami, P. Muthusamy, and K. Chidambaram, Screening of Actinomycetes from Mangrove Ecosystem for L-asparaginase Activity and Optimisation by Response Surface Methodology, *Polish Journal of Microbiology*, 60(3), 213–221, (2011).

223. K. Muralidharan, Six Sigma for Organisational Excellence: A Statistical Approach, 1st ed. India: Springer, 1999.

224. M. Pant, K. Deep, A. Nagar, and J. C. Bansal, Proceedings of the Third International Conference on Soft Computing for Problem Solving: SocProS 2013, 2nd ed. New York: Springeri, 2013.

225. G.-C. Yang, Transactions on Engineering Technologies: International MultiConference of Engineers and Computer Scientists, 1st ed. New York: Springer, 2014.

226. H. M. Bush, Biostatistics: An Applied Introduction for the Public Health Practitioner, 1st ed. U.S.A: Delmar Cengage Learning, 2012.

227. S. Rabe-Hesketh and B. Everitt, A Handbook of Statistical Analyses Using Stata, 4th ed. Florida: Chapman and Hall, 2007.

228. P. Wyatt, Property Valuation, 2nd ed. New York: John Wiley and Sons, 2013.

229. N. Pfenning, Elementary Statistics, 1st ed. U.S.A: Cengage Learning, 2011.

230. J. I. Vélez, J. C. Correa, and F. Marmolejo-Ramos, A New Approach to the Box–Cox Transformation, *Frontiers in Applied Mathematics and Statistics*, 1(1), 12, (2015).

231. M. J. Anderson and P. J. Whitcomb, RSM Simplified: Optimizing Processes Using Response Surface Methods for Design of Experiments, 1st ed. U.S.A: Productivity Press, 2005.

232. W. Smith, Experimental Design for Formulation, 1st ed. Philadelphia: Society for Industrial and Applied Mathematics (SIAM), 2005.

233. R. W. Mee, A Comprehensive Guide to Factorial Two-Level Experimentation, 1st ed. Philadelphia: Springer-Verlag, 2009.

234. S. Singh, Proceedings of the International Conference on Research and Innovations in Mechanical Engineering : ICRIME-2013, 1st ed. India: Springer, 2013.

235. S. Ahuja and S. Scypinski, Handbook of Modern Pharmaceutical Analysis, 2nd ed. New York: Elsevier, 2011.

236. H. G. Brittain, Profiles of Drug Substances, Excipients and Related Methodology, 1st ed. New York: Academic Press, 2003.

237. H. Merdjan, C. Bonnat, E. Singlas, and B. Diquet, Measurement of Ornidazole by High Performance Liquid Chromatography, *Journal of Chromatography B: Biomedical Sciences and Applications*, 273(2), 475–480, (1983).

238. R. Smith, Retention and Selectivity in Liquid Chromatography: Prediction, Standardisation, and Phase Comparisons, 1st ed. New York: Elsevier, 1995.

239. M. Swartz and I. S. Krull, Handbook of Analytical Validation, 1st ed. Florida: CRC Press, 2012.

240. O. McPolin, The Validation of Analytical Methods for Pharmaceutical Analysis, 1st ed. United Kingdom: Mourne Training Services, 2009.

241. ICH Harmonised Tripartite Guideline. Validation of Analytical Procedures: Text and Methodolgy. ICH Topic (Q2)R1, (2005).

242. S. K. Bansal, T. Layloff. E.Bush, M.Hamilton, Hankison.E, *et al.*, Qualification of Analytical Instruments for Use in the Pharmaceutical Industry: A Scientific Approach, *American Association of Pharmaceutical Scientists PharmSciTech*, 5(1), 1–10, (2004).

243. United States Pharmacopoeia-National Formulary, USP-28/NF-. Rockville: United States Pharmacopoeial Convention Inc, 2005.

244. G. Shabir, Validation of High Performance Liquid Chromatography Methods for Pharmaceutical Analysis: Understanding the Differences and Similarities between Validation, *Journal of Chromatography A*, 987(1), 57–66, (2003).

245. L. Felton, Remington Essentials of Pharmaceutics, 1st ed. United Kingdom: Pharmaceutical Press, 2012.

246. Institute of Medicine (U.S.). Committee on Food Chemicals Codex., Food Chemicals Codex, 5th ed. Washington: National Academy Press, 2003.

247. C. M. Riley, T. W. Rosanske, and S. Riley, Specification of Drug Substances and Products : Development and Validation of Analytical Methods, 1st ed. New York: Elsevier, 2013.

248. O. Wurl, Practical Guidelines for the Analysis of Seawater, 1st ed. Florida: CRC Press, 2009.

249. A. Fajgelj and A. Ambrus, Principles and Practices of Method Validation, 1st ed. United Kingdom: Royal Society of Chemistry, 2000.

250. C. C. Chan, Y. Lee, H. Lam, and X. M. Zhang, Analytical Method Validation and Instrument Performance Verification, 1st ed. New Jersey: John Wiley and Sons, 2004.

251. P. De Bièvre and H. Günzler, Validation in Chemical Measurement, 1st ed. New York: Springer, 2005.

252. S. B. Karch, Workplace Drug Testing, 1st ed. Florida: CRC Press, 2008.

253. Food and Drug Administration:Guidance for Industry: Validation of Analytical Procedures and Methodology, Topic Q2B. Centre for Drug Evaluation and Research (CDER), USA, (1996).

254. T. C. Paino and A. D. Moore, Determination of the LOD and LOQ of an HPLC Method Using Four Different Techniques, *Pharmaceutical Technology*, 23(10), 86–92, (1999).

255. M. Blessy, R. D. Patel, P. N. Prajapati, and Y. Agrawal, Development of Forced Degradation and Stability Indicating Studies of Drugs: A Review, *Journal of Pharmaceutical Analysis*, 4(3), 159–165, (2014).

256. ICH Harmonised Tripartite Guideline Stability Testing: Photostability Testing of New Drug Substances and Products Q1B Photostability Testing of New Drug Substances and Products. USA, 1996.

257. G. Ngwa, Forced Degradation as an Integral Part of HPLC Stability Indicating Method Development, *Drug Delivery Technology June*, 10(5), (2010).

258. Food and Drug Administration: Guidance for Industry:Photostability Testing of New Drug Substances and Products, Topic Q1B. Centre for Drug Evaluation and Research (CDER), USA, 301–827, (1996).

259. T. Rawat and I. P. Pandey, Forced Degradation Studies for Drug Substances and Drug Products Scientific and Regulatory Considerations, *Journal of Pharmaceutical Sciences and Research*, 7(5), 238–241, (2015).

260. P. Hamrapurkar, P. Patil, M. Desai, M. Phale, and S. Pawar, Stress Degradation Studies and Development of a Validated Stability Indicating Assay Method for Determination of Diacerein in Presence of Degradation Products., *Pharmaceutical methods*, 2(1), 30–35, (2011).

261. Y. Wu and R. Fassihi, Stability of Metronidazole, Tetracyline HCL and Famotidine Alone and in Combination, *International Journal of Pharmaceutics*, 290(1–2), pp.1-13, (2005).

262. M. Bakshi and S. Singh, Development of Validated Stability Indicating Assay Methods: Critical Review, *Journal of Pharmaceutical and Biomedical Analysis*, 28(6), 1011–1040, (2002).

263. S. Chaudhari and P. Patil, Pharmaceutical Excipients: A Review, *International Journal of advances in Pharmacy, biology and chemistry*, 1(1), 21–34, (2012).

264. J. Roy, An Introduction to Pharmaceutical Sciences: Production, Chemistry, Techniques and Technology, 1st ed. Oxford: Woodhead Publishing Series in Biomedicine, 2012.

265. L. L. Augsburger and S. W. Hoag, Pharmaceutical Dosage Forms: Tablets, 3rd ed. New York: Informa Healthcare, 2008.

266. V. B. Patravale, J. I. Disouza, and M. Rustomjee, Pharmaceutical Product Development: Insights into Pharmaceutical Processes, Management and Regulatory Affairs, 1st ed. New York: Taylor and Francis, 2016.

267. A. C. Cartwright and B. Matthews, International Pharmaceutical Product Registration, 2nd ed. New York: Informa Healthcare, 2009.

268. G. Chaurasia, A Review on Pharmaceutical Preformulation Studies in Formulation and Development of New Drug Molecules, *International Journal of Pharmaceutical Sciences and Research*, 7(6), 2313–2320, (2016).

269. A. Tilak, Significance of Preformulation Studies in Designing, Fabricating for Pharmaceutical Dosage Forms, *Journal of Biomedical and Pharmaceutical Research*, 4(6), 35–45, (2016).

270. G. S. Banker and C. T. Rhodes, Modern Pharmaceutics, 4th ed. New York: Marcel Dekker, 2002.

271. P. Kumar, P. K. Desu, G. Vaishnavi, K. Divya, U. Lakshmi, and D. P. Kumar, An Overview on Preformulation Studies, *Indo American Journal of Pharmacetical Sciences*, 2(10), 1399–1407, (2015).

272. International Conference on Harmonisation. ICH of Technical Requirements for Registration of Pharmaceuticals for Human Use. ICH Harmonised Tripartite Guideline, Pharmaceutical Development Q8 (R2), (2009).

273. Food and Drug Administration:Guidance for Industry: Nonclinical Studies for the Safety Evaluation of Pharmaceutical Excipients. Center for Drug Evaluation and Research (CDER).U.S.A, (2005).

274. A. Katdare and M. V. Chaubal, Excipient Development for Pharmaceutical, Biotechnology, and Drug Delivery Systems, 1st ed. New York: Informa Healthcare, 2006.

275. R. C. Rowe, Handbook of Pharmaceutical Excipients, 6th ed. United Kingdom: Pharmaceutical Press, 2009.

276. D. Phadtare, G. Phadtare, and M. Asawat, Hypromellose : A Choice of Polymer in Extended Release Tablet Formulation, *World Journal of Pharmacy and Pharmaceutical Sciences*, 3(9), 551–566, (2014).

277. P. Timmins, S. Pygall, and C. D. Melia, Hydrophilic Matrix Tablets for Oral Controlled Release, 1st ed. New York: Springer, 2014.

278. I. Uchegbu and A. Schatzlein, Polyemrs in Drug Delivery, 1st ed. Florida: CRC Press, 2006.

279. M. Jenkins, Biomedical Polymers, 1st ed. New York: Woodhead Publishing Series in Biomedicine, 2007.

280. D. S. Jones, Pharmaceutical Applications of Polymers for Drug Delivery, 1st ed. United Kingdom: Rapra Technology Ltd, 2004.

281. A. Nokhodchi, S. Raja, P. Patel, and K. Asare-Addo, The Role of Oral Controlled Release Matrix Tablets in Drug Delivery Systems., *BioImpacts*, 2(4), 175–87, (2012).

282. S. M. Samani, H. Montaseri, and A. Kazemi, The Effect of Polymer Blends on Release Profiles of Diclofenac Sodium from Matrices, *European Journal of Pharmaceutics and Biopharmaceutics*, 55(3), 351–355, (2003).

283. Y. Perrie and T. Rades, Pharmaceutics: Drug Delivery and Targeting, 2nd ed. United Kingdom: Pharmaceutical Press, 2012.

284. V. Thakur and M. Thakur, Handbook of Polymers for Pharmaceutical Technologies, 1st ed. New Jersey: Scrivener Publishing, 2015.

285. Y. Qiu, Y. Chen, Z. Lawrence, and Rao.Mintri, Developing Solid Oral Dosage Forms: Pharmaceutical Theory and Practice, 2nd ed. United Kingdom: Academic Press, 2017.

286. V. Nikam, K. Kotade, V. Gaware, and R. Dolas, Eudragit a Versatile Polymer: A Review, *Pharmacologyonline*, 1(1), 152–164, (2011).

287. A. Sonje and A. Chandra, Comprehensive Review on Eudragit Polymers, *International Research Journal of Pharmacy*, 4(5), 71–74, (2013).

288. S. Singh, S. Arora, and Y. Singla, An Overview of Multifaceted Significance of Eudragit Polymers in Drug Delivery Systems, *Asian Journal of Pharmaceutical and Clinical Research*, 8(5), 1–6, (2015).

289. F. Hoobakht, G. Fariba, E. Vasheghani-Farahani, and M. Mousavi, Eudragit RS PO Nanoparticles for Sustained Release of Pyridostigmine Bromide, *Journal of Nanoparticle Research*, 15(9), 1912–1917, (2013).

290. A. Sarker Apu, A. H. Pathan, D. Shrestha, G. Kibria, and R. Jalil, Investigation of In vitro Release Kinetics of Carbamazepine from Eudragit RS PO and RL PO Matrix Tablets, *Pharm Res Tropical Journal of Pharmaceutical Research*, 8(2), 145–152, (2009).

291. S. Indira, P. Amareshwar, and P. Srinivas, Preparation and Charecterisation of Gastroretentive Floating Microspheres of Balofloxacin, *World Journal of Pharmacy and Pharmaceutical Sciences*, 4(9), 1022–1035, (2015).

292. M. Fukuda, N. A. Peppas, and J. W. McGinity, Floating Hot-melt Extruded Tablets for Gastroretentive Controlled Drug Release System, *Journal of Controlled Release*, 115(2), 121–129, (2006).

293. G. Vijaya Baskar, N. Narayanan, R. Gaikwad, and S. Abdul, Formulation and Evaluation of Gastro-retentive Floating Multi-particulate System of Metoprolol Tartarate, *Tropical Journal of Pharmaceutical Research*, 9(2), 181–186, (2010).

294. R. Sushma and N. Sriram, Preparation and Evaluation of Floating Microspheres of Repaglinide, *International Journal of Advanced Pharmaceutics*, 3(1), 30–36, (2013).

295. P. Gupta, M. Kumar, and N. Sachan, An Overview on Polymethacrylate Polymers in Gastroretentive Dosage Forms, *Open Pharmaceutical Sciences Journal*, 2(1), 31–42, (2015).

296. N. Terinte, R. Ibbett, and K. C. Schuster, Overview on Native Cellulose and Microcrystalline Cellulose I Structure Studied by X-ray Diffraction (WAXD): Comparison between Measurement Techniques, *Lenzinger Berichte*, 89(1), 118–131, (2011).

297. T. Vehovec, A. Gartner, O. Planinšek, and A. Obreza, Influence of Different Types of Commercially Available Microcrystalline Cellulose on Degradation of Perindopril Erbumine and Enalapril Maleate in Binary Mixtures, *Acta Pharmaceutica*, 62(4), 515–528, (2012).

298. R. S. Gaud, S. J. Surana, G. S. Talele, and S. B. Gokhale, Natural Excipients, 2nd ed. Mumbai: Nirali Prakashan, 2008.

299. G. Thoorens, F. Krier, B. Leclercq, B. Carlin, and B. Evrard, Microcrystalline Cellulose, A Direct Compression Binder in a Quality by Design Environment: A Review, *International Journal of Pharmaceutics*, 473(1), 64–72, (2014).

300. P. Patel, K. Ahir, V. Patel, L. Manani, and C. Patel, Drug-Excipient Compatibility Studies: First Step for Dosage Form Development, *The Pharma Innovation Journal*, 14(45), 14–20, (2015).

301. S. Bohanec, T. Peteka, P. Bohanec, A. Krivec et al., Using Different Experimental Designs in Drug-Excipient Compatibility Studies During the Preformulation Development of a Stable Solid Dosage Formulation, *Acta Chimica Slovenica*, 57(4), 895–903, (2010).

302. S. C. Gad, Pharmaceutical Manufacturing Handbook: Production and Processes, 1st ed. New York: John Wiley and Sons, 2008.

303. A. Ravi, S. Saxena, and N. Nagpal, A Concise Understanding of Pharmaceutical Excipients, *International Journal of Pharmacy and Pharmaceutical Research*, 3(3), 122–136, (2015).

304. A. Narang, D. Desai, and S. Badawy, Impact of Excipient Interactions on Solid Dosage Form Stability, *Pharmaceutical Research*, 29(10), 2660–2683, (2012).

305. K. Jackson, D. Young, and S. Pant, Drug Excipient Interactions and their Effect on Absorption, *Pharmaceutical Science and Technology Today*, 3(10), 336–345, (2000).

306. S. Bharate, S. Bharate, and A. Bajaj, Interactions and Incompatibilities of Pharmaceutical Excipients with Active Pharmaceutical Ingredients: A Comprehensive Review, *Journal of Excipients and Food Chemistry*, 1(3), 3–26, (2010).

307. K. Gohil, P. Patel, and N. Patel, Application of Analytical Techniques in Preformulation Study: A Review, *International Journal of Pharmaceutical and Biological Archives*, 2(5), 1319–1326, (2011).

308. R. Chadha and S. Bhandari, Drug-Excipient Compatibility Screening: Role of Thermoanalytical and Spectroscopic Techniques, *Journal of Pharmaceutical and Biomedical Analysis*, 87(1), 82–97, (2014).

309. G. Bruni, L. Amici, V. Berbenni, A. Marini, and A. Orlandi, Drug-Excipient Compatibility Studies: Search of Interaction Indicators, *Journal of Thermal Analysis and Calorimetry*, 68(2), 561–573, (2002).

310. R. Gao, Y. Jin, Q.-Y. Yang, B.-W. Sun, and J. Lin, Study of Stability and Drug-Excipient Compatibility of Estradiol and Pharmaceutical Excipients, *Journal of Thermal Analysis and Calorimetry*, 120(1), 839–845, (2015).

311. L. L. Chaves, L. Rolim, M. Goncalves, A. Vieira, L.Alves *et al.*, Study of Stability and Drug-Excipient Compatibility of Diethylcarbamazine Citrate, *Journal of Thermal Analysis and Calorimetry*, 111(3), 2179–2186, (2013).

312. M. Akers, Excipient-Drug Interactions in Parenteral Formulations, *Journal of Pharmaceutical Sciences*, 91(11), 2283–2300, (2002).

313. K. Hotha, S. Roychowdhury, and V. Subramanian, Drug-Excipeint Interactions: Case Studies and Overview of Drug Degradation Pathways, *American Journal of Analytical Chemistry*, 7(1), 107–140, (2016).

314. S. Bozdag-Pehlivan, B. Subasi, I. Vural, N. Unlu, and Y. Cpan, Evaluation of Drug-Excipient Interaction in the Formulation of Celecoxib Tablets, *Acta Poloniae Pharmaceutica*, 68(3), 423–433, (2011).

315. N. Fathima, T. Mamatha, H. K. Qureshi, N. Anitha, and J. V. Rao, Drug-Excipient Interaction and its Importance in Dosage Form Development, *Journal of Applied Pharmaceutical Science*, 1(2011), 66–71, (2011).

316. J. Zheng, Formulation and Analytical Development for Low-dose Oral Drug Products, 1st ed. New York: John Wiley and Sons, 2009.

317. A. Dash, S. Singh, and J. Tolman, Pharmaceutics: Basic Principles and Application to Pharmacy Practice, 1st ed. New York: Elsevier, 2013.

318. A. S. Narang and S. H. S. Boddu, Excipient Applications in Formulation Design and Drug Delivery, 1st ed. New York: Elsevier, 2014.

319. J. L. Arias, Nanotechnology and Drug Delivery, 1st ed. Florida: CRC Press, 2014.

320. R. M. Richards, J. Z. Xing, and K. M. Mackay, Excipient Interaction with Cetylpyridinium Chloride Activity in Tablet Based Lozenges., *Journal of Pharmaceutical research*, 13(8), 1258–1264, (1996).

321. M. Barzegar-Jalali, S. Ghanbarzadeh, K.Adikia, H.Valizadeh, S. Bibak *et al.*, Development and Characterisation of Solid Dispersion of Piroxicam for Improvement of Dissolution Rate Using Hydrophilic Carriers., *BioImpacts*, 4(3), 141–8, (2014).

322. M. Newa, K. Bhandari, K. Jong Oh, I Jong Seob, A. Jung Ae *et al.*, Enhancement of Solubility, Dissolution and Bioavailability of Ibuprofen in Solid Dispersion Systems, *Chemical and Pharmaceutical bulletin*, 56(4), 569–74, (2008).

323. D. Ravishanker, K. Vijaya Sri, and C. A. Kumar, Formulation Development of Ritonavir Tablets Containing Solid Dispersions Employing Montmorillonite: Dissolution Rate Enhancement, *Asian Journal of Pharmaceutical and Clinical*, 6(2), 206–208, (2013).

324. R. Panakanti and A. S. Narang, Impact of Excipient Interactions on Drug Bioavailability from Solid Dosage Forms, *Journal of Pharmaceutical research*, 29(10), 2639–2659, (2012).

325. D. Zhou, Understanding Physicochemical Properties for Pharmaceutical Product Development and Manufacturing II: Physical and Chemical Stability and Excipient Compatibility, *Journal of Validation Technology*, 1(1), 36–47, (2009).

326. L. Jinjiang and Y. Yongemi, Lubricants in Pharmaceutical Dosage Forms, *Lubricants*, 2(2), 21–43, (2014).

327. K. J. Hartauer, G. Arbuthnot, S. Baertschi, R. Johnson *et al.*, Influence of Peroxide Impurities in Povidone and Crospovidone on the Stability of Raloxifene Hydrochloride in Tablets: Identification and Control of an Oxidative Degradation Product, *Journal of Pharmaceutical Development and Technology*, 5(3), 303–310, (2000).

328. Y. Wu, J. Levons, A. S. Narang, K. Raghavan, and V. M. Rao, Reactive Impurities in Excipients: Profiling, Identification and Mitigation of Drug-Excipient Incompatibility, *American Association of Pharmaceutical Scientists PharmSciTech*, 12(4), 1248–1263, (2011).

329. A. K. Pahari and B. S. Chauhan, Enginering Chemistry, 1st ed. New Delhi: Laxmi Publications, 2006.

330. P. Schattschneider, Linear and Chiral Dichroism in the Electron Microscope, 1st ed. U.S.A: Pan Stanford Publishing, 2012.

331. X. Fu, D. Huck, L. Makein, B. Armstrong, U. Willen, and T. Freeman, Effect of Particle Shape and Size on Flow Properties of Lactose Powders, *Particuology*, 10(2), 203–208.

332. P. W. Cleary, The Effect of Particle Shape on Simple Shear Flows, *Powder Technology*, 179(3), 144–163, (2008).

333. R. A. Carlton, Pharmaceutical Microscopy, 1st ed. New York: Springer, 2011.

334. A. Kar, Pharmaceutical Drug Analysis, 2nd ed. New Delhi: New Age International Publishers, 2005.

335. B. C. Smith, Fundamentals of Fourier Transform Infrared Spectroscopy, 2nd ed. Florida: CRC Press, 2011.

336. R. Mehta, A. Chawla, P. Sharma, and P. Pawar, Formulation and In vitro Evaluation of Eudragit S-100 Coated Naproxen Matrix Tablets for Colon-Targeted Drug Delivery System., *Journal of Advanced Pharmaceutical Technology and Research*, 4(1), 31–41, (2013).

337. H. Kumar Mukhopadhyay, H. Das, B. Manas, S. Ray, R. Rajabalaya *et al.*, Preparation and Characterisation of Polymethacrylate-based Matrix Microspheres of Carbamazepine Using Solvent Evaporation Method, *Farmacia*, 62(1), 137–158, (2014).

338. E. S. Ben, R. Nofita, S. Rusdi, M. Suardi, and A. Djamaan, Use of Eudragit RS PO in the Formulation of Acyclovir Hollow Microspheres by Solvent Evaporation Technique, *Der Pharmacia Lettre*, 8(11), 53–59, (2016).

339. T. R. Sekharan, S. Palanichamy, S. Tamilvanan, S. Shanmuganathan, and A. T. Thirupathi, Formulation and Evaluation of Hydroxypropyl Methylcellulose-based Controlled Release Matrix Tablets for Theophylline, *Indian Journal of Pharmaceutical Sciences*, 73(4), 451–6, (2011).

340. H. Akinosho, S. Hawkins, and L. Wicker, Hydroxypropyl Methylcellulose Substituent Analysis and Rheological Properties, *Carbohydrate Polymers*, 98(1), 276–281, (2013).

341. H. Biao, T. Li-rong, D. Da-song, O. Wen, L. Tao, and C. Xue-rong, Biomaterials Science and Engineering, 1st ed. Europe: InTech, 2011.

342. P. Gill, T. T. Moghadam, and B. Ranjbar, Differential Scanning Calorimetry Techniques: Applications in Biology and Nanoscience, *Journal of Biomolecular Techniques*, 21(4), 167–193, (2010).

343. G. W. H. Höhne, W. F. Hemminger, and H.-J. Flammersheim, Differential Scanning Calorimetry: An Introduction for Practitioners, 1st ed. New York: Springer Science and Business Media, 1996.

344. P. Gabbot, Principles and Applications of Thermal Analysis, 1st ed. United Kingdom: Blackwell Publishing, 2008.

345. F. Balestrieri, A. D. Magrì, A. L. Magrì, D. Marini, and A. Sacchini, Application of Differential Scanning Calorimetry to the Study of Drug-Excipient Compatibility, *Thermochimica Acta*, 285(2), 337–345, (1996).

346. D. Kiss, R. Zelkó, C. Novák, and Z. Éhen, Application of DSC and NIRS to Study the Compatibility of Metronidazole with Different Pharmaceutical Excipients, *Journal of Thermal Analysis and Calorimetry*, 84(2), 447–451, (2006).

347. M. C. Adeyeye and H. G. Brittain, Preformulation in Solid Dosage Form Development. U.S.A: Informa Healthcare, 2008.

348. A. Mesnukul, K. Yodkhum, and T. Phaechamud, Solid Dispersion Matrix Tablet Comprising Indomethacin-PEG-HPMC Fabricated with Fusion and Mold Technique, *Indian Journal of Pharmaceutical Sciences of Pharmaceutical Sciences*, 74(4), 413–420, (2009).

349. Scintag Inc.Basics of X-ray Diffraction,Providing Solutions to Your Diffraction Needs.Scintag Inc.California. 1–25, 1999.

350. R. Myers, The Basics of Physics, 1st ed. London: Greenwood Press, 2006.

351. Y. Waseda, E. Matsubara, and K. Shinoda, X-Ray Diffraction Crystallography: Introduction, Examples and Solved Problems, 1st ed. New York: Springer, 2011.

352. C. Hammond, The Basics of Crystallography and Diffraction, 4th ed. United Kingdom: Oxford University Press, 2015.

353. H. Wen and K. Park, Oral Controlled Release Formulation Design and Drug Delivery, 1st ed. U.S.A: John Wiley and Sons, 2011.

354. R. K. Verma, D. M. Krishna, and S. Garg, Formulation Aspects in the Development of Osmotically Controlled Oral Drug Delivery Systems, *Journal of Controlled Release*, 79(1–3), 7–27, (2002).

355. A. Hjalmarson. S. Goldstien, B. Fagerberg, H. Wedel *et al.*, Effects of Controlled-release Metoprolol on Total Mortality, Hospitalisations, and Well-Being in Patients with Heart Failure, *Journal of American Medical Association*, 283(10), 1295–302, (2000).

356. J. S. Gimbel, P. Richards, and R. K. Portenoy, Controlled-release Oxycodone for Pain in Diabetic Neuropathy: A Randomised Controlled Trial, *Neurology*, 60(6), 927–34, (2003).

357. B. Singh, S. K. Chakkal, and N. Ahuja, Formulation and Optimisation of Controlled Release Mucoadhesive Tablets of Atenolol Using Response Surface Methodology, *Journal of the American Association of Pharmaceutical Scientists*, 7(1), 19–28, (2006).

358. Effect of Metoprolol CR/XL in Chronic Heart Failure: Metoprolol CR/XL Randomised Intervention Trial in Congestive Heart Failure (MERIT-HF), *Lancet*, 353(9169), 2001–2007, (1999).

359. A. J. Gelenberg, R. B. Lydiard, R. L. Rudolph, L. Aguiar, J. T. Haskins, and E. Salinas, Efficacy of Venlafaxine Extended-release Capsules in Nondepressed Outpatients with Generalised Anxiety Disorder, *Journal of American Medical Association*, 283(23), 3082–3088, (2000).

360. J. Kane, F. Canas, M. Krammer, L. Ford, P. Lim *et al.*, Treatment of Schizophrenia with Paliperidone Extended-release Tablets: A 6-week Placebo-Controlled Trial, *Schizophrenia Research*, 90(1–3), 147–161, (2007).

361. K. E. Uhrich, S. M. Cannizzaro, R. S. Langer, and K. M. Shakesheff, Polymeric Systems for Controlled Drug Release, *Chemical Reviews*, 99(11), 3181–3198, (1999).

362. T. Salsa, F. Veiga, and M. E. Pina, Oral Controlled-release Dosage Forms. I. Cellulose Ether Polymers in Hydrophilic Matrices, *Drug Development and Industrial Pharmacy*, 239(239), 929–938, (1997).

363. R. D. Shami and B. Rao, Microencapuslation Technology and Applications, *Defence Science Journal*, 59(1), 82–95, (2009).

364. K. Teshima, Synthesis of Trimellitic Anhydride Microcapsule Toner by Liquid-Phase Separation, *Journal of Applied Polymer Science*, 90(14), 3822–3826, (2003).

365. Z. Tianyong, F. Xuening, S. Jian, and Z. Chunlong, Properties of Copper Phthalocyanine Microencapsulated in Polystyrene by Phase Separation, *Dyes and Pigments*, 44(1), 1–7, (1999).

366. N. Agnihotri, R. Mishra, C. Goda, and M. Arora, Microencapsulation: A Novel Approach in Drug Delivery: A Review, *Indo Global Journal of Pharmaceutical Sciences*, 2(1), 1–20, (2012).

367. M. N. Singh, K. S. Y. Hemant, M. Ram, and H. G. Shivakumar, Microencapsulation: A Promising Technique for Controlled Drug Delivery, *Research in Pharmaceutical Sciences*, 5(2), 65–77, (2010).

368. S. K. Ghosh, Self-healing Materials: Fundamentals, Design Strategies, and Applications, 1st ed. Weinheim: Wiley-VCH, 2009.

369. S. K. Das, R. Rajabalaya, H. Mukohopadhyay, T. Halder *et al.*, Microencapsulation Techniques and its Practices, *International Journal of Pharmaceutical Science and Technology*, 6(2), 1–23, (2011).

370. K. A. S. Khan, Using Metallic Foams with Macro-encapsulated Paraffin to Enhance the Charging and Dis-charging Processes, *Journal of Mechanical and Civil Engineering*, 12(4), 9–22, (2015).

371. M. F. Al-Omran, S. A. Al-Suwayeh, A. M. El-Helw, and S. I. Saleh, Taste Masking of Diclofenac Sodium using Microencapsulation, *Journal of Microencapsulation*, 19(1), 45–52, (2002).

372. A. Gupta and B. Dey, Microencapsulation for Controlled Drug Delivery: A Comprehensive Review, *Sunsari Technical College Journal*, 1(1), 48–54, (2012).

373. M. Momin, S. Rathod, and S. Kar, Taste Masking Techniques for Bitter Drugs -An Overview, *International Journal of Phamracy and Technology*, 4(2), 2100–2118, (2012).

374. S. Dutta Roy, S. Nandy, and S. Banerjee, Microencapsulation: Convenient Mode of Drug Delivery in Novel Drug Delivery System, *Internation Journal of Pharmacy and Life Sciences*, 3(3), 1555–1562, (2012).

375. V. Dash, S. K. Mishra, M. Singh, A. K. Goyal, and G. Rath, Release Kinetic Studies of Aspirin Microcapsules from Ethyl Cellulose, Cellulose Acetate Phthalate and their Mixtures by Emulsion Solvent Evaporation Method, *Scientia pharmaceutica*, 78(1), 93–101, (2010).

376. H. Yoshizawa, Trends in Microencapsulation Research, *KONA Powder and Particle Journal*, 22(1), 23–30, (2004).

377. V. Jyothi, M. Prasanna, S. Sakarkar, S. Prabha, S. Ramaiah, and G. Srawan, Microencapsulation Techniques, Factors Influencing Encapsulation Efficiency, *Journal of Microencapsulation*, 27(3), 187–197, (2010).

378. A. Jamekhorshid, S. M. Sadrameli, and M. Farid, A Review of Microencapsulation Methods of Phase Change Materials (PCMs) as a Thermal Energy Storage (TES) Medium, *Renewable and Sustainable Energy Reviews*, 31(1), 531–542, (2014).

379. C. Perignon, G. Ongmayeb, R. Neufeld, Y. Frere, and D. Poncelet, Microencapsulation by Interfacial Polymerisation: Membrane Formation and Structure, *Journal of Microencapsulation*, 32(1), 1–15, (2015).

380. D. Saihi, I. Vroman, S. Giraud, and S. Bourbigot, Microencapsulation of Ammonium Phosphate with a Polyurethane Shell. Part II. Interfacial Polymerisation Technique, *Reactive and Functional Polymers*, 66(10), 1118–1125, (2006).

381. M. K. Mishra, Handbook of Encapsulation and Controlled Release, 1st ed. Florida: CRC Press, 2015.

382. S. K. Ghosh, Functional Coatings: By Polymer Microencapsulation, 1st ed. Weinheim: John Wiley and Sons, 2006.

383. P. Girotra, S. Singh, and K. Nagpal, Supercritical Fluid Technology: A Promising Approach in Pharmaceutical Research, *Pharmaceutical Development and Technology*, 18(1), 22–38, (2013).

384. L. Maharaj, M. Gupta, and A. Gada, Microsphere: A Novel Tool for Controlled Drug Delivery, *World Journal of Pharmacy and Pharmaceutical Sciences*, 4(9), 126–141, (2015).

385. M. J. Cocero, Á. Martín, F. Mattea, and S. Varona, Encapsulation and Co-precipitation Processes with Supercritical Fluids: Fundamentals and Applications, *Journal of Supercritical Fluids*, 47(1), 546–555, (2009).

386. J. Sris and S. Prabha, Microencapsulation: A Review, *International Journal of Pharmacy and Biological Sciences*, 3(1), 509–531, (2012).

387. R. Rai and J. Bai, Beneficial Microbes in Fermented and Functional Foods. Florida: CRC Press, 2015.

388. S. Singh, N. Shanthi, and A. Mahato, Formulation and Evaluation of Metronidazole Tabletted Microspheres for Colon Drug Delivery, *Asian Journal of Pharmaceutical and Clinical Research*, 9(3), 398–403, (2016).

389. S. Ramukutty and E. Ramachandran, Crystal Growth by Solvent Evaporation and Characterisation of Metronidazole, *Journal of Crystal Growth*, 351(1), 47–50, (2012).

390. G. Tiwari, Release Studies of Metronidazole and Doxycycline From Polycaprolactone Films Prepared By Solvent Evaporation, *International Journal of ChemTech Research*, 2(3), 974–4290.

391. A. Vaidya, A. Jain, P. Khare, R. K. Agrawal, and S. K. Jain, Metronidazole Loaded Pectin Microspheres for Colon Targeting, *Journal of Pharmaceutical Sciences*, 98(11), 4229–4236, (2009).

392. J. Ravi, K. Reddy, K. Gnanaprakash, A. V Badarinath, C. Madhu, and S. Chetty, Formulation and Evaluation of Microparticles of Metronidazole, *Journal of Pharmaceutical Sciences and Research*, 1(10), 131–136, (2009).

393. M. Li, O. Rouaud, and D. Poncelet, Microencapsulation by Solvent Evaporation: State of the art for Process Engineering Approaches, *International Journal of Pharmaceutics*, 363(1), 26–39, (2008).

394. F. Ito, H. Fujimori, and K. Makino, Factors Affecting the Loading Efficiency of Water-soluble Drugs in PLGA Microspheres, *Colloids and Surfaces B: Biointerfaces*, 61(1), 25–29, (2008).

395. S. Tiwari and P. Verma, Microencapsulation Technique by Solvent Evaporation Method (Study of Effect of Process Variables), *International Journal of Pharmacy and Life Sciences*, 2(8), 998–1005, (2011).

396. N. T. Hwisa, P. Katakam, B. R. Chandu, and S. K. Adiki, Solvent Evaporation Techniques as Promising Advancement in Microencapsulation, *Vedic Research International Biological Medicinal Chemistry*, 1(1), 8–22, (2013).

397. P. B. O'Donnell and J. W. McGinity, Preparation of Microspheres by the Solvent Evaporation Technique, *Advanced Drug Delivery Reviews*, 28(1), 25–42, (1997).

398. T. Farheen, S. Hasnain, and A. Nayak, Microencapsulation of Pharmaceuticals by Solvent Evaporation Technique: A Review, *Elixir Pharmacy*, 47(1), 8821–8827, (2012).

399. N. V Satheesh Madhav and S. Kala, Review on Microparticulate Drug Delivery System, *International Journal of PharmTech Research*, 3(3), 1242–1254, (2011).

400. R. Maji, S. Ray, B. Das, and A. K. Nayak, Ethyl Cellulose Microparticles Containing Metformin HCl by Emulsification-solvent Evaporation Technique: Effect of Formulation Variables, *International Scholarly Research Notices Polymer Science*, 1(1), 1–7, (2012).

401. G. Spenlehauer, M. Veillard, and J. P. Benoît, Formation and Characterisation of Cisplatin Loaded Poly(d,l-Lactide) Microspheres for Chemoembolisation, *Journal of Pharmaceutical Sciences*, 75(8), 750–755, (1986).

402. Y. Miyazaki, Y. Onuki, S. Yakou, and K. Takayama, Effect of Temperature-increase Rate on Drug Release Characteristics of Dextran Microspheres Prepared by Emulsion Solvent Evaporation Process, *International Journal of Pharmaceutics*, 324(2), 144–151, (2006).

403. A. Lajoinie, E. Henin, B. Kassai, and D. Terry, Solid Oral Dosage Forms Availability in children: A Cost Saving Investigation, *British Journal of Clinical Pharmacology*, 78(5), 1080–9, (2014).

404. F. Liu, S.Ranmal, H. Batchelor, M. Orlu-Gul, E. Terry *et al.*, Patient-centred Pharmaceutical Design to Improve Acceptability of Medicines: Similarities and Differences in Paediatric and Geriatric Populations, *Drugs*, 74(16), 1871–89, (2014).

405. L. E. Wroblewski, R. M. Peek, K. T. Wilson, and K. T. Wilson, Helicobacter pylori and Gastric Cancer: Factors that Modulate Disease Risk, *Clinical Microbiology Reviews*, 23(4), 713–39, (2010).

406. A. O. Adebisi and B. R. Conway, Preparation and Characterisation of Gastroretentive Alginate Beads for Targeting Helicobacter pylori, *Journal of Microencapsulation*, 31(1), 58–67, (2014).

407. A. O. Adebisi and B. R. Conway, Modification of Drug Delivery to Improve Antibiotic Targeting to the Stomach, *Therapeutic Delivery*, 6(6), 741–762, (2015).

408. H. Strid, M. Simrén, P. Stotzer, H. Abrahamsson, and E. S. Björnsson, Delay in Gastric Emptying in Patients with Chronic Renal Failure, *Scandinavian Journal of Gastroenterology*, 39(6), 516–520, (2004).

409. M. Horowitz, J. M. Wishart, K. L. Jones, and G. S. Hebbard, Gastric Emptying in Diabetes: An Overview, *Diabetic medicine*, 13(9), 16–22, (1996).

410. S. Sarojini and R. Manavalan, An Overview on Various Approaches to Gastroretentive Dosage Forms, *International Journal of Drug Development and Research*, 4(1), 1–13, (2012).

411. A. Streubel, J. Siepmann, and R. Bodmeier, Gastroretentive Drug Delivery Systems, *Expert Opinion on Drug Delivery*, 3(2), 217–233, (2006).

412. P. Veerareddy, S. Sanka, R. Jukanti, S. Bandari, R. Ajemru, and A. Potu, Formulation

and Evaluation of Gastroretentive Dosage Form of Ofloxacin, *Stanford Journal of Pharmaceutical Sciences*, 4(1), 9–18, (2011).

413. R. Garg and G. Gupta, Progress in Controlled Gastroretentive Delivery Systems, *Tropical Journal of Pharmaceutical Research*, 7(3), 1055–1066, (2008).

414. E. A. Klausner, E. Lavy, M. Friedman, and A. Hoffman, Expandable Gastroretentive Dosage Forms, *Journal of Controlled Release*, 90(1), 143–162, (2003).

415. A. Hafeez, A. Maurya, J. Singh, A. Mittal, and L. Rana, An Overview on Floating Microsphere: Gastro Retention Floating Drug Delivery System (FDDS), *The Journal of Phytopharmacology*, 2(23), 1–12, (2013).

416. S. U. Zate, P. I. Kothawade, G. H. Mahale, K. P. Kapse, and S. P. Anantwar, Gastroretentive Bioadhesive Drug Delivery System: A Review, *International Journal of PharmTech Research*, 2(2), 1227–1235, (2010).

417. P. L. Bardonnet, V. Faivre, W. J. Pugh, J. C. Piffaretti, and F. Falson, Gastroretentive Dosage Forms: Overview and Special Case of Helicobacter pylori, *Journal of Controlled Release*, 111(1), 1–18, (2006).

418. U. K. Mandal, B. Chatterjee, and F. G. Senjoti, Gastroretentive Drug Delivery Systems and their In vivo Success: A Recent Update, *Asian Journal of Pharmaceutical Sciences*, 11(5), 575–584, (2016).

419. S. Dey, S. Dutta, and B. Mazumder, Formulation and Evaluation of Floating Matrix Tablet of Atenolol for Gastro-retentive Drug Delivery, *International Journal of Pharmacy and Pharmaceutical Sciences*, 3(3), 433–437, (2012).

420. H. P. Singh, A. Kaur, and I. Kaur, Formulation and Evaluation of Effervescent Floating Tablet of Famotidine with Natural Polymer Chitosan, *Asian Pacific Journal of Health Sciences*, 1(4), 517–523, (2014).

421. V. Bhardwaj and N. Harikumar, Floating Drug Delivery System: A Review, *Pharmacophore*, 4(1), 26–38, (2013).

422. K. Reddy, K. Kavitha, R. Kumar, J. Singh, S. Srinivasan, and M. Jyothi, A Review on Floating Drug Delivery Systems, *World Journal of Pharmacy and Pharmaceutical Sciences*, 3(7), 508–522, (2014).

423. S. Arora, J. Ali, A. Ahuja, R. K. Khar, and S. Baboota, Floating drug delivery systems: A review, *International Journal for Pharmaceutical Research Scholars*, 2(1), 61–70, (2013).

424. Hydrophilic Polyemrs in Gastric Floating Drug Delivery Systems, *Indo American Journal of Pharmaceutical Research*, 4(4), 2259–2267, (2014).

425. J. K. Amit, R. Rammulrajsinh, D. Sonali, P. Kinal, A. Pradeep, and M. Gandhi, Hydrodynamically Balanced Systems (HBS): Innovative Approach of Gastroretention: A Review, *International Journal of PharmTech Research*, 3(3), 1495–1508, (2011).

426. P. Rajak, A. Bhattacharya, N. Sharma, M. S. Kataki, and A. Rajkumari, Gastroretentive Floating Drug Delivery System: An Approach in Gastroretentive Drug Delivery, *International Journal for Pharmaceutical Sciences*, 3(4), 9–16, (2011).

427. M. R. Kumar, A Comprehensive Review on Gastroretentive Drug Delivery System, *Acta Chimica Pharmaceutica Indica*, 3(2), 149–164, (2013).

428. S. Kumar and N. Yagnesh, An Update on Gastroretentive Floating Systems, *World Journal of Pharmacy and Pharmaceutical Sciences*, 5(11), 476–525, (2016).

429. K. Venkateswara Rao and V. Venkatachalam, Recent Advances in Gastroretentive Drug Delivery Systems, *International Journal of Pharmaceutical Sciences and Nanotechnology*, 9(3), 3221–3225, (2016).

430. S. Punitha, G. Sabitha, V. Kalal, and S. Rajasekar, Floating Drug Delivery System-Chronotherapeutic Approach, *International Journal for Pharmacy*, 2(4), 38–45, (2011).

431. R. A. H. Ishak, G. A. S. Awad, N. D. Mortada, and S. A. K. Nour, Preparation, In vitro and In vivo Evaluation of Stomach-specific Metronidazole-loaded Alginate Beads as Local Anti-Helicobacter pylori Therapy, *Journal of Controlled Release*, 119(2), 207–214, (2007).

432. P. Sriamornsak, N. Thirawong, and S. Puttipipatkhachorn, Emulsion Gel Beads of Calcium Pectinate Capable of Floating on the Gastric Fluid: Effect of some Additives, Hardening Agent or Coating on Release Behavior of Metronidazole, *European Journal of Pharmaceutical Sciences*, 24(4), 363–373, (2005).

433. L. Yang, J. Eshraghi, and R. Fassihi, A New Intragastric Delivery System for the Treatment of Helicobacter pylori Associated Gastric Ulcer: In vitro Evaluation, *Journal of Controlled Release*, 57(3), 215–22, (1999).

434. P. S. Rajinikanth, J. Balasubramaniam, and B. Mishra, Development and Evaluation of a Novel Floating In situ Gelling System of Amoxicillin for Eradication of Helicobacter pylori, *International Journal of Pharmaceutics*, 335(1–2), 114–122, (2007).

435. L. Bhardwaj, P. Kumar Sharma, and R. Malviya, A Short Review on Gastroretentive Formulations for Stomach Specific Drug Delivery: Special Emphasis on Floating In situ Gel Systems, *African Journal of Basic and Applied Sciences*, 3(6), 300–312, (2011).

436. A. De, S. Chakraborty, A. Mukherjee, J. Chattopadhyay, and B. C. Roy, Techniques of Gastroretentive Floating Drug Delivery Advancement: A Review, *Rajiv Ghandi University of Health Sciences Journal of pharmaceutical sciences*, 4(3), 93–102, (2014).

437. A. Lohani and G. Chaudhary, Mucoadhesive Microspheres: A Novel Approach to Increase Gastroretention, *Chronicles of Young Scientists*, 3(2), 121–128, (2012).

438. A. Alexander, S. Sharma, and M. J. Khan, Theories and Factors Affecting Mucoadhesive Drug Delivery Systems, *International Journal of Research in Ayurveda and Pharmacy*, 2(24), 1155–1161, (2011).

439. V. N. Gupta and H. G. Shivakumar, Preparation and Characterisation of Superporous Hydrogels as Gastroretentive Drug Delivery System for Rosiglitazone Maleate, *Daru: Journal of Pharmaceutical Sciences*, 18(3), 200–210, (2010).

440. M. Nagpal, S. K. Singh, and D. Mishra, Superporous Hydrogels as Gastroretentive Devices, *Acta Pharmaceutica Scienca*, 53(1), 7–24, (2011).

441. R. Gröning, M. Berntgen, and M. Georgarakis, Acyclovir Serum Concentrations Following Peroral Administration of Magnetic Depot Tablets and the Influence of Extracorporal Magnets to Control Gastrointestinal Transit, *European Journal of Pharmaceutics and Biopharmaceutics*, 46(3), 285–291, (1998).

442. H. Chhetri and P. Thapa, An Overview of Gastroretentive Drug Delivery System,

Journal of Science, Engineering and Technology, 10(1), 90–103, (2014).

443. M. M. Yousfi, H. M. El-Zimaity, M. T. Al-Assi, R. A. Cole, R. M. Genta, and D. Y. Graham, Metronidazole, Omeprazole and Clarithromycin: An Effective Combination Therapy for Helicobacter pylori Infection, *Alimentary Pharmacology and Therapeutics*, 9(2), 209–12, (1995).

444. L. Meurer and D. Bower, Management of Helicobacter pylori Infection, *American Family Physician*, 65(7), 1327–1337, (2002).

445. P. Singh, V. Kumar, P. Verma, A. Singh, and V. Yadav, Multiunit Floating Drug Delivery System a Significant Tool for the Treatment of Peptic Ulcer Disease, *International Journal of Pharmaceutical Sciences and Research*, 4(4), 1351–1362, (2015).

446. P. Sharma, S. Garg, and M. Mann, Recent Advancement in Floating Drug Delivery System and Current Approaches, *World Journal of Pharmacy and Pharmaceutical Sciences*, 4(3), 317–314, (2014).

447. K. Rajkumar, S. Sai, G. Sainath, and E. Reddy, Floating Microspheres: A Novel Approach in Drug Delivery, *Journal of Drug Delivery Research*, 1(4), 1–20, (2012).

448. R. Kumar and S. Sahoo, Formulation and Evaluation of Floating Microspheres by Using Eudragit RSPO, *Journal of Medical and Pharmaceutical Innovation*, 2(12), 7–12, (2015).

449. M. Yelugam, D. Koteshwara, and S. Reddy, Gastro-retentive Floating Microspheres of Carvedilol: Formulation, Characterisation and In-vitro Evaluation, *International Journal of Pharmacy and Pharmaceutical Sciences*, 5(3), 686–690, (2013).

450. S. Monteiro, S. Kamath, S. Nayak, S. Prabhu, and A. Shabaraya, Development and In-vitro Evaluation of Floating Microspheres of Clarithromycin Using Rate Controlling Polymer, *International Journal of Pharmaceutical Research and Bio-Science*, 3(3), 282–297, (2014).

451. S. Mishra and S. Khatri, Formulation and Evaluation of Sustained Release Gastro-retentive Drug Delivery System of Acyclovir Leading to Enhanced Bioavailability, *British Journal of Pharmaceutical Research*, 7(6), 428–439, (2015).

452. A. Matharu, M. Motto, M. Patel, A. Simonelli, and R. Dave, Evaluation of Hydroxypropyl methylcellulose Matrix Systems as Swellable Gastro-retentive Drug Delivery Systems, *Journal of Pharmaceutical Sciences*, 100(151–163), (2011).

453. H. SL and A. Sharma, Development and Evaluation of Bromhexine Hydrochloride Floating Microparticulates, *Asian Journal of Pharmaceutics*, 6(1), 38–43, (2014).

454. K. Punitha, S. Khadhir, and V. Nagar, Intragastric Floating Drug Delivery System of Ranitidine Hydrochloride: Formulation and Evaluation, *International Journal of Pharmacy and Pharmaceutical Sciences*, 2(4), 106–108, (2010).

455. S. Patil, J. Venkatesh, C. Nagesh, and J. Rabadia, Intragastric Floating Drug Delivery System of Levofloxacin: Formulation and Evaluation, *Journal of Pharmaceutical Sciences and Research*, 3(6), 1265–1268, (2011).

456. K. Karthikeyan, Effect of Different Viscosity Grades of HPMC on Drug Release Profile, *Journal of Pharmacy Research*, 1(1), 23–28, (2008).

457. S. M. Khamanga and R. B. Walker, The Use of Response Surface Methodology in the Evaluation of Captopril Microparticles Manufactured Using an Oil in Oil Solvent Evaporation Technique, *Journal of Microencapsulation*, 29(1), 39–53, (2012).

458. M. Sharma, S. Kohli, and A. Dinda, In-vitro and In-vivo Evaluation of Repaglinide Loaded Floating Microspheres Prepared from Different Viscosity Grades of HPMC Polymer, *Saudi Pharmaceutical Journal*, 23(6), 675–682, (2015).

459. S. M. M. Khamanga and R. B. Walker, In vitro Dissolution Kinetics of Captopril from Microspheres Manufactured by Solvent Evaporation, *Dissolution Technologies*, 19(1), 42–51, (2012).

460. M. Abdel-Mottaleb and A. Lamrecht, Standardised In vitro Drug Release Test for Colloidal Drug Carriers Using Modified USP Dissolution Apparatus I, *Drug Development and Industrial Pharmacy*, 37(2), 178–184, (2011).

461. A. Semalty and A. Semwal, Gastroretentive Floating Microspheres of Nateglinide: Formulation, Evaluation and Effect of Drug-polymer Ratio, *Indian Drugs*, 51(6), 37–43, (2014).

462. S. Prajapati, L. Patel, and C. Patel, Polymers for Floating Drug Delivery System, *Polymers in floating drug delivery system*, 2(1), 1–7, (2011).

463. M. Sharma and S. Kholi, Floating Drug Delivery of Antidiabetic Drugs: An Overview, *International Journal of Pharmacy and Biological Sciences*, 3(4), 456–471, (2012).

464. J. Vysloužil, M. Kejdušová, K. Dvořáčkov, and D. Vetchý, Influence of Formulation and Process Parameters on the Characteristics of PLGA-based Microparticles with Controlled Drug Release, *Ceska a Slovenska farmacie*, 62(3), 120–126, (2013).

465. N. Sharma, P. Madan, and S. Lin, Effect of Process and Formulation Variables on the Preparation of Parenteral Paclitaxel-loaded Biodegradable Polymeric Nanoparticles: A Co-surfactant Study, *Asian Journal of Pharmaceutical Sciences*, 11(3), 404–416, (2016).

466. J. Sameni, K. Krigstin, and M. Sain, Effect of Preparation Parameters on the Formation of Lignin Acetate Microspheres, *International Journal of Engineering and Innovative Technology*, 4(8), 2277–3754, (2015).

467. P. B. O'Donnell and J. W. McGinity, Preparation of Microspheres by the Solvent Evaporation Technique, *Advanced Drug Delivery Reviews*, 28(1), 25–42, (1997).

468. P. Watts, M. Davies, and C. Melia, Microencapsulation Using Emulsification/Solvent Evaporation: An Overview of Techniques and Applications, *Critical Reviews in Therapeutic Drug Carrier Systems*, 7(3), 235–250, (1990).

469. S. Freitas, H. Merkle, and B. Gander, Microencapsulation by Solvent Extraction/Evaporation: Reviewing the State of The Art of Microsphere Preparation Process Technology, *Journal of Controlled Release*, 102(2), 313–332, (2004).

470. H. Zhao, J. Gagnon, and U. O. Häfeli, Process and Formulation Variables in the Preparation of Injectable and Biodegradable Magnetic Microspheres, *Biomagnetic Research and Technology*, 5(2), 1–11, (2007).

471. T. Ishikawa, Y. Watanabe, K. Takayama, H. Endo, and M. Matsumoto, Effect of Hydroxypropylmethylcellulose (HPMC) on the Release Profiles and Bioavailability of a Poorly Water-soluble Drug from Tablets Prepared Using Macrogol and HPMC, *International Journal of Pharmaceutics*, 202(1–2), 173–178, (2000).

472. F. A. A. Mohamed, M. Roberts, L. Seton, J. L. Ford, M. Levina, and A. R. Rajabi-Siahboomi, The Influence of HPMC Concentration on Release of Theophylline or Hydrocortisone from Extended Release Mini-tablets, *Drug Development and Industrial Pharmacy*, 39(8), 1167–1174, (2013).

473. M. M. Rahman, S. Roy, S. Das, M. Jha, T.Begum *et al.*, Evaluation of Various Grades of Hydroxypropylmethylcellulose Matrix Systems as Oral Sustained Release Drug Delivery Systems, *Journal of Pharmaceutical Sciences and Research*, 3(1), 930–938, (2011).

474. P. S. Hiremath and R. N. Saha, Controlled Release Hydrophilic Matrix Tablet Formulations of Isoniazid: Design and In vitro Studies, *American Association of Pharmaceutical Scientists PharmSciTech*, 9(4), 1171–1178, (2008).

475. X. Lin, J. Wang, Y. Xu, X. Tang *et al.*, Tracking the Effect of Microspheres Size on the Drug Release from a Microsphere/Sucrose Acetate Isobutyrate Hybrid Depot In vitro and In vivo, *Drug Development and Industrial Pharmacy*, 42(9), 1455–1465, (2016).

476. L. Hu, L. Li, X. Yang, W. Liu, and J. Yang, Floating Matrix Dosage Form for Dextromethorphan Hydrobromide Based on Gas Forming Technique: In vitro and In vivo Evaluation in Healthy Volunteers, *European Journal of Pharmaceutical Sciences*, 42(1–2), 99–105, (2011).

477. R. Patel and R. Kamani, Formulation Optimisation and Evaluation of Mometasone Furoate Cream, *Journal of Pharmacy Research*, 2(10), 1565–1569, (2009).

478. M. Kim, J. Jeong, Y. Yeon, S. Lee *et al.*, Development and Optimisation of a Novel Oral Controlled Delivery System for Tamsulosin Hydrochloride Using Response Surface Methodology, *International Journal of Pharmaceutics*, 341(1–2), 97–104, (2007).

479. S. Nazzal, M. Nutan, A. Palamakula, R. Shah, A. . Zaghloul, and M. . Khan, Optimisation of a Self-Nanoemulsified Tablet Dosage Form of Ubiquinone Using Response Surface Methodology: Effect of Formulation Ingredients, *International Journal of Pharmaceutics*, 240(1), 103–114, (2002).

480. U. Mandal, V. Gowda, A. Ghosh, S. Selvan, S. Solomon, and T. K. Pal, Formulation and Optimisation of SusUained Release Matrix Tablet of Metformin HCl 500 mg Ssing Response Surface Methodology, *Journal of the Pharmaceutical Society of Japan*, 127(8), 1281–90, (2007).

481. S. Ferreira, R. Bruns, C. Quintella *et al.*, Statistical Designs and Response Surface Techniques for the Optimisation of Chromatographic Systems, *Journal of Chromatography A*, 1158(1), 2–14, (2007).

482. G. Hanrahan and K. Lu, Application of Factorial and Response Surface Methodology in Modern Experimental Design and Optimisation, *Critical Reviews in Analytical Chemistry*, 36(3–4), 141–151, (2006).

483. J. Felhofer, G. Hanrahan, and C. D. García, Univariate and Multivariate Optimisation of the Separation Conditions for the Analysis of Five Bisphenols by Micellar Electrokinetic Chromatography, *Talanta*, 77(3), 1172–1178, (2009).

484. S. N. H. Shah, S. Asghar, M. A. Choudhry, M. S. H. Akash, N. ur Rehman, and S. Baksh, Formulation and Evaluation of Natural Gum-based Sustained Release Matrix Tablets of Flurbiprofen Using Response Surface Methodology, *Drug Development and Industrial Pharmacy*, 35(12), 1470–1478, (2009).

485. S. Dash, P. N. Murthy, L. Nath, and P. Chowdhury, Kinetic Modeling on Drug Release from Controlled Drug Delivery Systems, *Acta poloniae pharmaceutica*, 67(3), 217–23, (2010).

486. N. Ahuja, O. P. Katare, and B. Singh, Studies on Dissolution Enhancement and Mathematical Modeling of Drug Release of a Poorly Water-soluble Drug Using Water-soluble Carriers, *European Journal of Pharmaceutics and Biopharmaceutics*, 65(1), 26–38, (2007).

487. P. Costa and J. M. Sousa Lobo, Modeling and Comparison of Dissolution Profile, *European Journal of Pharmaceutical Sciences*, 13(2), 123–133, (2001).

488. J. Siepmann and A. Göpferich, Mathematical Modeling of Bioerodible, Polymeric Drug Delivery Systems, *Advanced Drug Delivery Reviews*, 48(2), 229–247, (2001).

489. C.-C. Lin and A. T. Metters, Hydrogels in Controlled Release Formulations: Network Design and Mathematical Modeling, *Advanced Drug Delivery Reviews*, 58(12), 1379–1408, (2006).

490. A. Palmieri, Dissolution Theory, Methodology, and Testing, 1st ed. Delaware: Dissolution Technologies, Incorporated, 2007.

491. H. K. Shaikh, Mathematical Models for Drug Release Characterisation: A Review, *World Journal of Pharmacy and Pharmaceutical Sciences*, 4(4), 324–338, (2015).

492. G. Singhvi and M. Singh, Review: In-vitro Drug Release Characterisation Models, *International Journal of Pharmaceutical Studies and Research*, 2(1), 77–84, (2011).

493. M. A. Kalam, M. Humanuni, S. Yadav *et al.*, Release Kinetics of Modified Pharmaceutical Dosage Forms: A Review, *Continental Journal of Pharmaceutical Sciences*, 1(1), 30–35, (2007).

494. C. A. Salome, O. C. Godswill, and O. I. Ikechukwu, Kinetics and Mechanisms of Drug Release from Swellable and Non Swellable Matrices: A Review, *Research Journal of Pharmaceutical, Biological and Chemical Sciences*, 4(2), 975–8585, (2013).

495. S. Ramakrishna, V. Mihira, K. Raja Vyshnavi, and V. Ranjith, Design and Evaluation of Drug Release Kinetics of Meloxicam Sustained Release Matrix Tablets, *International Journal of Current Pharmaceutical Reasearch*, 4(1), 90–99, (2012).

496. J. Siepmann and N. A. Peppas, Modeling of Drug Release from Delivery Systems Based on Hydroxypropyl methylcellulose (HPMC), *Advanced Drug Delivery Reviews*, 48(1), 139–157, (2001).

497. A. Tiwari and L. Uzun, Advanced Molecularly Imprinting Materials, 1st ed. New York: John Wiley and Sons, 2016.

498. M. Fanun, Colloids in Drug Delivery, 1st ed. Florida: CRC Press, 2010.

499. J. Siepmann and N. A. Peppas, Higuchi Equation: Derivation, Applications, Use and Misuse, *International Journal of Pharmaceutics*, 418(1), 6–12, (2011).

500. J. Wang, D. Flanagan, A. Noyes, W. Nerst *et al.*, General Solution for Diffusion-Controlled Dissolution of Spherical Particles, *Journal of pharmaceutical sciences*, 88(7), 731–8, (1999).

501. M. Jafari and B. Kaffashi, Mathematical Kinetic Modeling on Isoniazid Release from Dex-HEMA-PNIPAAm Nanogels, *Nanomedicine Research Journal*, 102(12), 90–9690, (2016).

502. O. Bagade, S. Dhole, N. Nemlekar, R. Pujari, and A. Shete, Assessment on Dissolution Testing and Contrasting Models for Drugs, *World Journal of Pharmacy and Pharmaceutical Sciences*, 3(9), 865–895, (2014).

503. M. A. Malana and R. Zohra, The Release Behavior and Kinetic Evaluation of Tramadol HCl from Chemically Cross Linked Ter Polymeric Hydrogels, *DARU Journal of Pharmaceutical Sciences*, 21(10), 1–10, (2013).

504. P. L. Ritger and N. A. Peppas, A Simple Equation for Description of Solute Release II. Fickian and Anomalous Release from Swellable Devices, *Journal of Controlled Release*, 5(1), 37–42, (1987).

505. D. Sinha Roy and B. D. Rohera, Comparative Evaluation of Rate of Hydration and Matrix Erosion of HEC and HPC and Study of Drug Release from their Matrices, *European Journal of Pharmaceutical Sciences*, 16(3), 193–199, (2002).

506. A. Budhian, S. J. Siegel, and K. I. Winey, Controlling the In Vitro Release Profiles for a System of Haloperidol-Loaded PLGA, *International Journal of Pharmaceutics*, 346(12), 151–159, (2008).

507. N. Chomcharn and M. Xanthos, Properties of Asprin Modified Enteric Polymer Prepared by Hot-melt Mixing, *International Journal of Pharmaceutics*, 450(1), 259–267, (2013).

508. W. Donald, Handbook of Pharmaceutical Controlled Release Technology, 1st ed. New York: Marcel Dekker, 2000.

509. H. N. A. Ram, P. Lachake, U. Kaushik, and C. S. Shreedhara, Formulation and Evaluation of Floating Tablets of Liquorice Extract., *Pharmacognosy research*, 2(5), 304–318, (2010).

510. A.-M. Oprea, M.-T. Nistor, L. Profire, M. I. Popa, C. E. Lupusoru, and C. Vasile, Evaluation of the Controlled Release Cability of Theophylline from Xanthan/Chondroitin Sulfate Hydrogels, *Journal of Biomaterials and Nanobiotechnology*, 4(2), 123–131, (2013).

511. V. A. de Mello and E. Ricci-Júnior, Encapsulation of Naproxen in Nanostructured System: Structural Characterisation and In vitro Release Studies, *Química Nova*, 34(6), 933–939, (2011).

512. G. Fu and W. . Soboyejo, Swelling and Diffusion Characteristics of Modified Poly(N-isopropylacrylamide) Hydrogels, *Materials Science and Engineering C*, 8(13), 8–13, (2010).

513. Y. Zhang, M. Huo, J. Zhou, W. Li *et al.*, DDSolver: An Add-in program for Modeling and Comparison of Drug Dissolution Profiles., *American Association of Pharmaceutical Scientists*, 12(3), 263–71, (2010).

514. J. Osborne, Improving Your Data Transformations: Applying the Box-Cox Transformation, *Practical Assessment Research and Evaluation*, 15(12), 1–9, (2010).

515. X. Huang and C. S. Brazel, On the Importance and Mechanisms of Burst Release in Matrix-controlled Drug Delivery Systems, *Journal of Controlled Release*, 73(2), 121–136, (2001).

516. S. B. Tiwari, T. K. Murthy, M. Raveendra Pai, P. R. Mehta, and P. B. Chowdary, Controlled Release Formulation of Tramadol Hydrochloride Using Hydrophilic and Hydrophobic Matrix System, *American Association of Pharmaceutical Scientists*, 4(3), 18–23, (2003).

517. S. Agarwal and R. S. R. Murthy, Effect of Different Polymer Concentration on Drug Release Rate and Physicochemical Properties of Mucoadhesive Gastroretentive Tablets, *Indian Journal of Pharmaceutical Sciences*, 77(6), 705–14, (2015).

518. J. Nerurkar, H. W. Jun, J. C. Price, and M. O. Park, Controlled-release Matrix Tablets of Ibuprofen Using Cellulose Ethers and Carrageenans: Effect of Formulation Factors on Dissolution Rates, *European Journal of Pharmaceutics and Biopharmaceutics*, 61(1–2), 56–68, (2005).

519. K. C. Sung *et al.*, Effect of Formulation Variables on Drug and Polymer Release from HPMC-based Matrix Tablets, *International Journal of Pharmaceutics*, 142(1), 53–60, (1996).

520. M. M. Talukdar, A. Michoel, P. Rombaut, and R. Kinget, Comparative Study on Xanthan Gum and Hydroxypropylmethyl cellulose as Matrices for Controlled-release Drug Delivery I. Compaction and In Vitro Drug Release Behaviour, *International Journal of Pharmaceutics*, 129(1), 233–241, (1996).

521. B. Sanjay, S. Dinesh, and N. Sakhuja, Stability Testing of Pharmaceutical Products, *Journal of Applied Pharmaceutical Science*, 2(3), 129–138, (2012).

522. B. Kommanaboyi and C. . Rhodes, Trends in Stability Testing, with Emphasis on Stability During Distribution and Storage, *Drug Development and Industrial Pharmacy*, 25(7), 1–10, (1999).

523. C. F. Poole, Gas Chromatography, 1st ed. U.S.A: Elsevier, 2012.

524. H. M. McNair and J. M. Miller, Basic Gas Chromatography, 2nd ed. New York: John Wiley and Sons, 2009.

525. G. Guiochon and C. Guillemin, Quantitative Gas Chromatography for Laboratory Analyses and On-line Process, 1st ed. New York: Elsevier, 1988.

526. K. D. Bartle and P. Myers, History of Gas Chromatography, *TrAC Trends in Analytical Chemistry*, 21(9–10), 547–557, (2002).

527. R. Scott, Introduction to Analytical Gas Chromatography, 2nd ed. New York: Marcel Dekker, 1998.

528. C. F. Poole, The essence of chromatography, 1st ed. Amsterdam: Elsevier, 2003.

529. K. Robards, P. . Jackson, and P. Haddad, Principles and Practice of Modern Chromatographic Methods, 1st ed. Amsterdam: Elsevier, 2004.

530. J. Peinado, F. Lopez-Soriano, and J. Argiles, Gas Chromatographic Method for the Estimation of Acetone and its Metabolites in Biological Samples, *Journal of Chromatography*, 415(1), 372–376, (1987).

531. D. Palma de Oliveira and M. Bastos de Siqueira, A Simple and Rapid Method for Urinary Acetone Analysis by Headspace/ Gas Chromatography, *Quim Nova*, 30(5), 1362–1364, (2007).

532. H. Pontes *et al.*, GC Determination of Acetone, Acetaldehyde, Ethanol, and Methanol in Biological Matrices and Cell Culture, *Journal of Chromatographic Science*, 47(1), 272–278, (2009).

533. E. Quirk, A. Doggett, and A. Bretnall, Determination of Residual Acetone and Acetone Releated Impurities in Drug Product Intermediates Prepared as Spray Dried Dispersions (SDD) using Gas Chromatography with Headspace Autosampling (GCHS), *Journal of Pharmaceutical and Biomedical Analysis*, 96(1), 37–44, (2016).

534. G. Mishra, V. Saxena, S. Jawla, and V. Srivastava, Method Development and Validation for the Determination of Residual Solvents in Omeprazole API by Using Headspace Gas Chromatography, *Asian Journal of Pharmaceutical and Clinical Research*, 7(1), 54–56, (2014).

535. S. Pandey, P. Pandey, R. Kumar, and N. Singh, Residual Solvent Determination by Head Space Gas Chromatography with Flame Ionisation Detector in Omeprazole API, *Brazilian Journal of Pharmaceutical Sciences*, 47(2), 379–384, (2011).

536. J. Manwar, K. Mahadik, A. Paradkar, S. Patil, L. Sathiyanarayanan, and R. Manmode, Gas Chromatography Method for the Determination of Non-ethanol Volatile Compounds in Herbal Formulation, *International Journal of Analytical and Bioanalytical Chemistry*, 3(1), 12–17, (2013).

537. P. Lima Gomes, E. Andrea, and C. Mendes, Determination of Benzene, Toluene and N-hexane in Urine and Blood by Headspace Solid-Phase Microextraction/Gas Chromatography for the Biomonitering of Occupational Exposure, *Journal of Brazilian Chemistry Society*, 21(1), 119–126, (2010).

538. Q. Chan Li and K. Cohen, A Capillary Gas Chromatography Procedure for the Analysis of Nine common Residual Solvents in Water-insoluble Bulk Pharmaceuticals, *Journal of Chromatographic Science*, 36(1), 119–124, (1998).

539. C. Ramos, Development and Validation of a Headspace Gas Chromatographic Method for the Determination of Reisdual Solvents in Five Drug Substances, *International Journal of Pharmaceutical Science Invention*, 2(3), 36–41, (2013).

540. A. Gupta, Y. Singh, K. S. Srinivas, G. Jain, V. B. Sreekumar, and V. P. Semwal, Development and Validation of a Headspace Gas Chromatographic Method for the Determination of Residual Solvents in Arterolane (RBx11160) Maleate Bulk Drug, *Journal of Pharmacy and BioAllied Sciences*, 2(1), 32–37, (2010).

541. D.-W. K and W. Engewald, Practical Gas Chromatography: A Comprehensive Reference. Springer Science and Business Media, 2014.

542. K. Goh, W. Chan, S. Shiota, and Y. Yamaoka, Epidemiology of Helicobacter pylori Infection and Public Health Implications, *Helicobacter*, 16(1), 1–9, (2011).

543. S. Hong, J. Seo, K. Moon, Advanced Materials, Mechanical and Structural Engineering, 1st ed. New York: CRC Press, 2015.

APPENDIX I
BATCH PRODUCTION RECORD FOR MTZ-001

LABORATORY SCALE MANUFACTURE

Only one solvent evaporation record for batch MTZ-001 is included in this thesis. The batch production records for all other batches are provided electronically on a disk.

RHODES UNIVERSITY, FACULTY OF PHARMACY,
GRAHAMSTOWN, 6140 SOUTH AFRICA

BATCH PRODUCTION RECORD FOR MTZ-001

Product name		Metronidazole
Batch		MTZ-001
Batch Size		4.25g
Batch record issued by:	**Date:**	
Batch record issued by:	**Date:**	

EQUIPMENT VERIFICATION

Description	Type	Verified by	Confirmed by
Weighing balance	Mettler® Model AE 163 analytical balance (Mettler®, Zurich, Switzerland)		
Homogenizer	Four- blade "butterfly" propeller of 50mm diameter linked to a homogenizer (Virtis Company, New York, USA)		
Sieve	# 20 mesh size		

RHODES UNIVERSITY, FACULTY OF PHARMACY,
GRAHAMSTOWN, 6140 SOUTH AFRICA

BATCH PRODUCTION RECORD FOR MTZ-001

Product name	Metronidazole
Batch	MTZ-001
Batch Size	4.25g

MASTER FORMULA AND BATCH FORMULA

BATCH FORMULA				
Material	**Quantity %m/m or m/v**	**Amount Dispensed**	**Dispensed by**	**Checked by**
MTZ	23.53			
Eudragit® RS PO	23.53			
Methocel® K100M	47.06			
Avicel® PH102	5.882			
Span® 80	1.2ml			
Light liquid paraffin	120ml			
Acetone	20ml			

PROCESSING PARAMETERS	
Homogenisation time hours	**Homogenisation speed rpm**
5	500

RHODES UNIVERSITY, FACULTY OF PHARMACY,
GRAHAMSTOWN, 6140 SOUTH AFRICA

BATCH PRODUCTION RECORD FOR MTZ-001

Product name	Metronidazole
Batch	MTZ-001
Batch Size	4.25g

MANUFACTURING DIRECTIONS

Step	Procedure	Time	Done by	Checked by
1	Screen the following materials through a #20 mesh separately MTZ, polymers and Avicel® PH102			
2	Weigh the excipients and MTZ separately on the analytical balance			
3	Measure 20 ml of acetone in a measuring cylinder and transfer to a 100ml beaker			
4	Disperse the polymers and Avicel® PH102 in a beaker containing the acetone			
5	Add 1 gram of MTZ in this acetone solution containing the polymers			
6	Measure 120 ml of light liquid paraffin using a measuring cylinder and transfer to a separate 400ml beaker			
7	Add 1.2ml of Span® 80 to the light liquid paraffin			
8	Agitate the light liquid paraffin containing Span® 80 with a four- blade "butterfly" propeller of 50mm diameter linked to a homogenizer at 1000 rpm for 5 minutes			
9	Mix the acetone dispersion with the contents in a 400mL beaker and homogenise at 500 rpm			
10	After 2 hours add 10ml of n-hexane to harden the microcapsules and continue stirring for a further 3 hours			
11	Collect microcapsules in a Buchner funnel, wash 2 -3 times with n-hexane and dry in an oven at 25°C for 24 hours. Transfer microcapsules to airtight amber coloured container,			

APPENDIX II
BATCH SUMMARY RECORDS

FACULTY OF PHARMACY, GRAHAMSTOWN, SOUTH AFRICA
BATCH SUMMARY RECORD

Formulator	Anjana Makan	**Batch size**	4.25 g
Product	Metronidazole microcapsules	**Homogenisation time (hours)**	5
Batch ID	MTZ-001	**Homogenisation speed (rpm)**	500
Temperature	22.3°C	**Date of manufacture**	05/09/16

Formula		
Material	**Amount added**	**Rhodes batch number**
MTZ	1.00 g	RM000338
Eudragit® RS PO	1.00 g	RM000023
Methocel® K100M	2.00 g	RM000602
Avicel® PH102	0.25g	RM000038
Span® 80	1% v/v	-
Light liquid paraffin	120ml	-
Acetone	20ml	-

Dissolution profile

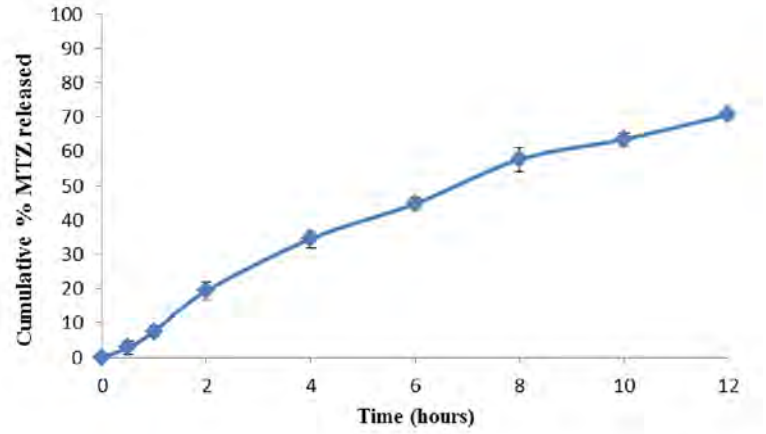

SEM

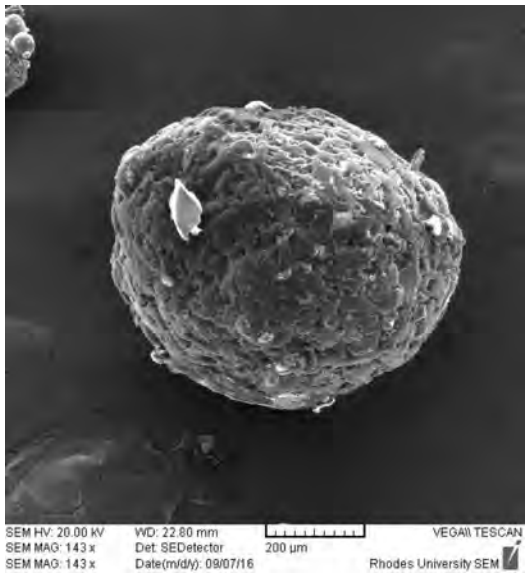

Encapsulation efficiency (%):78.63 ±3.38
Buoyancy (%): 61.47 ± 2.88
Yield (%): 95.12 ± 2.08
Particle size (µm): 653.33 ± 3.64
Shape and morphology: Spherical shaped microcapsule with rough surface

FACULTY OF PHARMACY, GRAHAMSTOWN, SOUTH AFRICA
BATCH SUMMARY RECORD

Formulator	Anjana Makan	**Batch size**	4.25 g
Product	Metronidazole microcapsules	**Homogenisation time (hours)**	5
Batch ID	MTZ-002	**Homogenisation speed (rpm)**	500
Temperature	22.7°C	**Date of manufacture**	06/09/16

Formula		
Material	**Amount added**	**Rhodes batch number**
MTZ	1.00g	RM000338
Eudragit® RS PO	1.00g	RM000023
Methocel® K100M	1.00g	RM000602
Avicel® PH102	1.25g	RM000038
Span® 80	1% v/v	-
Light liquid paraffin	120ml	-
Acetone	20ml	-

Dissolution profile

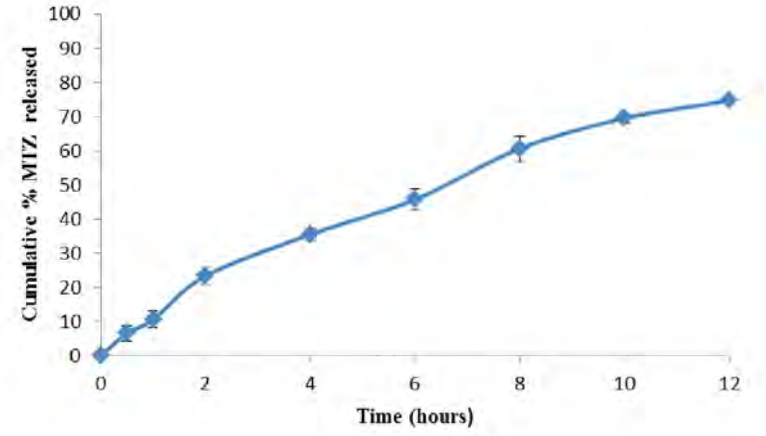

SEM

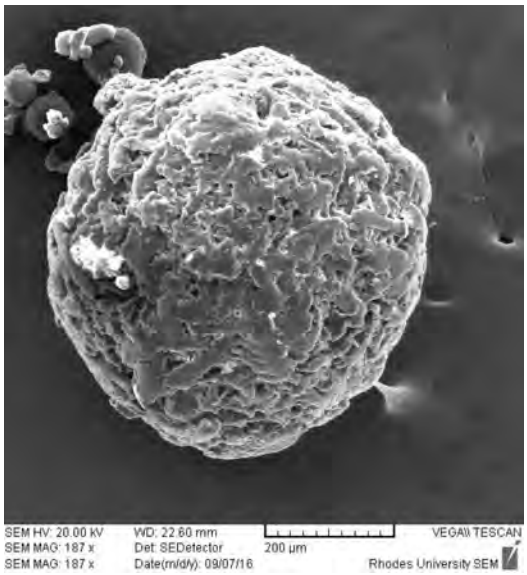

Encapsulation efficiency (%):72.02 ± 1.55
Buoyancy (%): 56.75 ± 4.01
Yield (%): 96.45 ± 2.28
Particle size (µm): 599.52 ± 1.84
Shape and morphology: Spherical shaped microcapsule with rough surface and particles on the surface

FACULTY OF PHARMACY, GRAHAMSTOWN, SOUTH AFRICA
BATCH SUMMARY RECORD

Formulator	Anjana Makan	**Batch size**	4.25 g
Product	Metronidazole microcapsules	**Homogenisation time (hours)**	5
Batch ID	MTZ-003	**Homogenisation speed (rpm)**	500
Temperature	22.5°C	**Date of manufacture**	07/09/16

Formula		
Material	**Amount added**	**Rhodes batch number**
MTZ	1.00g	RM000338
Eudragit® RS PO	1.00g	RM000023
Methocel® K15M	2.00g	RM000250
Avicel® PH102	0.25g	RM000038
Span® 80	1% v/v	-
Light liquid paraffin	120ml	-
Acetone	20ml	-

Dissolution profile

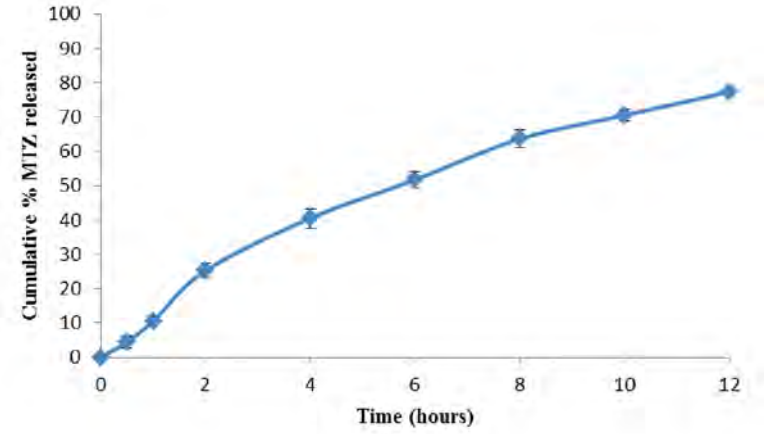

SEM

Encapsulation efficiency (%): 77.21 ± 2.64
Buoyancy (%): 61.89 ± 1.89
Yield (%): 96.47 ± 2.63
Particle size (µm): 494.09 ± 4.15
Shape and morphology: Spherical microcapsule with particles on surface

FACULTY OF PHARMACY, GRAHAMSTOWN, SOUTH AFRICA
BATCH SUMMARY RECORD

Formulator	Anjana Makan	**Batch size**	4.25 g
Product	Metronidazole microcapsules	**Homogenisation time (hours)**	5
Batch ID	MTZ-004	**Homogenisation speed (rpm)**	500
Temperature	22.7°C	**Date of manufacture**	08/09/16

Formula		
Material	**Amount added**	**Rhodes batch number**
MTZ	1.00g	RM000338
Eudragit® RS PO	1.00g	RM000023
Methocel® K15M	1.00g	RM000250
Avicel® PH102	1.25g	RM000038
Span® 80	1% v/v	-
Light liquid paraffin	120ml	-
Acetone	20ml	-

Dissolution profile

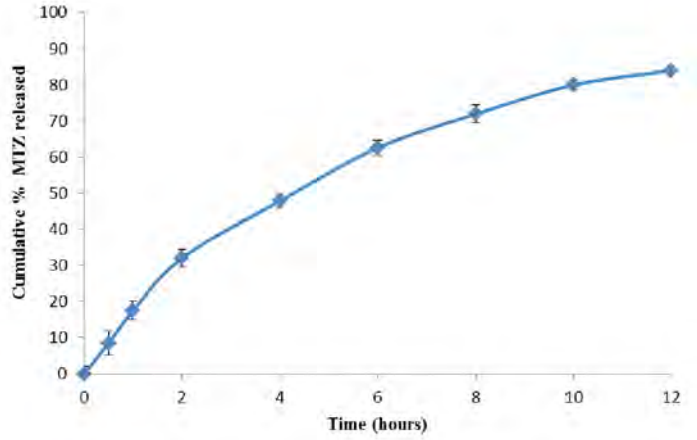

SEM

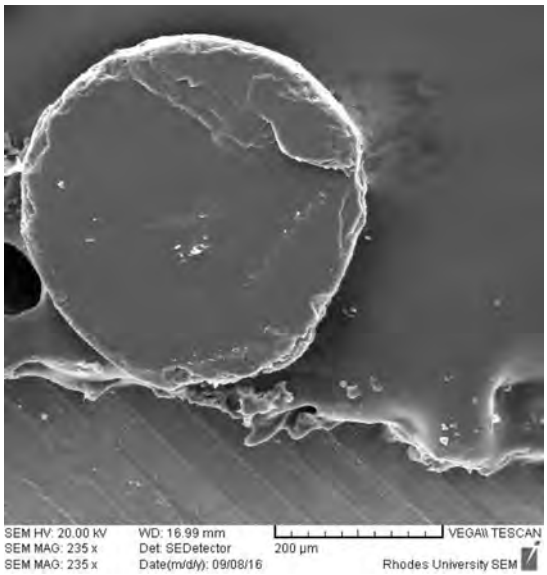

Encapsulation efficiency (%):70.65 ±2.77
Buoyancy (%): 57.45 ± 3.65
Yield (%): 94.67 ± 2.03
Particle size (µm): 491.73 ± 4.47
Shape and morphology: Spherical microcapsule with particles in the surface

FACULTY OF PHARMACY, GRAHAMSTOWN, SOUTH AFRICA
BATCH SUMMARY RECORD

Formulator	Anjana Makan	**Batch size**	4.25 g
Product	Metronidazole microcapsules	**Homogenisation time (hours)**	5
Batch ID	MTZ-005	**Homogenisation speed (rpm)**	500
Temperature	22.2°C	**Date of manufacture**	09/09/16

Formula		
Material	**Amount added**	**Rhodes batch number**
MTZ	1.00g	RM000338
Eudragit® RS PO	1.50g	RM000023
Methocel® K15M	1.00g	RM000250
Avicel® PH102	0.75g	RM000038
Span® 80	1% v/v	-
Light liquid paraffin	120ml	-
Acetone	20ml	-

Dissolution profile

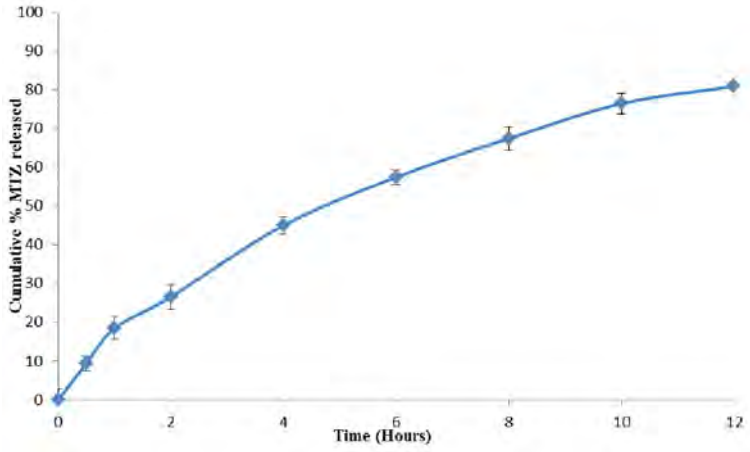

SEM

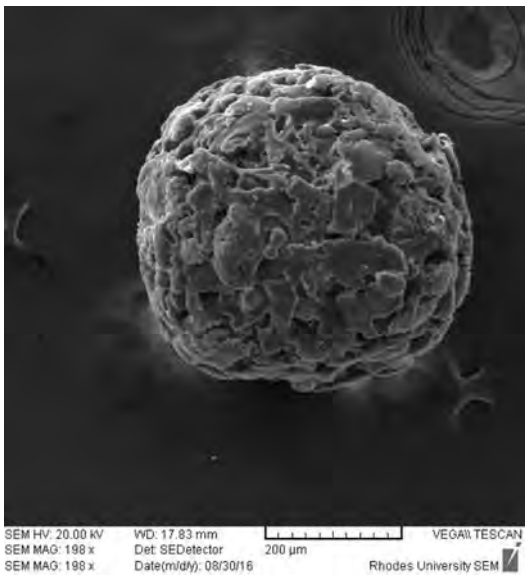

Encapsulation efficiency (%):71.32 ±0.83
Buoyancy (%): 57.10 ± 2.26
Yield (%): 95.75 ± 2.69
Particle size (µm): 421.20 ± 4.37
Shape and morphology: Spherical shaped microcapsule with rough surface

FACULTY OF PHARMACY, GRAHAMSTOWN, SOUTH AFRICA
BATCH SUMMARY RECORD

Formulator	Anjana Makan	**Batch size**	4.25 g
Product	Metronidazole microcapsules	**Homogenisation time (hours)**	6
Batch ID	MTZ-006	**Homogenisation speed (rpm)**	500
Temperature	22.7°C	**Date of manufacture**	06/09/16

Formula		
Material	**Amount added**	**Rhodes batch number**
MTZ	1.00g	RM000338
Eudragit® RS PO	1.50g	RM000023
Methocel® K15M	1.00g	RM000250
Avicel® PH102	0.75g	RM000038
Span® 80	1% v/v	-
Light liquid paraffin	120ml	-
Acetone	20ml	-

Dissolution profile

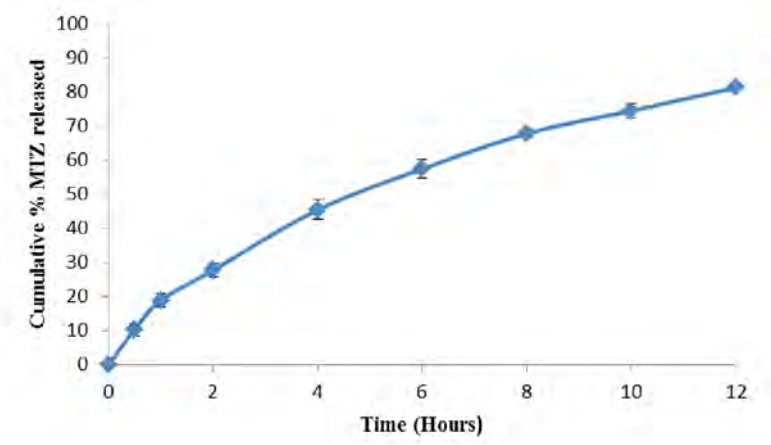

SEM

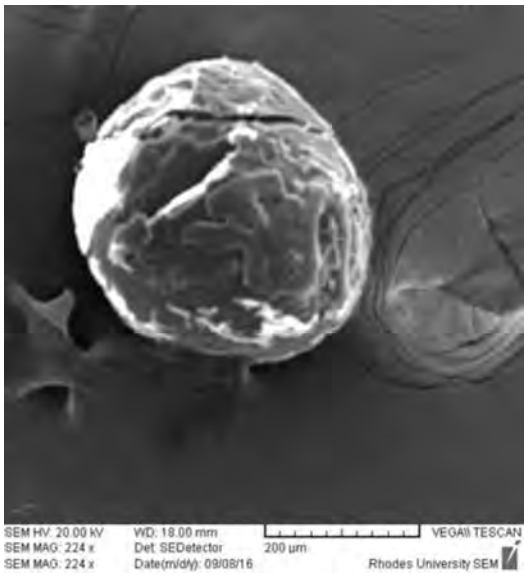

Encapsulation efficiency (%):70.89 ± 2.84
Buoyancy (%): 57.49 ± 2.75
Yield (%): 96.42 ± 3.17
Particle size (µm): 386.60 ± 2.21
Shape and morphology: Spherical shaped microcapsule with rough surface

FACULTY OF PHARMACY, GRAHAMSTOWN, SOUTH AFRICA
BATCH SUMMARY RECORD

Formulator	Anjana Makan	**Batch size**	4.25 g
Product	Metronidazole microcapsules	**Homogenisation time (hours)**	6
Batch ID	MTZ-007	**Homogenisation speed (rpm)**	1500
Temperature	21.6°C	**Date of manufacture**	06/09/16

Formula		
Material	**Amount added**	**Rhodes batch number**
MTZ	1.00g	RM000338
Eudragit® RS PO	1.50g	RM000023
Methocel® K15M	1.00g	RM000250
Avicel® PH102	0.75g	RM000038
Span® 80	1% v/v	-
Light liquid paraffin	120ml	-
Acetone	20ml	-

Dissolution profile

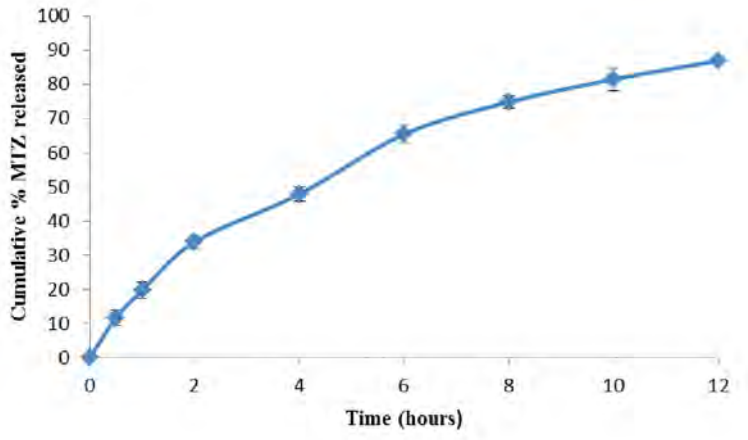

SEM

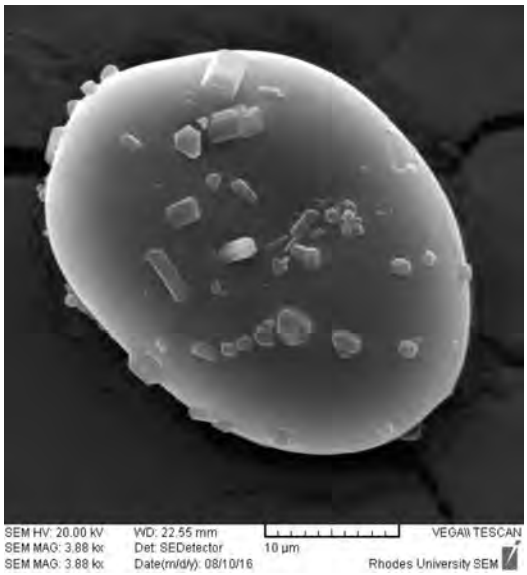

Encapsulation efficiency (%):68.54 ± 1.86
Buoyancy (%): 56.74 ± 1.62
Yield (%): 91.45 ± 2.54
Particle size (µm): 61.01 ± 3.62
Shape and morphology: Spherical shaped with smooth surface and particles on the surface

FACULTY OF PHARMACY, GRAHAMSTOWN, SOUTH AFRICA
BATCH SUMMARY RECORD

Formulator	Anjana Makan	**Batch size**	4.25 g
Product	Metronidazole microcapsules	**Homogenisation time (hours)**	6
Batch ID	MTZ-008	**Homogenisation speed (rpm)**	1000
Temperature	21.3°C	**Date of manufacture**	20/09/16

Formula		
Material	**Amount added**	**Rhodes batch number**
MTZ	1.00g	RM000338
Eudragit® RS PO	1.25g	RM000023
Methocel® K15M	1.25g	RM000250
Avicel® PH102	0.75g	RM000038
Span® 80	1% v/v	-
Light liquid paraffin	120ml	-
Acetone	20ml	-

Dissolution profile

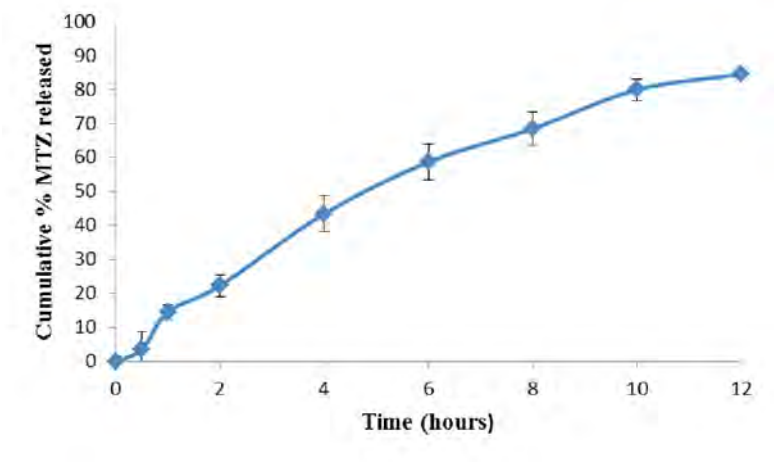

SEM

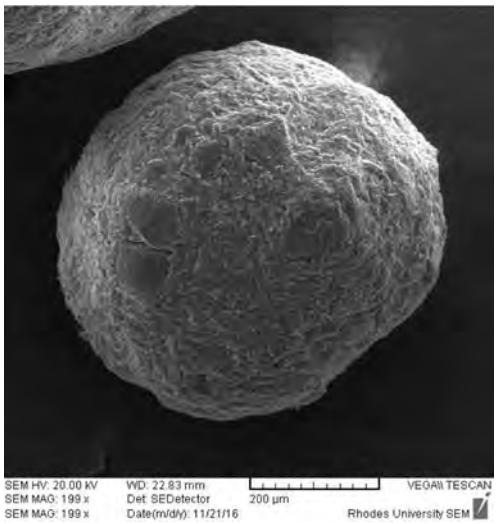

Encapsulation efficiency (%):73.70 ± 2.79
Buoyancy (%): 58.34 ± 2.21
Yield (%): 96.94 ± 2.17
Particle size (µm): 199.71 ± 3.21
Shape and morphology: Spherical shaped microcapsule with smooth surface

FACULTY OF PHARMACY, GRAHAMSTOWN, SOUTH AFRICA
BATCH SUMMARY RECORD

Formulator	Anjana Makan	**Batch size**	4.25 g
Product	Metronidazole microcapsules	**Homogenisation time (hours)**	6
Batch ID	MTZ-009	**Homogenisation speed (rpm)**	1000
Temperature	22.5°C	**Date of manufacture**	21/09/16

Formula		
Material	**Amount added**	**Rhodes batch number**
MTZ	1.00g	RM000338
Eudragit® RS PO	1.25g	RM000023
Methocel® K15M	1.25g	RM000250
Avicel® PH102	0.75g	RM000038
Span® 80	1% v/v	-
Light liquid paraffin	120ml	-
Acetone	20ml	-

Dissolution profile

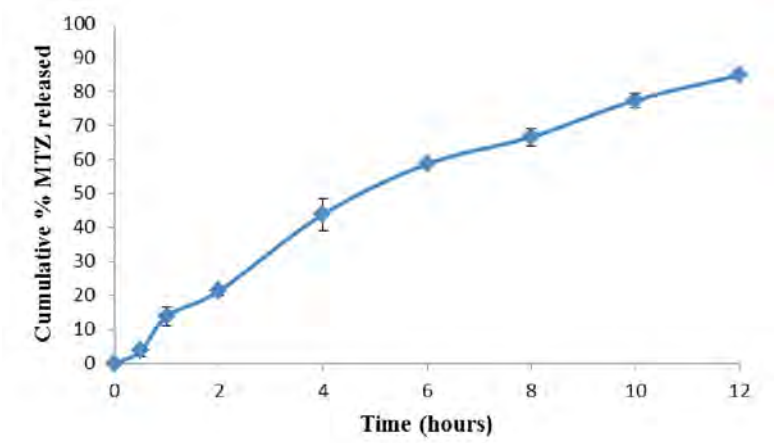

SEM

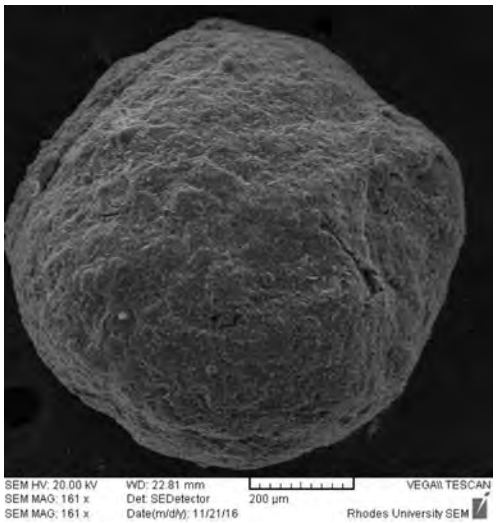

Encapsulation efficiency (%):72.51 ± 2.65
Buoyancy (%): 58.45 ± 1.98
Yield (%): 96.47 ± 1.75
Particle size (µm):233.80 ± 2.72
Shape and morphology: Spherical shaped microcapsule with smooth surface

FACULTY OF PHARMACY, GRAHAMSTOWN, SOUTH AFRICA
BATCH SUMMARY RECORD

Formulator	Anjana Makan	**Batch size**	4.25 g
Product	Metronidazole microcapsules	**Homogenisation time (hours)**	7
Batch ID	MTZ-010	**Homogenisation speed (rpm)**	1500
Temperature	22.0°C	**Date of manufacture**	22/09/16

Formula		
Material	**Amount added**	**Rhodes batch number**
MTZ	1.00g	RM000338
Eudragit® RS PO	1.50g	RM000023
Methocel® K15M	1.00g	RM000250
Avicel® PH102	0.75g	RM000038
Span® 80	1% v/v	-
Light liquid paraffin	120ml	-
Acetone	20ml	-

Dissolution profile

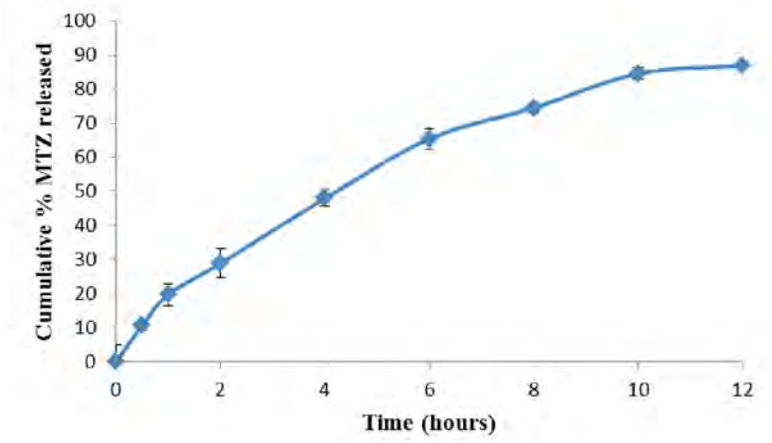

SEM

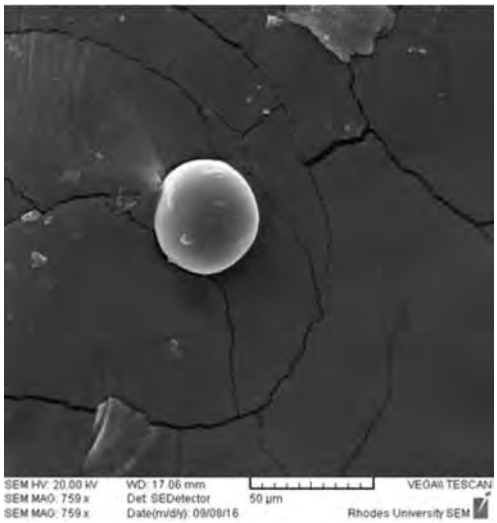

Encapsulation efficiency (%):70.81 ±2.09
Buoyancy (%): 56.42 ± 1.67
Yield (%): 91.76 ± 1.65
Particle size (µm): 43.96 ± 0.78
Shape and morphology: Spherical shaped microcapsule with smooth surface

FACULTY OF PHARMACY, GRAHAMSTOWN, SOUTH AFRICA
BATCH SUMMARY RECORD

Formulator	Anjana Makan	**Batch size**	4.25 g
Product	Metronidazole microcapsules	**Homogenisation time (hours)**	7
Batch ID	MTZ-011	**Homogenisation speed (rpm)**	500
Temperature	23.1°C	**Date of manufacture**	23/09/16

Formula		
Material	**Amount added**	**Rhodes batch number**
MTZ	1.00g	RM000338
Eudragit® RS PO	1.00g	RM000023
Methocel® K15M	1.00g	RM000250
Avicel® PH102	1.25g	RM000038
Span® 80	1% v/v	-
Light liquid paraffin	120ml	-
Acetone	20ml	-

Dissolution profile

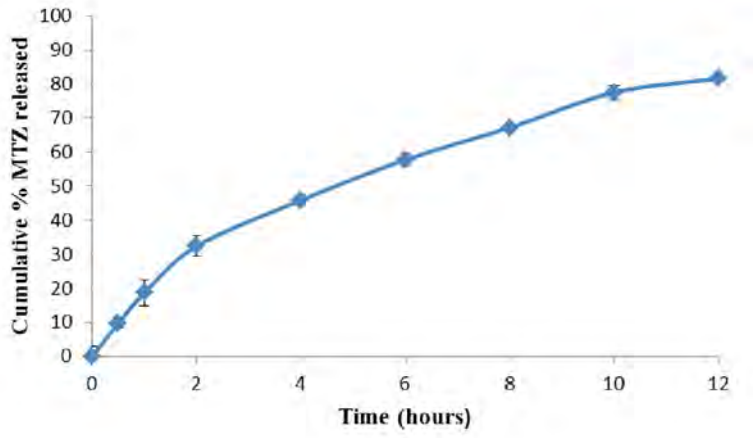

SEM

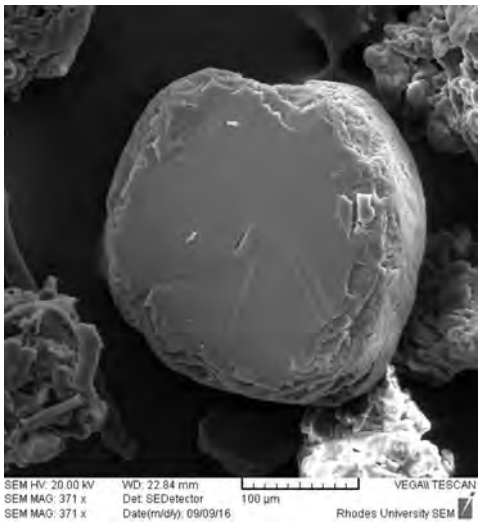

Encapsulation efficiency (%): 71.97 ± 2.27
Buoyancy (%): 57.15 ± 3.05
Yield (%): 94.88 ± 2.17
Particle size (µm): 280.67 ± 1.86
Shape and morphology: Irregular shaped microcapsule with rough surface

FACULTY OF PHARMACY, GRAHAMSTOWN, SOUTH AFRICA
BATCH SUMMARY RECORD

Formulator	Anjana Makan	**Batch size**	4.25 g
Product	Metronidazole microcapsules	**Homogenisation time (hours)**	7
Batch ID	MTZ-012	**Homogenisation speed (rpm)**	500
Temperature	22.0°C	**Date of manufacture**	24/09/16

Formula		
Material	**Amount added**	**Rhodes batch number**
MTZ	1.00g	RM000338
Eudragit® RS PO	1.50g	RM000023
Methocel® K15M	1.50g	RM000250
Avicel® PH102	0.25g	RM000038
Span® 80	1% v/v	-
Light liquid paraffin	120ml	-
Acetone	20ml	-

Dissolution profile

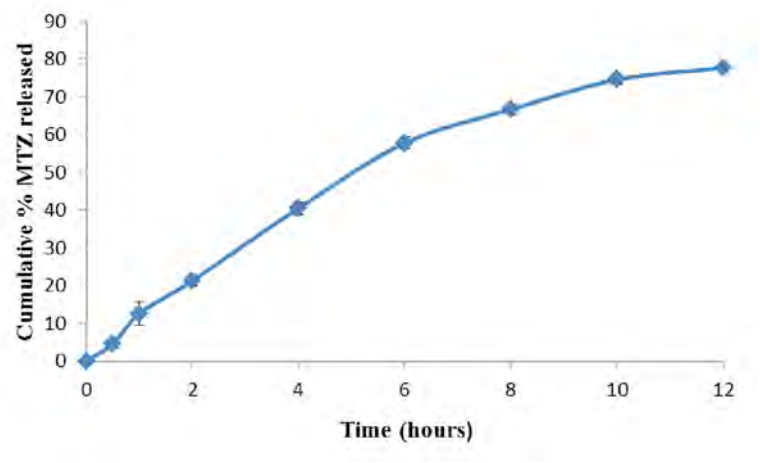

SEM

Encapsulation efficiency (%): 74.90 ± 1.39
Buoyancy (%): 60.55 ± 1.02
Yield (%): 95.71 ± 1.08
Particle size (µm): 303.93 ± 3.73
Shape and morphology: Irregular shaped microcapsule with particles on the surface

FACULTY OF PHARMACY, GRAHAMSTOWN, SOUTH AFRICA
BATCH SUMMARY RECORD

Formulator	Anjana Makan	**Batch size**	4.25 g
Product	Metronidazole microcapsules	**Homogenisation time (hours)**	5
Batch ID	MTZ-013	**Homogenisation speed (rpm)**	1500
Temperature	22.4°C	**Date of manufacture**	26/09/16

Formula		
Material	**Amount added**	**Rhodes batch number**
MTZ	1.00g	RM000338
Eudragit® RS PO	1.00g	RM000023
Methocel® K15M	1.50g	RM000250
Avicel® PH102	0.75g	RM000038
Span® 80	1% v/v	-
Light liquid paraffin	120ml	-
Acetone	20ml	-

Dissolution profile

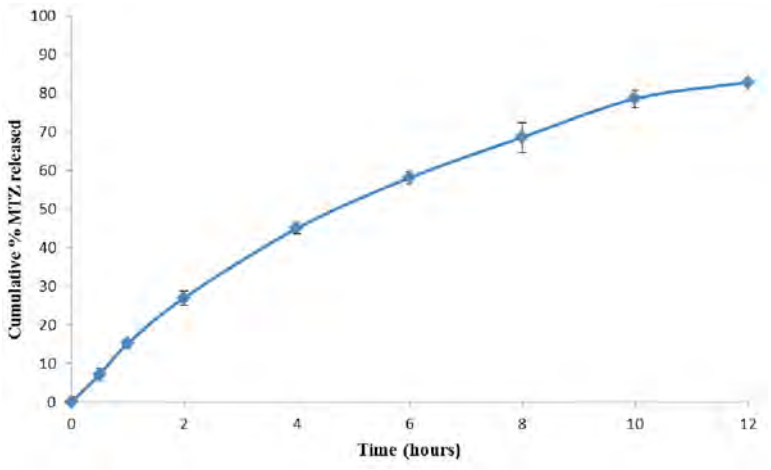

SEM

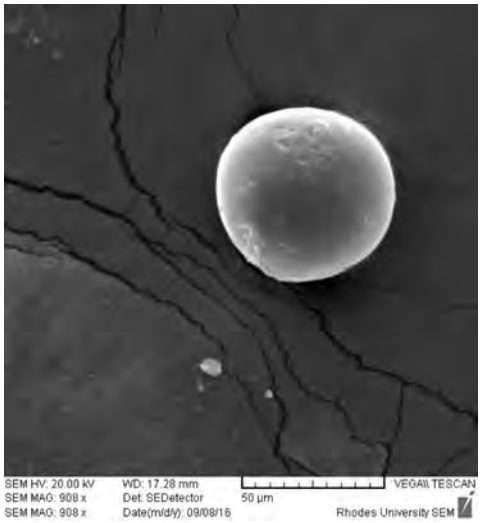

Encapsulation efficiency (%): 69.77 ± 1.54
Buoyancy (%): 61.52 ± 1.76
Yield (%): 92.82 ± 1.15
Particle size (µm): 61.91 ± 2.26
Shape and morphology: Spherical shaped microcapsule with smooth surface

FACULTY OF PHARMACY, GRAHAMSTOWN, SOUTH AFRICA
BATCH SUMMARY RECORD

Formulator	Anjana Makan	**Batch size**	4.25 g
Product	Metronidazole microcapsules	**Homogenisation time (hours)**	5
Batch ID	MTZ-014	**Homogenisation speed (rpm)**	1500
Temperature	22.2°C	**Date of manufacture**	27/09/16

Formula

Material	Amount added	Rhodes batch number
MTZ	1.00g	RM000338
Eudragit® RS PO	1.50g	RM000023
Methocel® K15M	1.00g	RM000250
Avicel® PH102	0.75g	RM000038
Span®80	1% v/v	-
Light liquid paraffin	120ml	-
Acetone	20ml	-

Dissolution profile

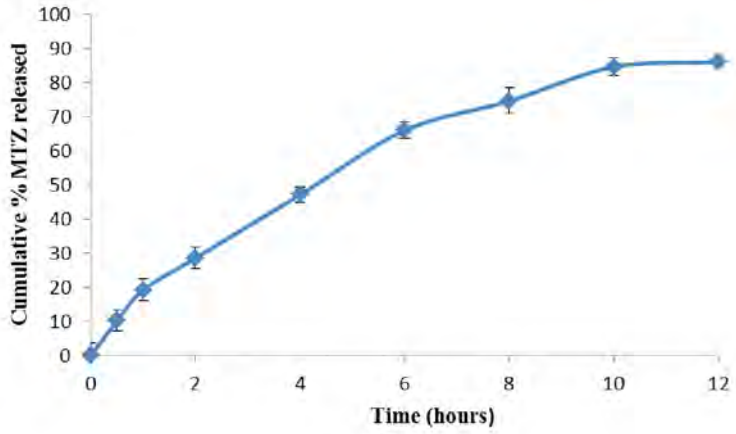

SEM

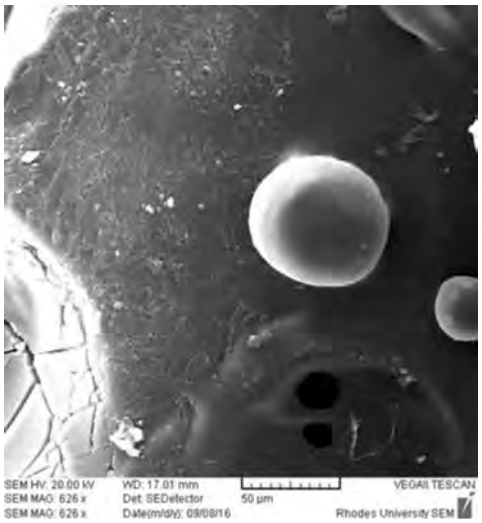

Encapsulation efficiency (%): 70.11 ± 3.06
Buoyancy (%): 56.55 ± 1.79
Yield (%): 90.24 ± 1.97
Particle size (µm): 70.67 ± 2.26
Shape and morphology: Spherical shaped microcapsule with smooth surface

FACULTY OF PHARMACY, GRAHAMSTOWN, SOUTH AFRICA
BATCH SUMMARY RECORD

Formulator	Anjana Makan	**Batch size**	4.25 g
Product	Metronidazole microcapsules	**Homogenisation time (hours)**	5
Batch ID	MTZ-015	**Homogenisation speed (rpm)**	500
Temperature	22.5°C	**Date of manufacture**	28/09/16

Formula		
Material	**Amount added**	**Rhodes batch number**
MTZ	1.00g	RM000338
Eudragit® RS PO	1.00g	RM000023
Methocel® K15M	1.00g	RM000250
Avicel® PH102	1.25g	RM000038
Span®80	1% v/v	-
Light liquid paraffin	120ml	-
Acetone	20ml	-

Dissolution profile

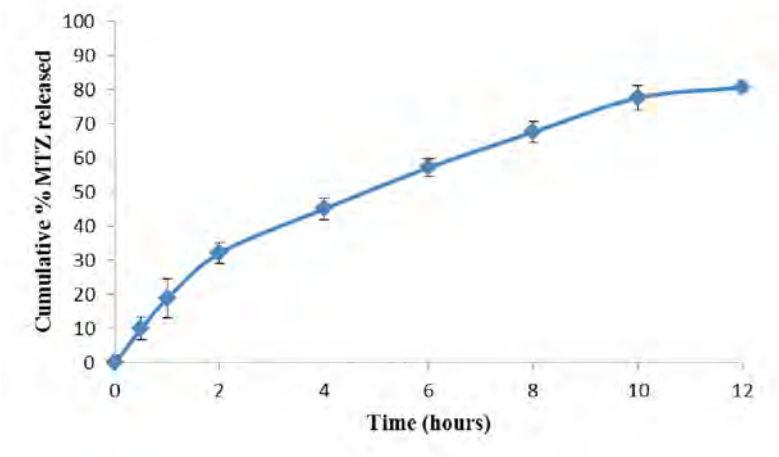

SEM

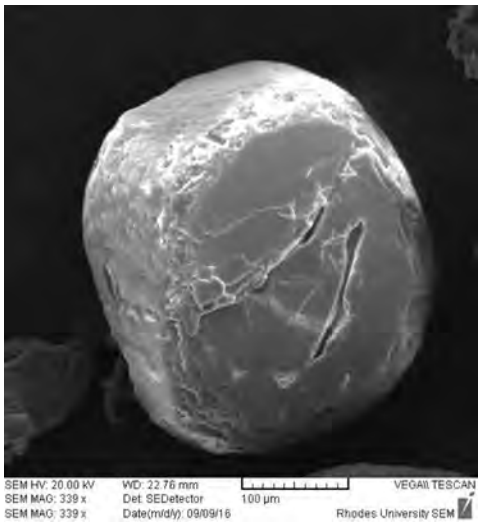

Encapsulation efficiency (%): 70.93 ± 1.58
Buoyancy (%): 57.13 ± 2.13
Yield (%): 94.76 ± 2.06
Particle size (µm): 349.11 ± 2.57
Shape and morphology: Spherical shaped microcapsule with rough surface

FACULTY OF PHARMACY, GRAHAMSTOWN, SOUTH AFRICA
BATCH SUMMARY RECORD

Formulator	Anjana Makan	**Batch size**	4.25 g
Product	Metronidazole microcapsules	**Homogenisation time (hours)**	6
Batch ID	MTZ-016	**Homogenisation speed (rpm)**	1000
Temperature	22.6°C	**Date of manufacture**	29/09/16

Formula		
Material	**Amount added**	**Rhodes batch number**
MTZ	1.00g	RM000338
Eudragit® RS PO	1.25g	RM000023
Methocel® K15M	1.25g	RM000250
Avicel® PH102	0.75g	RM000038
Span®80	1% v/v	-
Light liquid paraffin	120ml	-
Acetone	20ml	-

Dissolution profile

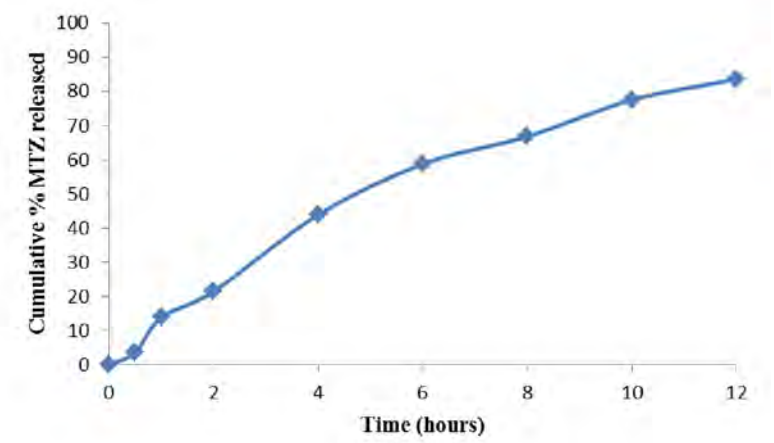

SEM

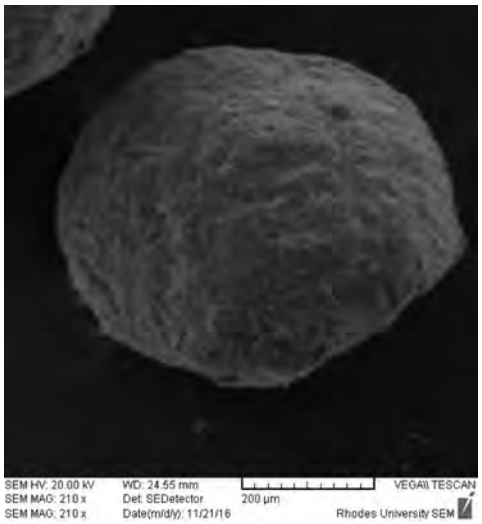

Encapsulation efficiency (%): 72.91 ± 1.19
Buoyancy (%): 58.22 ± 1.99
Yield (%): 96.94 ± 2.16
Particle size (µm): 191.75 ± 4.15
Shape and morphology: Irregular shaped microcapsule with smooth surface

FACULTY OF PHARMACY, GRAHAMSTOWN, SOUTH AFRICA
BATCH SUMMARY RECORD

Formulator	Anjana Makan	**Batch size**	4.25 g
Product	Metronidazole microcapsules	**Homogenisation time (hours)**	7
Batch ID	MTZ-017	**Homogenisation speed (rpm)**	1500
Temperature	22.9°C	**Date of manufacture**	30/09/16

Formula		
Material	**Amount added**	**Rhodes batch number**
MTZ	1.00g	RM000338
Eudragit® RS PO	1.50g	RM000023
Methocel® K15M	1.50g	RM000250
Avicel® PH102	0.25g	RM000038
Span®80	1% v/v	-
Light liquid paraffin	120ml	-
Acetone	20ml	-

Dissolution profile

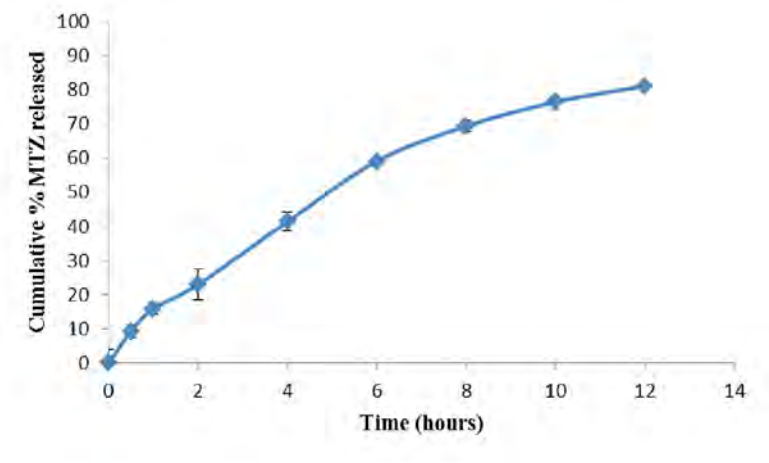

SEM

Encapsulation efficiency (%): 71.29 ± 2.53
Buoyancy (%): 60.15 ± 1.30
Yield (%): 92.18 ± 4.81
Particle size (µm): 38.74 ± 2.54
Shape and morphology: Spherical shaped microcapsule with particles on the smooth surface

FACULTY OF PHARMACY, GRAHAMSTOWN, SOUTH AFRICA
BATCH SUMMARY RECORD

Formulator	Anjana Makan	**Batch size**	4.25 g
Product	Metronidazole microcapsules	**Homogenisation time (hours)**	6
Batch ID	MTZ-018	**Homogenisation speed (rpm)**	500
Temperature	22.3°C	**Date of manufacture**	1/10/16

Formula		
Material	**Amount added**	**Rhodes batch number**
MTZ	1.00g	RM000338
Eudragit® RS PO	1.25g	RM000023
Methocel® K15M	1.25g	RM000250
Avicel® PH102	0.75g	RM000038
Span®80	1% v/v	-
Light liquid paraffin	120ml	-
Acetone	20ml	-

Dissolution profile

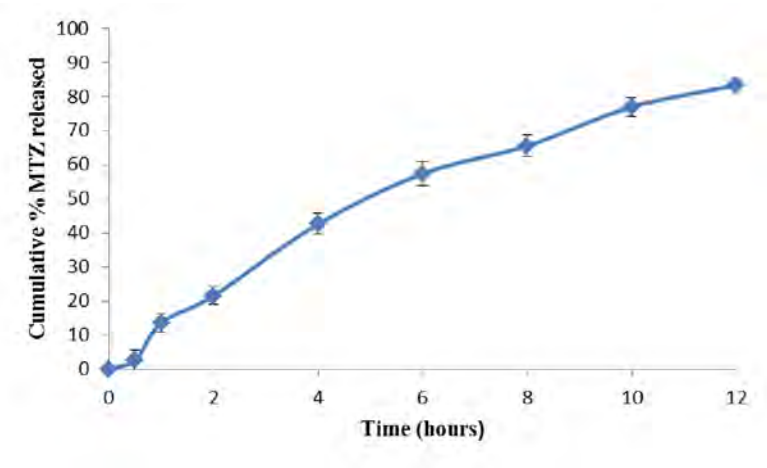

SEM

Encapsulation efficiency (%): 73.58 ± 1.66
Buoyancy (%): 59.60 ± 0.96
Yield (%): 94.71 ± 3.02
Particle size (µm): 332.74 ± 2.54
Shape and morphology: Irregular shaped microcapsule with particles on rough surface

FACULTY OF PHARMACY, GRAHAMSTOWN, SOUTH AFRICA
BATCH SUMMARY RECORD

Formulator	Anjana Makan	**Batch size**	4.25 g
Product	Metronidazole microcapsules	**Homogenisation time (hours)**	7
Batch ID	MTZ-019	**Homogenisation speed (rpm)**	500
Temperature	22.0°C	**Date of manufacture**	2/10/16

Formula		
Material	**Amount added**	**Rhodes batch number**
MTZ	1.00g	RM000338
Eudragit® RS PO	1.00g	RM000023
Methocel® K15M	1.50g	RM000250
Avicel® PH102	0.75g	RM000038
Span®80	1% v/v	-
Light liquid paraffin	120ml	-
Acetone	20ml	-

Dissolution profile

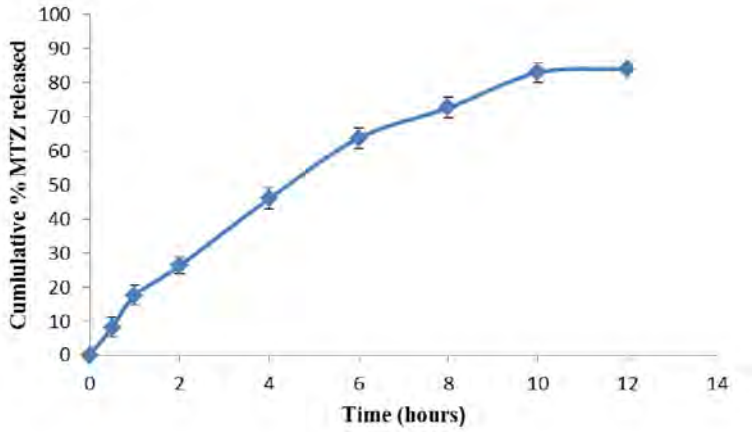

SEM

Encapsulation efficiency (%): 71.79 ± 2.02
Buoyancy (%): 57.45 ± 2.67
Yield (%): 96.76 ± 0.50
Particle size (µm): 279.05 ± 2.07
Shape and morphology: Irregular shaped microcapsule with rough surface and particles on the surface

FACULTY OF PHARMACY, GRAHAMSTOWN, SOUTH AFRICA
BATCH SUMMARY RECORD

Formulator	Anjana Makan	**Batch size**	4.25 g
Product	Metronidazole microcapsules	**Homogenisation time (hours)**	6
Batch ID	MTZ-020	**Homogenisation speed (rpm)**	1000
Temperature	21.9°C	**Date of manufacture**	3/10/16

Formula

Material	Amount added	Rhodes batch number
MTZ	1.00g	RM000338
Eudragit® RS PO	1.25g	RM000023
Methocel® K15M	1.25g	RM000250
Avicel® PH102	0.75g	RM000038
Span®80	1% v/v	-
Light liquid paraffin	120ml	-
Acetone	20ml	-

Dissolution profile

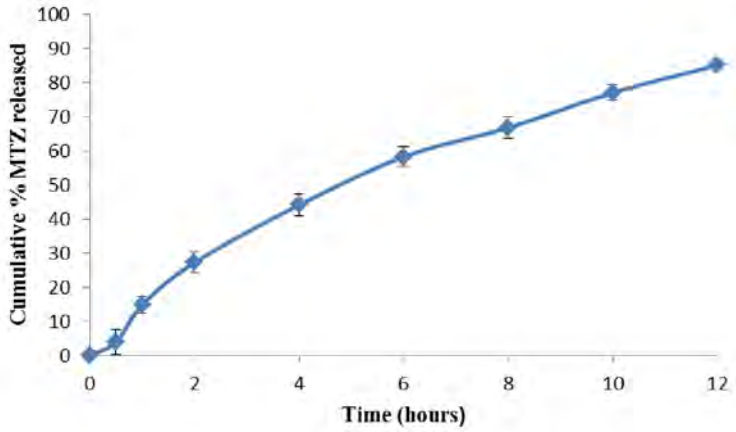

SEM

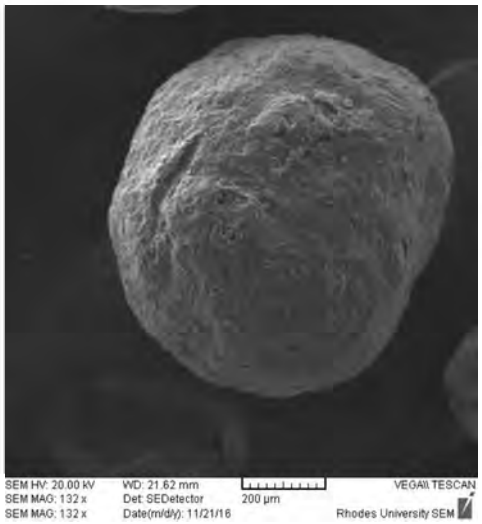

Encapsulation efficiency (%): 73.41 ± 1.99
Buoyancy (%): 59.21 ± 1.19
Yield (%): 94.12 ± 2.07
Particle size (µm): 190.86 ± 3.62
Shape and morphology: Spherical shaped microcapsule with smooth surface

FACULTY OF PHARMACY, GRAHAMSTOWN, SOUTH AFRICA
BATCH SUMMARY RECORD

Formulator	Anjana Makan	**Batch size**	4.25 g
Product	Metronidazole microcapsules	**Homogenisation time (hours)**	7
Batch ID	MTZ-021	**Homogenisation speed (rpm)**	500
Temperature	22.5°C	**Date of manufacture**	4/10/16

Formula		
Material	**Amount added**	**Rhodes batch number**
MTZ	1.00g	RM000338
Eudragit® RS PO	1.00g	RM000023
Methocel® K15M	1.50g	RM000250
Avicel® PH102	0.75g	RM000038
Span®80	1% v/v	-
Light liquid paraffin	120ml	-
Acetone	20ml	-

Dissolution profile

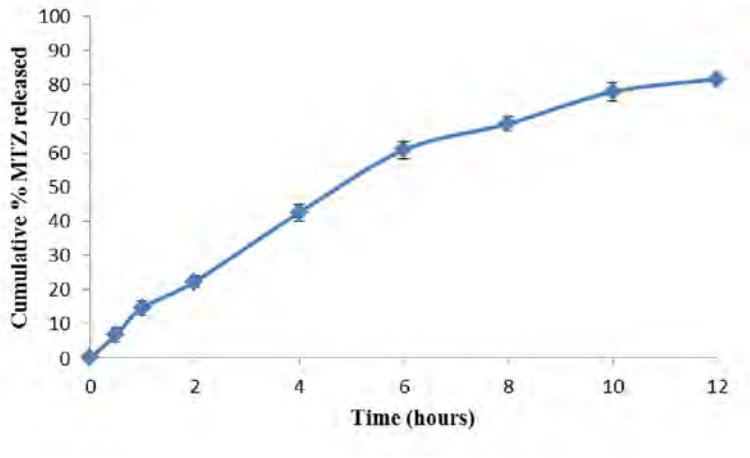

SEM

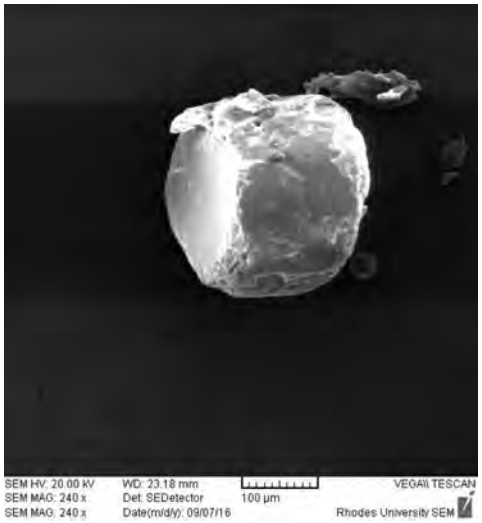

Encapsulation efficiency (%):74.25 ± 2.56
Buoyancy (%): 62.54 ± 0.94
Yield (%): 96.94 ± 2.14
Particle size (µm):267.89 ± 4.56
Shape and morphology: Irregular shaped microcapsule with rough surface

FACULTY OF PHARMACY, GRAHAMSTOWN, SOUTH AFRICA
BATCH SUMMARY RECORD

Formulator	Anjana Makan	**Batch size**	4.25 g
Product	Metronidazole microcapsules	**Homogenisation time (hours)**	6
Batch ID	MTZ-022	**Homogenisation speed (rpm)**	1000
Temperature	21.9°C	**Date of manufacture**	5/10/16

Formula		
Material	**Amount added**	**Rhodes batch number**
MTZ	1.00g	RM000338
Eudragit® RS PO	1.50g	RM000023
Methocel® K15M	1.25g	RM000250
Avicel® PH102	0.50g	RM000038
Span®80	1% v/v	-
Light liquid paraffin	120ml	-
Acetone	20ml	-

Dissolution profile

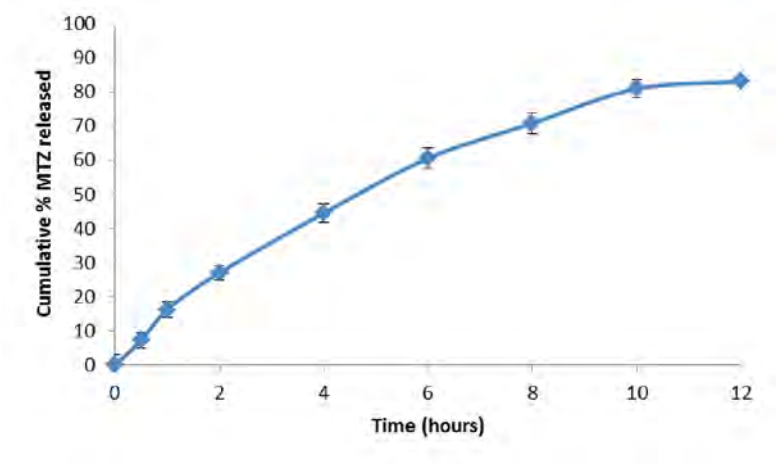

SEM

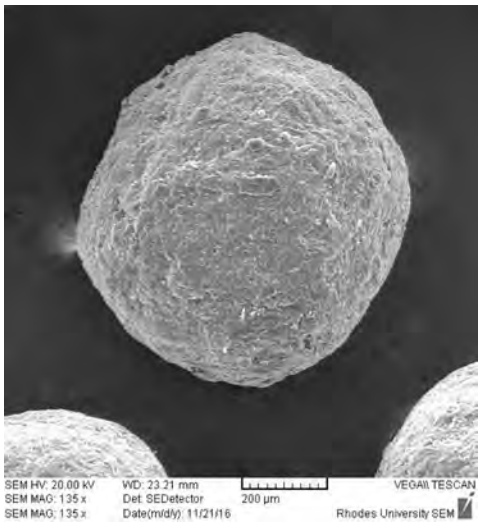

Encapsulation efficiency (%):71.12 ± 2.28
Buoyancy (%): 58.54 ± 2.21
Yield (%): 96.94 ± 1.72
Particle size (µm):181.55 ± 3.57
Shape and morphology: Spherical microcapsule with smooth surface

FACULTY OF PHARMACY, GRAHAMSTOWN, SOUTH AFRICA
BATCH SUMMARY RECORD

Formulator	Anjana Makan	**Batch size**	4.25 g
Product	Metronidazole microcapsules	**Homogenisation time (hours)**	5
Batch ID	MTZ-023	**Homogenisation speed (rpm)**	1000
Temperature	22.0°C	**Date of manufacture**	6/10/16

Formula		
Material	**Amount added**	**Rhodes batch number**
MTZ	1.00g	RM000338
Eudragit® RS PO	1.25g	RM000023
Methocel® K15M	1.25g	RM000250
Avicel® PH102	0.75g	RM000038
Span®80	1% v/v	-
Light liquid paraffin	120ml	-
Acetone	20ml	-

Dissolution profile

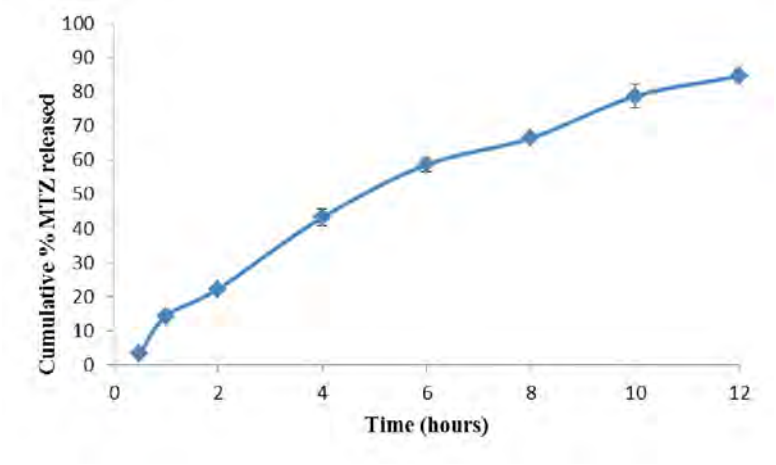

SEM

Encapsulation efficiency (%):72.57 ± 2.03
Buoyancy (%): 58.46 ± 1.99
Yield (%): 93.76 ± 2.53
Particle size (µm):244.43 ± 1.68
Shape and morphology: Spherical shaped microcapsule with particles on surface

FACULTY OF PHARMACY, GRAHAMSTOWN, SOUTH AFRICA
BATCH SUMMARY RECORD

Formulator	Anjana Makan	**Batch size**	4.25 g
Product	Metronidazole microcapsules	**Homogenisation time (hours)**	6
Batch ID	MTZ-024	**Homogenisation speed (rpm)**	1000
Temperature	21.9°C	**Date of manufacture**	7/10/16

Formula		
Material	**Amount added**	**Rhodes batch number**
MTZ	1.00g	RM000338
Eudragit® RS PO	1.25g	RM000023
Methocel® K15M	1.25g	RM000250
Avicel® PH102	0.75g	RM000038
Span®80	1% v/v	-
Light liquid paraffin	120ml	-
Acetone	20ml	-

Dissolution profile

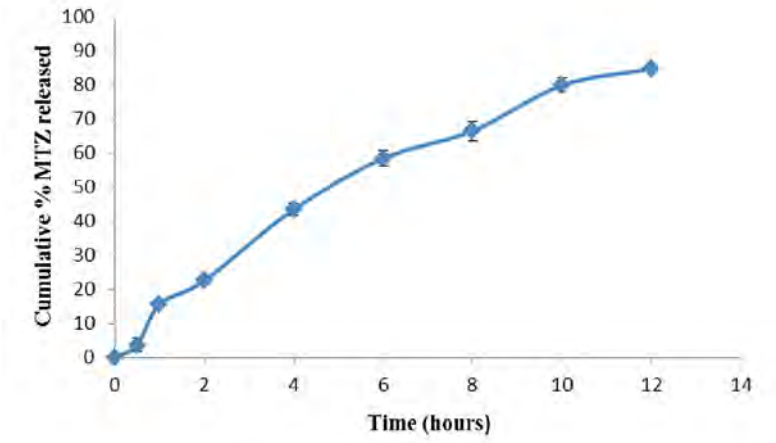

SEM

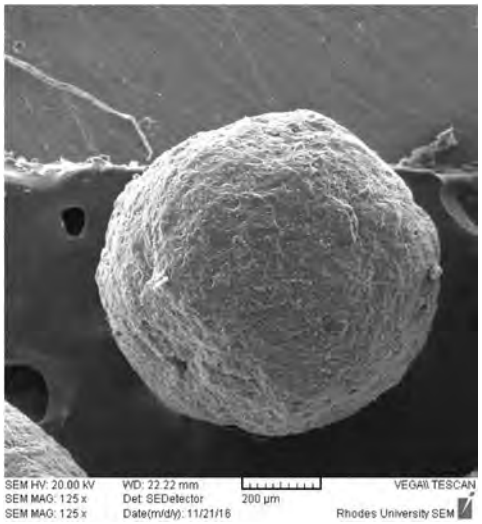

Encapsulation efficiency (%):73.35 ± 2.01
Buoyancy (%): 57.51 ± 1.68
Yield (%): 94.35 ± 2.74
Particle size (µm):175.92 ± 3.21
Shape and morphology: Spherical shaped microcapsule with smooth surface

FACULTY OF PHARMACY, GRAHAMSTOWN, SOUTH AFRICA
BATCH SUMMARY RECORD

Formulator	Anjana Makan	**Batch size**	4.25 g
Product	Metronidazole microcapsules	**Homogenisation time (hours)**	6
Batch ID	MTZ-025	**Homogenisation speed (rpm)**	1000
Temperature	21.9°C	**Date of manufacture**	8/10/16

Formula		
Material	**Amount added**	**Rhodes batch number**
MTZ	1.00g	RM000338
Eudragit® RS PO	1.25g	RM000023
Methocel® K15M	1.25g	RM000250
Avicel® PH102	0.75g	RM000038
Span®80	1% v/v	-
Light liquid paraffin	120ml	-
Acetone	20ml	-

Dissolution profile

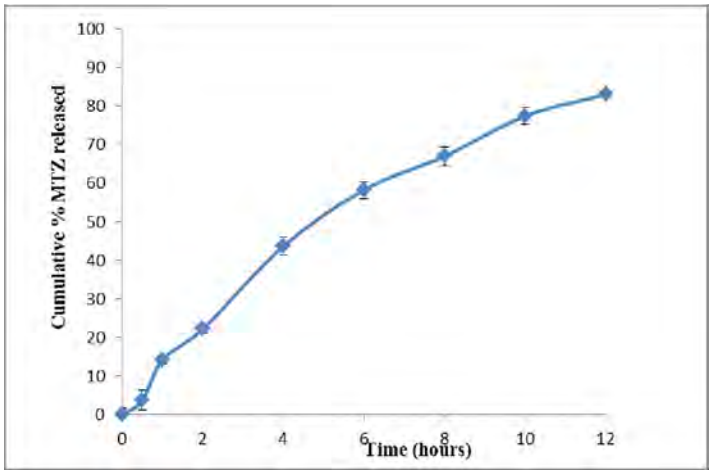

SEM

Encapsulation efficiency (%):74.49 ± 3.04
Buoyancy (%): 58.40 ± 23.0
Yield (%): 96.47 ± 1.98
Particle size (µm):180.94 ± 2.53
Shape and morphology: Irregular shaped microcapsule with rough surface

FACULTY OF PHARMACY, GRAHAMSTOWN, SOUTH AFRICA
BATCH SUMMARY RECORD

Formulator	Anjana Makan	**Batch size**	4.25 g
Product	Metronidazole microcapsules	**Homogenisation time (hours)**	5
Batch ID	MTZ-026	**Homogenisation speed (rpm)**	500
Temperature	22.4°C	**Date of manufacture**	9/10/16

Formula		
Material	**Amount added**	**Rhodes batch number**
MTZ	1.00g	RM000338
Eudragit® RS PO	1.00g	RM000023
Methocel® K15M	1.50g	RM000250
Avicel® PH102	0.75g	RM000038
Span®80	1% v/v	-
Light liquid paraffin	120ml	-
Acetone	20ml	-

Dissolution profile

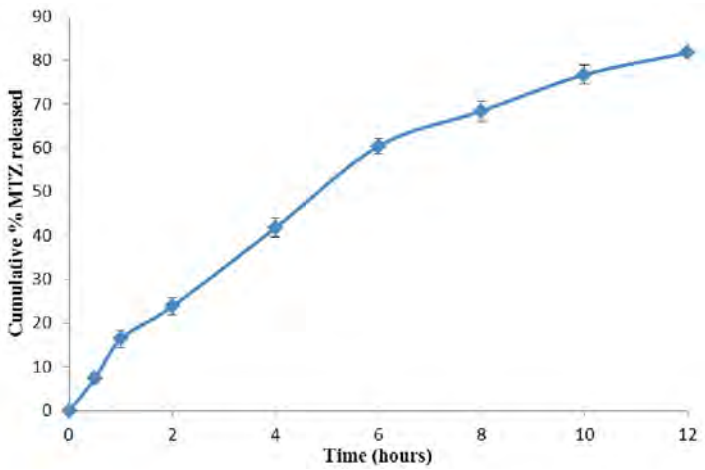

SEM

Encapsulation efficiency (%):74.49 ± 1.89
Buoyancy (%): 61.88 ± 1.11
Yield (%): 96.47 ± 1.98
Particle size (µm):402.22 ± 1.10
Shape and morphology: Spherical microcapsule with smooth surface

FACULTY OF PHARMACY, GRAHAMSTOWN, SOUTH AFRICA
BATCH SUMMARY RECORD

Formulator	Anjana Makan	**Batch size**	4.25 g
Product	Metronidazole microcapsules	**Homogenisation time (hours)**	5
Batch ID	MTZ-027	**Homogenisation speed (rpm)**	500
Temperature	22.3°C	**Date of manufacture**	10/10/16

Formula		
Material	**Amount added**	**Rhodes batch number**
MTZ	1.00g	RM000338
Eudragit® RS PO	1.50g	RM000023
Methocel® K15M	1.50g	RM000250
Avicel® PH102	0.25g	RM000038
Span®80	1% v/v	-
Light liquid paraffin	120ml	-
Acetone	20ml	-

Dissolution profile

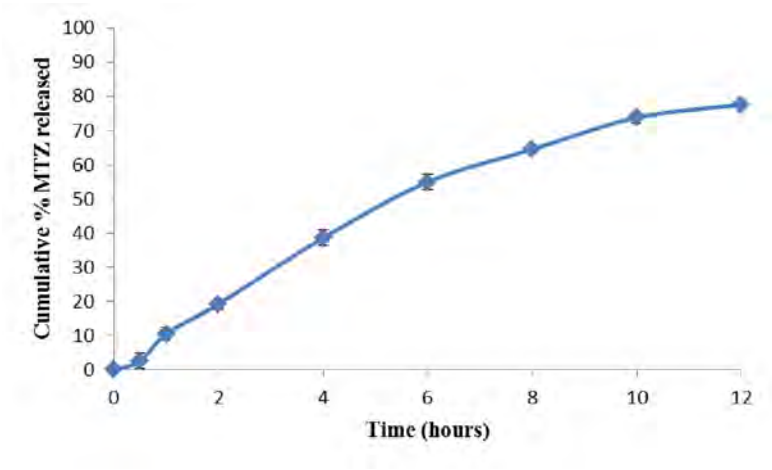

SEM

Encapsulation efficiency (%):75.03 ± 2.29
Buoyancy (%): 60.56 ± 1.89
Yield (%): 94.12 ± 2.07
Particle size (µm):357.27 ± 2.08
Shape and morphology: Irregular shaped microcapsule with rough surface

FACULTY OF PHARMACY, GRAHAMSTOWN, SOUTH AFRICA
BATCH SUMMARY RECORD

Formulator	Anjana Makan	**Batch size**	4.25 g
Product	Metronidazole microcapsules	**Homogenisation time (hours)**	7
Batch ID	MTZ-028	**Homogenisation speed (rpm)**	1500
Temperature	21.9°C	**Date of manufacture**	11/10/16

Formula		
Material	**Amount added**	**Rhodes batch number**
MTZ	1.00g	RM000338
Eudragit® RS PO	1.00g	RM000023
Methocel® K15M	1.50g	RM000250
Avicel® PH102	0.75g	RM000038
Span®80	1% v/v	-
Light liquid paraffin	120ml	-
Acetone	20ml	-

Dissolution profile

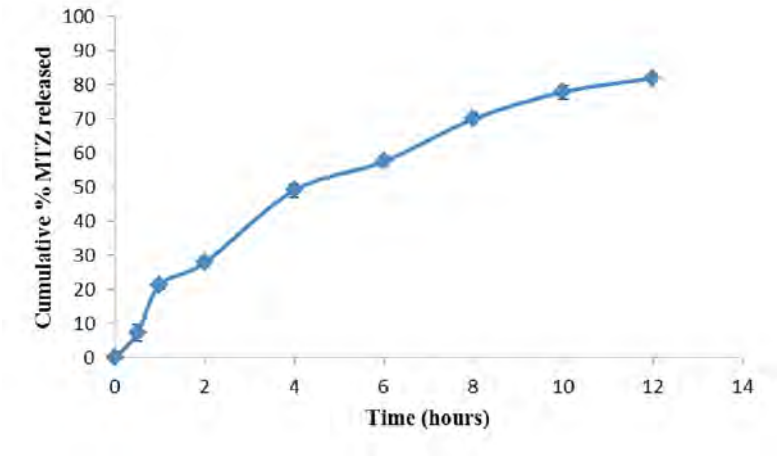

SEM

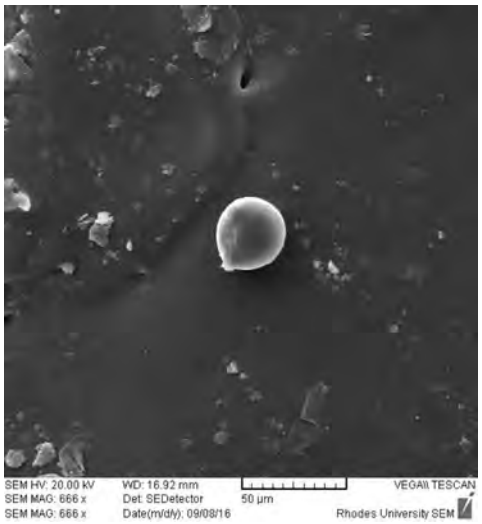

Encapsulation efficiency (%): 69.59 ± 2.04
Buoyancy (%): 59.55 ± 0.94
Yield (%): 90.01 ± 1.42
Particle size (µm):35.67 ± 0.43
Shape and morphology: Spherical shaped microcapsule with particles adhering to the surface

FACULTY OF PHARMACY, GRAHAMSTOWN, SOUTH AFRICA
BATCH SUMMARY RECORD

Formulator	Anjana Makan	**Batch size**	4.25 g
Product	Metronidazole microcapsules	**Homogenisation time (hours)**	5
Batch ID	MTZ-029	**Homogenisation speed (rpm)**	1500
Temperature	22.7°C	**Date of manufacture**	12/10/16

Formula		
Material	**Amount added**	**Rhodes batch number**
MTZ	1.00g	RM000338
Eudragit® RS PO	1.50g	RM000023
Methocel® K15M	1.50g	RM000250
Avicel® PH102	0.25g	RM000038
Span®80	1% v/v	-
Light liquid paraffin	120ml	-
Acetone	20ml	-

Dissolution profile

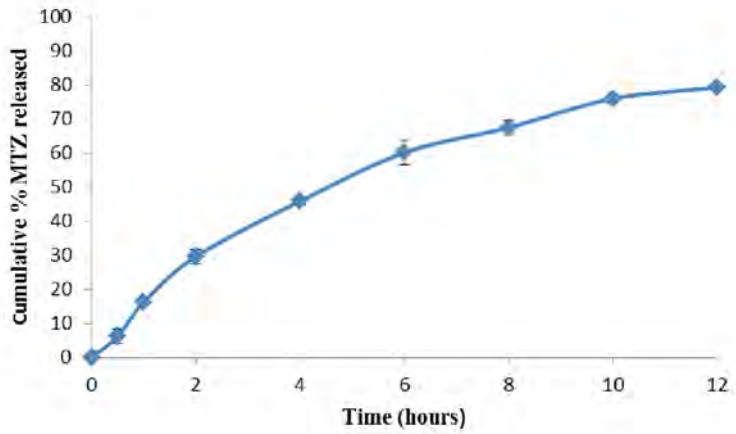

SEM

Encapsulation efficiency (%):70.89 ± 2.17
Buoyancy (%): 61.56 ± 2.09
Yield (%): 92.12 ± 2.07
Particle size (µm):54.09 ± 5.80
Shape and morphology: Spherical microcapsule with particles adhering to the surface

FACULTY OF PHARMACY, GRAHAMSTOWN, SOUTH AFRICA
BATCH SUMMARY RECORD

Formulator	Anjana Makan	**Batch size**	4.25 g
Product	Metronidazole microcapsules	**Homogenisation time (hours)**	7
Batch ID	MTZ-030	**Homogenisation speed (rpm)**	1000
Temperature	22.6°C	**Date of manufacture**	13/10/16

Formula		
Material	**Amount added**	**Rhodes batch number**
MTZ	1.00g	RM000338
Eudragit® RS PO	1.25g	RM000023
Methocel® K15M	1.25g	RM000250
Avicel® PH102	0.75g	RM000038
Span®80	1% v/v	-
Light liquid paraffin	120ml	-
Acetone	20ml	-

Dissolution profile

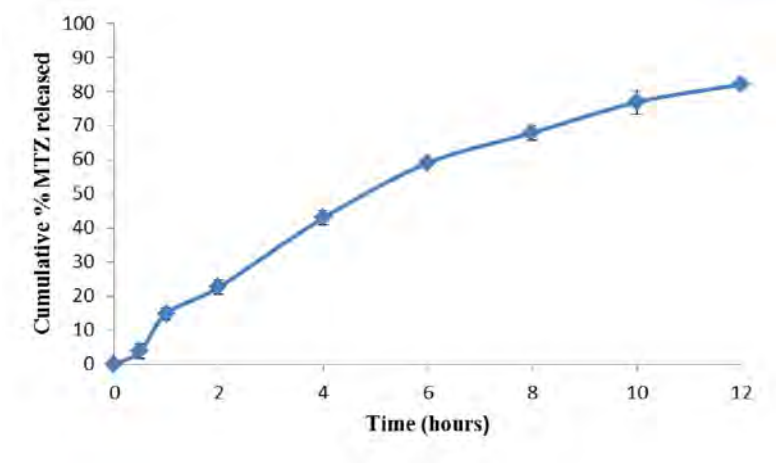

SEM

Encapsulation efficiency (%):73.4 ± 1.95
Buoyancy (%): 58.55 ± 1.90
Yield (%): Yield: 94.35 ± 2.02
Particle size (µm): 146.76 ± 2.38
Shape and morphology: Irregular shaped microcapsule with smooth surface

FACULTY OF PHARMACY, GRAHAMSTOWN, SOUTH AFRICA
BATCH SUMMARY RECORD

Formulator	Anjana Makan	**Batch size**	4.25 g
Product	Metronidazole microcapsules	**Homogenisation time (hours)**	6
Batch ID	MTZ-031	**Homogenisation speed (rpm)**	1000
Temperature	21.8°C	**Date of manufacture**	14/10/16

Formula		
Material	**Amount added**	**Rhodes batch number**
MTZ	1.00g	RM000338
Eudragit® RS PO	1.00g	RM000023
Methocel® K15M	1.25g	RM000250
Avicel® PH102	1.00g	RM000038
Span®80	1% v/v	-
Light liquid paraffin	120ml	-
Acetone	20ml	-

Dissolution profile

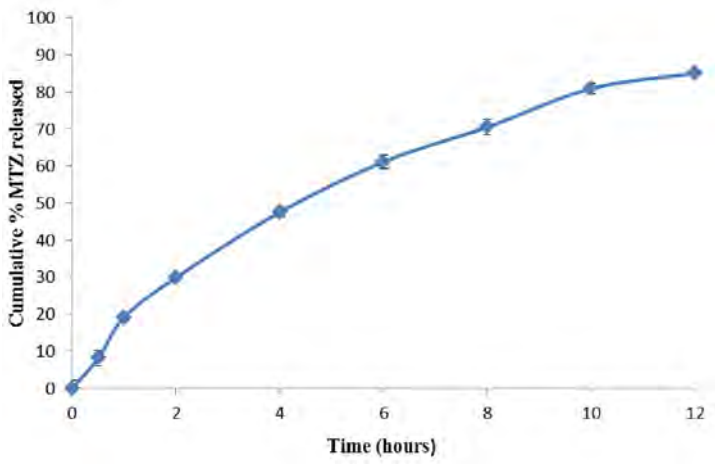

SEM

Encapsulation efficiency (%): 72.70 ± 1.96
Buoyancy (%): 57.54 ± 1.34
Yield (%): 96.09 ± 1.29
Particle size (µm):168.89 ± 3.05
Shape and morphology: Spherical microcapsule with smooth surface

FACULTY OF PHARMACY, GRAHAMSTOWN, SOUTH AFRICA
BATCH SUMMARY RECORD

Formulator	Anjana Makan	**Batch size**	4.25 g
Product	Metronidazole microcapsules	**Homogenisation time (hours)**	5
Batch ID	MTZ-032	**Homogenisation speed (rpm)**	500
Temperature	22.3°C	**Date of manufacture**	15/10/16

Formula		
Material	**Amount added**	**Rhodes batch number**
MTZ	1.00g	RM000338
Eudragit® RS PO	1.50g	RM000023
Methocel® K15M	1.00g	RM000250
Avicel® PH102	0.75g	RM000038
Span®80	1% v/v	-
Light liquid paraffin	120ml	-
Acetone	20ml	-

Dissolution profile

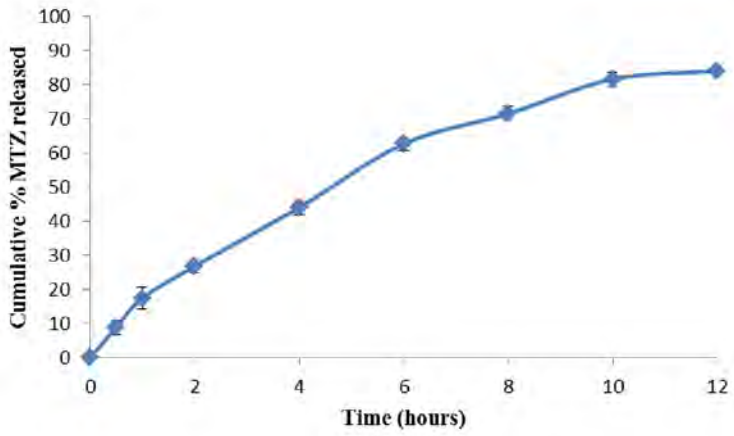

SEM

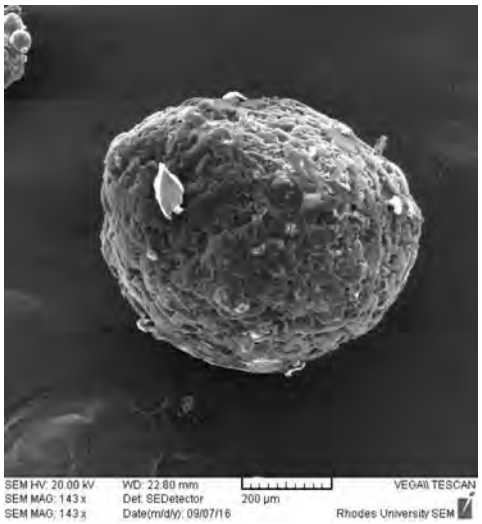

Encapsulation efficiency (%): 71.59 ± 2.75
Buoyancy (%): 55.90 ± 2.37
Yield (%): 94.11 ± 2.14
Particle size (µm): 653.33 ± 3.17
Shape and morphology: Irregular shaped microcapsule with rough surface and particles adhering to the surface

FACULTY OF PHARMACY, GRAHAMSTOWN, SOUTH AFRICA
BATCH SUMMARY RECORD

Formulator	Anjana Makan	**Batch size**	4.25 g
Product	Metronidazole microcapsules	**Homogenisation time (hours)**	6
Batch ID	MTZ-033	**Homogenisation speed (rpm)**	1000
Temperature	22.5°C	**Date of manufacture**	16/10/16

Formula		
Material	**Amount added**	**Rhodes batch number**
MTZ	1.00g	RM000338
Eudragit® RS PO	1.25g	RM000023
Methocel® K15M	1.00g	RM000250
Avicel® PH102	1.00g	RM000038
Span®80	1% v/v	-
Light liquid paraffin	120ml	-
Acetone	20ml	-

Dissolution profile

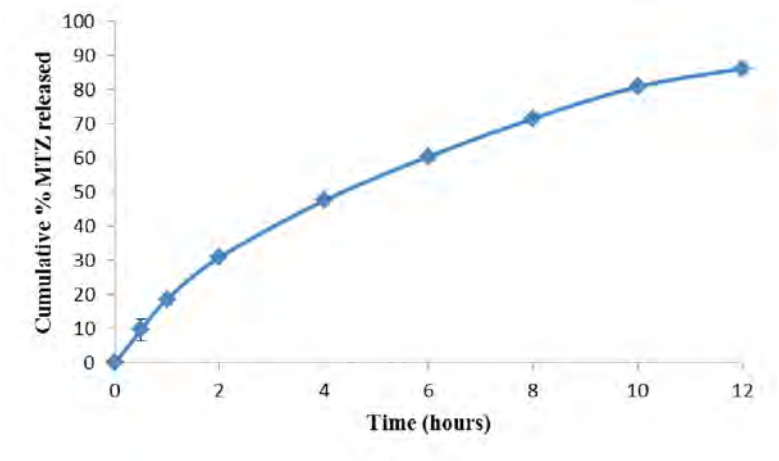

SEM

Encapsulation efficiency (%): 70.46 ± 1.74
Buoyancy (%): 58.55 ± 1.97
Yield (%): 95.49 ± 0.77
Particle size (µm): 165.21 ± 4.50
Shape and morphology: Spherical microcapsule with smooth surface

FACULTY OF PHARMACY, GRAHAMSTOWN, SOUTH AFRICA
BATCH SUMMARY RECORD

Formulator	Anjana Makan	**Batch size**	4.25 g
Product	Metronidazole microcapsules	**Homogenisation time (hours)**	6
Batch ID	MTZ-034	**Homogenisation speed (rpm)**	1500
Temperature	22.7°C	**Date of manufacture**	17/10/16

Formula

Material	Amount added	Rhodes batch number
MTZ	1.00g	RM000338
Eudragit® RS PO	1.25g	RM000023
Methocel® K15M	1.25g	RM000250
Avicel® PH102	0.75g	RM000038
Span®80	1% v/v	-
Light liquid paraffin	120ml	-
Acetone	20ml	-

Dissolution profile

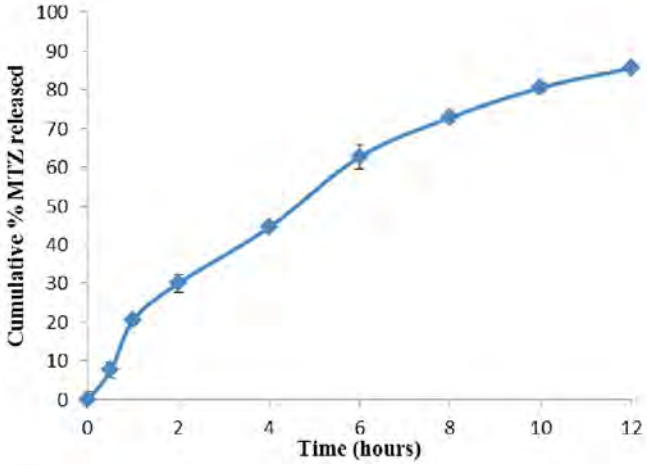

SEM

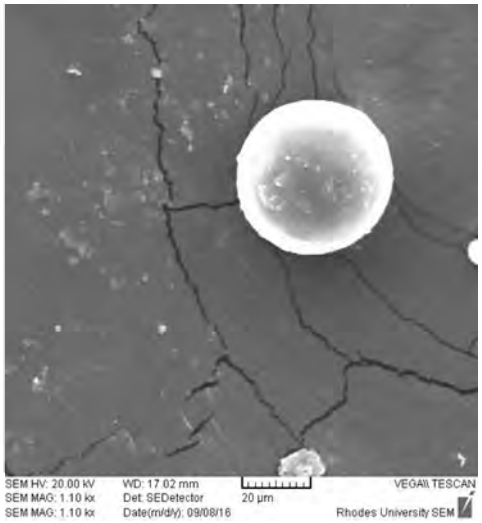

Encapsulation efficiency (%): 69.14 ± 2.01
Buoyancy (%): 56.50 ± 0.93
Yield (%): 90.88 ± 1.98
Particle size (µm): 45.49 ± 0.85
Shape and morphology: Spherical microcapsule with smooth surface

FACULTY OF PHARMACY, GRAHAMSTOWN, SOUTH AFRICA
BATCH SUMMARY RECORD

Formulator	Anjana Makan	**Batch size**	4.25 g
Product	Metronidazole microcapsules	**Homogenisation time (hours)**	7
Batch ID	MTZ-035	**Homogenisation speed (rpm)**	1500
Temperature	22.5°C	**Date of manufacture**	18/10/16

Formula		
Material	**Amount added**	**Rhodes batch number**
MTZ	1.00g	RM000338
Eudragit® RS PO	1.00g	RM000023
Methocel® K15M	1.00g	RM000250
Avicel® PH102	1.25g	RM000038
Span®80	1% v/v	-
Light liquid paraffin	120ml	-
Acetone	20ml	-

Dissolution profile

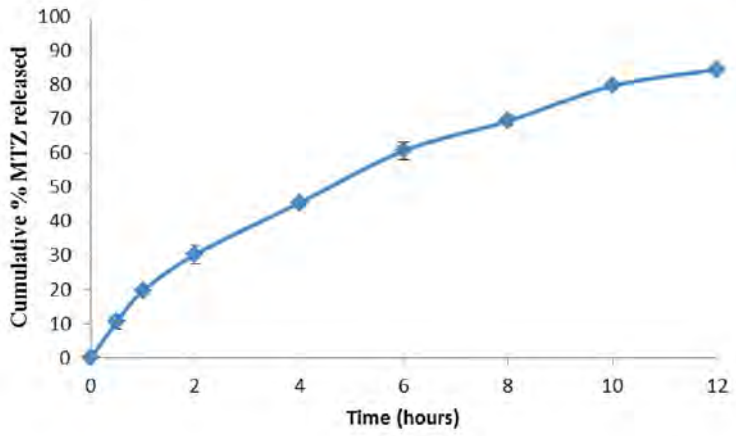

SEM

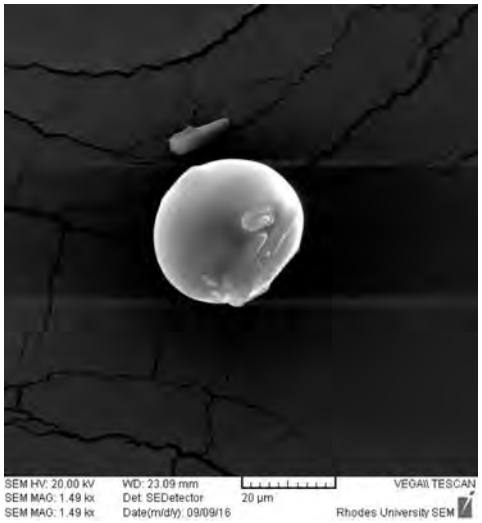

Encapsulation efficiency (%):69.59 ± 1.65
Buoyancy (%): 56.45 ± 1.75
Yield (%): 91.47 ± 1.06
Particle size (µm): 31.12 ± 5.21
Shape and morphology: Spherical microcapsule with particles adhering to the smooth surface

FACULTY OF PHARMACY, GRAHAMSTOWN, SOUTH AFRICA
BATCH SUMMARY RECORD

Formulator	Anjana Makan	**Batch size**	4.25 g
Product	Metronidazole microcapsules	**Homogenisation time (hours)**	5
Batch ID	MTZ-036	**Homogenisation speed (rpm)**	1500
Temperature	22.6°C	**Date of manufacture**	19/10/16

Formula		
Material	**Amount added**	**Rhodes batch number**
MTZ	1.00g	RM000338
Eudragit® RS PO	1.00g	RM000023
Methocel® K15M	1.00g	RM000250
Avicel® PH102	1.25g	RM000038
Span®80	1% v/v	-
Light liquid paraffin	120ml	-
Acetone	20ml	-

Dissolution profile

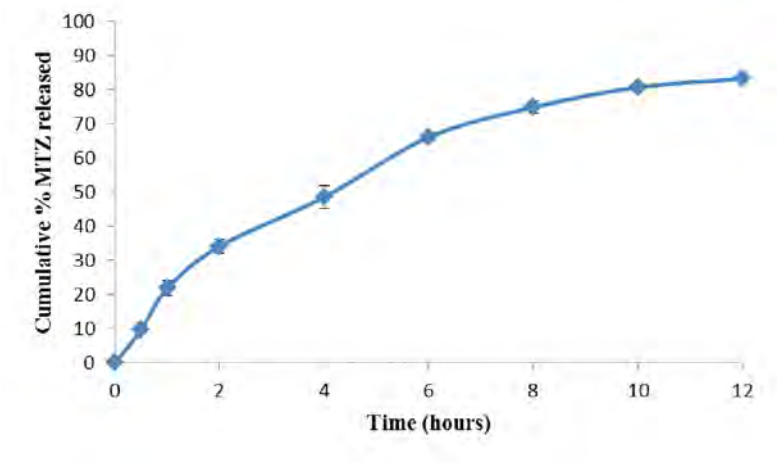

SEM

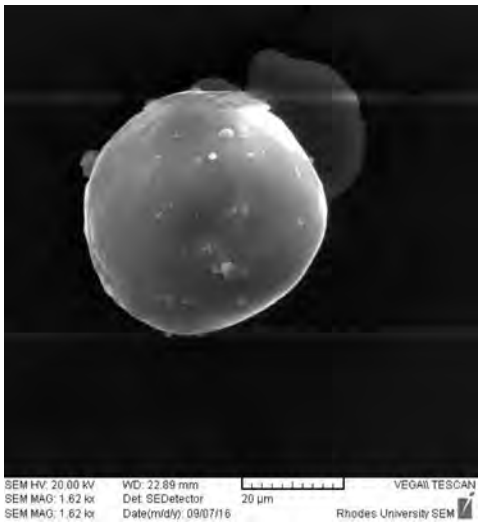

Encapsulation efficiency (%):68.06 ± 2.51
Buoyancy (%): 57.45 ± 2.54
Yield (%): 92.23 ± 1.28
Particle size (µm): 47.59 ± 0.04
Shape and morphology: Spherical microcapsule with smooth surface

FACULTY OF PHARMACY, GRAHAMSTOWN, SOUTH AFRICA
BATCH SUMMARY RECORD

Formulator	Anjana Makan	**Batch size**	4.25 g
Product	Metronidazole microcapsules	**Homogenisation time (hours)**	6
Batch ID	MTZ-037	**Homogenisation speed (rpm)**	1000
Temperature	21.9°C	**Date of manufacture**	20/10/16

Formula		
Material	**Amount added**	**Rhodes batch number**
MTZ	1.00g	RM000338
Eudragit® RS PO	1.25g	RM000023
Methocel® K15M	1.50g	RM000250
Avicel® PH102	0.50g	RM000038
Span®80	1% v/v	-
Light liquid paraffin	120ml	-
Acetone	20ml	-

Dissolution profile

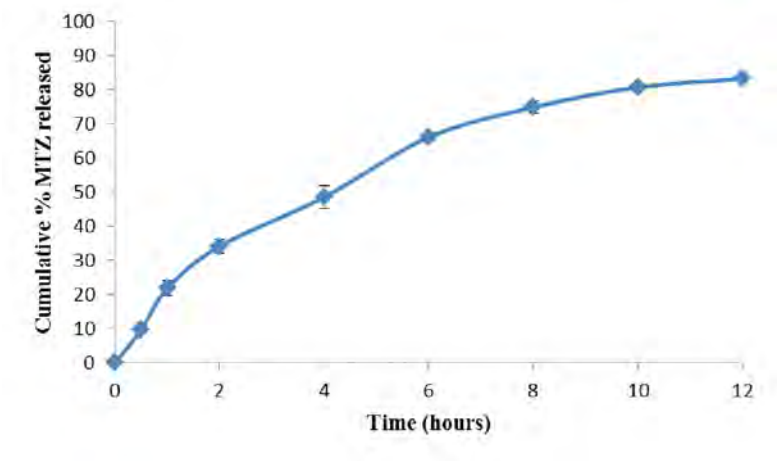

SEM

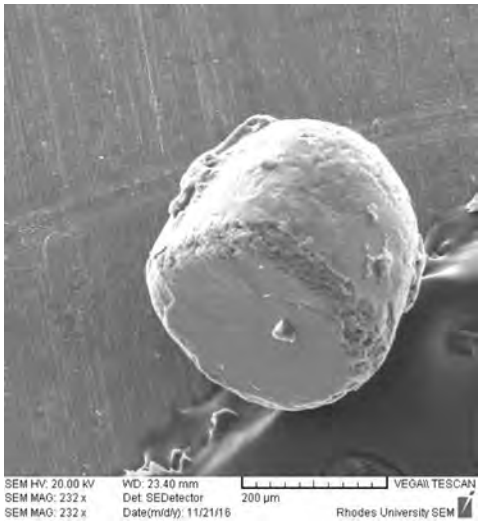

Encapsulation efficiency (%):71.42 ± 1.73
Buoyancy (%): 61.2 ± 2.12
Yield (%): 94.47 ± 2.00
Particle size (µm): 153.35 ± 3.48
Shape and morphology: Irregular shaped microcapsule with rough surface

FACULTY OF PHARMACY, GRAHAMSTOWN, SOUTH AFRICA
BATCH SUMMARY RECORD

Formulator	Anjana Makan	**Batch size**	4.25 g
Product	Metronidazole microcapsules	**Homogenisation time (hours)**	6
Batch ID	MTZ-038	**Homogenisation speed (rpm)**	1000
Temperature	21.5°C	**Date of manufacture**	24/10/16

Formula		
Material	**Amount added**	**Rhodes batch number**
MTZ	1.00g	RM000338
Eudragit® RS PO	1.49g	RM000023
Methocel® K15M	1.25g	RM000250
Avicel® PH102	0.51g	RM000038
Span®80	1% v/v	-
Light liquid paraffin	120ml	-
Acetone	20ml	-

Dissolution profile

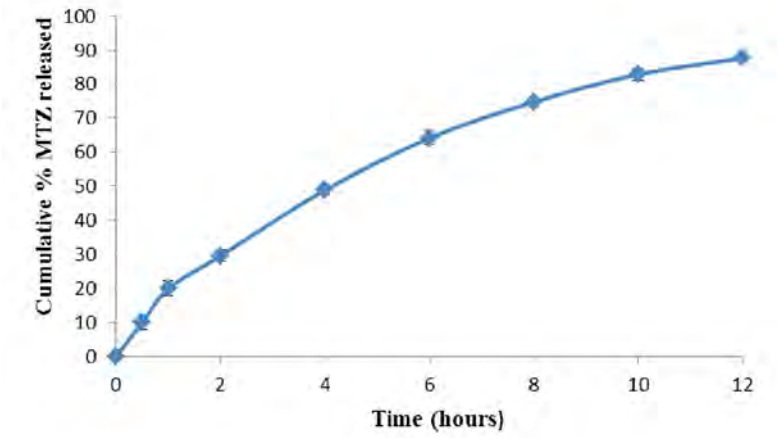

SEM

Encapsulation efficiency (%):72.60 ±1.67
Buoyancy (%): 58.41 ± 1.81
Yield (%): 96.83 ± 1.51
Particle size (µm): 153.35 ± 3.48
Shape and morphology: Spherical microcapsule with smooth surface

APPENDIX III

Diagnostic, two-dimensional and three-dimensional response surface plots used for optimisation with CCD for cumulative % MTZ released at 2 hours, (Y_2) and cumulative % MTZ released at 6 hours (Y_3) but not discussed in Chapter 5.

1. Diagnostic plots for the quadratic model for MTZ released at 2 hours (Y_2)

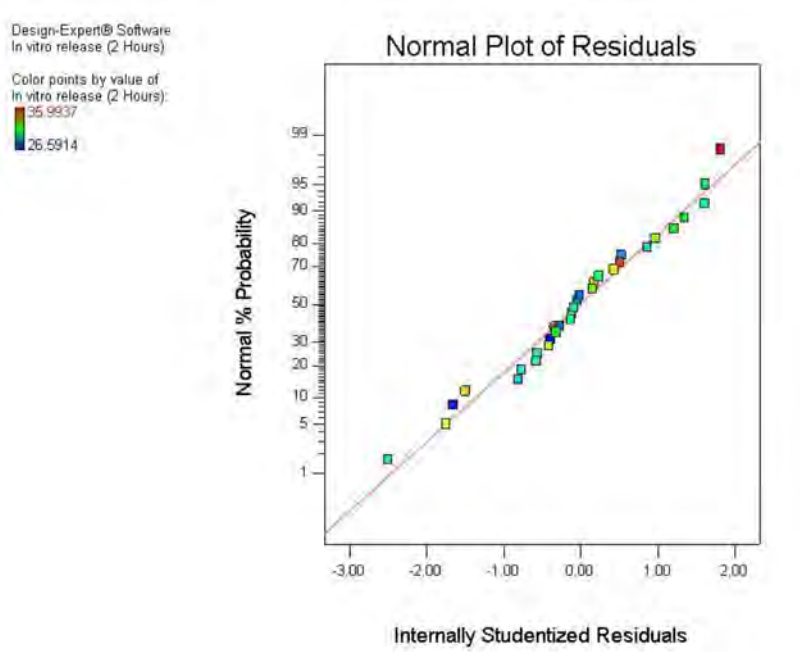

Figure Ap. 3.1 Normal plot of residuals for amount of MTZ released at 2 hrs (Y_2)

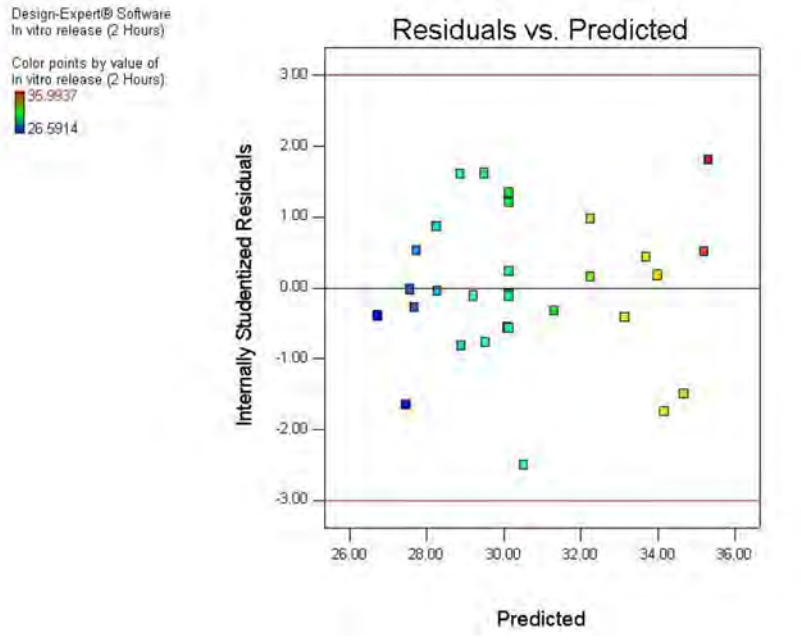

Figure Ap. 3.2 Plot of residuals vs. predicted response for amount of MTZ released at 2 hours (Y_2)

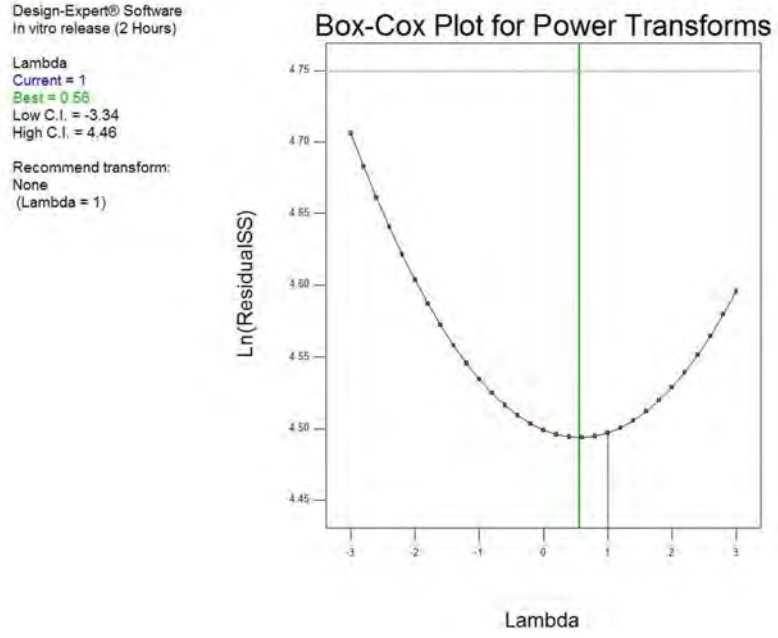

Figure Ap. 3.3 Box-Cox plot for amount of MTZ released at 2 hours (Y_2)

2. Response surface plots for the quadratic model for MTZ released at 2 hours (Y_2)

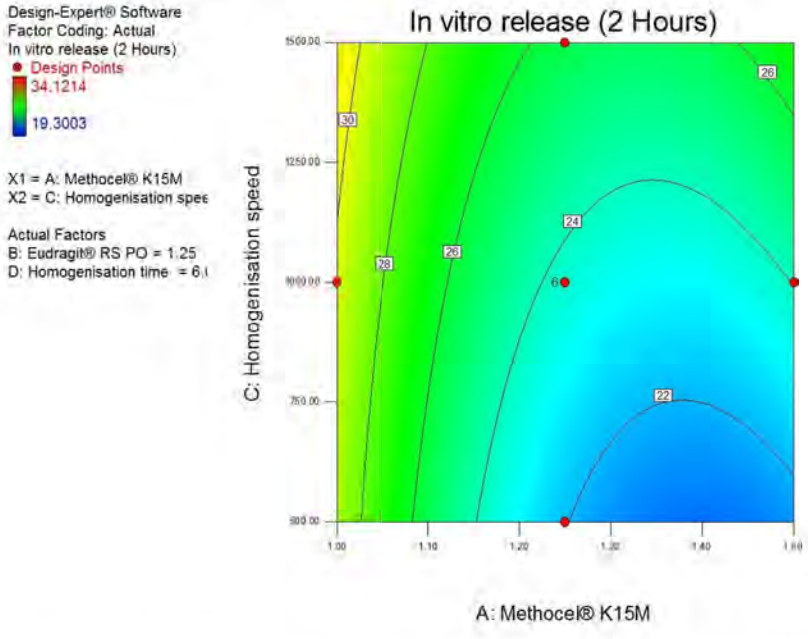

Figure Ap. 3.4 Contour plot depicting the impact of homogenisation speed and Methocel® K15M on amount of MTZ released at 2 hours (Y_2)

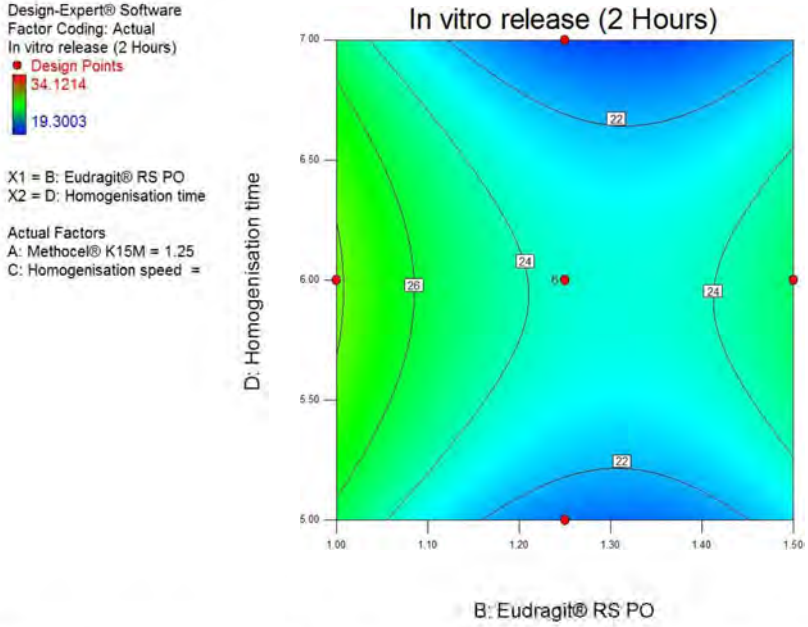

Figure Ap. 3.5 Contour plot depicting the impact of homogenisation time and Eudragit® RS PO on amount of MTZ released at 2 hours (Y_2)

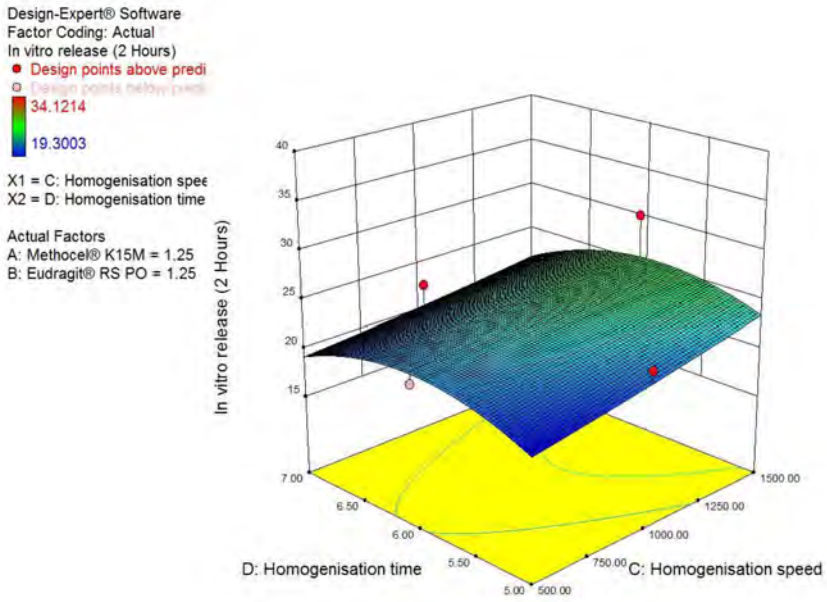

Figure Ap. 3.6 3D plot depicting the impact of homogenisation time and speed on the amount of MTZ released at 2 hours (Y_2)

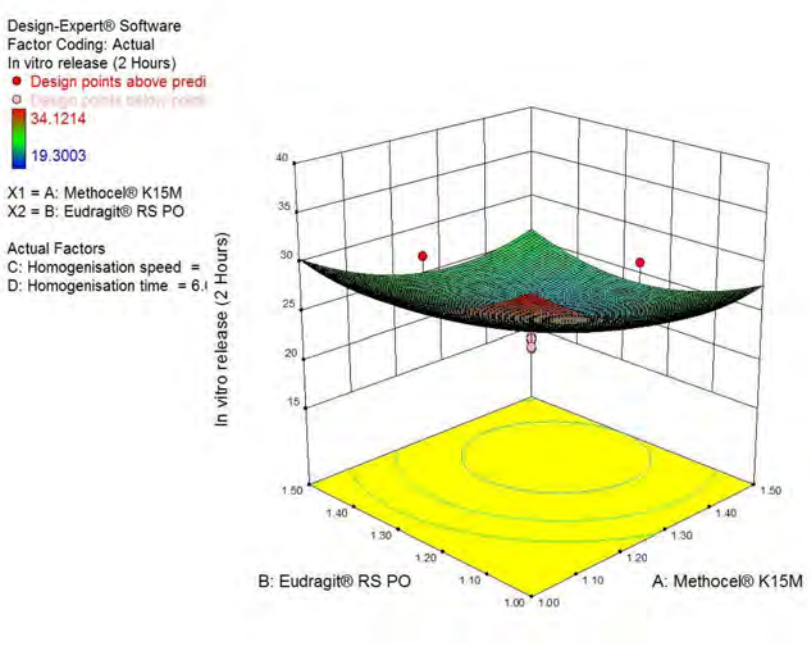

Figure Ap. 3.7 3D plot depicting the impact of Methocel® K15M and Eudragit® RS PO on the amount of MTZ released at 2 hours (Y_2)

3. Diagnostic plots for the quadratic model for MTZ released at 6 hours (Y_3)

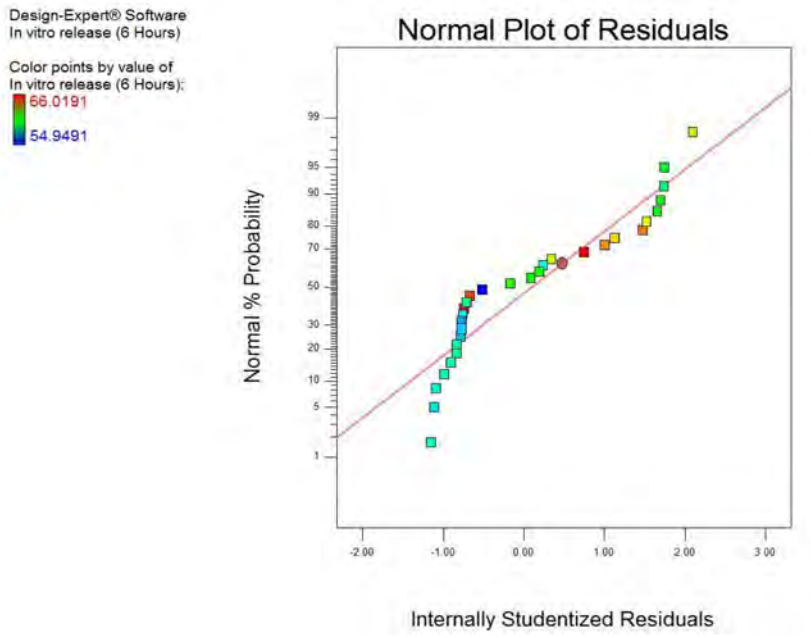

Figure Ap. 3.8 Normal plot of residuals for amount of MTZ released at 6 hrs (Y_3)

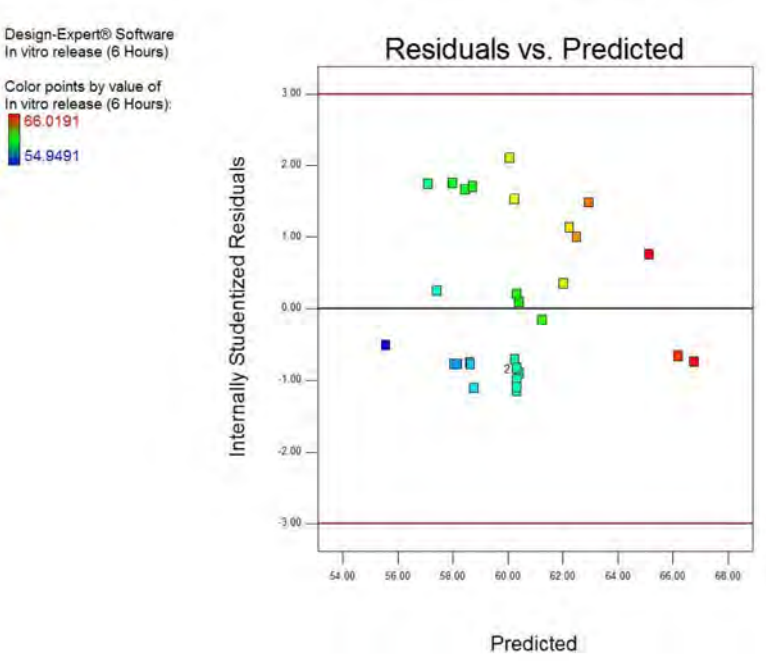

Figure Ap. 3.9 Plot of residuals vs. predicted response for amount of MTZ released at 6 hours (Y_3)

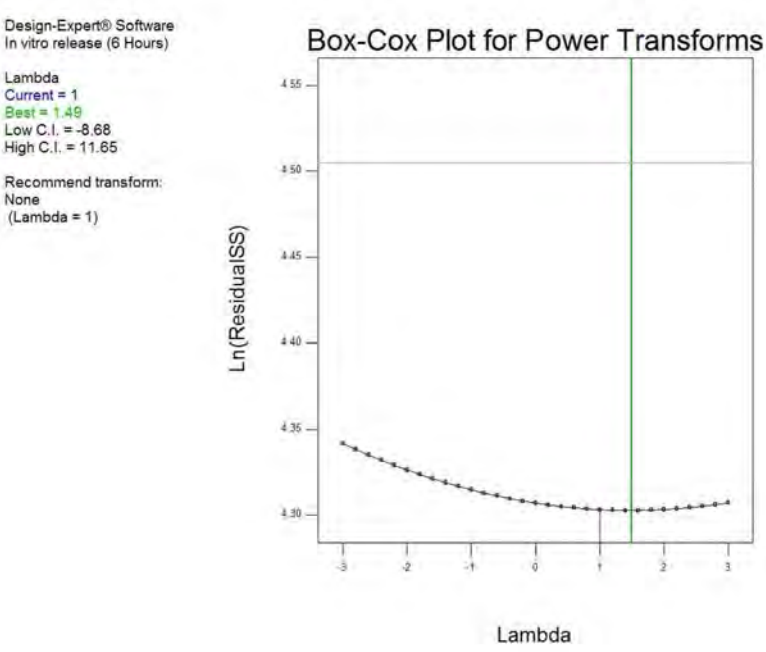

Figure Ap. 3.10 Box-Cox plot for amount of MTZ released at 6 hours (Y_3)

4. Response surface plots for the quadratic model for MTZ released at 6 hours (Y_3)

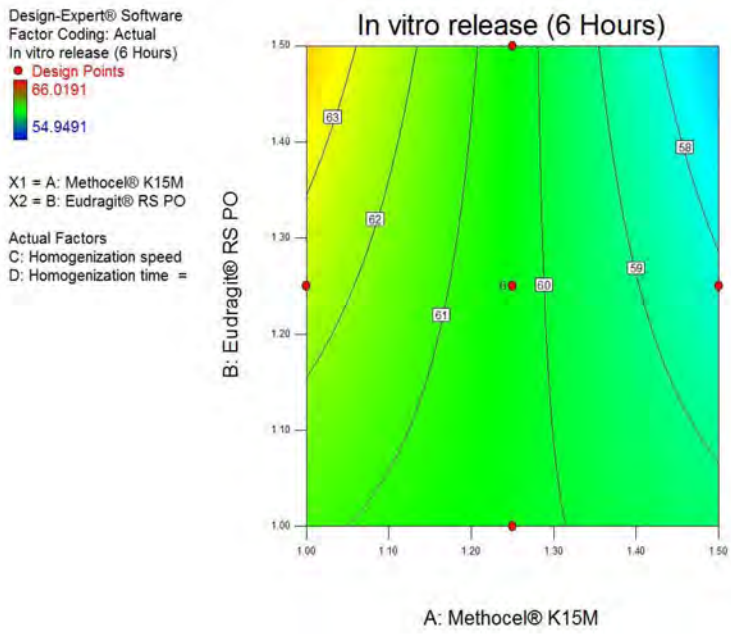

Figure Ap. 3.11 Contour plot depicting the impact of the amount of Methocel® K15M and amount of Eudragitl® RS PO on amount of MTZ released at 6 hours (Y_3)

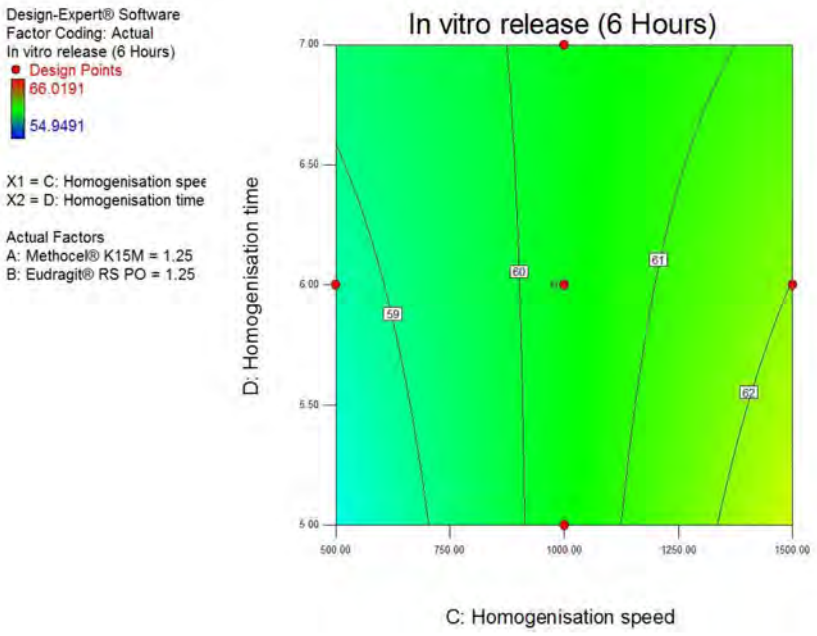

Figure Ap. 3.12 Contour plot depicting the impact of homogenisation speed and homogenisation time on amount of MTZ released at 6 hours (Y_3)

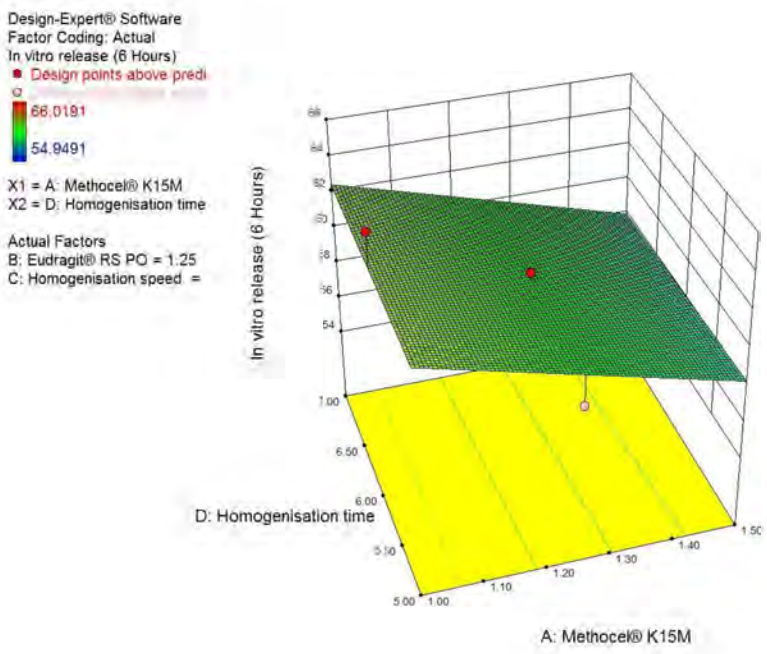

Figure Ap. 3.13 3D plot depicting the impact of homogenisation time and the amount of Methocel® K15M on amount of MTZ released at 6 hours (Y_3)

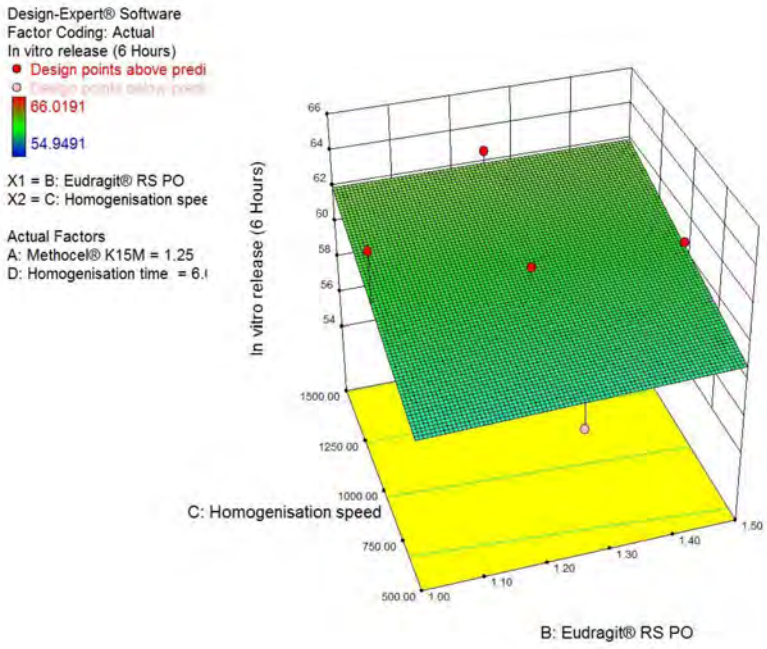

Figure Ap. 3.14 3D plot depicting the impact of homogenisation speed and the amount of Eudragit RS PO® on amount of MTZ released at 6 hours (Y_3)